UNCLASSIFIED

AD NUMBER

AD804730

LIMITATION CHANGES

TO:

Approved for public release; distribution is unlimited.

FROM:

Distribution: Further dissemination only as directed by Federal Aviation Agency, Washington, DC 20553, 06 SEP 1966, or higher DoD authority.

AUTHORITY

FAA ltr 2 Jul 1973

THIS PAGE IS UNCLASSIFIED

8047730

SUPERSONIC
TRANSPORT
DEVELOPMENT
PROGRAM

PHASE III PROPOSAL
AIRFRAME DESIGN REPORT PART E

AD No.
DDC FILE COPY

SST
V2-B2707-9

BOEING SUPERSONIC TRANSPORT DIVISION

SEPTEMBER 6, 1966

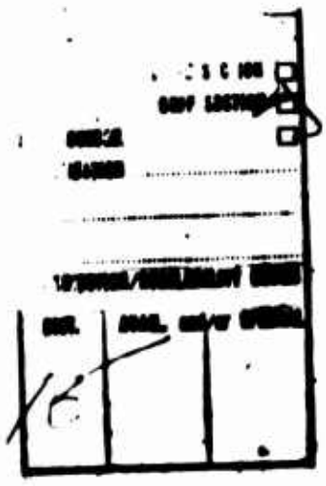
NOTICES

When Government drawings, specifications, o other data are used for any purpose other than in connection w a definitely related Government procurement operation, the United States Government thereby incurs no responsibility nor any obligation whatsoever; and the fact that the Government may have formulated, furnished, or in any way supplied the said drawings, specifications, or other data, is not to be regarded by implication or otherwise as in any manner licensing the holder or any other person or corporation, or conveying any rights or permission to manufacture, use, or sell any patented invention that may in any way be related thereto.

All distribution of this document is controlled. This document may be further distributed by any holder only with specific prior approval of:

Director of Supersonic Transport Development
Federal Aviation Agency
Washington, D. C. 20553

The distribution of this document is limited because it contains technology identifiable with items excluded from export by the Department of State (U. S. Export Control Act of 1949 as amended).



(6) Supersonic Transport Development Program.

Phase III Proposal.

BOEING MODEL 2707.

Volume II-9.

AIRFRAME DESIGN REPORT.
PART E.
STRUCTURAL TESTS,

(14) V2-B2707-9

September 6, 1966

(10) D.R. Donaldson

(11) 6 Sep 66

(12) 226 p.

PREPARED BY D.R. Donaldson APPROVED BY H. Armstrong

(15)

Contract FA-SS-66-5

Prepared for

FEDERAL AVIATION AGENCY

Office of Supersonic Transport Development Program

"THIS DOCUMENT CONTAINS SENSITIVE, COMPETITIVE, AND PROPRIETARY DATA, AND IS NOT TO BE REPRODUCED OR RELEASED OUTSIDE OF YOUR ORGANIZATION OR USED FOR ANY PURPOSE OTHER THAN SUPERSONIC TRANSPORT EVALUATION WITHOUT THE WRITTEN PERMISSION OF EITHER THE FEDERAL AVIATION AGENCY, OFFICE OF SUPERSONIC TRANSPORT DEVELOPMENT, ATTENTION: SS-30, OR THE BOEING COMPANY, SUPERSONIC TRANSPORT DIVISION, ATTENTION: CONTRACT ADMINISTRATION"

DDC RECEIVED JAN 13 1967 B

402 097

THE BOEING COMPANY
SUPERSONIC TRANSPORT DIVISION

FAA

A 139

ISSUE NO. 4

CONTENTS

		Page
1.0	INTRODUCTION AND SUMMARY	1
2.0	TEST PROGRAM PLANS	11
2.1	COMPONENT TESTS	11
2.2	MODEL TESTS	21
2.3	AIRPLANE TESTS	21
3.0	DEVELOPMENT TEST PROGRAM RESULTS	27
3.1	WING PIVOT TESTS	27
3.2	WING TESTS	43
3.3	FUSELAGE TESTS	72
3.4	EMPENNAGE TESTS	106
3.5	PROPULSION POD TESTS	115
3.6	FATIGUE TESTS	116
3.7	SONIC TEST	175
3.8	HONEYCOMB SANDWICH STRUCTURE DEVELOPMENT TESTS	187
3.9	LONG TIME EXPOSURE AND CREEP TESTS	198

VOLUME I

SUMMARY V1-B2707

Phase III Proposal Summary -1

Boeing Model 2707 Warranties -2

VOLUME II

AIRPLANE TECHNICAL REPORT V2-B2707

System Engineering Report -1

Mockup Plan -2

Aerodynamic Design -3

Airplane Performance (GE) -4

Airplane Performance (P&W) -5

Airframe Design Report. -6-1
Part A Weight & Balance

Airframe Design Report- -6-2
Part B Component Design

Airframe Design Report- -7
Part C
Design Criteria
Loads
Aerodynamic Heating
Flutter

Airframe Design Report- -8
Part D
Materials and Processes

Airframe Design Report- -9
Part E
Structural Tests

Systems Report-Part A -10
Environmental Control
Electric
Navigation & Communication

Systems Report-Part B -11
Hydraulics
Landing Gear
Auxiliary Systems

Propulsion Report-Part A -12
Engine, Inlet, & Controls

Propulsion Report-Part B -13
Engine Installation
Fuel System
Exhaust System

Propulsion Report-Part C -14
Engine Evaluation

VOLUME III

ENGINE CONTRACTORS ONLY

VOLUME IV

SYSTEM INTEGRATION V4-B2707

Operational Suitability -1

Sonic Boom Program -3

Airport & Community Noise Program -4

Internal Noise Program -5

System Safety Plan -6

Training & Training Equipment Program -7

Human Engineering Program -8

Test Integration & Management -10

Integrated Test Program -11

Simulation Program -12

Flight Simulation Program -13

Flight Test Program -14

Maintainability Program -15

Reliability Program -16

Quality Control Program -17

Value Engineering Program -18

Standardization Program -19

Product Support Program -20

Quality Assurance Program -21

VOLUME V

MANAGEMENT MANUFACTURING V5-B2707

Configuration Management Plan -1

Data Management Plan -2

Master Program Plan -3

Detail Work Plan -4

Procurement Program -5

Cost & Schedules Control Program -6

Facilities Program -7

Program Management -8

Manufacturing Program -9

VOLUME VI

COST V6-B2707

Cost Baseline Report Summary Data -1

Cost Baseline Report Cost Support Data -2

VOLUME VII

ECONOMICS V7-B2707

Economic Summary -1

Economic Summary - For Government Use Only -2

1.0 INTRODUCTION AND SUMMARY

1.1 INTRODUCTION

The Airframe Design Report is one of a series of documents in Volume II, Technical/Airplane, called for by the FAA Request for Proposal for Phase III of the Supersonic Transport Development Program. The Airframe Design Report consists of five documents: Weights and Balance — Part A, V2-B2707-6-1, Component Design — Part B, V2-B2707-6-2, Structural Criteria, Loads, Flutter and Aero Heating — Part C, V2-B2707-7, Materials and Processes — Part D, V2-B2707-8, and this document Structural Test-Part E, V2-B2707-9.

The Flight Test Program, V4-B2707-14 includes the accumulation of data for structural evaluation. The Integrated Test Program, V4-B2707-11 describes the structural tests of this report and integrates them into a complete program.

1.2 SUMMARY

A comprehensive development and verification test program has been established for the structure of the B-2707 airplane. It recognizes the more demanding usage and environment to which the airplane is subjected, and the use of relatively new structural materials and processes. Additionally, it recognizes the problems of contemporary airplanes and provides testing of proper magnitude and timing to preclude recurrence of similar problems on the SST. Structural areas of concern have been covered by systematic development tests to provide the maximum information possible prior to final design. Toward this end, Boeing has conducted development tests of the SST structure and materials to establish reliable strength, fatigue life, and fail-safe concepts continuously during the past 8-years.

Testing began with small specimens and progressed to full-scale specimens as the accumulation of data permitted. A typical example of this is illustrated by the wing pivot bearing development described in Sec. 3.0 which progresses from basic materials evaluation through 1/4-scale bearings to full-scale (36-in. dia) bearings and a final full-scale pivot structure test. Testing of basic materials and processes is a continuous operation to provide improved designs and is combined with the large specimen test data to define a proposed design for the airplane. Information from these tests will be used to finalize the airplane design. The airplane static, fatigue, and flight test programs will validate the design for the production article.

Much of the required development testing was accomplished during the Phase II-C Program. Material selections were made and allowables established for the airframe structure. Design criteria were established on the basis of the test results and subsequently verified with tests of large-scale specimens built to that criteria. Items tested include the following.

a. A full-scale fuselage pressure section (Fig. 1-1) was used to establish design criteria for passenger sections. Several panels were tested to determine crack growth rates for various skin-stringer combinations, and to establish fail-safe strap requirements versus skin gages. Guillotine tests to demonstrate fail-safety for instantaneous punctures of skin, skin and stiffeners, and skin and frame were also included.

b. A full-scale wing box (Fig. 1-2) was tested at room temperature and elevated temperatures to verify stresses, thermal distributions, and analysis methods. Tests in progress will evaluate fail-safe criteria established through panel tests and theoretical analysis.

c. A full-scale empennage box structure test (Fig. 1-3) was tested under simulated load and thermal environment to establish thermal buckling criteria for both the skin-stringer structure and the honeycomb sandwich structure.

d. A full-scale wing pivot bearing (Fig. 1-4) was tested for the equivalent of a full airplane life (30,000 cycles) without bearing failure. Supporting bearing programs included a 1/4-size pivot test and small-scale bearing material and process development tests.

e. Fatigue and fail-safe tests (Fig. 1-5) were conducted on specimens of many sizes representative of all areas of the airframe structure.

f. Wing compression panels, (Fig. 1-6) fuselage compression panels, wing spar structure, (Fig. 1-7), shear panels, and structural joints and splices were tested to determine allowables.

g. Sonic fatigue tests of skin-stringer (Fig. 1-8) were conducted in the sonic facility and behind a J-75 engine.

Results of these and other Phase II-C tests are presented in Sec. 3.0.

Fabrication and test preparation of certain large structural components began during Phase II-C when there appeared to be elements of risk in the design, or where long lead times were required to obtain data. Maximum technical information will be obtained from these components because they will be tested intensively in the beginning of Phase III, and the data will be available early for the airplane design. These tests include the following.

a. A full-scale pivot structure with adjoining wing box sections will be loaded to check stress distribution and deflection at various sweep angles. This will be followed by cyclic tests to check bearing wear characteristics and structure fatigue life. Fail-safe tests will be run following the cyclic test. Supporting tests include: a 1/4-scale photostress model tested in the latter part of Phase II-C to verify the pivot design prior to start of full-scale testing; a 36-in. full-scale bearing life test which is a continuation of the Phase II-C test; a 1/4-scale dynamic load bearing wear test to simulate pounding loads; continuation of the Phase II-C 1/4-scale pivot box test to check bearing configuration changes, and material and process evaluation using small diameter bearings.

b. Three full-scale wing boxes will be tested to improve the wing design fatigue quality, and to evaluate the effect of thermal cycles on fatigue life and the proposed full-scale airplane fatigue test methods.

c. A full-scale crew compartment will be tested to determine the integrity of the cab design under pressure and thermal loads, including the windshield and window structure. Window fail-safe and bird-strike characteristics will be verified.

d. A full-scale empennage box section with honeycomb leading and trailing edge sections will be tested to confirm the honeycomb panel design under combined bending and thermal loadings.

Structural Test Program plans for Phase III and IV are presented in Sec. 2.0. Overall test planning is presented in The Integrated Test Program, V4-B2707-11. The results of the development testing accomplished during Phase II-C are presented in Sec. 3.0 including the description of the wing fatigue box tests, wing pivot test, and other hardware which required more time to complete than was available during Phase II-C. Structural component allowable tests to validate the stress analysis of Airframe Design Report — Part B Component Design, V2-B2707-6-2 include compression and shear panels, joint strength tests, fracture toughness, and crack growth types of fail-safe tests, and sonic and component fatigue tests. The material, process, and basic allowable tests are presented in the Airframe Design Report — Part D Materials and Processes, V2-B2707-8.

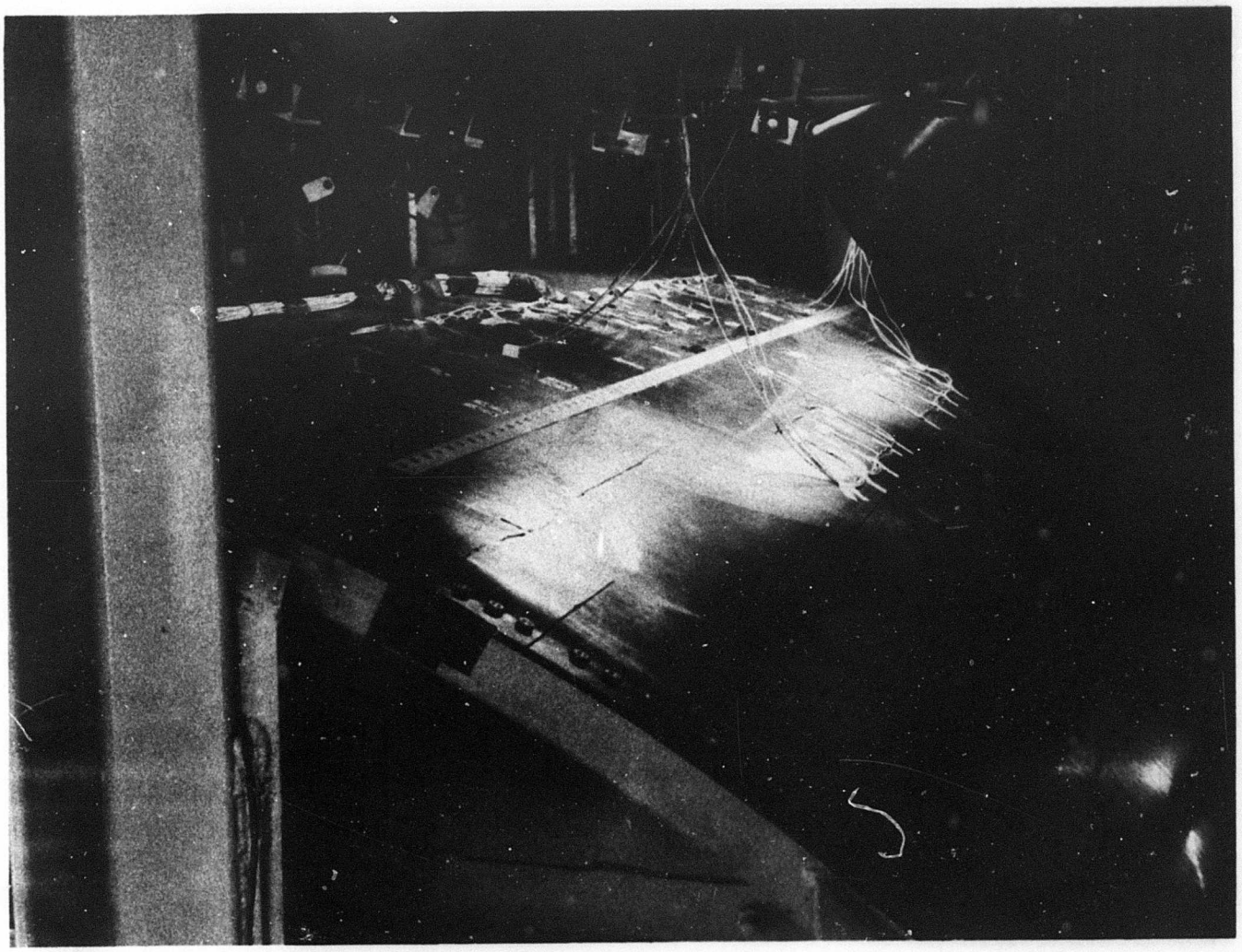


Figure 1-1. Fuselage Pressure Section

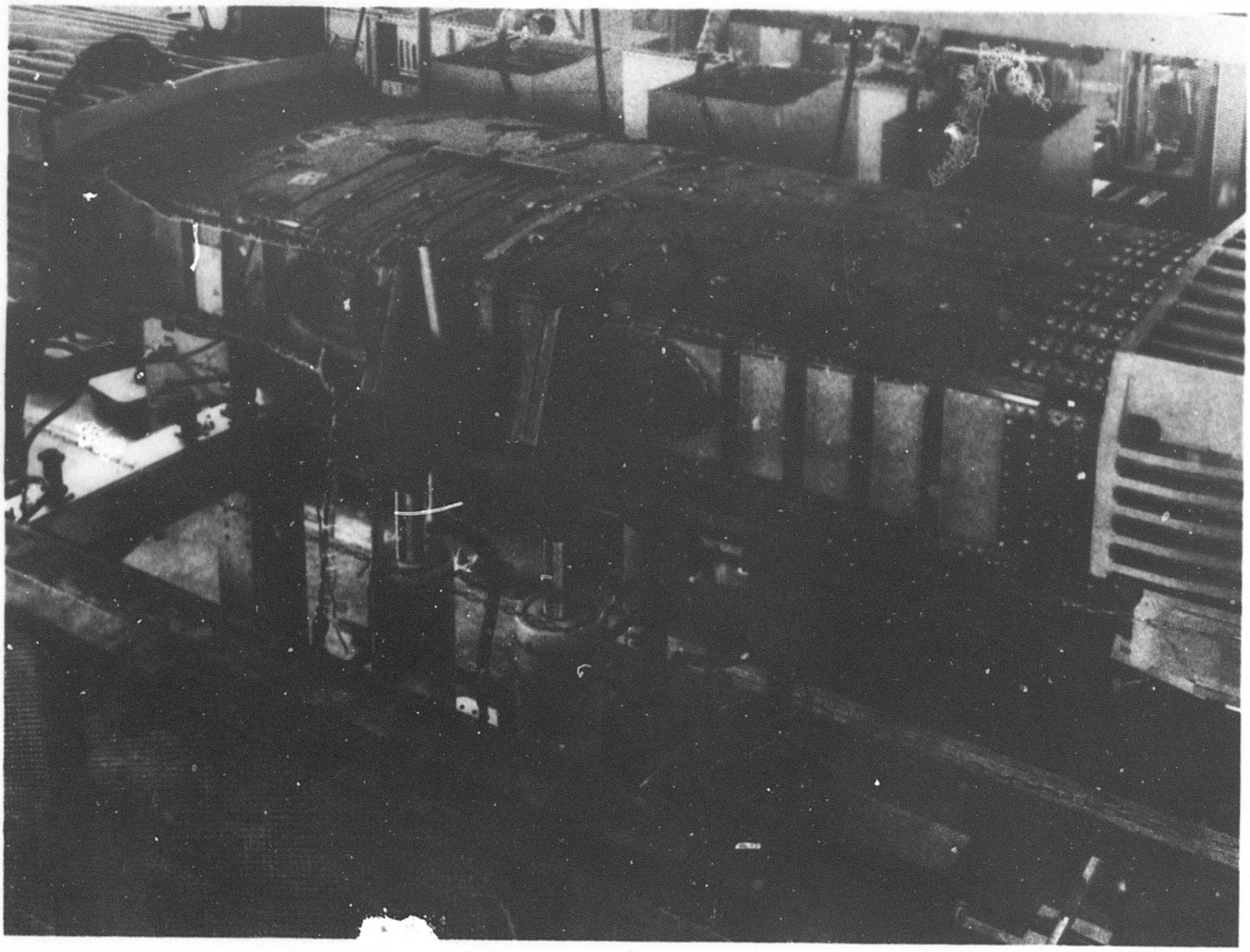


Figure 1-2. Wing Box

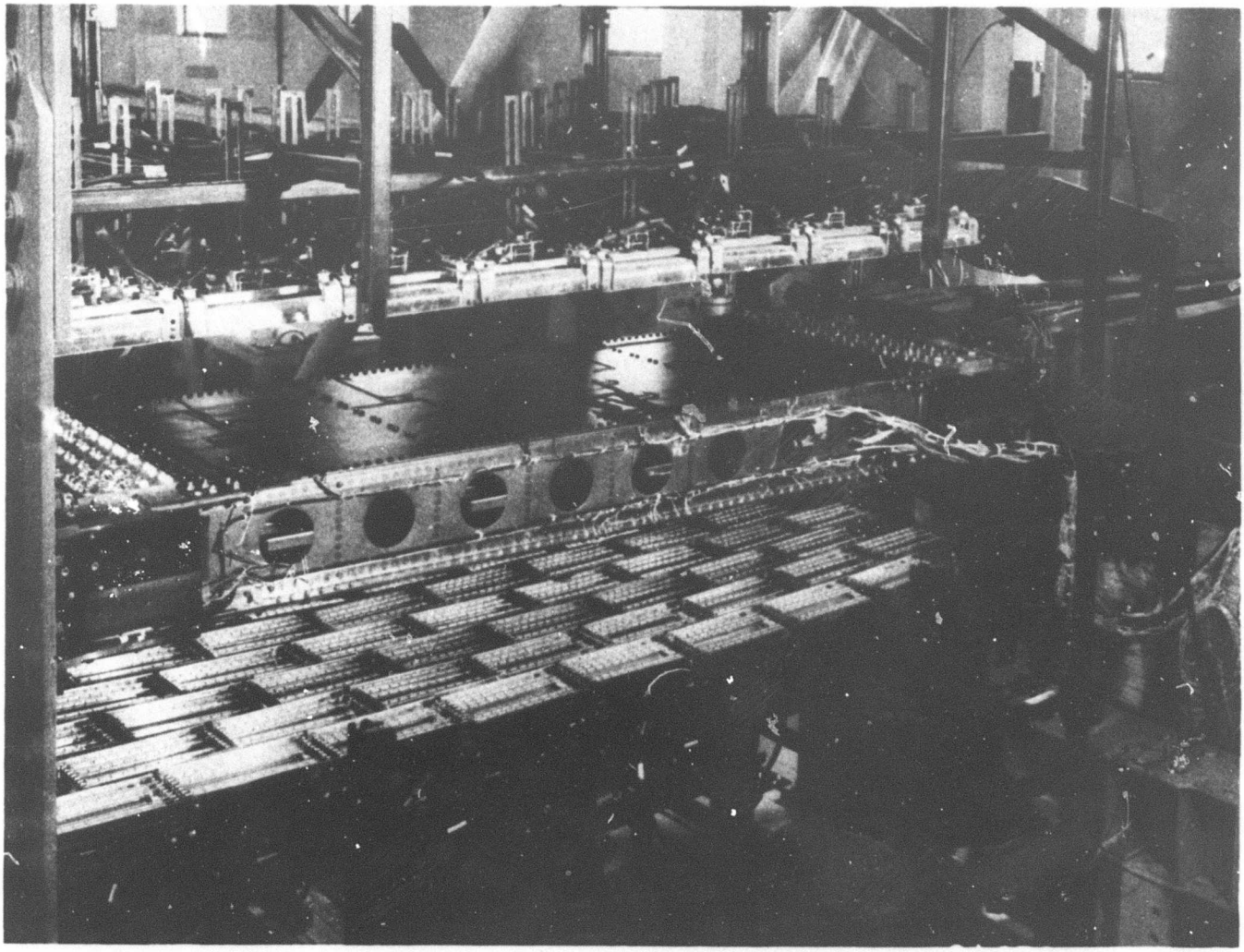


Figure 1-3. Empennage Box Structure Test

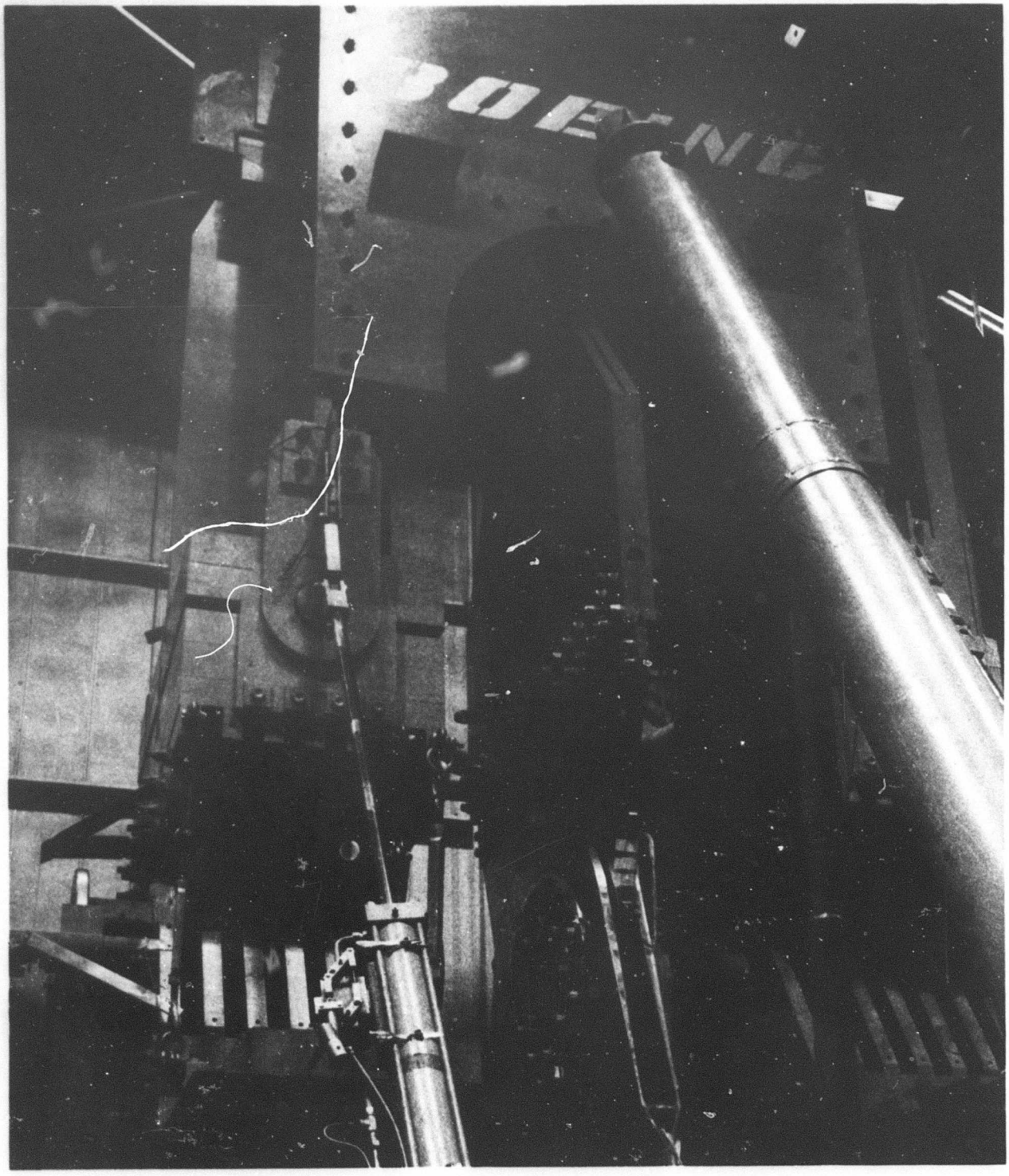


Figure 1-4. Wing Pivot Bearing

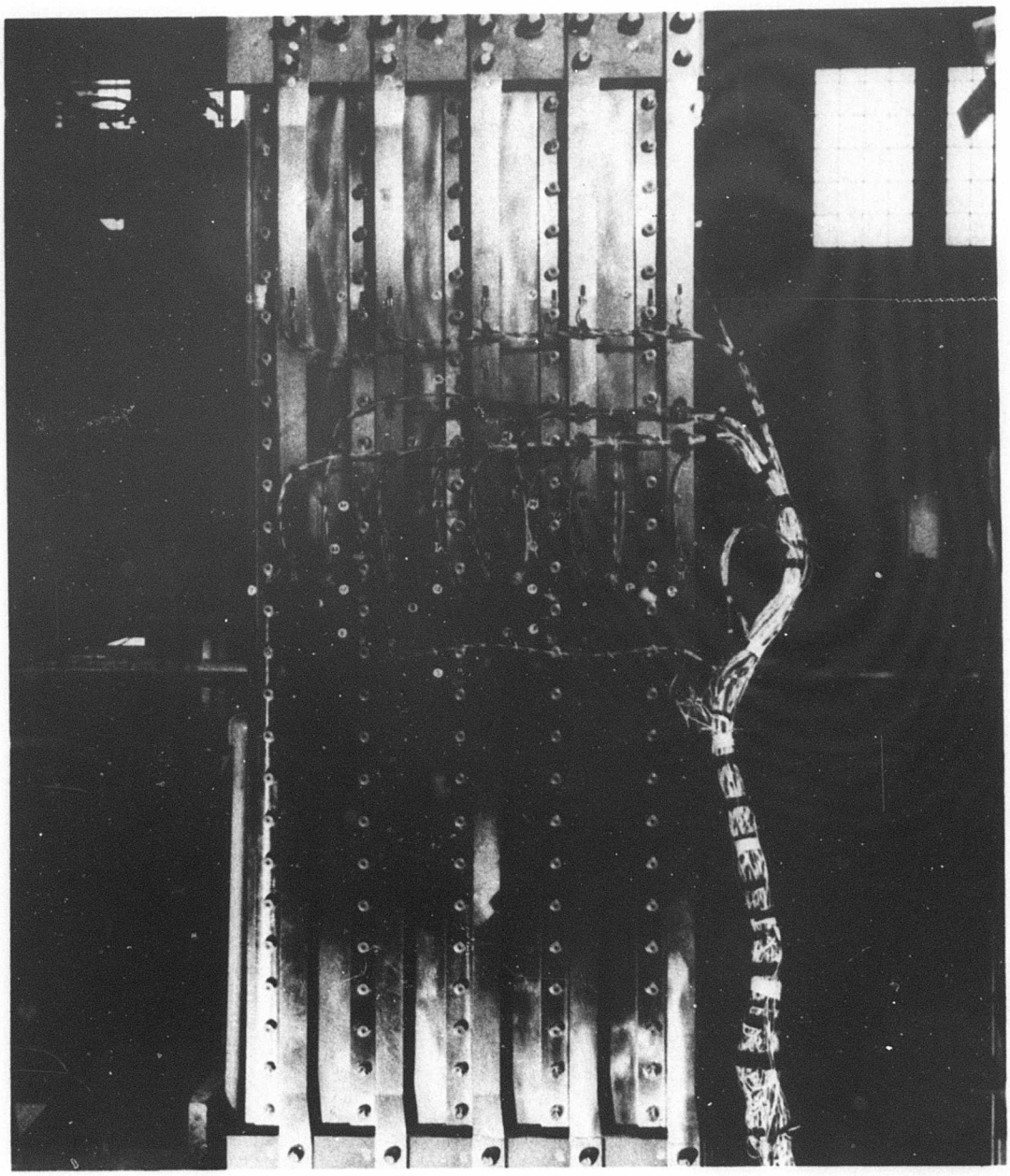


Figure 1-5. Fail-Safe Test Panel

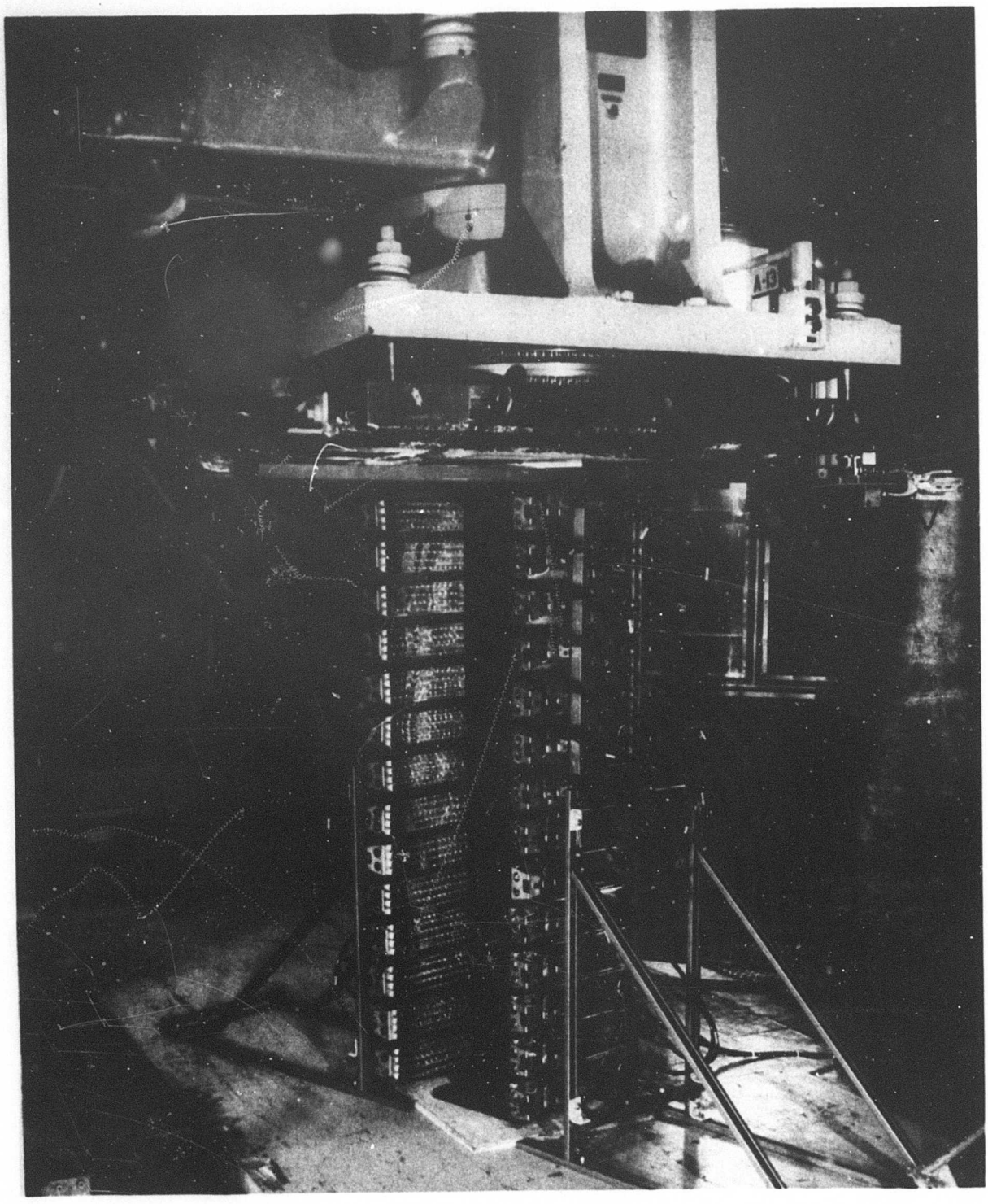


Figure 1-6. Compression Test Panel

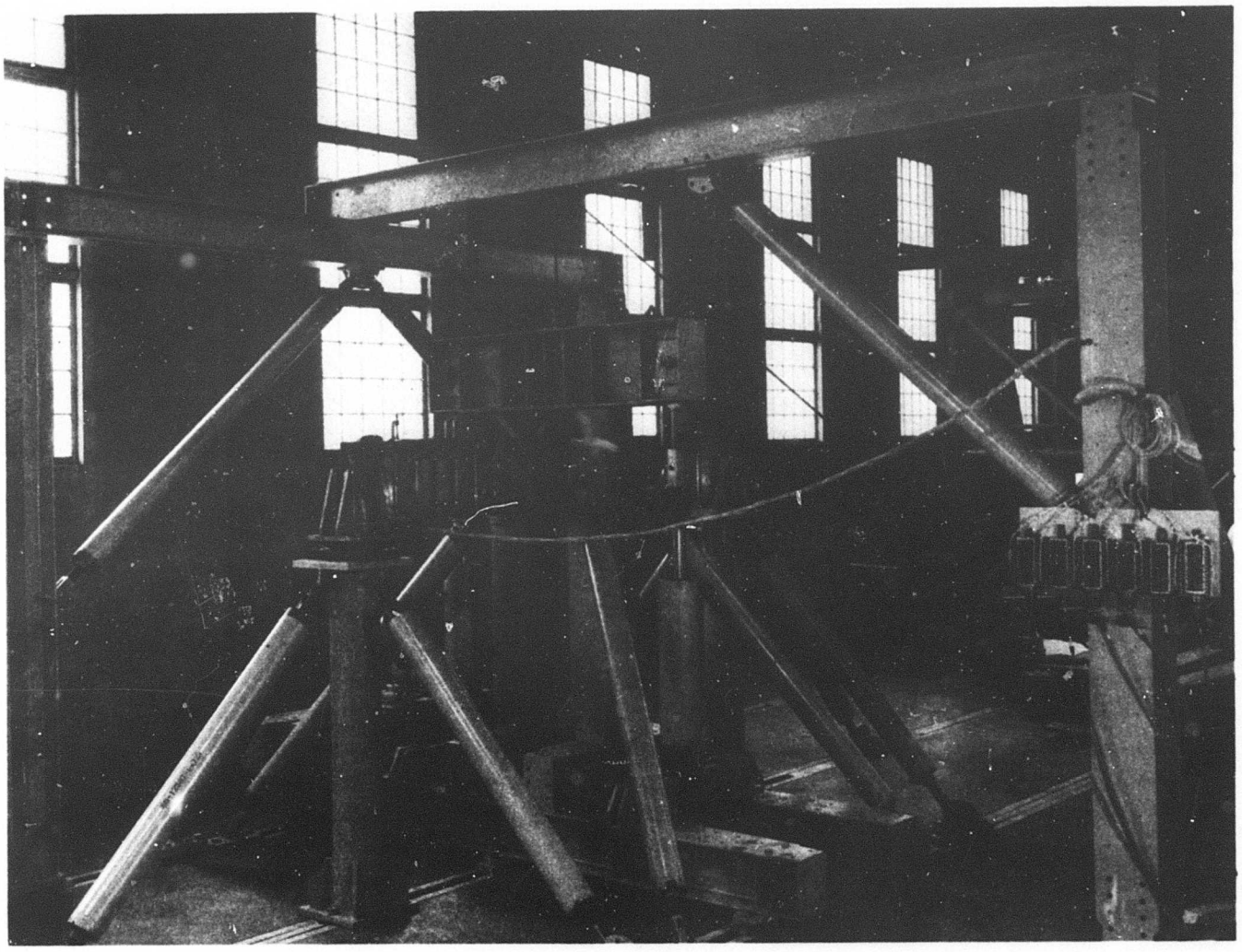


Figure 1-7. Wing Spar

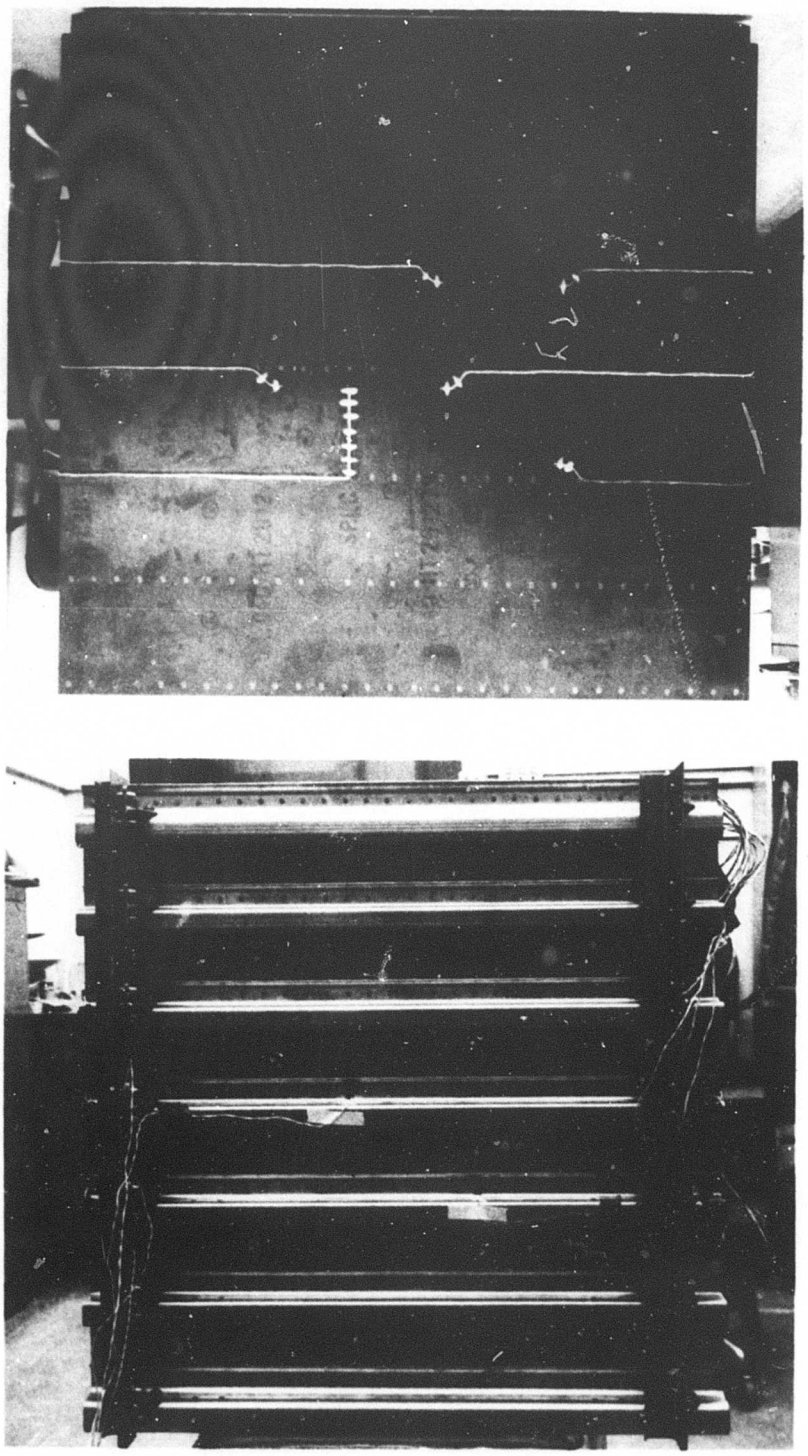


Figure 1-8. Sonic Test Panel

2.0 TEST PROGRAM PLANS

A summary plan is presented in Fig. 2-1, describing the tests of Phase II-C through Phase IV. Included are full-scale airframe test sections to be built from prototype tooling for refining the production design and advancing the flight envelope (gross weights, maneuver factors, and speed) through qualification of the prototype structure to maximum limits. These components are designated by an asterisk after the test titles of Par. 2.1 and the program plan.

2.1 COMPONENT TESTS

The development programs of Phase II-C will be continued with emphasis on programs directed toward hardware design verification. Included in these tests are structural allowables, windows, radomes, joints, fittings, panels, and fatigue specimens. Structures which involve any appreciable risks are built as components and tested in adequate time to incorporate possible changes into the production design and verify the integrity of the prototype airplane. These tests will provide a thorough check of the airplane structure integrity comparable to an airplane proof test. A detail breakdown of the test program is presented in the Integrated Test Program, V4-B2707-11. A summary of the more important tests follow.

2.1.1 Wing-to-Fuselage Joint Tests*

This is the most highly-loaded area for both fuselage and wing structures and this program will provide verification of the static and fatigue strength.

Proof test of the structure will apply landing gear, fuselage pressure, and wing loads, to meet the critical design limit load conditions. Stress distributions will be obtained through photostress analysis and strain deflection measurements. This test will be followed by a cyclic fatigue test to verify and improve structural fatigue life. The fatigue test will be based on full-scale airplane cyclic body pressure, landing gear, and wing loads.

The fatigue test will be followed by fail-safe tests of as much structure as is practical including lower wing surface, upper fuselage, lower longeron, landing gear attachment fittings, and fuselage bulkheads.

2.1.2 Empennage-to-Fuselage Joint Tests*

This program will verify the static and fatigue strength of the fin-stabilizer-fuselage intersection structure. A full-scale fuselage structure section complete with fin and stub stabilizer sections will be subjected to empennage and body design limit loads. Stress distribution will be obtained through photostress analysis and strain-deflection measurements. This test will be followed by a cyclic fatigue test to verify and improve the structural fatigue life. The fatigue test will duplicate the test proposed for the full-scale airplane cyclic test as closely as possible and will include fuselage pressure, vertical fin, and stabilizer loads.

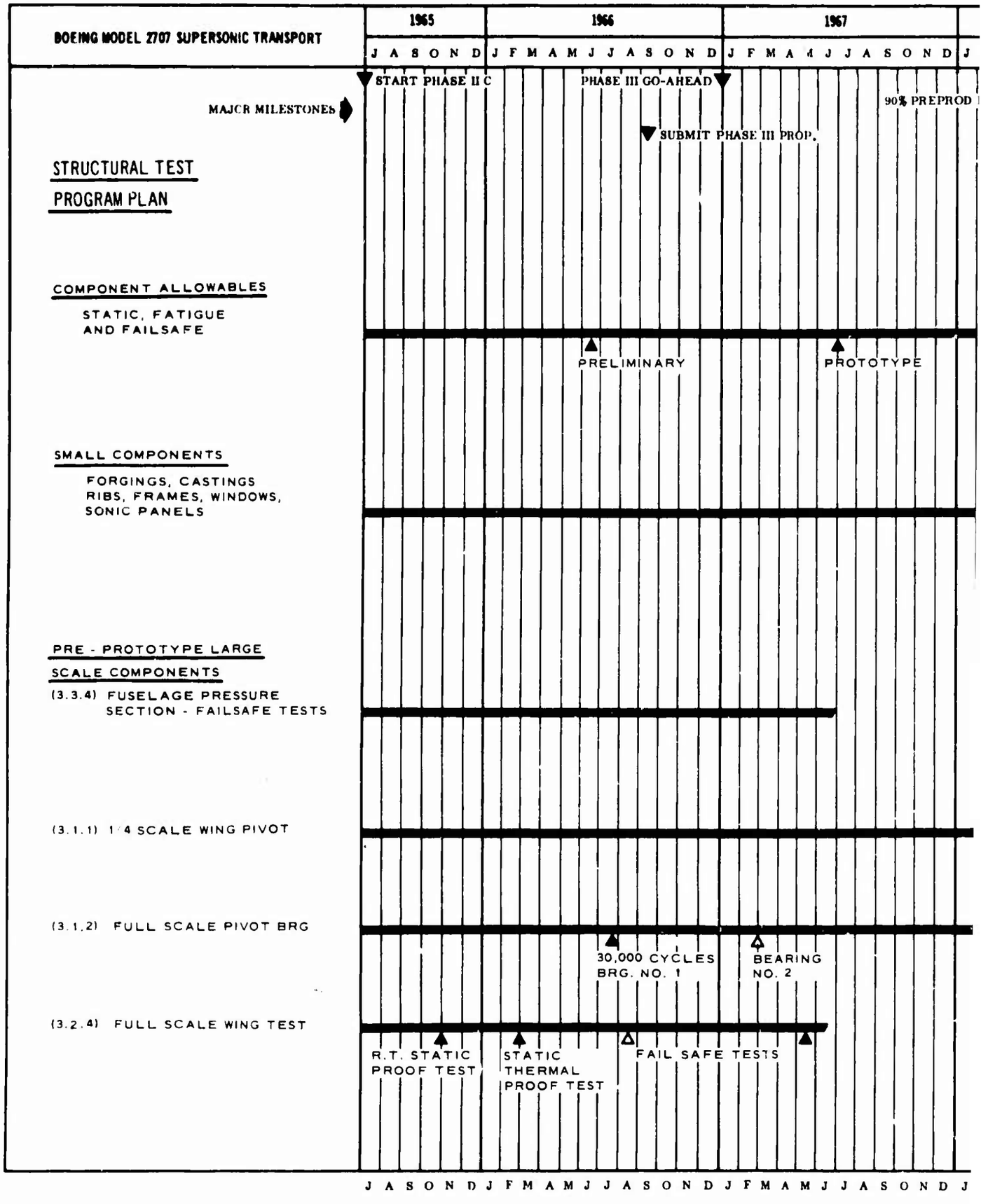
The fatigue test will be followed by fail-safe and crack-growth tests of empennage and fuselage panels and, critical joint and bulkhead structures. A full description is presented in the Integrated Test Program, "Horizontal Stabilizer to Body Joint Tests" and "Fin-Body-Ventral Joint Tests," V4-B2707-11.

2.1.3 Forward Body Compartment Tests*

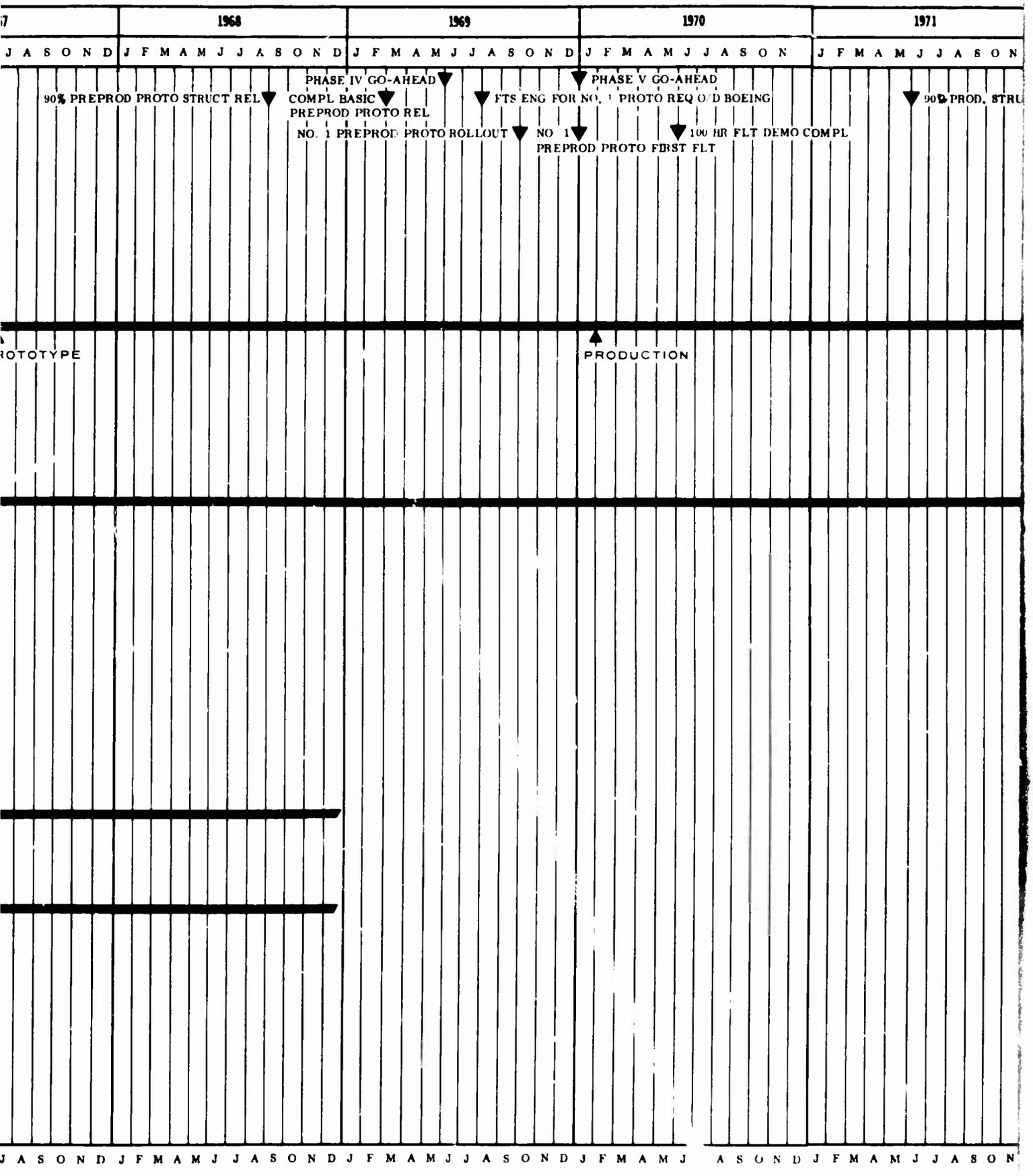
This program will demonstrate the structural integrity of the passenger pressure compartment. A full-scale fuselage section will be subjected to proof pressures and thermal loads. Pressure leakage and thermal distribution will be determined during proof-pressure test. Cyclic pressure will be applied to verify and improve the structural fatigue life. The fatigue test will be followed by fail-safe and crack-growth tests.

2.1.4 Outboard Wing Tests*

This program will demonstrate the structural integrity of the wing. A full-scale wing section complete from the pivot outboard to the wing-tail interlock (approx. 500 in.) will be subjected to a proof test which will apply critical design flight and ground limit loads. Stress distribution and deflections will be obtained at all critical locations. This test will be followed by a cyclic fatigue test to verify and improve fatigue life. (Par. 2.3.2) The fatigue test will then be followed by fail-safe tests of critical areas and additional proof testing to near ultimate loads.


BOEING MODEL 2707 SUPERSONIC TRANSPORT
1965
1966
1967
J A S O N D J F M A M J J A S O N D J F M A M J J A S O N D J F M A M J J A S O N D J
START PHASE II C
PHASE III GO-AHEAD
90% PREPROD
MAJOR MILESTONES
SUBMIT PHASE III PROP.
STRUCTURAL TEST PROGRAM PLAN
COMPONENT ALLOWABLES
STATIC, FATIGUE AND FAILSAFE
PRELIMINARY
PROTOTYPE
SMALL COMPONENTS
FORGINGS, CASTINGS RIBS, FRAMES, WINDOWS, SONIC PANELS
PRE - PROTOTYPE LARGE SCALE COMPONENTS
(3.3.4) FUSELAGE PRESSURE SECTION - FAILSAFE TESTS
(3.1.1) 1/4 SCALE WING PIVOT
(3.1.2) FULL SCALE PIVOT BRG
30,000 CYCLES BRG. NO. 1
BEARING NO. 2
(3.2.4) FULL SCALE WING TEST
R.T. STATIC PROOF TEST
STATIC THERMAL PROOF TEST
FAIL SAFE TESTS
J A S O N D J F M A M J J A S O N D J F M A M J J A S O N D J

A


1968
1969
1970
1971
J A S O N D J F M A M J J A S O N D J F M A M J J A S O N D J F M A M J J A S O N J F M A M J J A S O N
90% PREPROD PROTO STRUCT REL
PHASE IV GO-AHEAD
COMPL BASIC PREPROD PROTO REL
NO. 1 PREPROD PROTO ROLLOUT
FTS ENG FOR NO. 1 PROTO REQ O/D BOEING
PHASE V GO-AHEAD
NO. 1 PREPROD PROTO FIRST FLT
100 HR FLT DEMO COMPL
90% PROD. STRU
ROTOTYPE
PRODUCTION
J A S O N D J F M A M J J A S O N D J F M A M J J A S O N D J F M A M J J A S O N D J F M A M J J A S O N

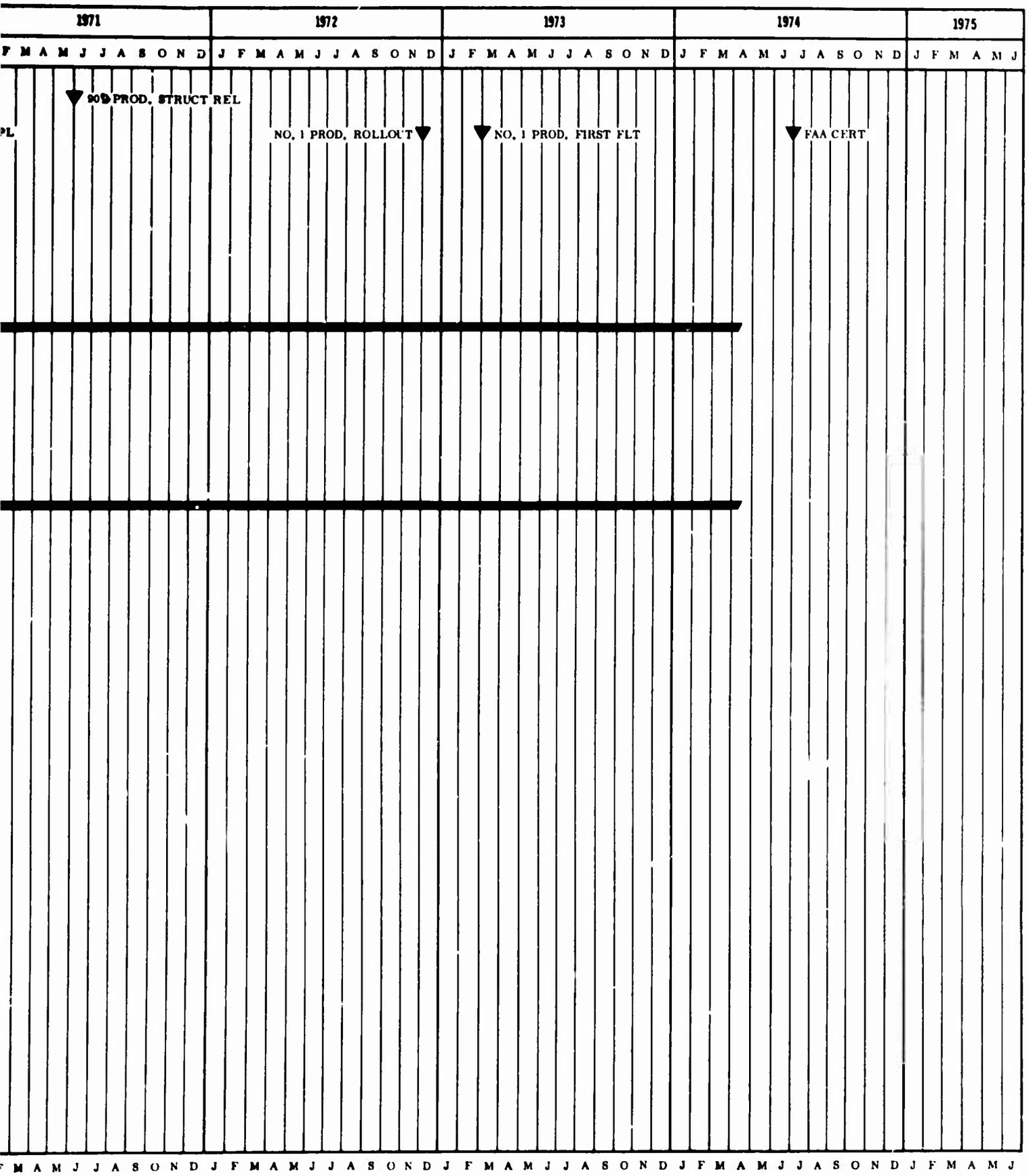
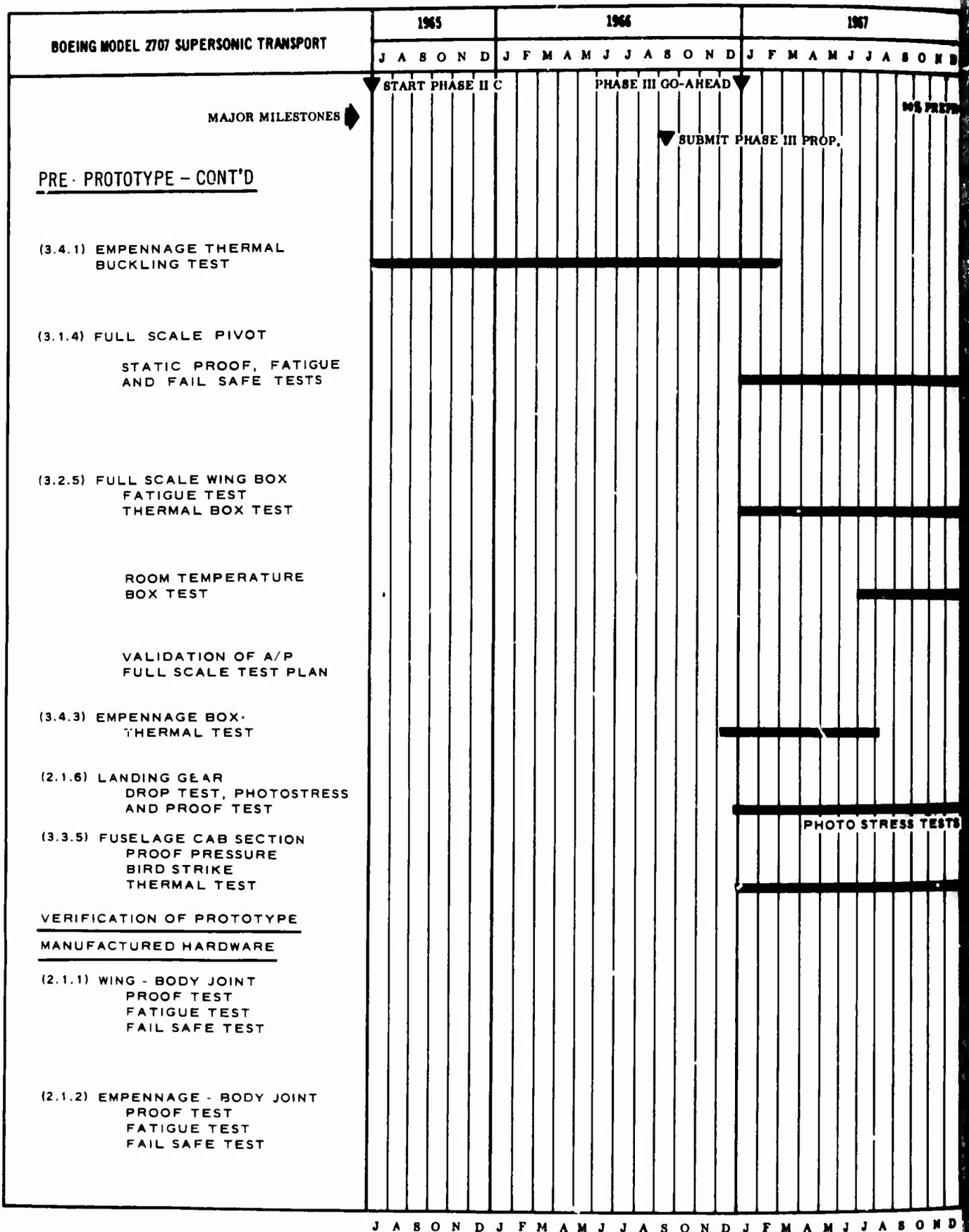
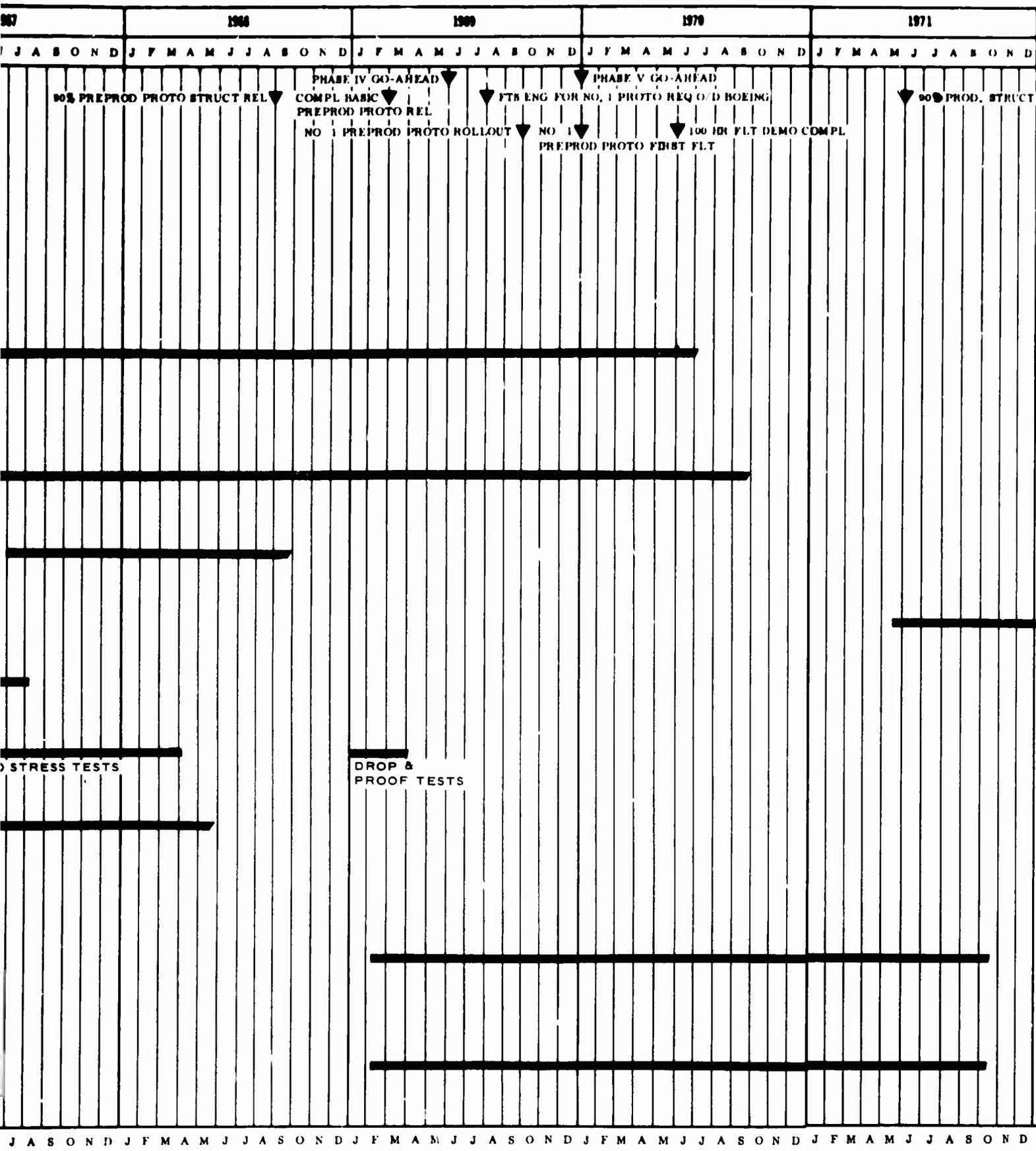


Figure 2-1. Test Program Plan


BOEING MODEL 2707 SUPERSONIC TRANSPORT
1965
1966
1967
J A S O N D J F M A M J J A S O N D J F M A M J J A S O N D
START PHASE II C
PHASE III GO-AHEAD
MAJOR MILESTONES
SUBMIT PHASE III PROP.
PRE · PROTOTYPE – CONT'D
(3.4.1) EMPENNAGE THERMAL BUCKLING TEST
(3.1.4) FULL SCALE PIVOT
STATIC PROOF, FATIGUE AND FAIL SAFE TESTS
(3.2.5) FULL SCALE WING BOX
FATIGUE TEST
THERMAL BOX TEST
ROOM TEMPERATURE BOX TEST
VALIDATION OF A/P FULL SCALE TEST PLAN
(3.4.3) EMPENNAGE BOX · THERMAL TEST
(2.1.6) LANDING GEAR
DROP TEST, PHOTOSTRESS AND PROOF TEST
PHOTO STRESS TESTS
(3.3.5) FUSELAGE CAB SECTION
PROOF PRESSURE
BIRD STRIKE
THERMAL TEST
VERIFICATION OF PROTOTYPE
MANUFACTURED HARDWARE
(2.1.1) WING - BODY JOINT
PROOF TEST
FATIGUE TEST
FAIL SAFE TEST
(2.1.2) EMPENNAGE - BODY JOINT
PROOF TEST
FATIGUE TEST
FAIL SAFE TEST
J A S O N D J F M A M J J A S O N D J F M A M J J A S O N D

A


1967
1968
1969
1970
1971
J A S O N D J F M A M J J A S O N D J F M A M J J A S O N D J F M A M J J A S O N D J F M A M J J A S O N D
90% PREPROD PROTO STRUCT REL
PHASE IV GO-AHEAD
COMPL BASIC PREPROD PROTO REL
NO 1 PREPROD PROTO ROLLOUT
FTS ENG FOR NO. 1 PROTO REQ O/D BOEING
PHASE V GO-AHEAD
NO 1 PREPROD PROTO FDIST FLT
100 HR FLT DEMO COMPL
90% PROD. STRUCT
STRESS TESTS
DROP & PROOF TESTS
J A S O N D J F M A M J J A S O N D J F M A M J J A S O N D J F M A M J J A S O N D J F M A M J J A S O N D

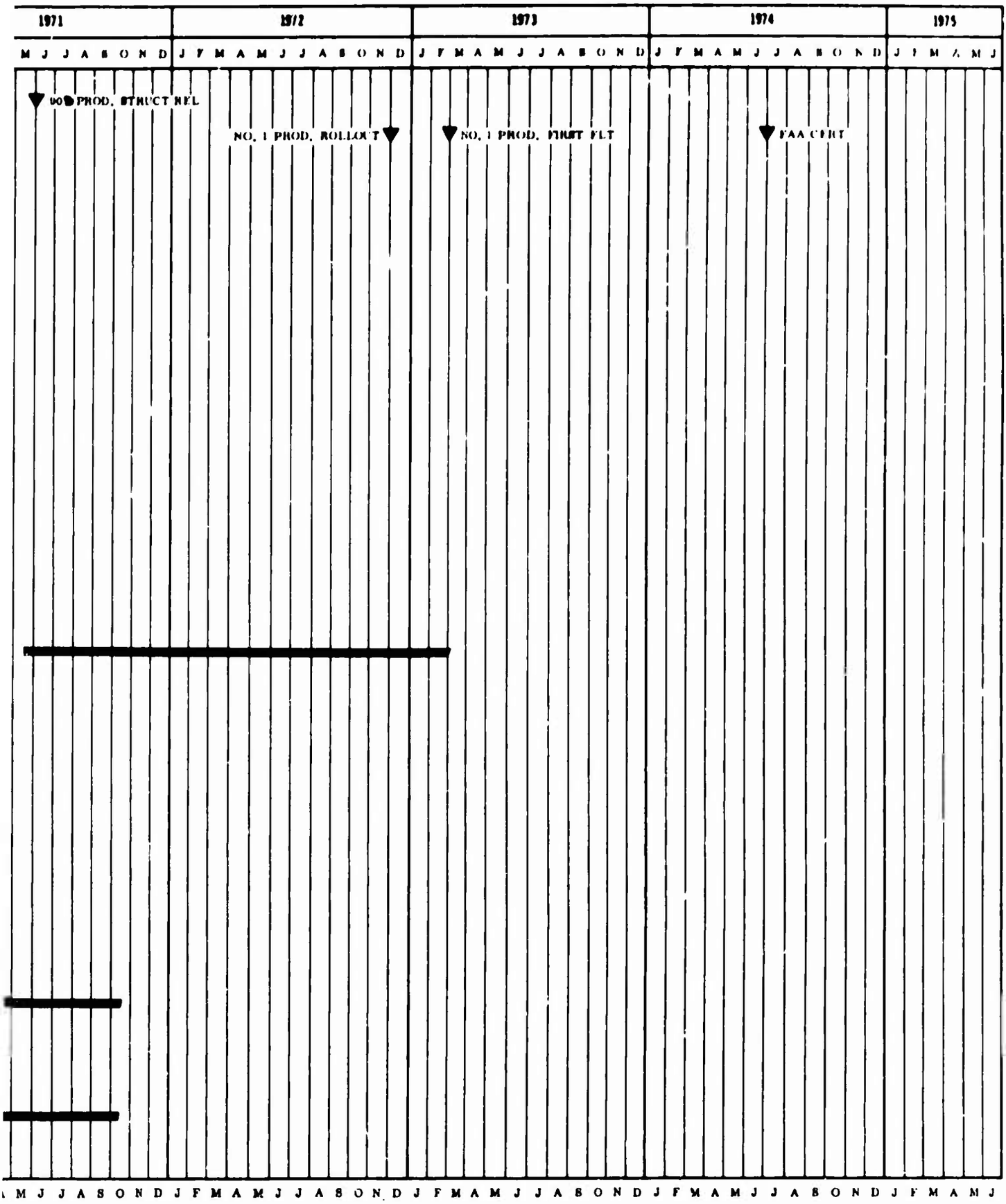
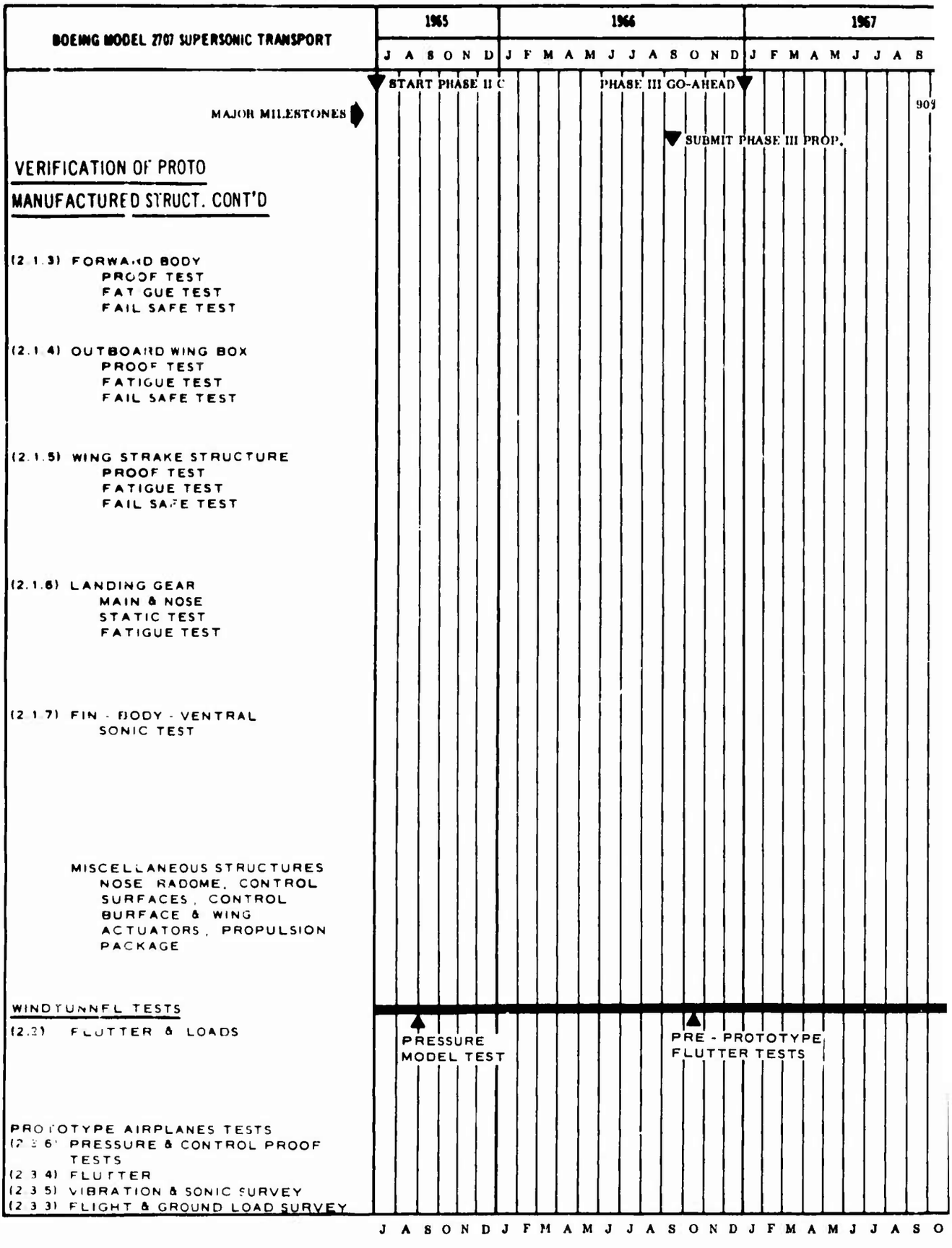
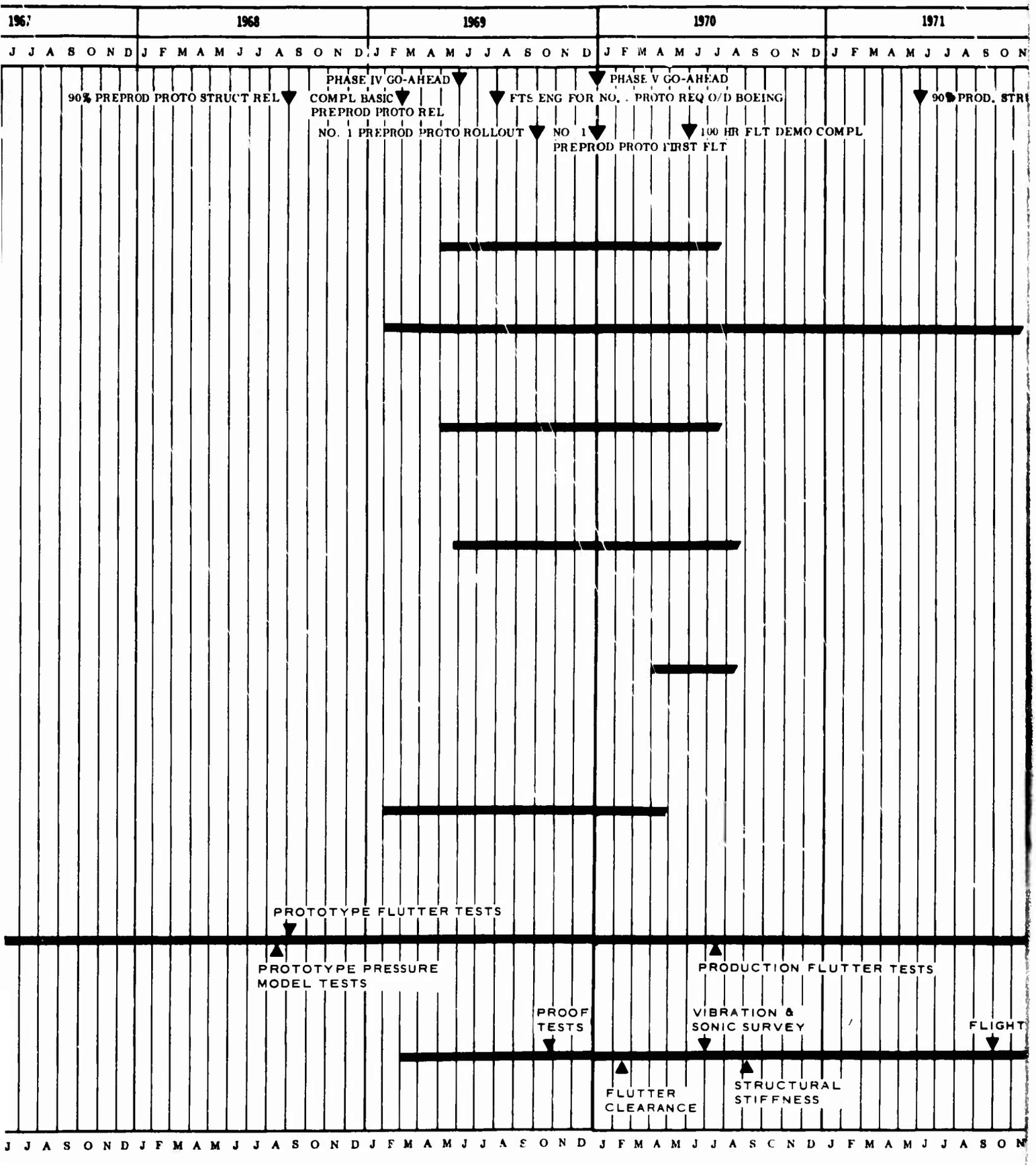


Figure 2-1. (Continued)


BOEING MODEL 2707 SUPERSONIC TRANSPORT
1965
1966
1967
J A S O N D J F M A M J J A S O N D J F M A M J J A S
START PHASE II C
PHASE III GO-AHEAD
MAJOR MILESTONES
SUBMIT PHASE III PROP.
VERIFICATION OF PROTO
MANUFACTURED STRUCT. CONT'D
(2.1.3) FORWARD BODY
PROOF TEST
FAT GUE TEST
FAIL SAFE TEST
(2.1.4) OUTBOARD WING BOX
PROOF TEST
FATIGUE TEST
FAIL SAFE TEST
(2.1.5) WING STRAKE STRUCTURE
PROOF TEST
FATIGUE TEST
FAIL SAFE TEST
(2.1.6) LANDING GEAR
MAIN & NOSE
STATIC TEST
FATIGUE TEST
(2.1.7) FIN - BODY - VENTRAL
SONIC TEST
MISCELLANEOUS STRUCTURES
NOSE RADOME, CONTROL SURFACES, CONTROL BURFACE & WING ACTUATORS, PROPULSION PACKAGE
WINDTUNNEL TESTS
(2.2) FLUTTER & LOADS
PRESSURE MODEL TEST
PRE - PROTOTYPE FLUTTER TESTS
PROTOTYPE AIRPLANES TESTS
(2.3.6) PRESSURE & CONTROL PROOF TESTS
(2.3.4) FLUTTER
(2.3.5) VIBRATION & SONIC SURVEY
(2.3.3) FLIGHT & GROUND LOAD SURVEY
J A S O N D J F M A M J J A S O N D J F M A M J J A S O

A


1967
1968
1969
1970
1971
J J A S O N D J F M A M J J A S O N D J F M A M J J A S O N D J F M A M J J A S O N D J F M A M J J A S O N
90% PREPROD PROTO STRUCT REL
PHASE IV GO-AHEAD
COMPL BASIC PREPROD PROTO REL
NO. 1 PREPROD PROTO ROLLOUT
FTS ENG FOR NO. . PROTO REQ O/D BOEING
PHASE V GO-AHEAD
NO 1 PREPROD PROTO FIRST FLT
100 HR FLT DEMO COMPL
90% PROD. STR
PROTOTYPE FLUTTER TESTS
PROTOTYPE PRESSURE MODEL TESTS
PROOF TESTS
FLUTTER CLEARANCE
VIBRATION & SONIC SURVEY
STRUCTURAL STIFFNESS
PRODUCTION FLUTTER TESTS
FLIGHT
J J A S O N D J F M A M J J A S O N D J F M A M J J A S O N D J F M A M J J A S O N D J F M A M J J A S O N

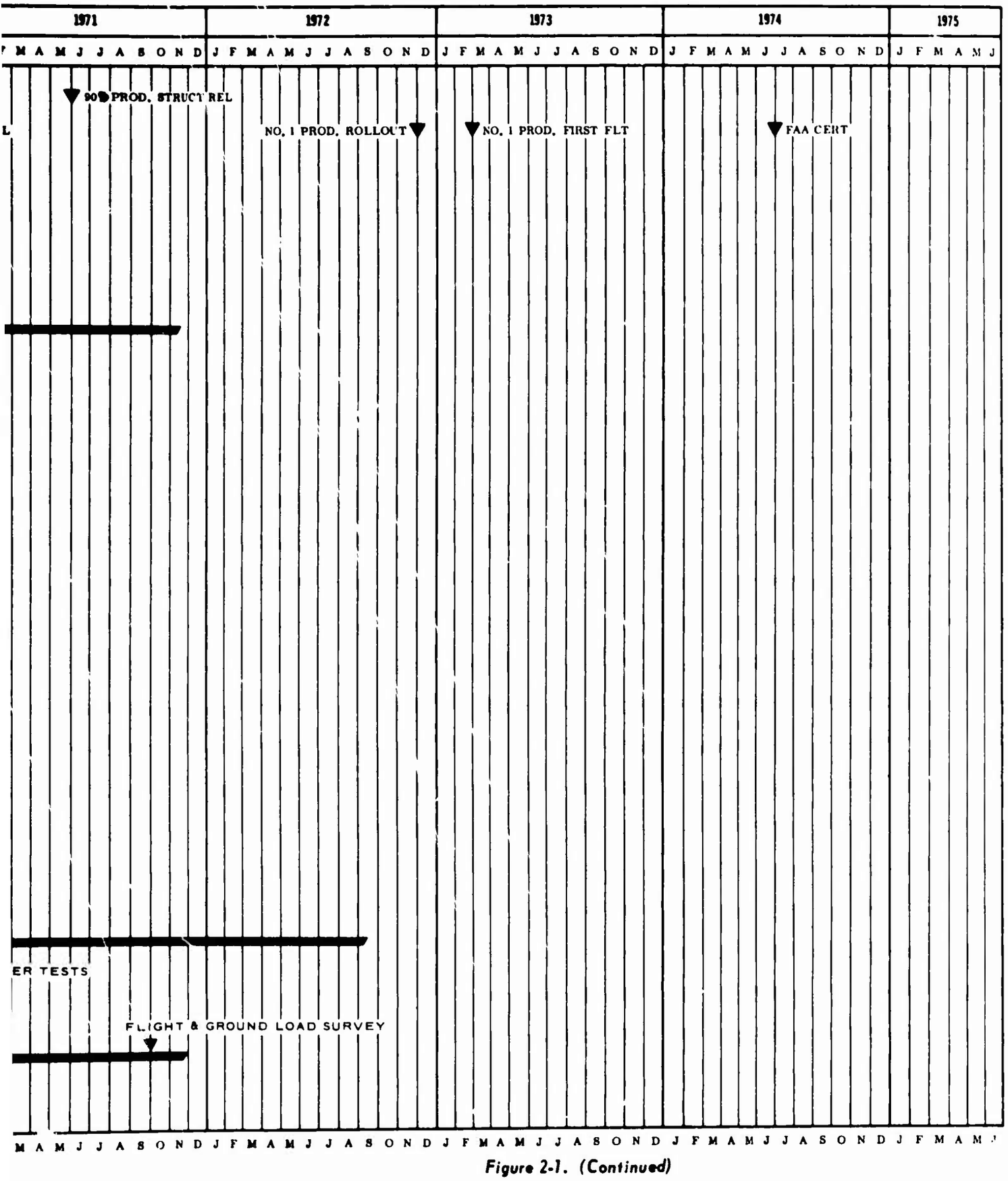
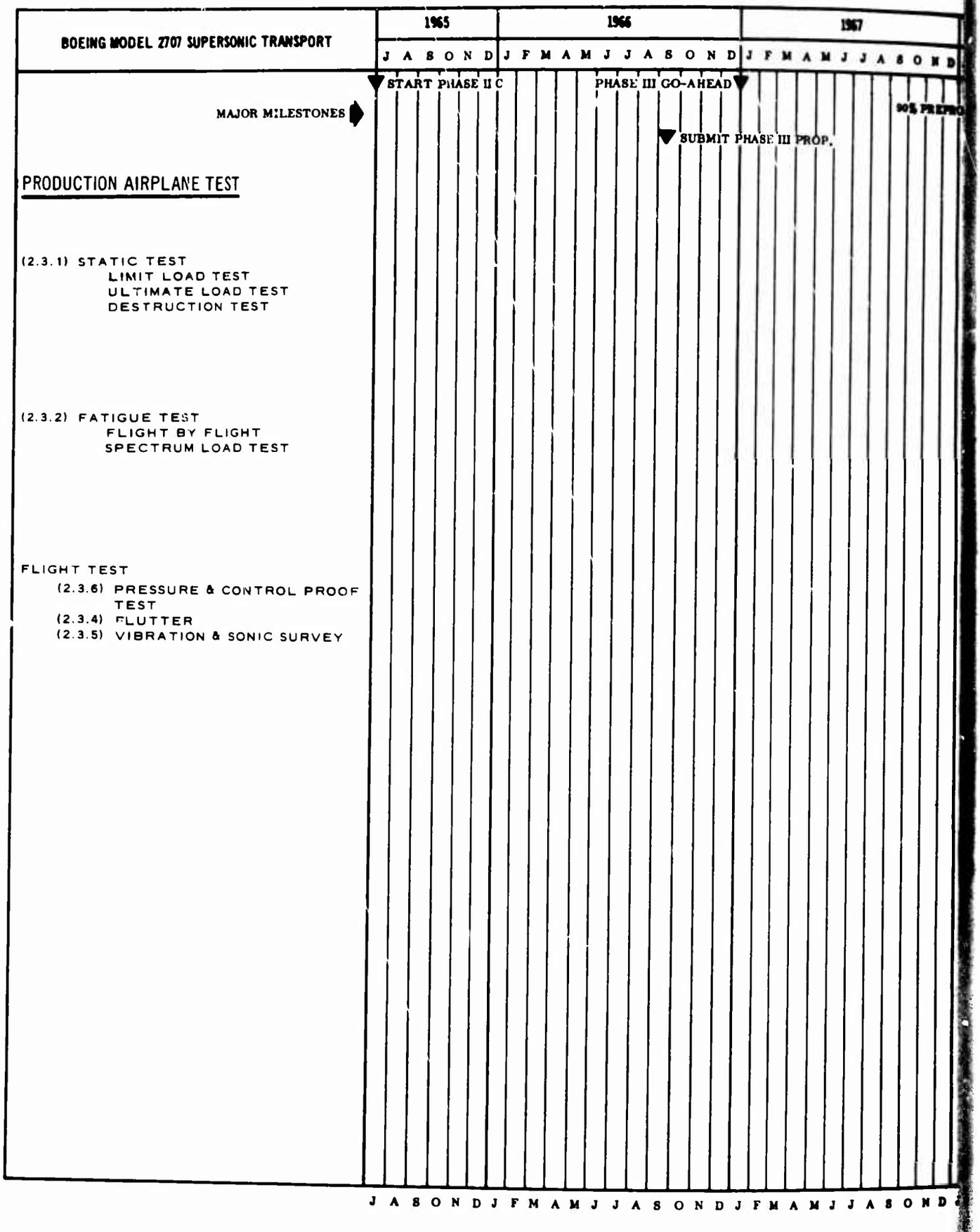
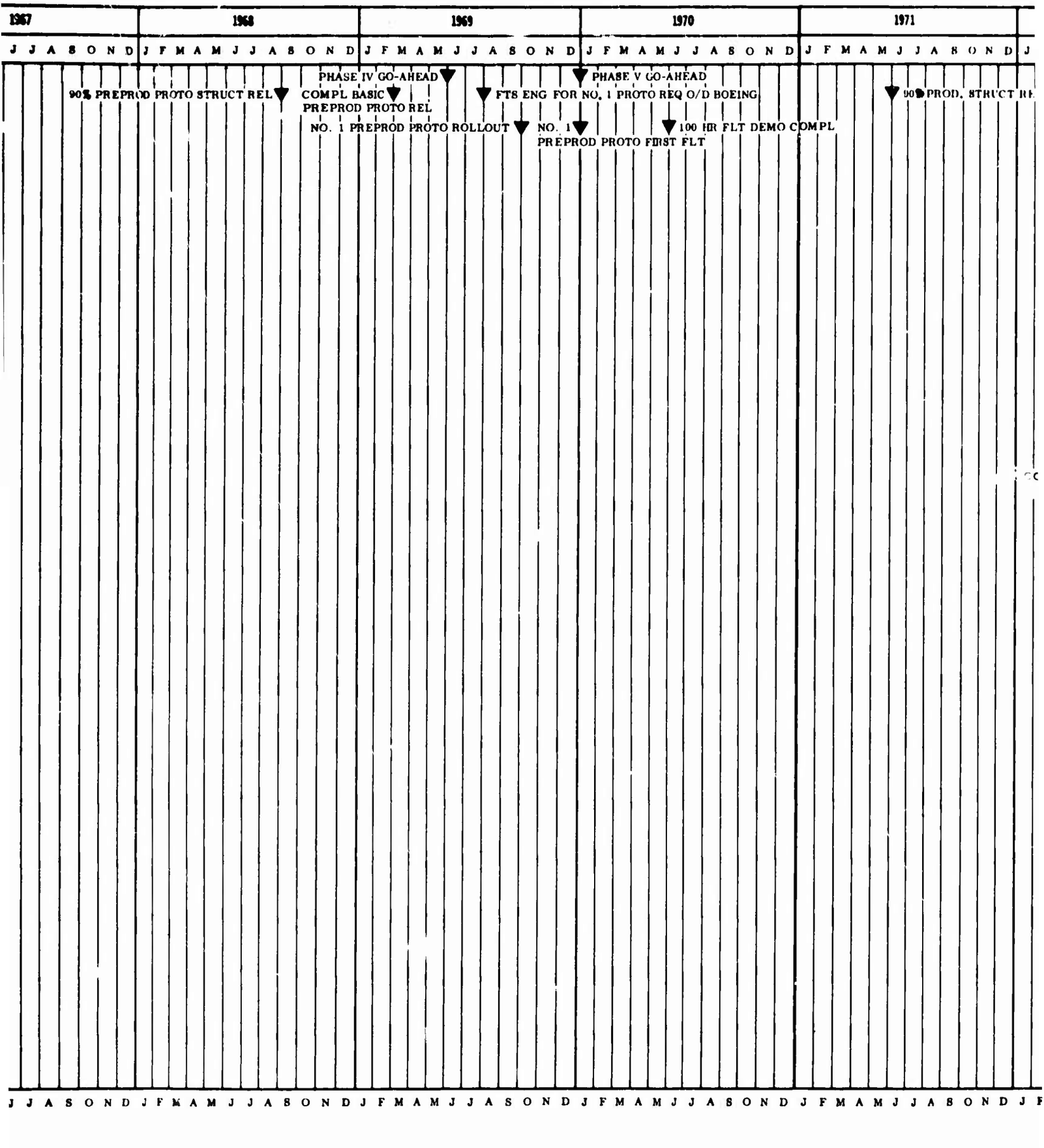


Figure 2-1. (Continued)


BOEING MODEL 2707 SUPERSONIC TRANSPORT
1965
1966
1967
J A S O N D J F M A M J J A S O N D J F M A M J J A S O N D
START PHASE II C
PHASE III GO-AHEAD
MAJOR MILESTONES
SUBMIT PHASE III PROP.
PRODUCTION AIRPLANE TEST
(2.3.1) STATIC TEST
LIMIT LOAD TEST
ULTIMATE LOAD TEST
DESTRUCTION TEST
(2.3.2) FATIGUE TEST
FLIGHT BY FLIGHT
SPECTRUM LOAD TEST
FLIGHT TEST
(2.3.6) PRESSURE & CONTROL PROOF TEST
(2.3.4) FLUTTER
(2.3.5) VIBRATION & SONIC SURVEY
J A S O N D J F M A M J J A S O N D J F M A M J J A S O N D

A


1967
1968
1969
1970
1971
J J A S O N D J F M A M J J A S O N D J F M A M J J A S O N D J F M A M J J A S O N D J F M A M J J A S O N D J
90% PREPROD PROTO STRUCT REL
PHASE IV GO-AHEAD
COMPL BASIC PREPROD PROTO REL
NO. 1 PREPROD PROTO ROLLOUT
FTS ENG FOR NO. 1 PROTO REQ O/D BOEING
PHASE V GO-AHEAD
NO. 1 PREPROD PROTO FIRST FLT
100 HR FLT DEMO COMPL
90% PROD. STRUCT RE
J J A S O N D J F M A M J J A S O N D J F M A M J J A S O N D J F M A M J J A S O N D J F M A M J J A S O N D J F

B

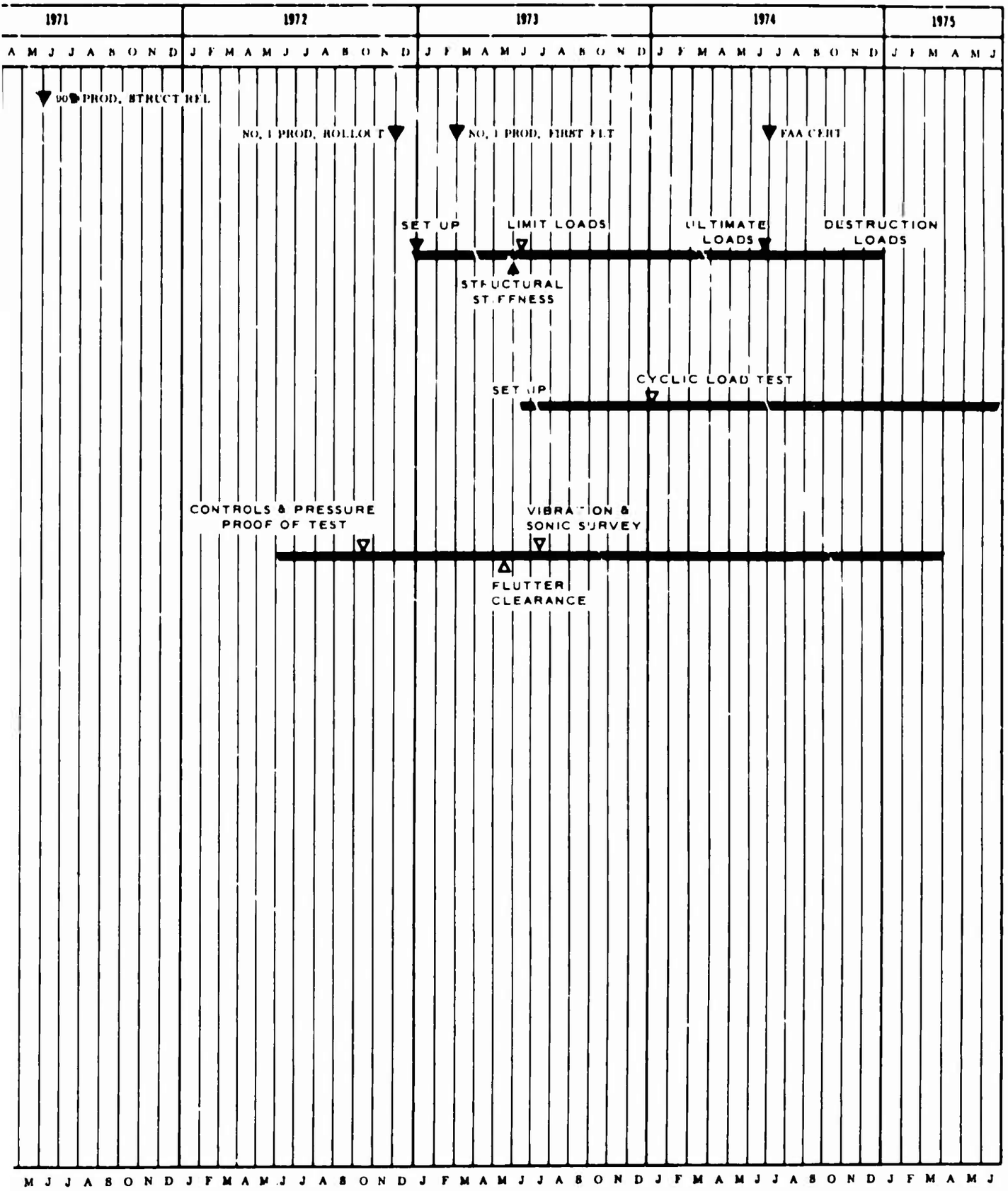


Figure 2-1. (Concluded)

BLANK PAGE

2.1.5 Wing Strake to Body Tests*
This program will demonstrate the structural integrity of the wing strake, strake fuel compartment, and strake attachment to fuselage structure. A full-scale section of the wing strake will be proof tested with limit design fuel pressure, thermal, and bending loads. Stress distribution and deflection measurements will be obtained for the critical design load conditions. This test will be followed by a cyclic fatigue test which applies fuel pressure and bending loads simulating airplane usage to improve the fatigue life. Fail-safe tests will be conducted after completion of the fatigue tests.

2.1.6 Landing Gear Tests
The following tests will be conducted on both nose gear and main gear structures.

2.1.6.1 Drop Tests
Drop tests will be made on each of the gears to develop proper load-stroke characteristics. These tests will use a full gear assembly loaded with a simulated airplane mass. Drops will be made at varying weights and drop heights with wheels spun up to represent landing speeds. Final drops will demonstrate gear energy absorption capacity for maximum sink rates at design landing weights and at maximum gross airplane weight. Gear loads, stresses, and deflection will be obtained through instrumentation on the test rig and landing gear structure. These data will prove the structural integrity of the gears.

2.1.6.2 Experiment Stress Survey
This program will provide a method for refining detail gear design through elimination of excessive material and reduction of stress concentrations. Replicas of the gear structure made to preliminary machining drawings are coated with bi-refingent-sensitive plastic and loaded to proportionate values representative of the critical design conditions. Examination of the loaded gear under polarized light permits definition of either low or excessive stresses. The specimen is reshaped to provide an improved distribution of stresses and the material is then retested. This design-test-design iteration will continue until the gear details are optimized.

2.1.6.3 Static and Fatigue Tests*
This program will demonstrate the structural integrity of the landing gear components. Complete gear structure, except for wheels, brakes, and tires, will be subjected to design ultimate load tests to establish gear strength, growth potential, and possible weight reduction. Loads will be applied in increments through design ultimate for all critical conditions. A final destruction test will follow completion of all design conditions.

Additional gears will be cyclic-fatigue tested to verify and improve fatigue life. Loads will be applied in blocks representing landing, taxi, and ground handling operations. The total test will provide a life demonstration of a minimum of 50,000-hr airplane service (30,000 takeoffs) times a factor of four. Specific components may be shown adequate for a factor of two if the particular structure is easily replaceable.

2.1.7 Fin-Body-Ventral Sonic Tests*
The fin-body-ventral assembly described in Par. 2.1.2 will be set up for sonic testing after completion of the earlier tests. All fuel lines, ducts, electrical, and hydraulic components in these sections will be installed. The combined structure will be tested in the presence of an operating engine to simulate actual airplane sonic environment. The test will be used to validate or improve the structure design for a time equivalent to the airplane service life. See the Integrated Test Program, V4-B2707-11, for complete description.

2.2 MODEL TESTS
Wind tunnel load and flutter model tests are presented in the Airframe Design Report, Part C, "Design Criteria, Loads, Aerodynamic Heating and Flutter," V2-B2707-7.

The model tests will provide load and flutter design information. Included in the program are low-speed transonic and supersonic pressure model tests for design load distribution; flutter models for stiffness verification of wing and tail coupled to the body; dynamic landing simulations to establish landing-load factors; engine air induction pressure tests which use a 1/3-scale operating engine mounted in a wind tunnel, and a hydrodynamic test to investigate the behavior and loads during a water ditching operation.

2.3 AIRPLANE TESTS

2.3.1 Static Test
Static strength integrity will be developed through knowledge of environment, criteria development, design, analysis, and test. The design will be developed and substantiated by static testing of

parts, panels, and components. As a final demonstration and substantiation of static strength integrity, tests will be conducted on combinations of inter-related parts to be accomplished by testing a full-scale static test airframe.

A full-scale static test will be conducted on a production certification airframe that is structurally complete with the exception of the landing gear, high lift devices, and control surfaces on one side. Tests will be conducted for critical conditions on the fuselage, wing, empennage, landing gear, nacelles, and control surfaces. The tests will progress in a logical sequence through the stages of proof tests to limit load, design ultimate load and, in some instances, to destruction. The fuselage will be pressurized during proof and ultimate flight conditions. Provisions will be made to conduct tests with the wing in any sweep position. The landing gear will be static tested as a separate item prior to conducting the full airframe test.

The flight load survey on the prototype airplane will be completed prior to the start of full-scale static and fatigue tests to allow for final adjustment of design loads and temperatures.

Preliminary analyses of the B-2707 indicate that some critical design conditions occur at a time when the structure is hot and maximum thermal gradients exist. Provisions will be made for heating during test. Heat will also be applied without mechanical load, to determine thermal gradients and resultant thermal stresses.

A complete description of the test facilities is presented in the Integrated Test Program, V4-B2707-11.

2.3.2 Fatigue Test

A full-scale fatigue test will be conducted on a production airframe that is structurally complete except for the landing gear, high lift devices, and control surfaces on the left side. The landing gear will be fatigue tested in a separate test as shown in Par. 2.1.6. This test will be similar to those conducted by Boeing on the B-47, B-52, KC-135, and the Model 727. The 727 test article in preparation for test is shown in Fig. 2-2. The objectives of the airplane cyclic test are as follows:

- Locate fatigue-critical areas of the airplane at the earliest possible time.
- Provide test data for analytical service life prediction.
- Evaluage fail-safe characteristics of major structural parts.
- Develop inspection and maintenance procedures for the airlines.

To accomplish these objectives, the airplane fatigue test must be accomplished as early in the overall airplane program as possible so that necessary structural changes can be incorporated in the production run early and thus minimize retrofitting. Additionally, the necessary lead time of test flight hour accumulation over service hours can be maintained.

The SST is the first commercial airplane which will encounter significant elevated temperatures during normal operations. Elevated temperature can affect the structural fatigue life of an SST in several ways: thermal stresses resulting from temperature gradients; soak at elevated temperature and the resulting change in behavior, and the change in fatigue life. Considerable research effort is being expended to increasing the understanding of such effects.

The basic ways in which the airplane fatigue test could be conducted to account for the thermal effects are as follows:

- Real time at elevated temperature. The supersonic portion of each flight of the fatigue test airplane would be of the same time duration as that for an actual flight.
- Shorten the test time spent at elevated temperature by compressing the holding period at temperature.
- Test at constant temperatures and eliminate the thermal stress cycle.
- Test at room temperature and account for thermal effects through test loading adjustments and in the interpretation of the results.

For a test with real time at elevated temperature, as described in Par. 2.3.2(a), the time required to conduct the test would increase many times above that for a room temperature test. Assuming that an SST would spend about 30,000 hr.

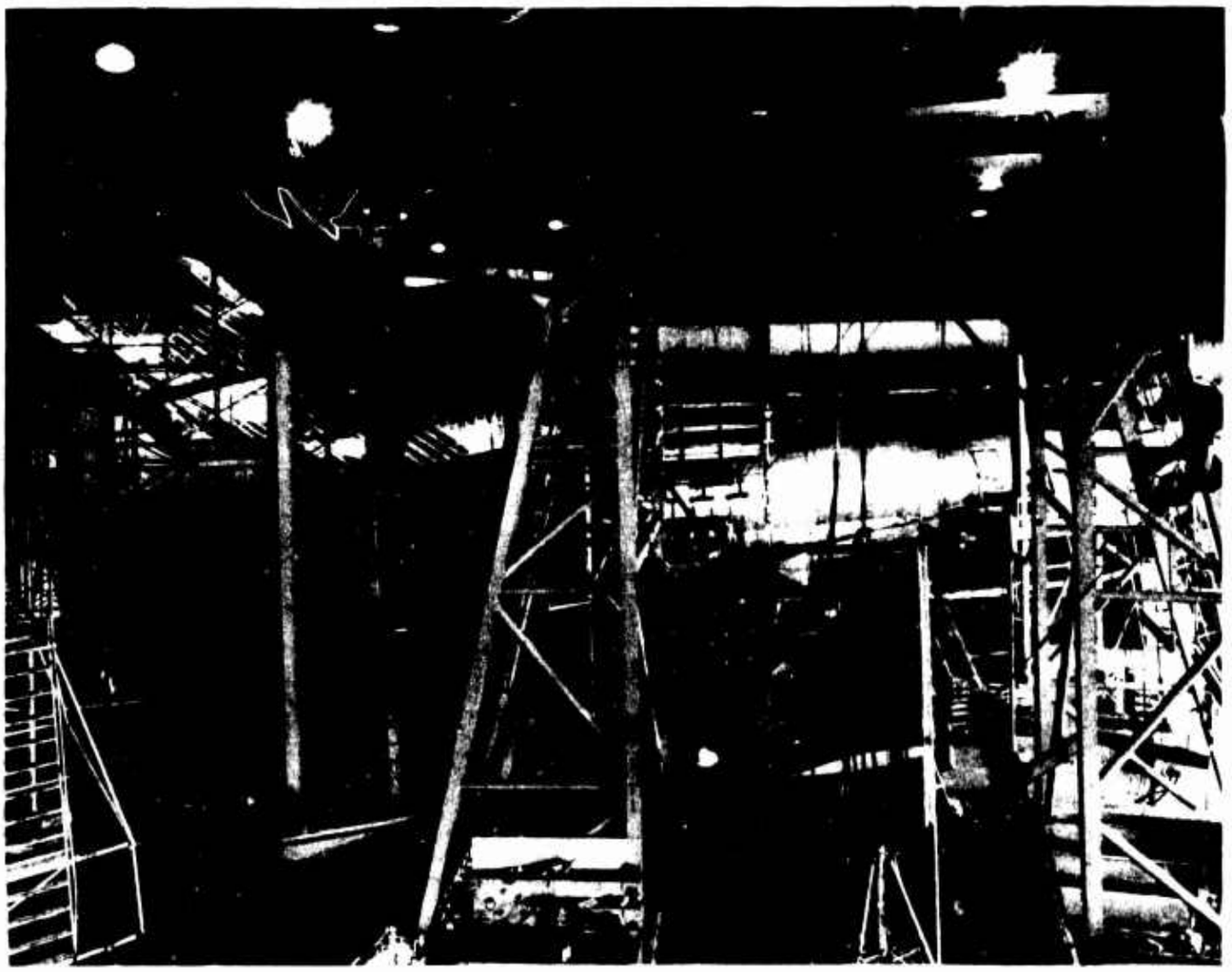


Figure 2-2. Model 727 Cyclic Test

of its service life at elevated temperature, and recognizing that airplane fatigue tests are normally conducted for at least twice the service life and that some down time is a necessary part of the test, it follows that the duration of such a test would approach the useful life of the airplane. It is recognized that the thermal test is subject to the same approximations in loading spectra definition and application as the accelerated tests, plus significant additional approximations in the temperature definition and application.

By using the type of test described in Par. 2.3.2(b), in which the time at elevated temperature is reduced, the test duration could be shortened. All other problems associated with elevated temperature testing, however, would still be present. The test time would still be considerably longer than for a room temperature test because of the time involved in achieving a reasonable buildup and decay of temperature and temperature gradients. Supporting test programs and analysis would still be required to quantitatively evaluate the effects on the fatigue life of the reduced time at temperature.

The method listed in Par. 2.3.2(c) would permit testing almost as rapidly as a room temperature test but would prevent as typical of thermal fatigue tests, the necessary close inspection monitoring of the structure. In addition, the fatigue effects of the thermal stress gradient would not be accounted for, thus losing one of the primary reasons for conducting a thermal test.

The approach listed in Par. 2.3.2(d), would permit an on-time fatigue test, proper inspection at frequent intervals, and adequate monitoring through strain gage and crack detection instrumentation. The room temperature test would be accomplished more economically using supporting test programs and analysis to quantitatively evaluate the effects of the temperature omission.

In formulating the program for the B-2707 airplane fatigue test, the merits of the different types of tests and the significance of the temperature effects on fatigue life have been carefully considered. The program currently planned provides for sufficient pretest thermal exposure to account for creep effects around interference fit fasteners. The test will then be conducted at room temperature by replacing the thermal stresses in the critical elements with mechanical stresses and accounting for the differences between test and service conditions through supporting laboratory test programs and analysis.

Full-scale airplane fatigue tests have historically been conducted to simplified conditions. This has been necessary for both practical and technical reasons. The actual flight environment varies with each airplane and each flight, and can be only approximated by statistical average. For a well defined loading spectrum, the application to a complete test airframe presents complex problems. Accordingly, the loadings applied to the test article are reduced in number, increased in intensity, and applied in a reasonably simple sequence.

The loadings for the cyclic test will be derived from an analysis similar to that given in the Airframe Design Report Part B — Component Design V2-B2707-6-2, Sec. 5.0, using the operational profiles and airplane design characteristics of the B-2707. Cyclic cabin pressurization and wing sweep changes are included in the loading spectrum. The load spectra will be similar to those shown in Fig. 2-3 for the 727,

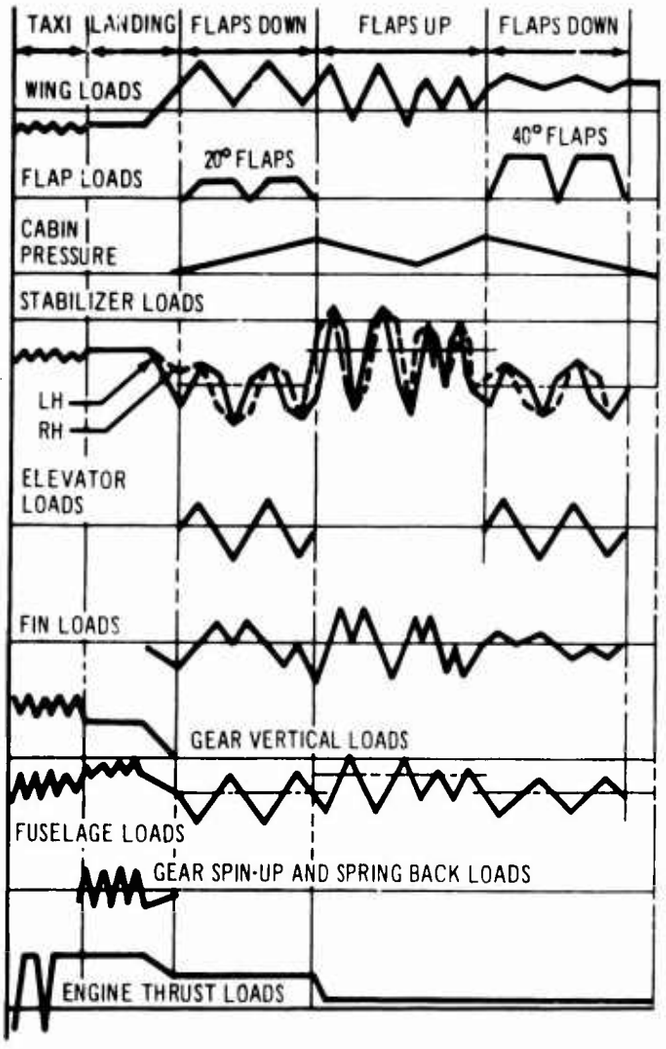


Figure 2-3. Model 727 Cyclic Load Spectrum Composition

although more extensive to account for the increased structural and environmental complexity.

Thermal stresses will be accounted for in the more critical structural elements by increasing the mechanical loading. For example, at a given section of skin and stiffener construction, the skin and the free flange of the stiffener will experience thermal stresses which add to one element and subtract from the other. Moreover, for either element, the sign of the thermal stress will be opposite during descent to that during climb and cruise. The test loading at that section would be a practical simulation of the more critically loaded of the two elements. For the other element, the test loading will be conservative.

The effects of elevated temperature and long time soak at elevated temperature on the fatigue resistance of the material will be accounted for.

Research work is currently being conducted by Boeing and other companies which will help to provide a firm basis for the planning and interpretation of the room temperature airplane fatigue test. Tests to evaluate the effects of long-time exposure to elevated temperature are currently in progress at Boeing. These tests will show the effects of exposure times up to 30,000 hr at 500°F and 650°F., with variable load and with and without steady load, on the subsequent fatigue life. Research work sponsored by Federal Aviation Agency (FAA), Department of Defence (DOD), and the National Aeronautics and Space Administration (NASA) is providing valuable data on the effects of elevated temperature on structure and materials.

A series of wing boxes will be tested in Phase III and IV (Par. 3.2.5) to provide data for the final fatigue test loading definition. These boxes will be tested with and without the thermal environment so that a correction factor can be determined for equating a room temperature fatigue test to a thermal environment fatigue test. It is planned that the airplane fatigue test will be run at room temperature following a thermal soak for the period of time necessary to permit creep of the structure around interference fit fasteners. Component tests of fatigue specimens have demonstrated that specimen fatigue life stabilizes at less than 500 hr of exposure at 500°F (Par. 3.6.2). On this basis, test planning will be for 1,000 hr exposure of the complete airframe at 450°F.

Additional testing will be accomplished in Phase III to fully validate the approach.

Tests loads will be applied through an automated programming system which sequentially applies loads in accordance with the spectra and continuously records the loads actually applied.

2.3.3 Flight and Ground Load Survey
Flight load survey is planned for Phase IV. Program integration and test description are shown in the Integrated Test Plan, V4-B2707-11.

2.3.4 Flutter and Ground Vibration Tests
Complete flutter and ground vibration test programs are planned for Phase III and IV. Details are presented in the Airframe Design Report — Part C, Design Criteria, Loads, Aerodynamic Heating, Flutter, V2-B2707-7. Program integration and test description are shown in the Integrated Test Plan, V4-B2707-11.

2.3.5 Sonic Noise and Vibration Survey
A full survey of sonic and vibration levels will be accomplished on the prototype airplane and on all subsequent models which have an appreciable engine thrust increase. The airplane will be fully instrumented with microphones and accelerometers to measure the sonic and vibration environment with engines at various power settings. Measurements will then be taken during all applicable flight conditions. Further, definition of the program is presented in the Airframe Design Report, Part C, V2-B2707-7, and the Integrated Test Plan, V4-B2707-11.

2.3.6 Airplane Proof Tests
A description of the prototype airplane proof tests is presented in the following paragraphs. Similar tests will be accomplished on the production airplane prior to first flight.

2.3.6.1 Fuselage Proof Pressure Test
A proof pressure test will be conducted on the fuselage of the first prototype airplane prior to first flight. Strain gages and deflection indicators will be located at critical points along the fuselage skin and frame structures to obtain data for verification of the stress and deflection analysis. Particular attention will be paid to the structure in the cab section and at the wing-fuselage and fuselage-empennage junctures. Pneumatic pressure will be applied in increments to 150 percent of the operating pressure (11.12 x 1.5 = 16.68 psig). Stresses and deflection will be recorded at each increment of pressure loading. This test will substantiate the design analysis of the pressure critical structure.

2.3.6.2 Fuel Cell Proof Pressure Test
A proof pressure test will be conducted prior to first flight on all fuel cells of the prototype airplanes. The airplane will be instrumented with strain gages and deflection indicators at critical structure locations to prevent over-pressurization during the test. Pressure will be applied to each tank to represent the fuel tank vent pressure levels. The test will verify the basic design for sustaining ground and inflight fuel pressures.

2.3.6.3 Flight Controls Proof Test

A test of the first prototype airplane control systems will be conducted prior to first flight. All primary control systems will be tested for the purpose of verifying structural integrity and control-system deflection. Limit static loads will be applied from the pilot's and co-pilot's stations and will be reacted at the mechanism control surfaces. Operation tests will be conducted by applying constant moments at the control surface attachment equal to 80 percent of the design limit load and reacting them at the cabin.

3.0 DEVELOPMENT TEST PROGRAM RESULTS

Test results and data are presented for the structural development accomplished in support of the SST design. Basic material testing is presented in the Airframe Report - Materials and Processes Part D V2-B2707-8. Summary results are shown herein where appropriate. Because this document precedes the completion of Phase II-C, complete test program results are not shown. However, a description of the remaining testing is provided and additional results will be provided for on-site review and through the monthly letter reports as they become available.

3.1 WING PIVOT TESTS

Wing pivot tests have been conducted continuously over the past six years by Boeing in conjunction with the SST and military airplane development programs. Because of this lengthy study, the bearing selected during the Phase I was near the final design and could be treated much the same as other structural component development.

The bearing program for developing material and processing concepts is described in Airframe Design Report — Part D, Material and Processes, V2-B2707-8. This program was augmented by a 1/4-scale full pivot test and a full-scale lug bearing test. Additional test work planned for Phase III will continue these tests and others on a full-scale pivot structural bearing constructed for the test. These test programs have demonstrated the bearing design for life equivalent to the design goals for the airplane. The programs are described in detail in the following paragraphs.

3.1.1 The 1/4-Scale Wing Pivot Bearing Test

This test was initiated to evaluate the effect of the bearing configuration and wing flexibility on bearing wear life with an elevated temperature environment. It also permits the evaluation of thrust bearing wear rate and pressure distribution. Future tests will include the effect of vibration and pounding loads on bearing life.

The test setup (Fig. 3-1) has two 1/4-scale pivot bearings installed in a simulated outboard wing pivot. Loads are transferred through the bearings to a shaft which was designed to simulate the flexural stiffness of the inboard wing. A constant shear load is applied to the wing box 70 in. from the pivot center line while the pivot joint is rotated back and forth through a 60-degree arc. The shear load is transferred through the test fixture by thrust bearings adjacent to the upper surface bearing as on the airplane design. Moment is transferred to the fixture by couple loads on the test bearings. The loads are chosen to produce a bearing pressure of 8,850 psi, and represent the critical supersonic flight conditions. After 300,000 cycles have been accumulated on a bearing, the test pressure is increased to 12,500 psi. All tests are conducted with a bearing temperature of 300°F, which is approximately 100° higher than maximum anticipated bearing temperature. Test bearing configurations are shown on Fig. 3-2.

The bearing surfaces consist of a highly compressed teflon-fabric bonded to the bearing races. The -3 configuration is considered superior because it has two bearing surfaces with a floating center race. This allows rotation on either bearing surface which provides a uniform wear rate on the entire periphery of the bearing. It also allows rotation after failure of one of the bearing surfaces. This theory has been verified by wear and failure observations on both surfaces of the -3 and -3 modified bearings which have been tested.

A summary of test results is given in Fig. 3-2. Based on 120,000 test cycles per airplane life, all but one of the -3 bearings tested have exceeded one equivalent airplane lifetime and most have exceeded three lives. Test results also show that the -3 modified bearings have the best wear life of all configurations tested. The early bearings used the AF-31 adhesive system for bonding the bearing

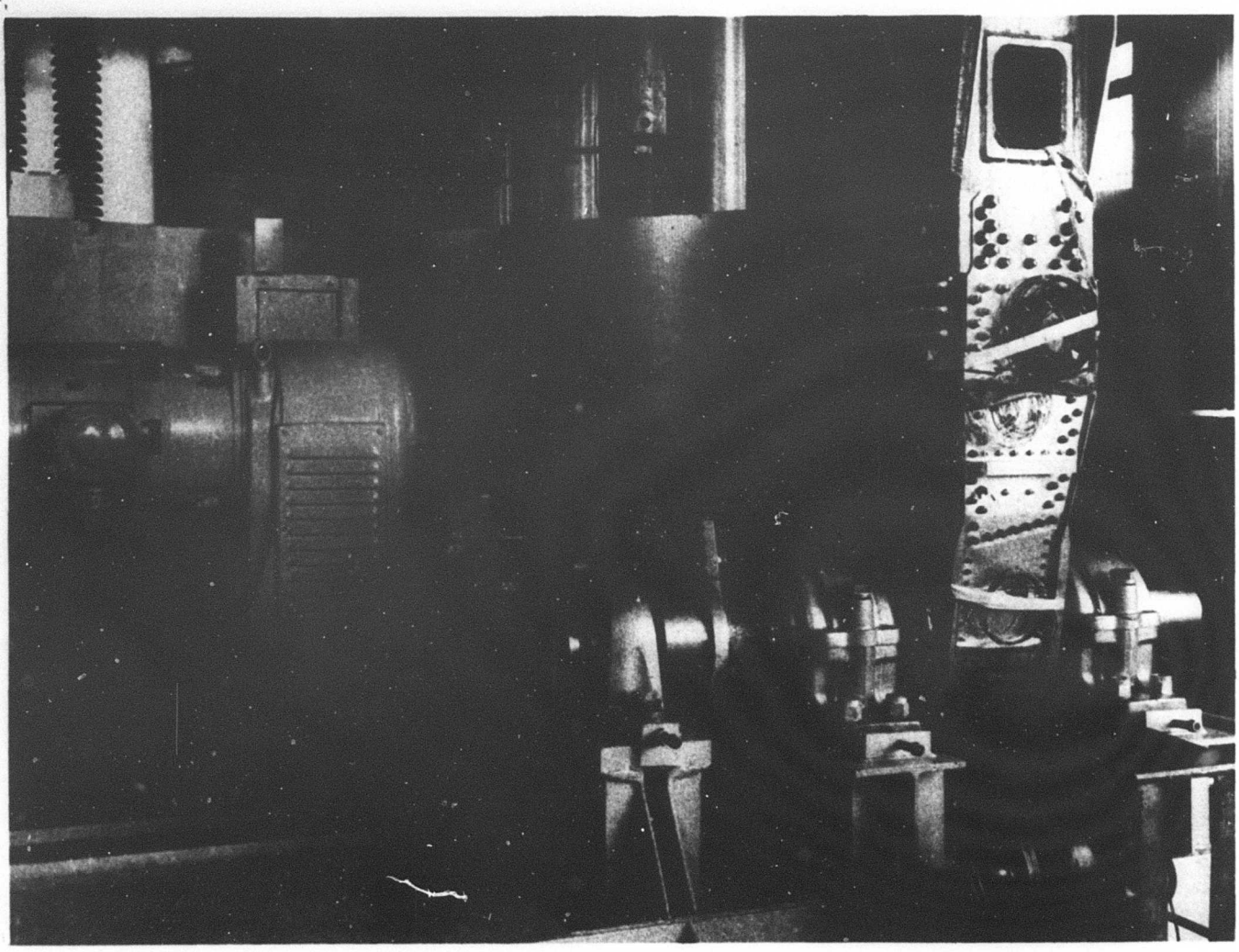


Figure 3-1. Quarter-Scale Wing Pivot Test Section

liners in place. Later bearings have used the Shell 957 adhesive system as a result of the development tests conducted on small-scale bearings, Ref. Airframe Design Report, Part D, Materials and Processes, V2-B2707-8 and have demonstrated the improvement shown with the smaller test specimens. Future specimens will utilize the Shell adhesive.

Periodic wear measurements are being made on a -3 modified bearing and show that after 200,000 cycles, bearing wear was negligible. After accumulating 400,000 cycles 90 percent of the bearing thickness remained. Measurements will continue to be taken to establish bearing wear-life expectancy.

The thrust bearing assembly which reacts the shear load consists of a teflon bronze thrust bearing bonded to a steel retainer plate. Thrust bearing wear and failure observations have shown average thrust bearing wear-life is approximately 400,000 cycles (more than three airplane lives).

3.1.2 Full-Scale Bearing Test

A full-scale specimen of the wing lower surface pivot joint was fabricated for use in a test program to evaluate bearing wear life and to determine stress distribution in the pivot lugs. The teflon bearing (Fig. 3-3) used in this first test was manufactured by Sheafer Bearing Division. The bearing is made of three rings of 17-4 PH corrosion resistant steel. Teflon-impregnated

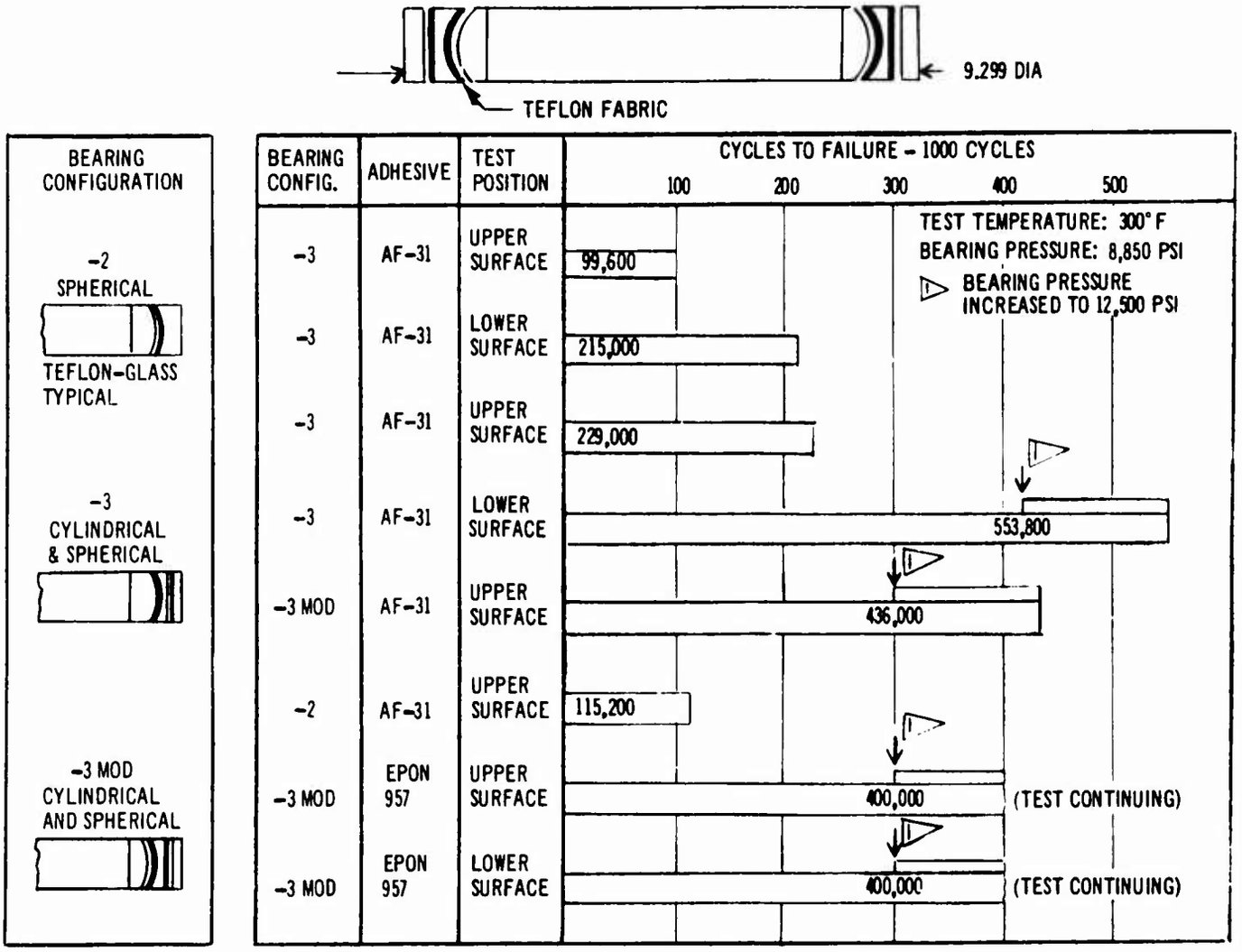


Figure 3-2. Quarter-Scale Wing Pivot Test Results

Dacron cloth is bonded to the spherical surface of the outer ring and cylindral surface of the center ring. (Fig. 3-3). The Teflon was bonded to the surface with a proprietory adhesive. A second bearing was manufactured by the Transport Dynamics Corporation for use in the next series of tests. Neither of these bearings was entirely representative of the optimum design that has been developed with the small 2-in. and 1/4-scale test programs and would be expected to have less life than those utilizing the Shell 957 adhesive and fiber glass retaining material. However, the first bearing was tested for a full airplane life without failure (30,000 cycles) and has demonstrated the validity of the design. The total test program will provide adequate information and data for full qualifications of the final design.

The specimen was installed in a test machine Fig. 1-4 capable of applying limit loads of 3.6 million pounds at appropriate sweep angles. A linearized

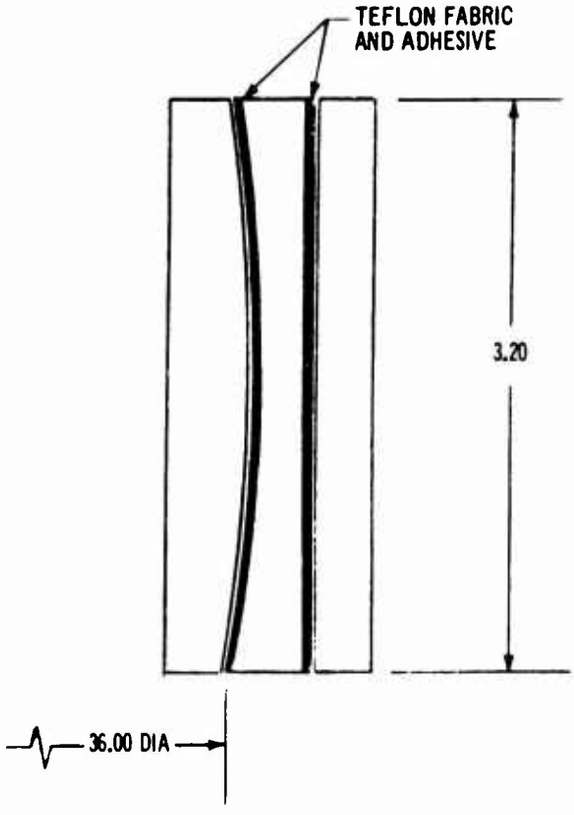


Figure 3-3. Bearing Details

load spectrum (Fig. 3-4) designed to simulate typical flight profile loads during a wing sweep was applied to the specimen. Because of problems with the attachment to the test fixture the sweep angle for room and reduced temperature conditions was changed slightly at 6,893 total cycles to obtain a less severe stress pattern on the inboard lug. At that time, 3,520 room temperature cycles 3,323 200°F temperature cycles and 50 of the -40°F temperature cycles had been applied. Proof loads of 2,400 kips were applied at 3,075 and 6,533 cycles. 3,600 kip proof loads were applied at 6,544 and 16,730 cycles. All proof loads were at 0 degrees angular displacement. Approximately 90 strain gages were installed on the specimen. Readings were taken at 10, 0, 10, 31 and 44 degrees for cyclic loads and the 2,400 kip proof loads.

The test was stopped for inspection and repair at 18,474 cycles because of a loud report which indicated a structural failure. At this time the lugs were disassembled and completely inspected. There was no evidence of any appreciable bearing wear, however, a crack had appeared at the corner of the triangular cutout as shown in Fig. 3-5. Also, inspection of the inboard lug and plug showed galling on the mating surfaces at random locations with a maximum depth of 0.017 in. after removal of local pits. To prevent recurrence, a protective coating of teflon was applied to the mating surfaces of the lug and plug and an anti-rotation system (Fig. 3-6) was installed to prevent relative rotation between the plug and inboard lug. Inspection of the lug following the test completion showed this to be an effective method for prevention of galling.

Results of a stress survey on 1/10-photoelastic models of the lug showed that stress concentrations existed at the corner of the tiangular cutout of sufficient magnitude to cause problems. Several cutout shapes were investigated and the cutout was reworked to the most favorable configuration. The crack was repaired by welding.

The lugs were reassembled and the testing continued without incident to 18,922 cycles. At this time a crack developed in the splice between the inboard lug and the test fixture. Fatigue tests of a similar splice configuration showed the original design stress to be excessive and that the early fatigue life predictions of Ti 8-1-1 were overly optimistic for the bolted joint. The specimen was repaired by moving the splice outboard about 8 in. Taper-Lok bolts were used in the new splice in place of the original straight shank bolts which had been installed in rather loosefit holes. Because of continued deteriotion of the under-designed lug joint, testing has been discontinued after slightly over one airplane equivalent life.

The program at this point had accumulated 150 cycles at -40°F, 13,340 cycles at 200°F and 16,611 cycles at room temperatures, slightly exceeding the airplane single life goal of 30,000 cycles, or the equivalent of 50,000 hours of airplane operation. Examination of the bearing shows it to be in serviceable condition. A photograph of the removed bearing is shown in Fig. 3-7 and the bearing will be available for on-site visual inspection.

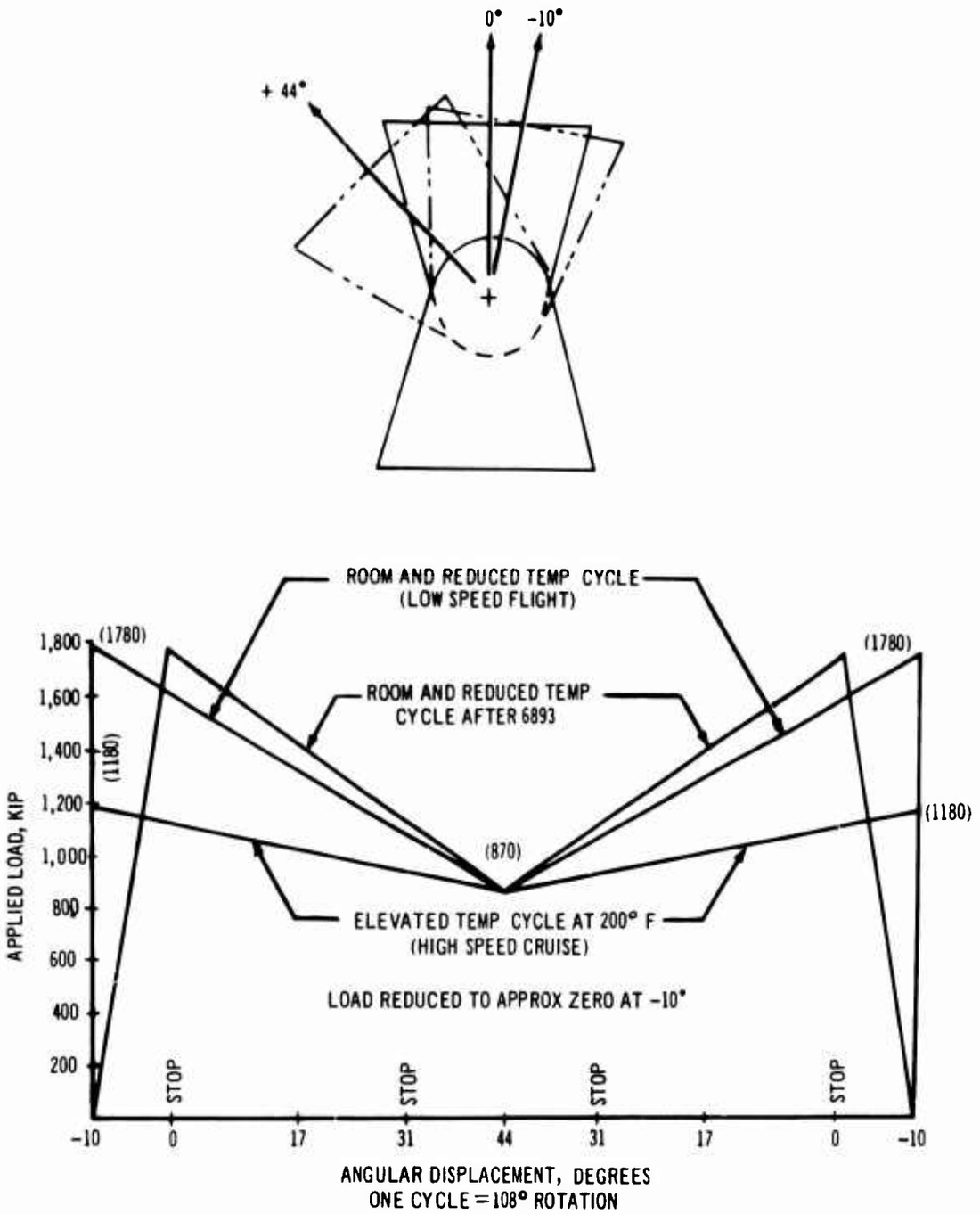


Figure 3-4. Test Load Spectrum

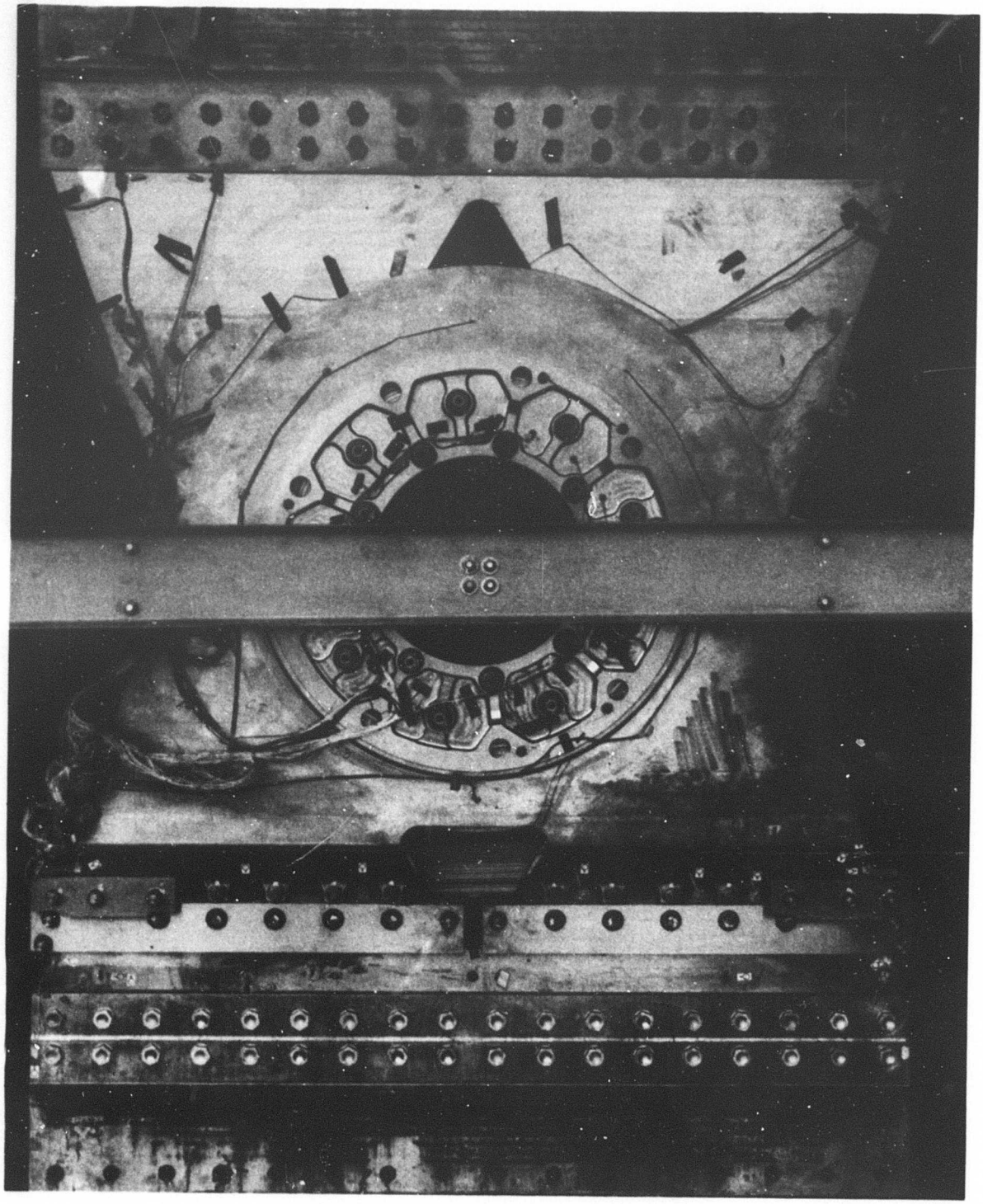


Figure 3-5. Pivot Bearing Lug Crack

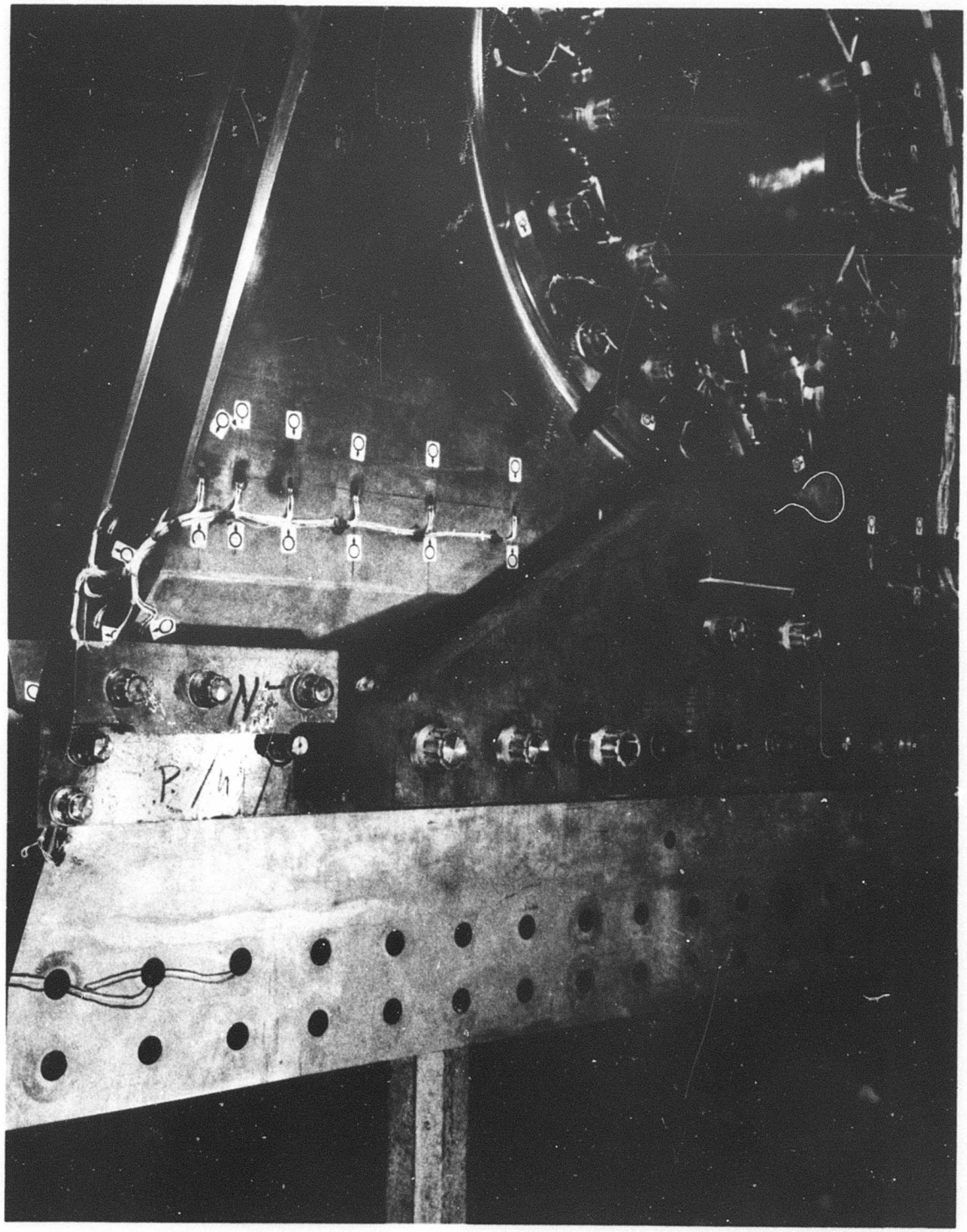


Figure 3-6. Inboard Lug Crack



Figure 3-7. Pivot Bearing After Life Test

A new inboard lug of Ti 6Al–4V mill annealed that incorporates airplane type splice joint design and stress levels is being fabricated and will be available to start testing of additional bearings in November of 1966. Design concepts were based on the full-scale pivot design, data from the stress survey conducted during this program, and a finite element solution using a computer program. The new design eliminates the triangular-shaped hole and other stress concentrations to be more nearly equivalent to the actual airplane design.

While the test specimen experienced structural fatigue problems, the test program accomplished the following goals established at its inception.

- Prove the feasibility of manufacture of full-scale titanium pivot bearing support structure.
- Demonstrate a bearing design for a life equivalent to the airplane design goals.

3.1.3 Quarter-Scale Photoelastic Pivot Test
The purpose of the quarter-scale photoelastic pivot test is to evaluate the validity of the parameters and load transfer methods used in the design of the full-scale titanium test box (Ref. Par. 3.1.4). Figure 3-8 shows the test section. The exterior surfaces are machined from a birefringent plastic (araldite 502). All ribs and interior lugs are made from Type G plexiglas. A plan view of the test setup and loading positions are shown in Fig. 3-9. Loads simulating actual airplane load distributions will be applied to the specimen.

Photoelastic techniques, supplemented by strain gages will then be used to determine load distribution on the surfaces with strain gages used to evaluate stresses in the inaccessible areas of the pivot structure and interior wing box. The results of this test will be used to aid in placing strain gages and photostress in critical areas of the full-scale titanium pivot test box and, if necessary, to effect changes in the specimen prior to critical loads and life testing.

3.1.4 Full-Scale Pivot Test
A wing pivot test box design which incorporates the knowledge and experience gained from the earlier pivot test programs is presently under construction. The deficiencies noted in the full-scale bearing test have been corrected and except for local structure revisions, the arrangement will be identical to that used on the B-2707 airplane. Results of this program will serve to eliminate the development risk and preclude possible maintenance problems with the pivot.

3.1.4.1 Test Specimen
The test section consists of a pivot fitting and wing structure extending 109-in. outboard and 100-in. inboard of the centerline of the pivot. The structural arrangement of the box is shown in Figs. 3-10 and 3-11. The pivot fitting consists of lugs at the uppor and lower wing surfaces. The outboard wing laminated single shear lug is sandwiched between the double shear lug in the inboard wing. A compression plug fits into the lugs and transfers loads from the outboard to the inboard wing lugs. The outboard wing rotates on the bearing while the plug remains stationary. The lugs are attached to the inboard and outboard wing sections by mechanical fasteners in a double shear splice. The inboard and outboard wing sections are conventional two-spar torque boxes.

The bearing for this test was made by the MICRO-PRECISION COMPANY. The bearing race configuration is identical to that used in the 36-in. dia bearing test except that improvements from the development test programs are incorporated to provide a teflon-impregnated fiber glass cloth bonded to the surfaces with Shell Epon 957 Adhesive.

The beam shear is reacted by a thrust bearing at the upper surface between the outboard wing lug and the upper plug. The plug transfers the shear to the inboard wing curved spar which is attached to the inner lugs of the inboard wing. The bending and torsional moments are transferred as couple loads in the upper and lower lugs. The torsional couple loads produce differential bending in the lugs which is reacted by the surfaces at the first rib adjacent to the centerline of the pivot. This load is sheared out in the spars and surfaces at the end ribs in the test specimen.

The titanium test box is fitted at each end with steel extensions to apply and react the test loads (Fig. 3-12). The shear moment and torsion on the test box are obtained by application of a single point load which rotates through 52 degrees at a radial distance 363 in. outboard of the pivot centerline. The bearing and lug design incorporates information gained during tests of the full-scale pivot (Ref. Par. 3.1.2) and the 1/4-scale pivot described in Par. 3.1.1. Ultimate design shears, moments, and torsions for the test box are shown in Table 3-A.

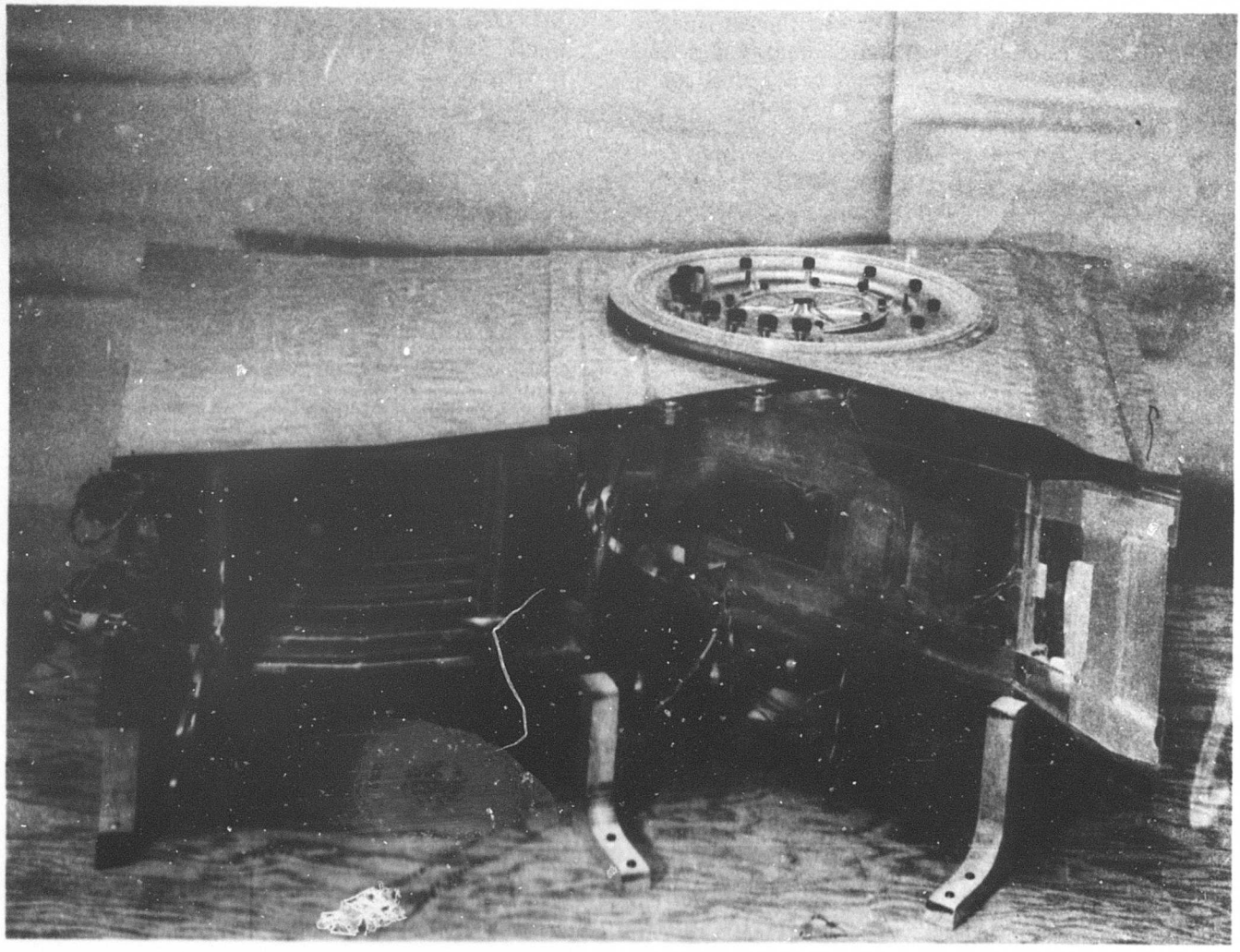


Figure 3-8. One-Quarter Scale Test Section

3.1.4.2 Program Objectives
The major objectives of the test program are as follows:

- To substantiate analytical calculations.
- To determine stress distribution in structure and effect of structural flexibility in the pivot area.
- To determine temperature distribution and thermal stresses in the structure.
- To prove structural integrity of the design including a limited fatigue life evaluation.
- To demonstrate fail-safe load paths.

3.1.4.3 Test Program

- Loads at 40 percent of ult, at sweep angles of 20 degrees, 42 degrees, and 72 degrees.

  Subsonic maneuver — flaps down $\Lambda = 20°$

  Subsonic flaps up $\Lambda = 42°$

  Transonic flaps up $\Lambda = 72°$

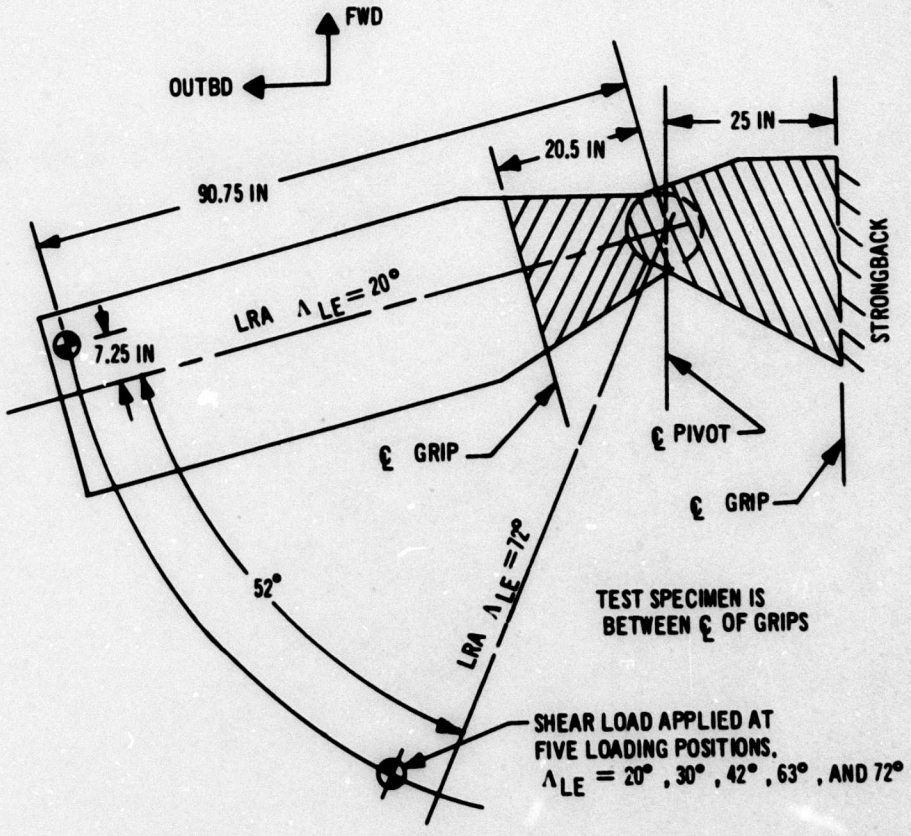


Figure 3-9. One-Quarter Scale Pivot Box Test Setup

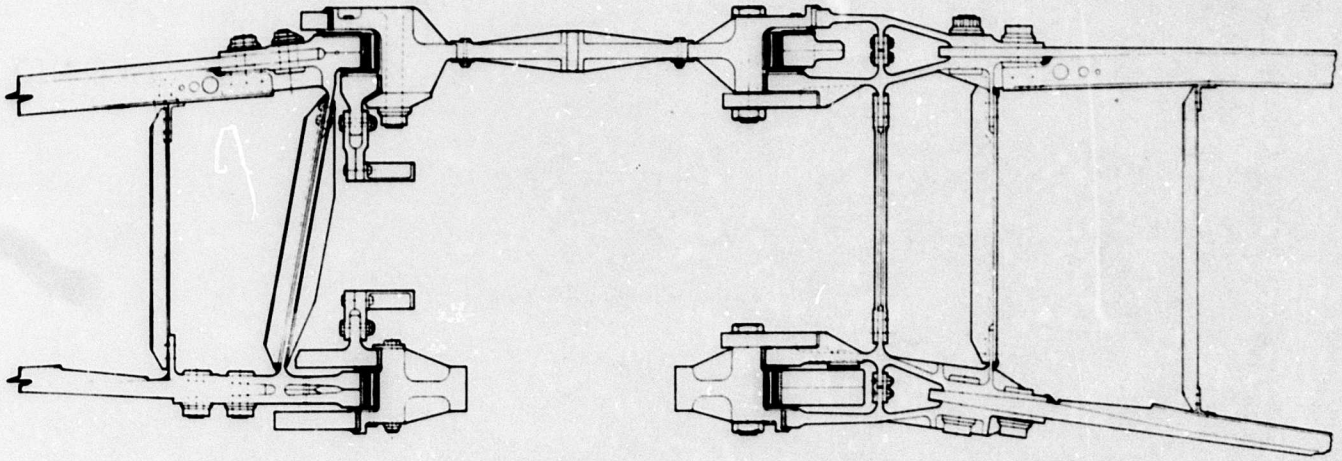


Figure 3-10. Pivot Test Section

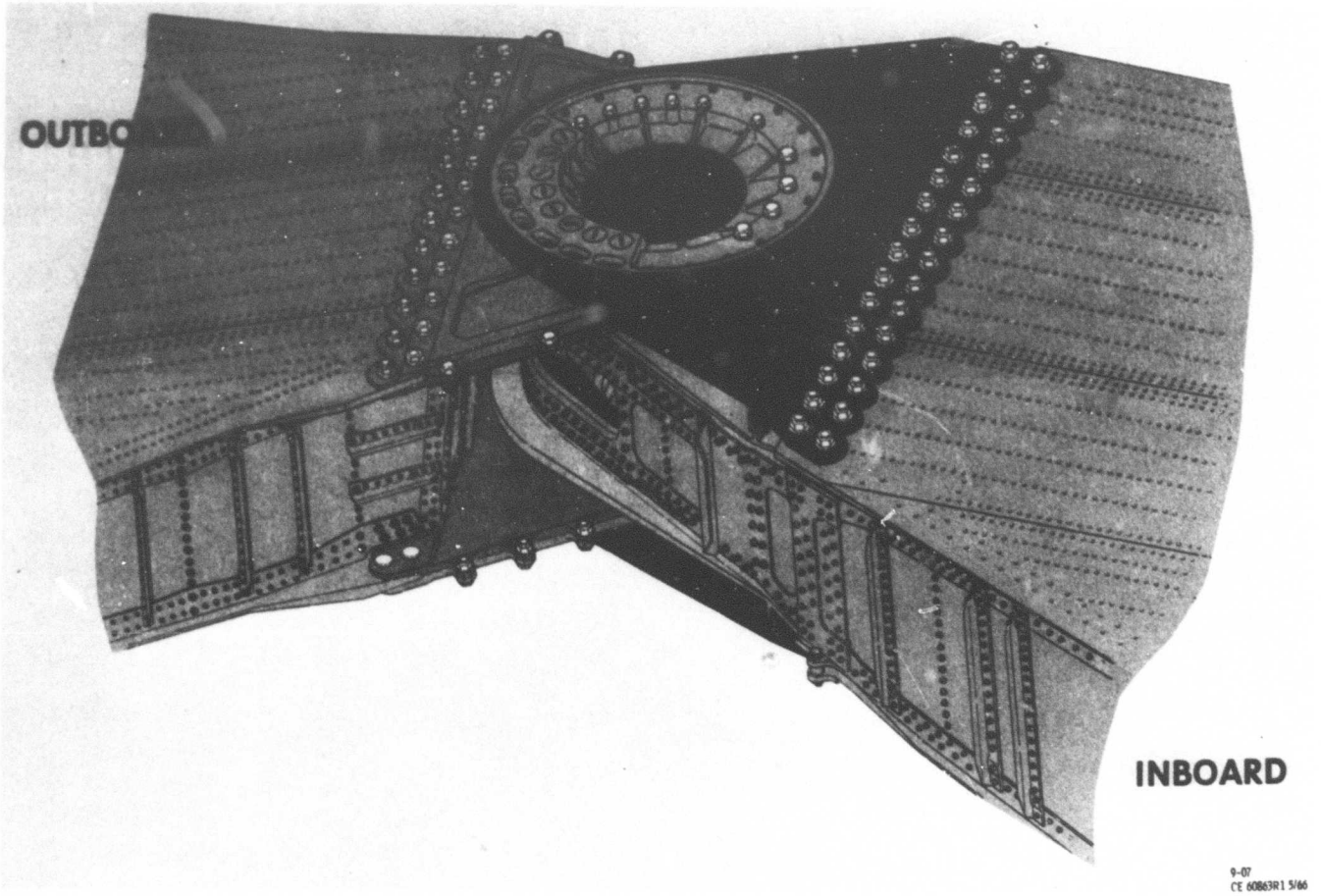


Figure 3-11. Pivot Test Section

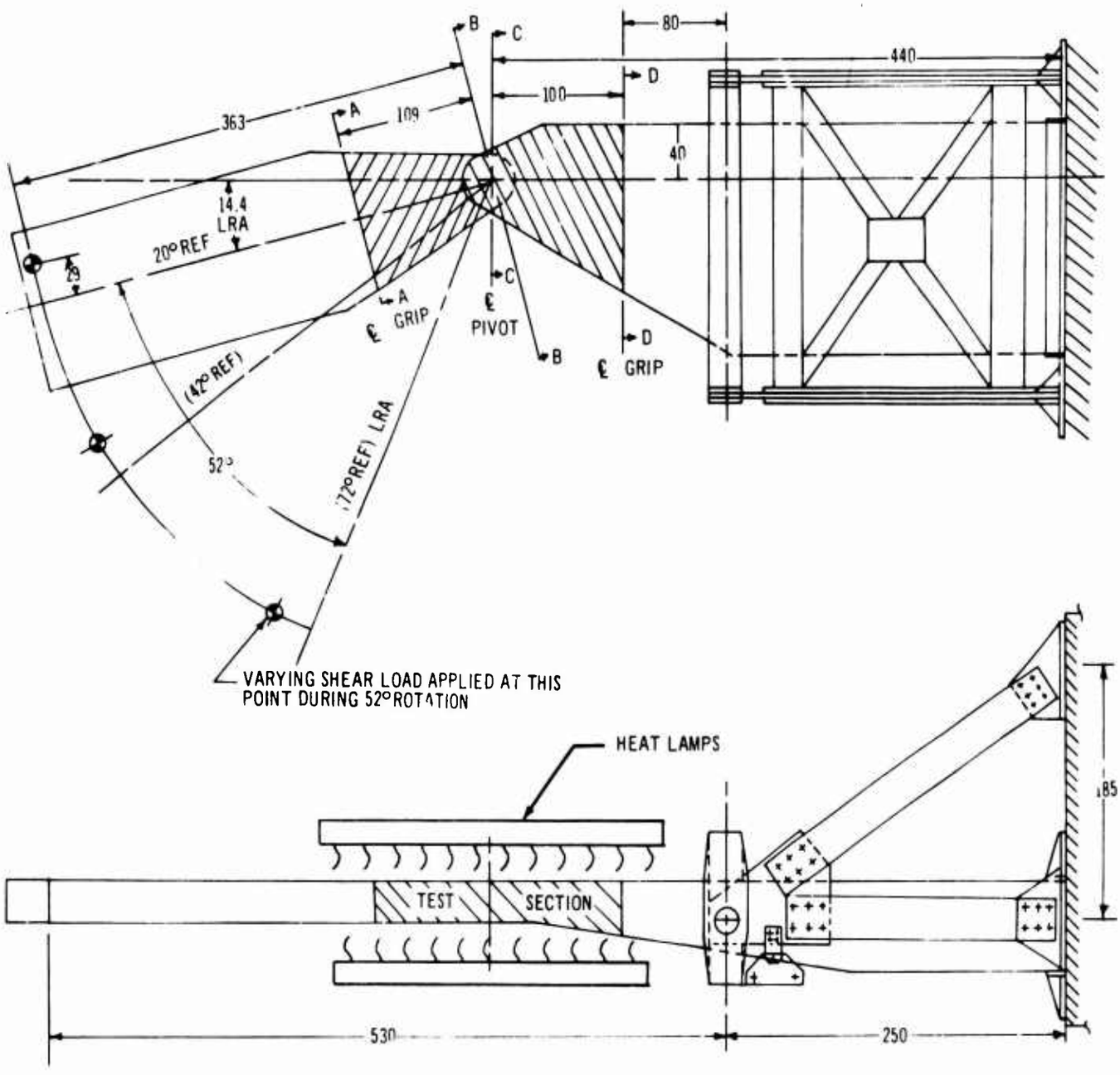


Figure 3-12. Pivot Test Setup

Table 3-A. Pivot Test Loads

Section [1]	L.E. Sweep Angle	Condition Number [2]	Ultimate Test Loads kips		
			kips	10^3 in kips	
			V	M	T
A-A	20°	1	430	109	12.5
	42°	2	305	100	11.5
	72°	3	286	73	8.3
	72°	4	265	67	7.7
B-B	20°	1	430	156	12.5
	42°	2	395	143	11.5
	72°	3	286	104	8.3
	72°	4	265	96	7.7
C-C	20°	1	430	151	-40
	42°	2	395	130	-77
	72°	3	286	46	-98
	72°	4	265	29	-92
D-D	20°	1	430	190	-55
	42°	2	395	146	-97
	72°	3	286	60	-99
	72°	4	265	56	-92

[1] Ref. Fig. 3-12 for location of sections

[2] 1 - Flaps Down

2 - Subsonic Maneuver

3 - Transonic Maneuver

4 - Supersonic Maneuver Including Environmental Temperature

- Cyclic loads of 30 percent of ultimate while sweeping the wing through 52 degrees.

- Fail-safe testing at 80 percent of limit. Planks in the wing lower surface will be saw cut and load will be applied to determine crack growth rate and demonstrate fail-safe load paths. Areas to be cut will be selected based on stress distributions determined from test data obtained during proof loading.

Extensive deflection, temperature, and stress measurements will be taken during testing. Approximately 100 sq ft of bi-refringent plastic will be applied to the upper and lower wing surfaces and exposed lug areas. Approximately 900 strain gages will be installed to evaluate stress distribution throughout the test specimen.

3.2 WING TESTS

The wing test program has included a large number of component specimen including a full-scale wing box, full-scale spar structure, compression panels, shear panels and fail-safe panels. A full-scale wing box fail-safe test is currently in test. Three full-scale wing boxes are being built for testing in the follow-on period. These boxes will be used to define the Ti 6-4 wing fatigue quality and to verify the full-scale airplane fatigue test methods.

Tests have been conducted at room temperature and at elevated temperature as appropriate to the problem definition. Individual tests are described in detail in the following paragraphs.

3.2.1 Compression Panel Tests

3.2.1.1 Program Objectives

Test programs have been conducted on Ti 8-1-1 and Ti 6Al-4V compression panels to verify analytical methods used for determining compressive allowables and to establish design allowables for skin stringer panels.

3.2.1.2 Panel Description

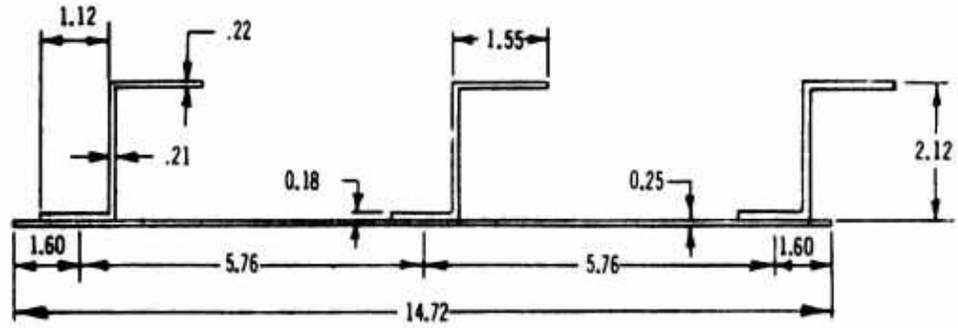
Initial tests were conducted on Ti 8-1-1 panels configurated as shown in Fig. 3-13a. These panels were representative of light and heavy section wing structure and light and medium fuselage structure. The panels were designed using the analysis methods given in Airframe Design Report — Part B — Component Design, V2-B2707-6-2. Attachment of skin to stringer was by spotwelding with attachment spacing consistent with the design practice of providing stability for inter-rivet buckling or, as required by panel shear. Panel lengths were varied to obtain slenderness ratio values over the optimum design range. Specimens of approximately 6 in. in length of both panel sections and individual stiffeners were used to determine crippling strengths. The Ti 8-1-1 panel sections shown in Fig. 3-13a were similar to those of Fig. 3-13b except that rivets were used instead of spotwelds for attachment of skin and stringer. In addition, hat section panels were included in this series of tests. The Ti 6-4 panels were designed as verification test panels typical of B-2707 wing, fuselage and empennage compression structure. An earlier series of tests of seven spotwelded panels similar to those of Fig. 3-13 a are not included. The test results showed reasonable correlation to predicted values; however, the spotwelding procedure used in the fabrication of these panels did not provide acceptable spotweld tension allowables and resulted in some nontypical panel failures. For all later panels, a revised spotwelding procedure was used.

3.2.1.3 Testing Procedure

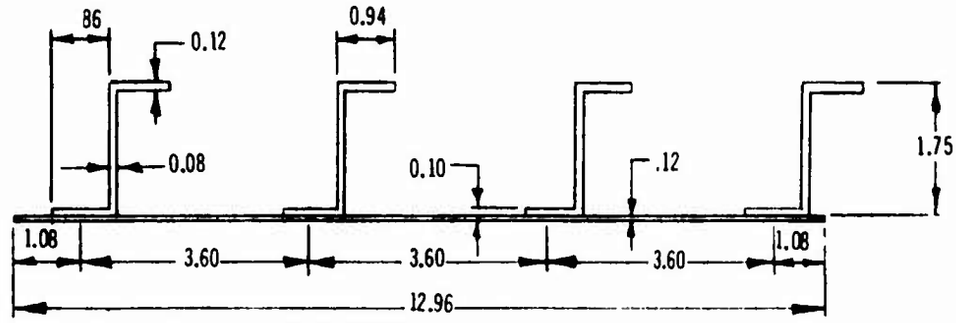
Column tests were performed at room temperature, 500°F, and with 200°F -500°F thermal gradients. Crippling tests were at room temperature and 500°F. Ends of the test parts were machined square so that when loaded by the flat test machine heads, an end fixity of approximately 3.5 would be developed.

Strain gages were applied at critical locations on the skins of the room temperature panels to indicate the load level at which skin buckling occurred. The point at which buckling occurred was determined from an analysis of strain gages installed back-to-back.

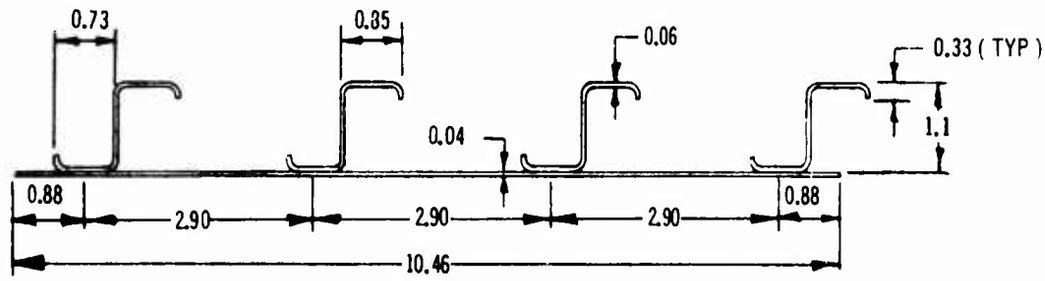
Radiant heat lamps were used for the elevated temperature conditions. Temperatures were monitored by thermocouples to ensure that desired level and distributions were obtained. For the thermal gradient tests a load of approximately 40 percent of the expected ultimate load was applied before heating was started. This procedure was necessary to prevent the reduction in end fixity that would occur with the application of thermal gradient with a small axial loading. Strain gage readings were taken with axial load only and again after the temperature condition had been established. The difference between the readings determined the stresses due to the thermal gradient. Panel ultimate loads were



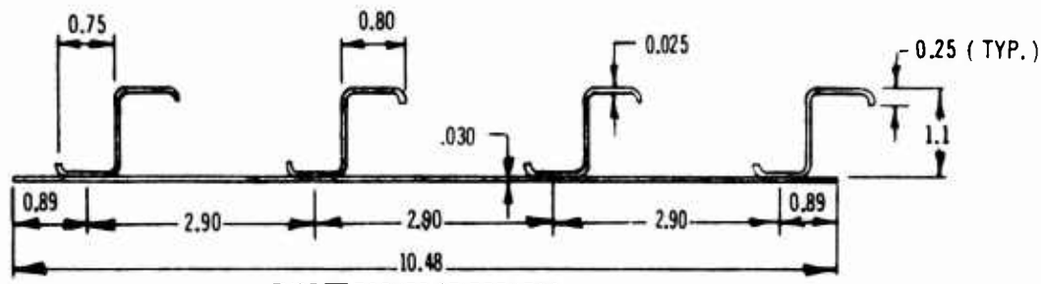
TYPE I EXTRUDED STIFFENERS



TYPE II EXTRUDED STIFFENERS



TYPE III FORMED STIFFENERS



TYPE IV FORMED STIFFENERS

Figure 3-13a. Compression Test Sections

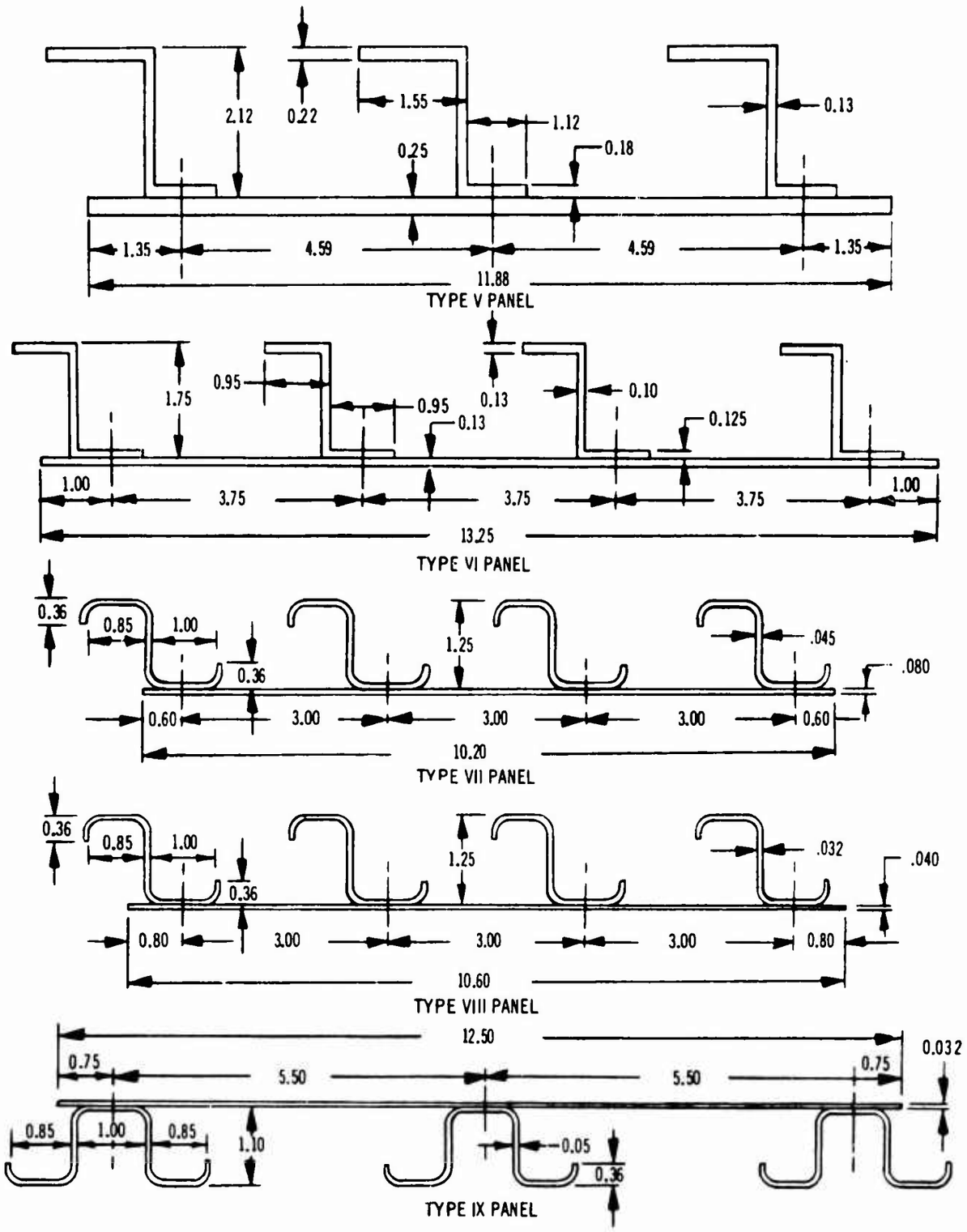


Figure 3–13b. Compression Test Sections

then determined. A typical test setup for an elevated temperature test is shown by Fig. 1-6.

Lateral deflections of the panels were measured. An indication of the actual end fixity of the column was determined from the deflected shape of the specimen.

To further evaluate the test end fixity, one panel was built with completely fixed ends. Results of this test indicated that an end fixity coefficient of 3.5 for flat end panels was reasonable.

A bowed condition was produced in the manufacturing of some panels. In general this condition was confined to the spotwelded panels. For these panels a load was applied to seat the panel ends against the test machine head. The deflection of the panel was then determined and this value was used as a measure of initial panel eccentricity.

3.2.1.4 Test Results
The results of compression tests are shown in Tables 3-B and 3-C and a comparison of test results and predicted column loads are presented in Fig. 3-14. In general, reasonable agreement was obtained between test and predicted load. Panel alignment in the test machine, end flatness and eccentricity are factors that influence loading. Small variations in these factors can materially change test results. The bowed condition of the spotwelded panels presented difficulties in accurate determination of panel eccentricities. However, using initial eccentricities based on panel deflection measurements resulted in reasonable agreement of test and predicted load. Test loads for the riveted Ti 6-4 panels averaged approximately ten percent lower than prediction for the heavier sections. The lighter formed stiffener sections showed generally good agreement. For the heavier sections, panel failure was initiated by premature stiffener roll. The premature stiffener roll resulted from a combination of end fixity reduction and inadequate simulation of the rib chord member. The simulated rib chord member used for outstanding flange stabilization was free to translate in the plane of the panel. Panel deflection data indicated a reduction of end fixity below the normally assumed coefficient of 3.5. The lower test end fixity resulted in an effective length change between rib chord stabilizing members and allowed premature stiffener roll. In the actual airplane structure, translation of the rib chord members are restrained and panel lengths are set by rib spacing. Evaluation of test results and test factors indicates that reliable structure design can be obtained using the analysis methods.

3.2.2 Shear Panel Tests

3.2.2.1 Program Objectives
Test programs have been conducted on Ti 8-1-1 and Ti 6-4 shear beams to verify analysis methods and to establish design allowables for intermediate-type shear webs having either riveted or spotwelded web to stiffener attachments. Test results have verified the adequacy of the analytical methods outlined herein.

3.2.2.2 Panel Design
The panels were designed using relation of web strength, strength of web stiffeners and stiffener to web attachments consistent with existing design methods. Webs were designed for a basic net area shear strength of 0.49 F_{tu}. Allowable stiffener strength was based on the method given by Kuhn in NACA TN 2661 Ref. 1 modified for titanium stiffeners as follows:

$$F_{ST} \quad 26000K^{2/3}\left(\frac{t_u}{t}\right)^{1/3}\left(\frac{F_{CY}}{37000}\right)^{0.38}\left(\frac{E}{10.5\times10^6}\right)^{0.83}$$

Web to stiffener fastener requirements for spotwelded construction was based on a tension loading per inch of 29 percent of the actual shear flow. The ratio of tension strength to shear strength of spotwelds was conservatively assumed to be 0.55.

Initial fastener strength requirements for riveted construction was based on a shear loading per inch of 85 percent of the web shear. Riveting for the final series of panels was reduced to 40 percent of web shear requirements consistent with design practice for aluminum shear webs. Testing performed to date has validated this reduction.

3.2.2.3 Ultimate Strength Tests
Ultimate strength tests were conducted on Ti 8-1-1 and Ti 6-4 panels having web gages varying from 0.025 to 0.125. Panel details are given by Fig. 3-15 and Table 3-D. Small specimen tension tests were used to determine material properties of the webs. All testing was at room temperature

Table 3-B. Compression Test Results

TEST VS CALCULATED LOADS -Ti 8-1-1 SPOTWELD PANEL

Panel Type Ref. Fig.13a	Length (in)	Test Temperature °F	Test Load kips	Predicted Load Johnson-Euler kips [1]	Predicted Load Init. Eccent. kips
I	73.5	70	388	472	380
	46.5	500	438	492	[2]
	73.5	500	326	379	303
	46.5	500-200	509	506	
	46.5	100-400	507	515	
II	70.0	70	161.5	160	
	52.5	500	170	189	
	52.5	500-200	169.5	168.4	
III	28.0	70	79.5	93.2	73.8
	28.0 [3]	70	82.0	96.1 [3]	77.8
	39.0	70	56.5	70.5	[2]
	28.0	500	62.5	70.0	56.9
	39.0	500	51.5	57.4	47.5
	28.0	500-200	66.0	76.6	60.3
IV	30.0	70	26.9	26.0	
	30.0	500	23.0	21.2	
	37.0	500	20.6	19.9	
	30.0	500-200	24.0	21.8	

[1] Based upon actual material properties and panel end fixity of 3.5 except as noted.

[2] No deflection data available.

[3] Fully fixed ends

Table 3-C. Compression Test Results

TEST VS CALCULATED LOADS

Panel Type Ref. Fig. 13b	Length, (in)	Test Temperature °F	Test Load kips	Predicted Load kips [2]
V	46.5	70	498	519 [1]
	73.5	70	319	392
	46.5	500	447	475
	73.5	500	300	333
Ti 6AL4V Riveted	46.5	500-200	454	495
	46.5	200-500	402	416 [1]
VI	52.5	70	244	286
	70.0	70	157.5	164
	52.5	500	212	229
Ti 6AL4V Riveted	70.0	500	135	143
	52.5	500-200	212	240
VII	28.0	70	80.0	84.5
	39.0	70	63.0	62.9
	28.0	500	62.9	69.8 [1]
Ti 6AL4V Riveted	39.0	500	51.0	54.9
	28.0	500-200	58.5	65.7
VIII	30.0	70	36.0	34.7
	37.0	70	35.1	34.9
	30.0	500	32.9	29.6
	37.0	500	30.5	28.2
Ti 6AL4V Riveted	30.0	500-200	32.0	26.9
	30.0	200-500	32.4	26.2
IX	37.0	70	49.9	53.8
Ti 6AL4V Riveted	37.0	500	42.0	44.8

[1] Using C 2 Based on Test Deflection Data

[2] Based on Standard Material Properties

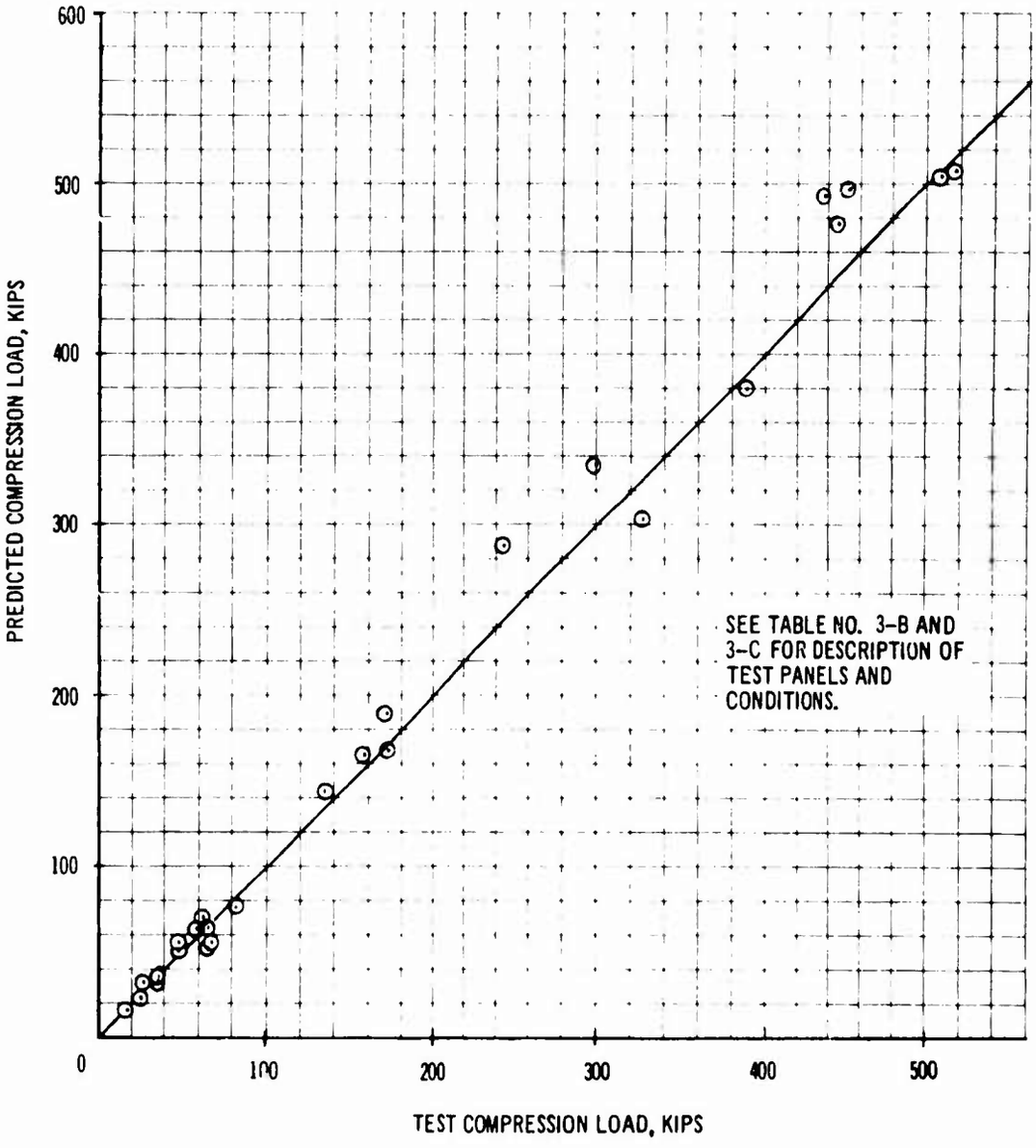


Figure 3-14. Test Versus Predicted Loads-Compression

The first series of tests were conducted on Ti 8-1-1 duplex annealed panels. Eight panels had spotwelded web to stiffener attachment and the remaining three were riveted. The panels were installed in the jig structure and loaded as cantilever beams. The jig structure served as chords and end stiffeners for the beam. Pin joints were used at the corners of the jig to prevent shear transfer through the jig by bent action. Figure 3-16 shows the testing jig with a panel installed. During the initial tests, it was determined that excessive jig chord rigidity was reducing the diagonal tension loading from the web on the stiffeners. To eliminate this and obtain more representative stiffener loading, the jig structure was redesigned to provide chord flexibility similar to that of actual shear beams. Four additional Ti 8-1-1 riveted panels were built and tested to verify the redesigned jig structure. After verification of the jig structure, ten Ti 6Al-4V riveted panels were tested to substantiate the B-2707 shear design allowables.

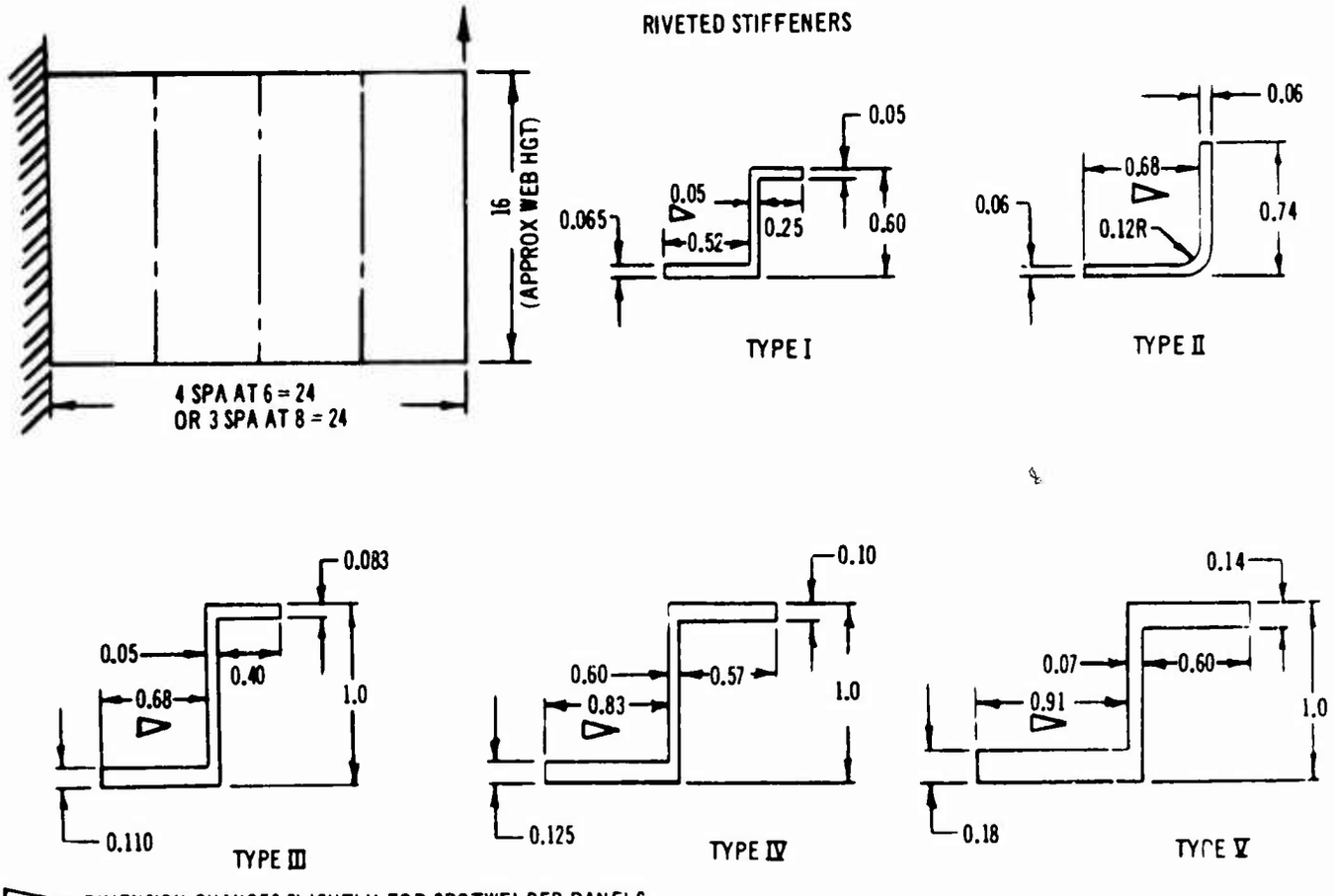


Figure 3-15. Shear Test Panels

Table 3-D. Shear Panel Configurations

Panel	Material	Web Gage	Stiff. Type	Stiff. Spacing	Stiffener-Web Fasteners
1	Ti 8-1-1 Duplex Ann.	0.025	I	6	S/W at 0.44
2		0.025	I	8	S/W at 0.44
3		0.025	II	6	S/W at 0.44
4		0.050	III	6	S/W at 0.88
5		0.050	III	8	S/W at 0.88
6		0.070	IV	6	S/W at 0.88
7		0.120	V	6	S/W at 1.03
8		0.120	V	8	S/W at 1.03
9		0.025	I	6	1/8 Rivets at 0.57
10		0.050	III	6	3/16 Rivets at 0.76
11		0.070	IV	6	1/4 Rivets at 0.95
12	Ti 8-1-1 Duplex Ann.	0.120	V	6	3/16 Bolts at 1.04
13	Ti 6-4 Cond. IV	0.025	I	6	1/8 Rivets at 0.75
14		0.025	II	6	1/8 Rivets at 0.75
15		0.050	III	6	3/16 Rivets at 0.98
16		0.060	IV	6	1/4 Rivets at 1.50
17	Ti 6-4 Cond. IV	0.125	V	6	3/16 Bolts at 1.50

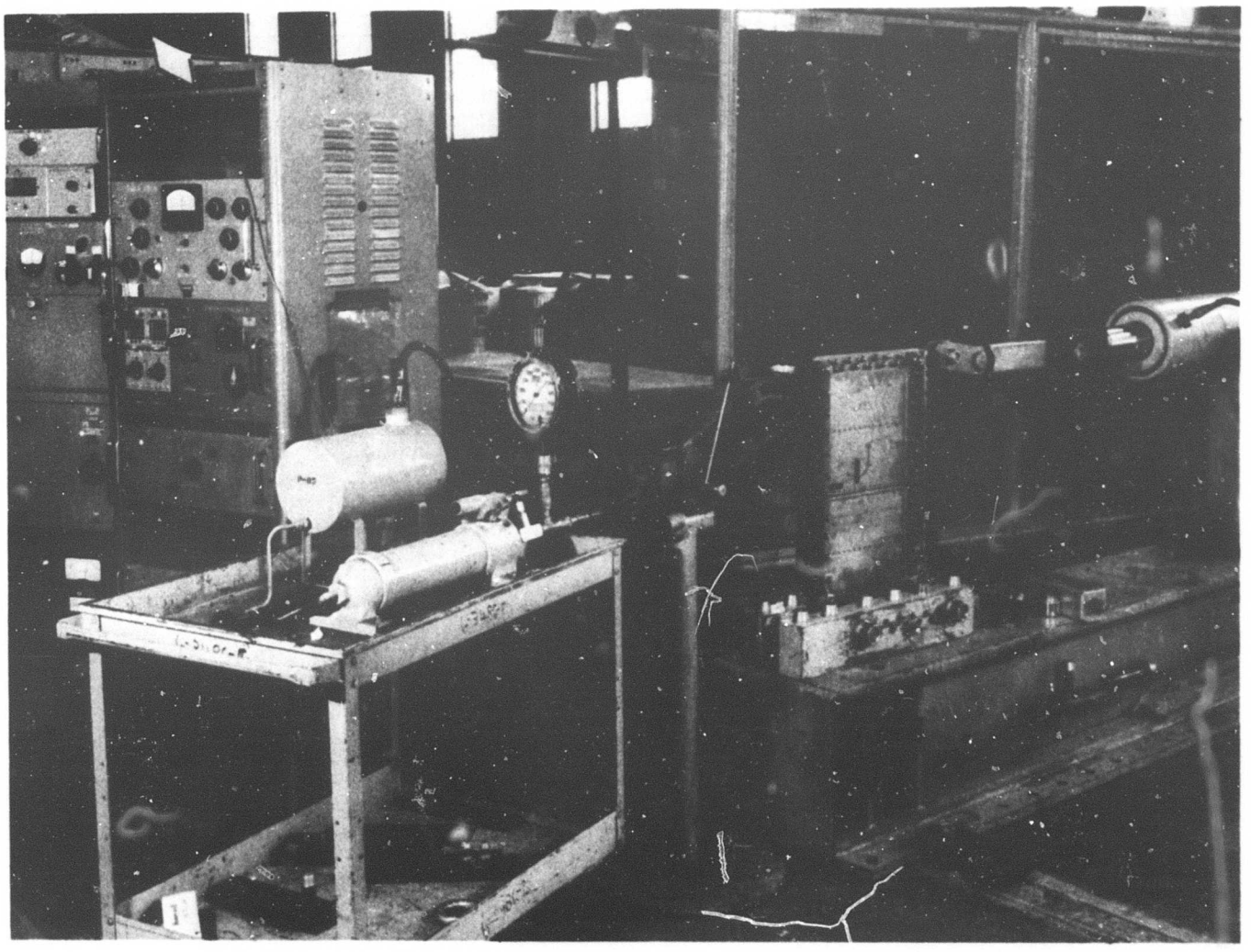


Figure 3-16. Test Panel Setup

The results of panel tests are given by Fig. 3-17 and show the close correlation between actual test loads and predicted values.

3.2.2.4 Fatigue Tests of Shear Webs
Normally, shear webs are not considered critical in fatigue. However, because of low spotwelded structure fatigue life, three light-gage shear panels have been life tested to evaluate the effects of repeated web buckling on the spotwelded attachments of web stiffeners and show no problems. The panels used 0.020 Ti 6Al-4V Condition I webs spotwelded to Ti 6Al-4V Condition III extruded zee-stiffeners. The panels were tested in a picture frame jig with loads applied at two diagonally opposite corners. A typical shear panel and test setup are shown in Fig. 3-18.

Cyclic tension loads varying from 150 lb minimum to 2,000 lb maximum were applied to the first panel. Panel shear flows resulting from the maximum tension load approximates maximum one factor loading on a typical wing rib. After 100,000 cycles produced no damage, the loads were increased to approximately a 3.1 factor loading (450 and 6,200 lb). After an additional 35,000 cycles, several small cracks were found in the web near the spotwelds. Panel failure occurred at 152,000 total cycles.

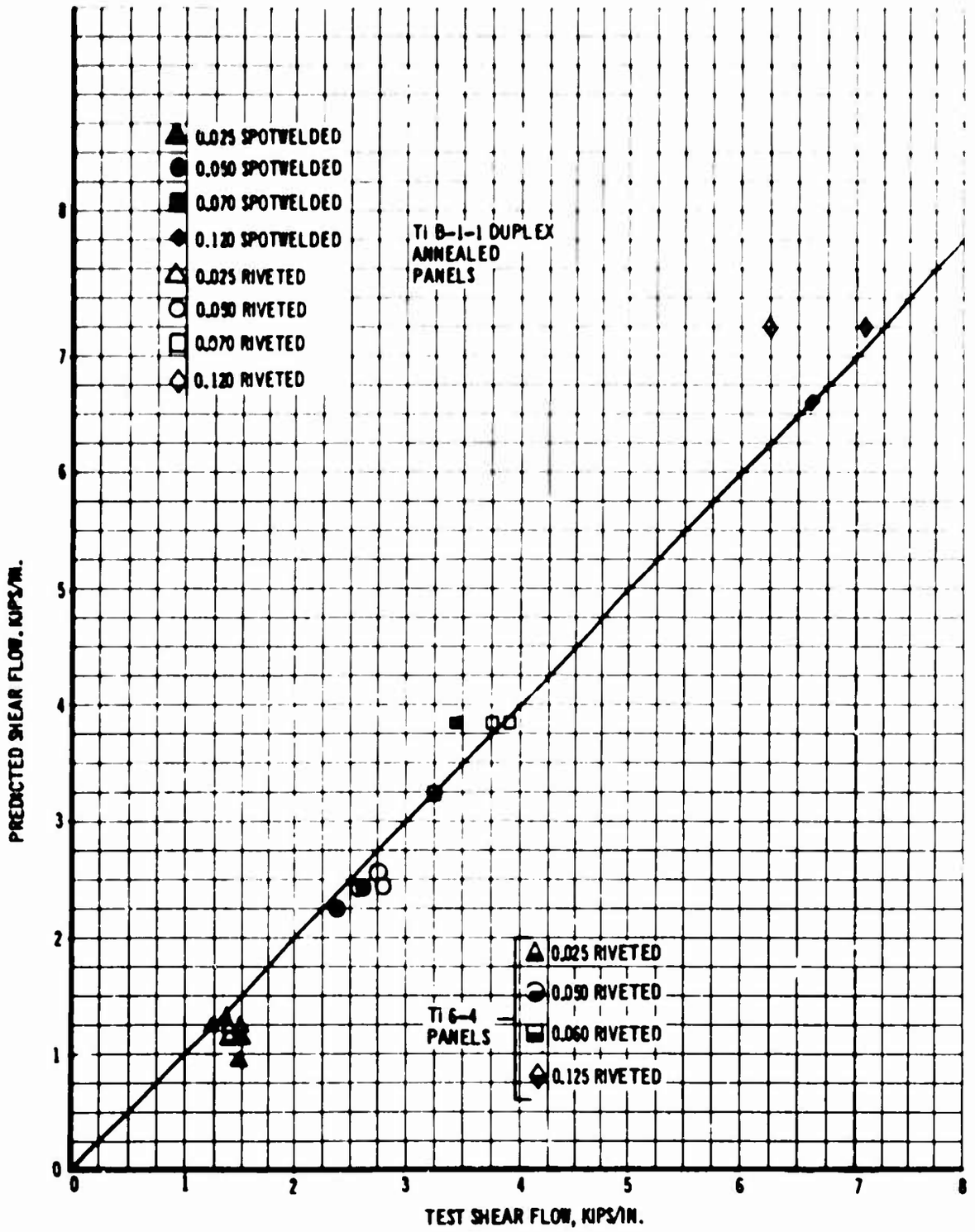


Figure 3-17. Test Versus Predicted Loads-Shear

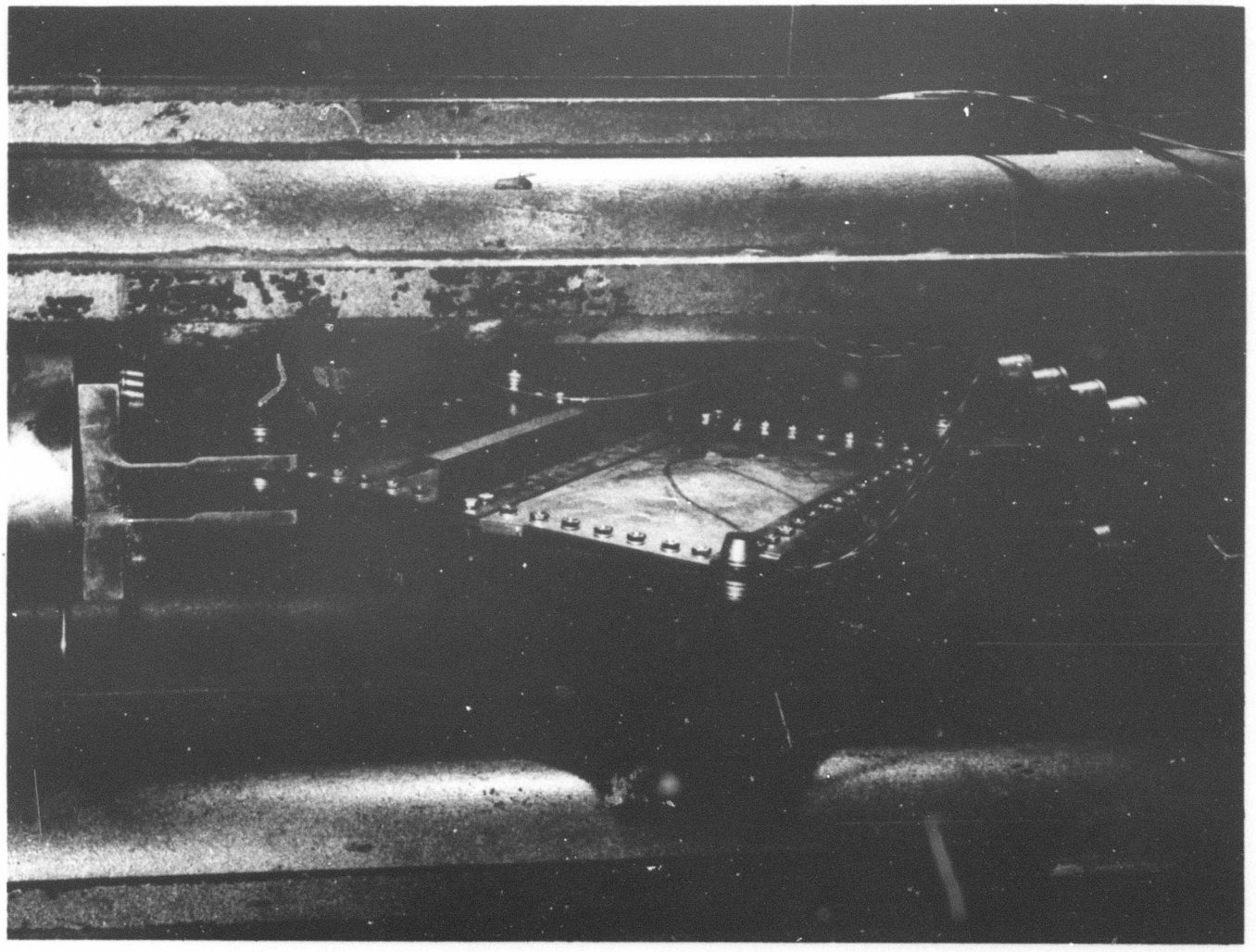


Figure 3-18. Fatigue Test Panel

In the second panel tested, small web cracks near spotwelds were found after 36,000 cycles of 450 to 6,200 lb loading. Panel failure occurred at 75,000 cycles.

Small cracks began in the third panel at 153,000 cycles for a 2.05 factor load condition (300 to 4,100 lb) and failure occurred at 380,000 cycles.

3.2.2.5 Summary of Test Results
The ultimate strength tests were in good agreement with prediction (Fig. 3-17) thus verifying proposed analysis methods and design allowables for shear webs.

The fatigue test results indicate that spotwelded attachments of web stiffeners are adequate for repeated applications of web buckling shear loads.

3.2.3 Access Panel

3.2.3.1 Program Objectives
A test program will be conducted the latter part of 1966 to evaluate stress distributions within a typical lower surface access panel. The objective of the program is to verify the panel design and to determine areas of unacceptable stress concentrations and areas of excessive material weight.

3.2.3.2 Test Panel Description

A one-half scale plastic model of the wing fatigue box lower surface access panels is being manufactured (Par. 3.2.4). The panel, shown in Fig. 3-19 has two access openings and a different transition configuration on either end. Out of plane support is provided by simulated rib structure spaced at 13-1/2 in. The panel is coated with a photoelastic material which allows visual stress measurements over the complete surface of the panel. The primary advantage of using a plastic model is that structural modifications can be easily accomplished by adding additional plastic material which then becomes part of the basic material. Sections can be reduced by simply removing material.

3.2.3.3 Test Program

Shear and axial load tests will be conducted on the model.

Initial testing will be for application of shear loads. The model will be installed in a picture frame jig with loading applied at two diagonally opposite corners. Stress distribution will be determined from the photostress patterns and areas determined where strain gages are required to obtain additional strain data. Modifications will be made as indicated by the stress distribution and the panel retested for verification of the modifications. Following the shear tests, axial load tests will be conducted to obtain stress distributions and determine areas of required modification.

The results of the plastic model test will be used in the followon design of a full-scale titanium part on which life tests will be conducted. These results will be transmitted as they become available.

3.2.4 Full-Scale Wing Box Test

3.2.4.1 Program Objectives

A test program has been conducted on a full-scale wing box section with the following objectives:

a. Demonstrate the structural integrity of the wing structure when subjected to a variety of applied and thermal load conditions, and

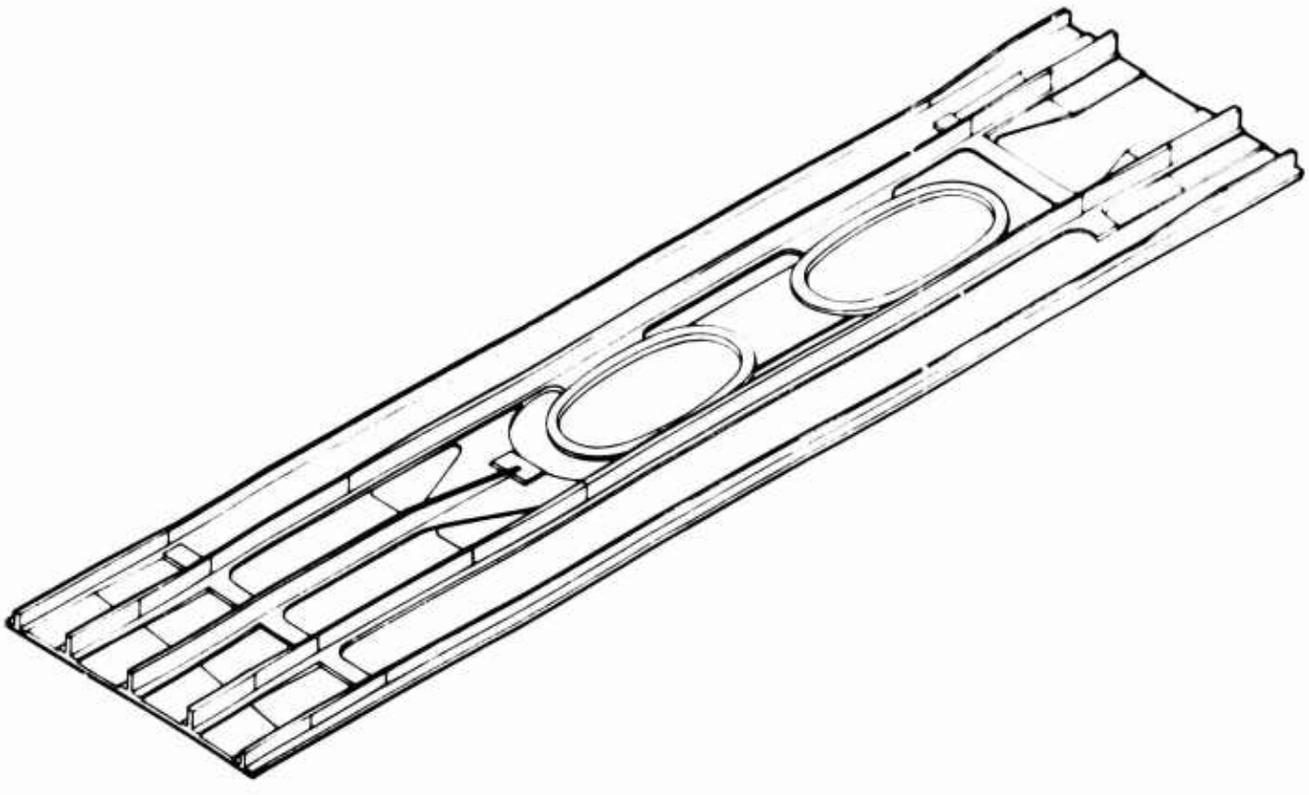


Figure 3-19. Access Panel – Plastic Model

b. Conduct load surveys for correlation of theoretical and experimental mechanical and thermal stresses.

3.2.4.2 Description of Wing Box

The test box shown in Fig. 3-2 is a typical single cell, two spar wing box having skin-stringer surfaces and stiffened web spars and ribs. The entire box was fabricated from Ti 8-1-1 material. The box is approximately 12 ft long, 5 ft wide and 1-1/2 ft deep. A wing box fuel cell having four inner tank ribs and two tank end ribs was included. All ribs were spaced at 24 in. The test section was supported by two steel extensions, each 19 ft long and designed to provide the proper moment distribution in the test section. The extensions were simple supported at the ends and could translate in the spanwise direction to allow thermal expansion. Loads were applied through fittings at the front and rear spars (Fig. 3-2). Elevated temperature test conditions were achieved by using radiant heat lamps on the upper and lower surfaces.

3.2.4.3 Test Program

Three room temperature and eleven elevated temperature tests were conducted. Fuel loadings of 3/4-full, 1/3-full, and empty were investigated for the elevated temperature conditions. An outline of the tests conducted is given by Table 3-E. Therminol, a heat transfer fluid, was used to simulate actual fuel. The substitution of Therminol for actual fuel has the advantage of being nonexplosive, yet has the same specific heat on a volume basis.

Table 3-E. Wing Box Test Outline

Temperature Condition	Loading Condition	Fuel Level
Room Temperature	Limit, Shear and Moment	No Fuel
Room Temperature	Torsion	No Fuel
Room Temperature	Limit, Shear, Moment and Torque	No Fuel
400°F at 30°/Min	No Load	No Fuel
500°F at 40°/Min	No Load	No Fuel
500°F at 60°/Min	No Load	No Fuel
500°F at 40°/Min	1.1g, Shear and Moment ▷1◁	No Fuel
400°F at 40°/Min	1.1g, Shear, Moment and Torque	No Fuel
500°F at 40°/Min	1.1g, Shear, Moment and Torque	No Fuel
500°F at 40°/Min	Limit, Shear and Moment ▷2◁	No Fuel
500°F at 40°/Min	No Load	3/4 Full
500°F at 40°/Min	1.1g, Shear, Moment and Torque	3/4 Full
500°F at 40°/Min	No Load	1/3 Full
500°F at 40°/Min	1.1g, Shear, Moment and Torque	1/3 Full

▷1◁ Load cycled to 1.8g at time of maximum ΔT across section

▷2◁ Elevated temperature limit 75% of Room Temperature limit

3.2.4.4 Testing Procedure
For the room temperature conditions, the distribution of loads was obtained for various load increments up to maximum load

The sequence of testing for the elevated temperature tests was as follows: A 1.0g static load was applied first and the temperature profile was started. When the temperature of the outer surfaces reached the desired test values, a hot soaked condition was simulated by maintaining the surface temperatures constant for approximately one hour. The heat was then shut off and the wing box allowed to cool. Data was taken during all phases of the test cycle

3.2.4.5 Analysis of Thermal and Applied Stresses
Span-wise and chord-wise thermal strains were calculated by determining the average strain of the cross section and subtracting the absolute strain of the individual point in question. Applied bending stresses were determined using standard bending theory and then modified to account for configuration and test condition influences. The effect of the shear lag which resulted from the loading arrangement was accounted for in the calculation of bending stresses. Calculated bending stresses also account for the redistribution of the applied bending load resulting from changes in section stiffness with thermal gradients. Secondary bending effects about both the span-wise and chord-wise axes due to an unsymmetrical temperature distribution were accounted for in the analysis. The restraint provided by the ribs to the chord-wise Poisson strain effect was also included.

The experimentally measured stresses were corrected for the effect of creep and drift of the strain gages.

3.2.4.6 Summary of Test Results
In general the test results indicated good agreement between actual and theoretical stresses for the various test conditions and substantiate the analysis methods for the B-2707. Typical test results and correlation with predicted stresses are shown in Figs. 3-20 and 3-21.

Figure 3-20 shows the distribution of temperatures and span-wise stresses for the elevated temperature limit load condition. Figure 3-21 shows the distribution of temperatures and chord-wise stresses at a tank end rib for a test condition with a 3/4-full fuel level. The data of both Figs. 3-20 and 3-21 were obtained at the time of maximum thermal gradient across the structure

3.2.5 Wing Box Fatigue Tests
A program is in work to fatigue test three full scale wing boxes. These tests are in support of the full-scale airplane fatigue test and will provide structural design information for the prototype and production airplanes.

All three test boxes are of identical construction and represent a 135-in. long section of the outboard wing primary structural box. They include upper and lower surface skin and stiffener cover panels, front and rear spars, four intermediate ribs, and two tank end ribs. Fittings are located on the front and rear spars for representative attachment of flaps, slats and ailerons and their actuators. A test box is shown in Fig. 3-22.

One box will be tested to represent as nearly as practical the actual wing and the loads and temperatures it will encounter in normal service. It will have programmed temperatures applied. The heating and cooling (climb and descent) portions of each test flight will be applied on a true-time basis to provide proper temperature gradients and thermal stresses. A fluid will be pumped into and out of the box each flight to provide the fuel heat sink effects. Properly proportioned external loads are applied through the flight from taxi to landing in proper time phase with the temperature changes. The applied loads are higher than would normally be encountered in typical usage to achieve meaningful results before start of the full airplane fatigue test on a production airplane. The type of test setup is shown in Fig. 3-23 and the box inboard end bending moments during the flight are shown in Fig. 3-24.

The other two boxes will be tested on an accelerated time basis. This is achieved by testing at room temperature and eliminating the heat-up and cool-down time required in the other test.

The second box to be tested at room temperature will complement the time-temperature box test. Loads on the box will be higher than normally encountered in flights to account for thermal effects. The exact level of the loads will not be established until the time-temperature box test is nearly completed. The loads will be established to obtain a correlation in number of flights before fatigue failures between this box and the time-temperature test box. This box test along

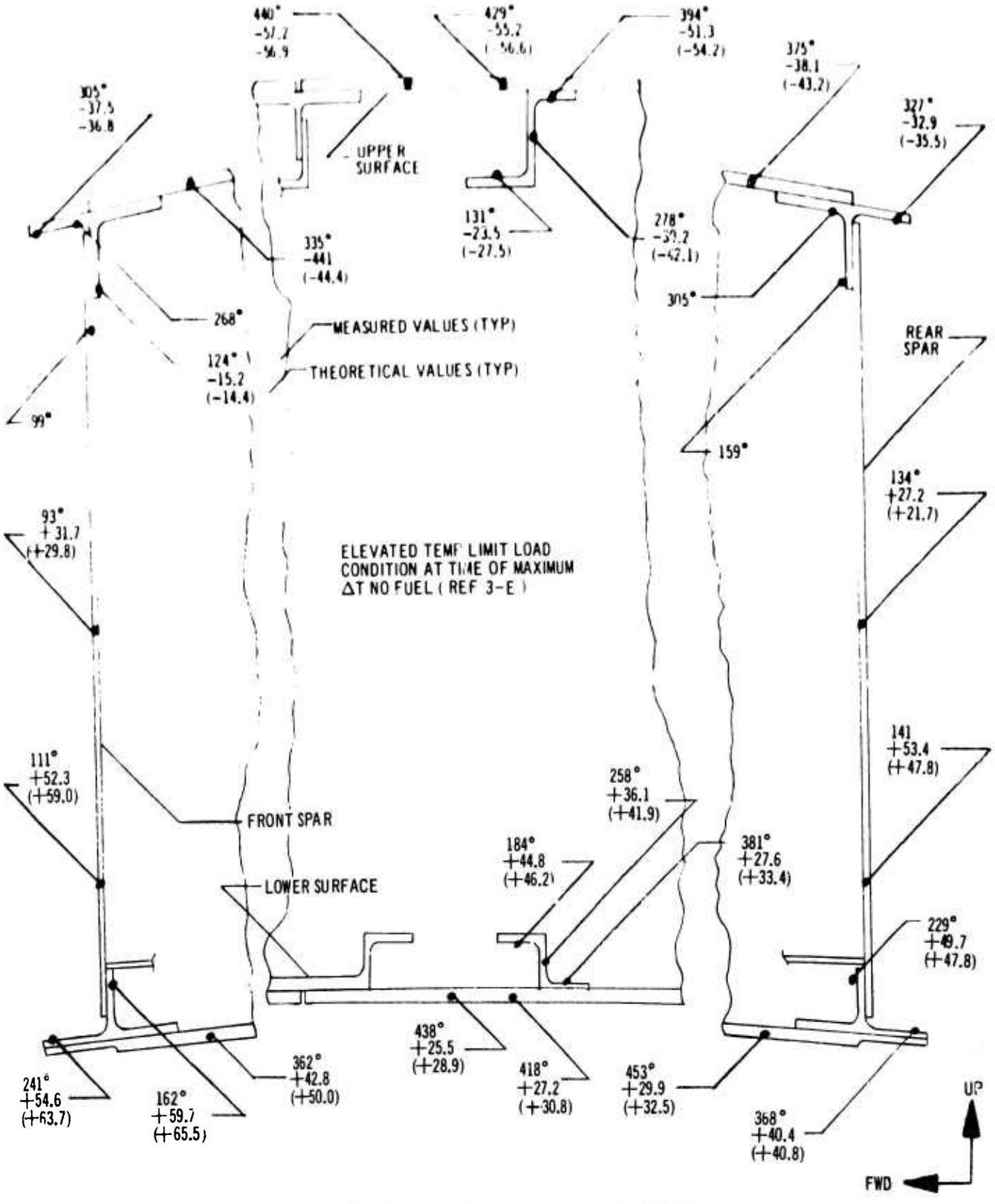


Figure 3-20. Spanwise Temperature-Stress Distribution

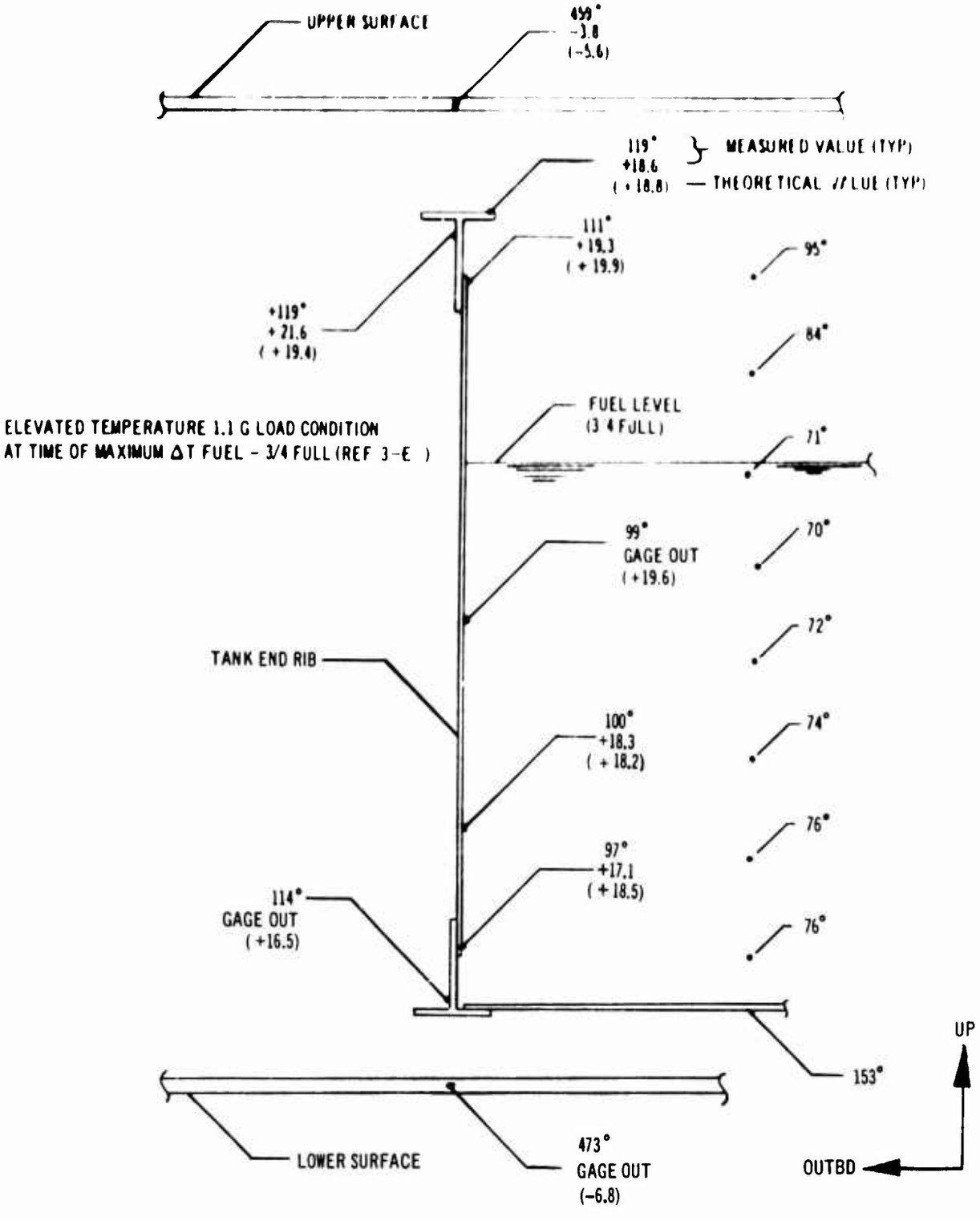


Figure 3-21. Chordwise Temperature-Stress Distribution

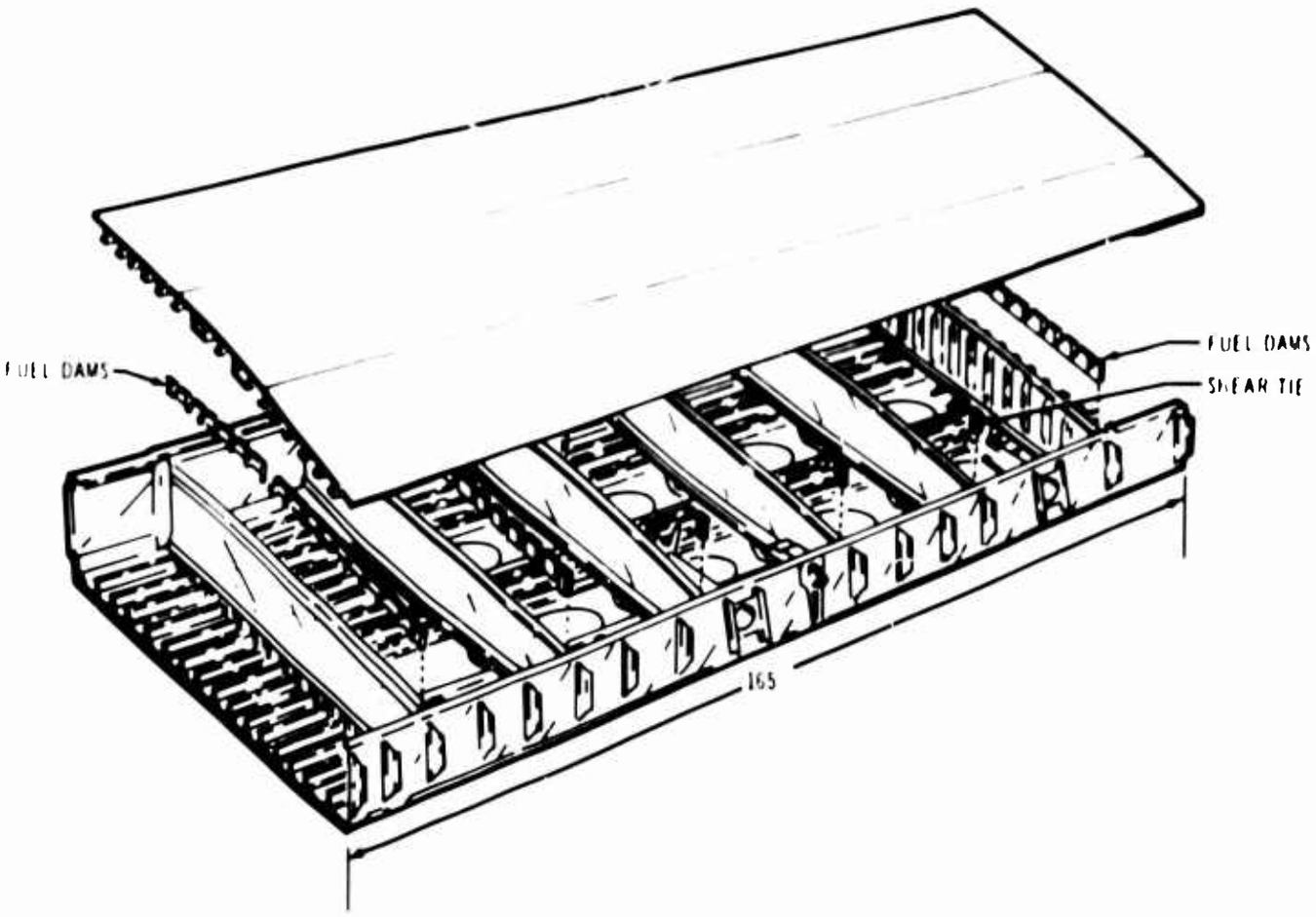


Figure 3-22. Wing Fatigue Box Test Section

with the time-temperature box test will provide very useful correlation data on failure locations and lives between realistic and accelerated type tests. This correlation data will be extremely important to assure that meaningful results are obtained from the full airplane test.

3.2.6 Fail-Safe Test — Panels

3.2.6.1 Program Objectives

A testing program to evaluate and verify fail-safe design for the wing lower surface is being conducted in three parts. In the first part a series of stiffened panels were tested to evaluate effects of stiffening ratios, stringer spacing, types of fasteners, fastener spacing, and stringer loads on crack growth rates and ultimate fracture strength. Test results were used for development of new design techniques and analysis methods and to provide experimental data for correlation of modifications of existing theoretical analysis. In the second part, fail-safe panels of the selected prototype material and design configurations will be tested to verify the designs. The third part of the program is a series of fail-safe tests for a variety of damage configurations on a full-scale test box. The details of this test program are given in Par. 3.2.7.

3.2.6.2 Description of Test Panels

The initial test configurations were simple skin panels of either Ti 8-1-1 or Ti 6Al-4V material stiffened by straps or zee stringers. Skin-to-stiffener attachments were either spotwelds or mechanical fasteners. Stiffener area ratios varied from 28 to 42 percent of the median section area. In general, the panel lengths were at least three times the panel width. The panel configurations are shown in Fig. 3-25 with the design parameters for these panels shown in Table 3-F.

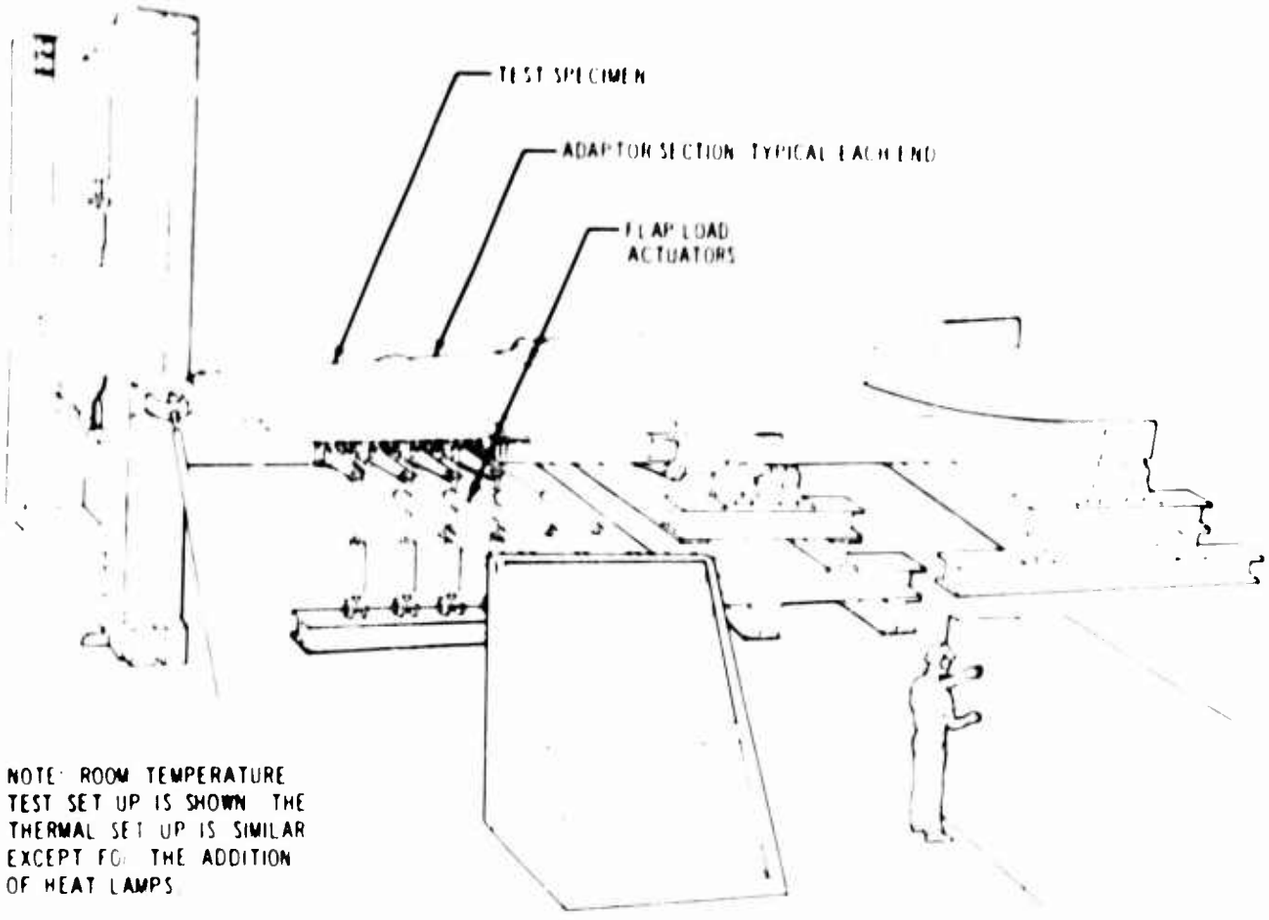


Figure 3-23. Wing Fatigue Box Test Set-Up

The test results from these panels were used to design the multiskin verification panels shown in Fig. 3-26. These panels have mechanically fastened Ti 6Al-4V skin and stiffeners and incorporate design parameters for fastener spacing, stiffener spacing and area ratio. Tests on these specimens are scheduled to begin in August, 1966.

3.2.6.3 Testing Procedure and Results

The panels were strain gaged to obtain data on stress distribution within the panel, local fastener loads, and stringer loads as cracks were extended to desired test length. High-speed recordings were used to obtain strain measurements for ultimate residual strength tests. For all panels, fatigue cracks were produced from starter cracks by fatigue cycling. Upon completion of crack extension, some panels were statically loaded to failure. Other panels were repaired in order to conduct additional tests.

The crack growth histories of the strap reinforced panels (I and II) are shown by Fig. 3-27. During fatigue cycling of the smaller strap area panel, a fatigue crack was initiated in the strap at the first spotweld away from the skin crack and complete strap failure occurred after 6,945 cycles. A fractographic examination of the larger area straps, after the static test of the panel, showed that a fatigue crack had also initiated on the center strap but had not grown completely through the straps before the static test was conducted.

The crack growth histories of Panels IIIa and IIIb are shown by Fig. 3-28. The Type III panels are zee-stiffened panels having the same stiffening ratio as the Type II strap reinforced panel. Panel IIIa had spotwelded skin stiffener attachments and IIIb had mechanical fasteners. The skin flange of the center stringer on Panel IIIa

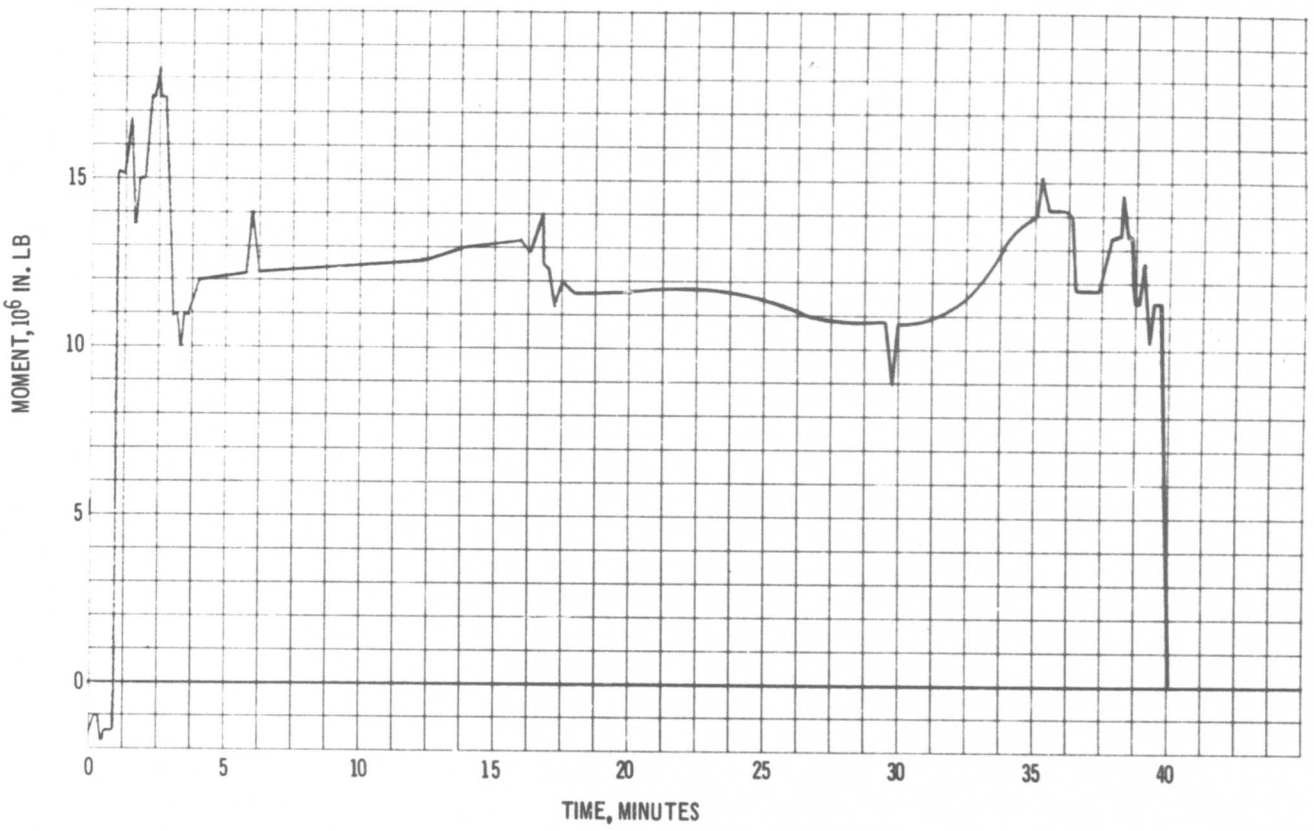


Figure 3-24. Fatigue Box Bending Moments

developed a fatigue crack at the edge of the first spotweld away from the skin crack. This crack was detected at a crack length of 5.92 in. The stringer was completely severed by sawcutting and cycling was continued at a reduced stress level to obtain growth data for a broken stringer configuration. Cyclic testing was discontinued after the crack had been extended to a length of 7.0 in. and the panel was statically loaded to failure. The skin crack in Panel IIIb was extended to 10.9 in. at 35-ksi maximum gross area stress without detectable fatigue damage to the center stringer. The damaged area of the panel is shown in Fig. 3-29 and the test setup in Fig. 1-5. Following the cyclic testing an ultimate load test was conducted. From the crack growth history curve, it is apparent that spotwelded structure tends to retard crack growth better than bolted structure; however, the fatigue life of the remaining intact spotweld structure is reduced below an acceptable level.

The crack growth rate histories of Panel I, II, IIIa, and IIIb are shown in Fig. 3-30. The crack growth rate of the spotwelded panels show very good agreement. Panel IIIb data shows the faster growth rate of the bolted structure. Analytical methods are being adjusted to account for this effect.

The comparison of predicted versus measured failure loads for the first four panels are shown by Fig. 3-31. Predicted loads are based on company-developed analysis methods for residual strength of damaged structure. The predictions are in good agreement with test results.

Panels IVa and IVb were tested as fatigue specimens prior to being used as fail-safe panels. After completion of fatigue testing (par. 3.6) the panels were modified for use as fail-safe panels. In general, the crack growth rates for these panels were higher than experienced for

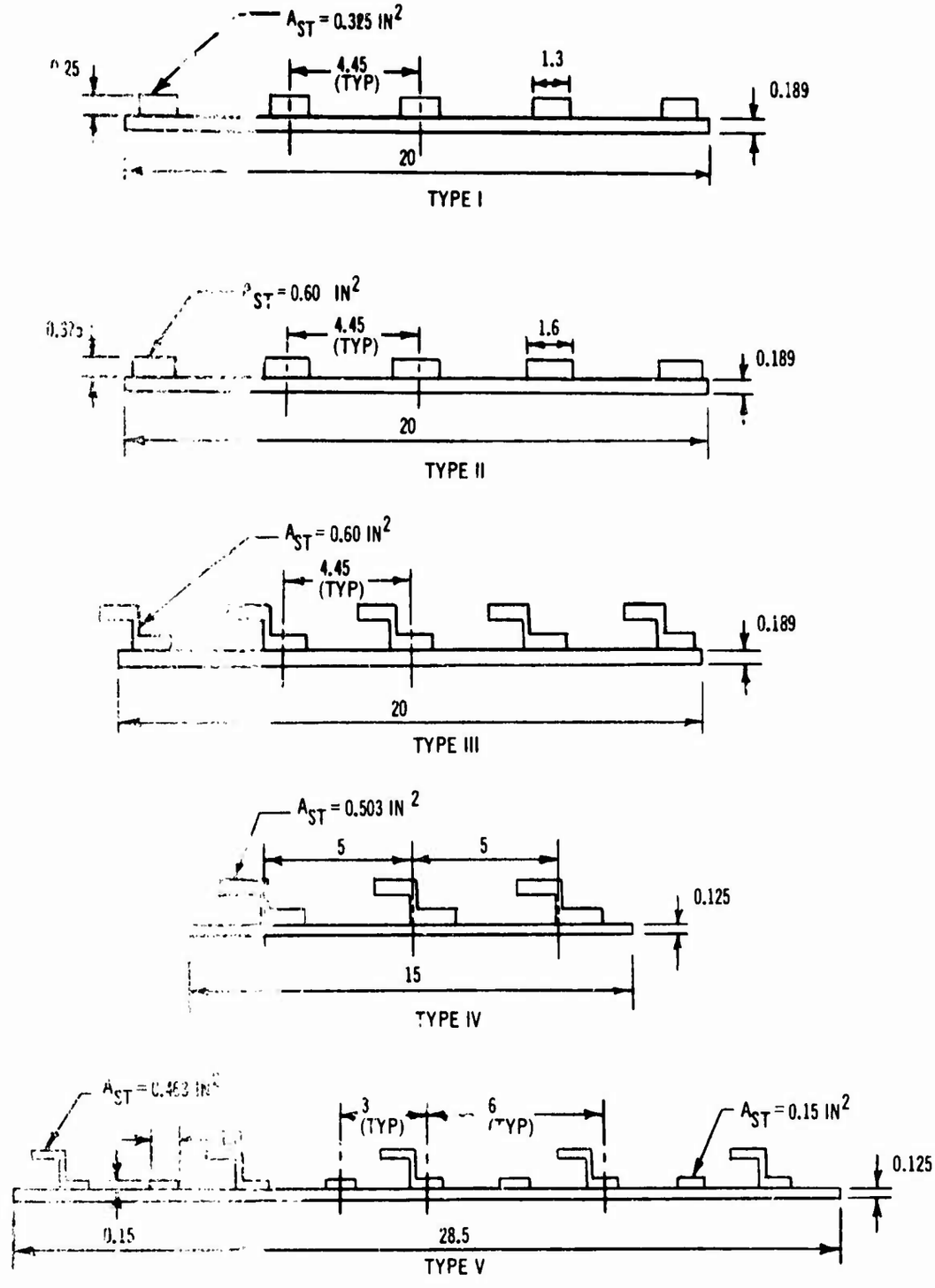


Figure 3-25. Fail-Safe Test Panels

Table 3-F. Panel Details

Panel Type	Skin Material	Stiffener Material	Fasteners & Spacing	Skin-Stiff Area Ratio%	Initial Damage	Maximum Cyclic Stress
I	TI 8-1-1 DA	TI 8-1-1 DA	Spotwelds at 1.5	70-30	Sawcut in skin only	35 ksi
II	TI 8-1-1 DA	TI 8-1-1 DA	Spotwelds at 1.5	56-44	Sawcut in skin only	35 ksi
III a	TI 8-1-1 DA	TI 8-1-1 Mill Anneal Extrusion	Spotwelds at 1.5	58-42	Sawcut in skin only	35 ksi
III b	TI 8-1-1 DA	TI 8-1-1 Mill Anneal Extrusion	Countersunk Lockbolts at 2.0	55-45	Sawcut in skin only	35 ksi
IV a	TI 8-1-1 DA	TI 8-1-1 Mill Anneal Extrusion	Spotwelds at 1.15	55-45	Sawcut Stiffener and skin	20 ksi
IV b	TI 8-1-1 DA	TI 8-1-1 Mill Anneal Extrusion	Hi-Loks at 1.5	55-45	Sawcut Stiffener only	20 ksi
V	TI 6-4 Condition III	TI 8-1-1 Strap Mill Anneal Extrusion TI 6-4 Cond. III	Countersunk Lockbolts at 1.5	54-46	Sawcut; skin skin & Stiff skin & Part Stiff	35 ksi 25, 40 ksi 40 ksi

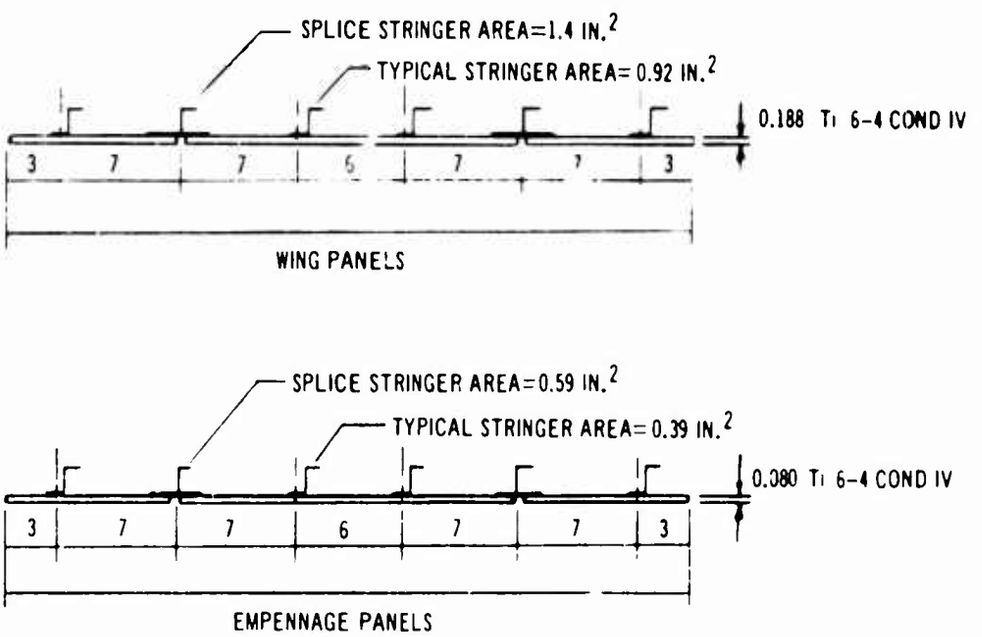


Figure 3-26. Fail-Safe Verification Test Panels

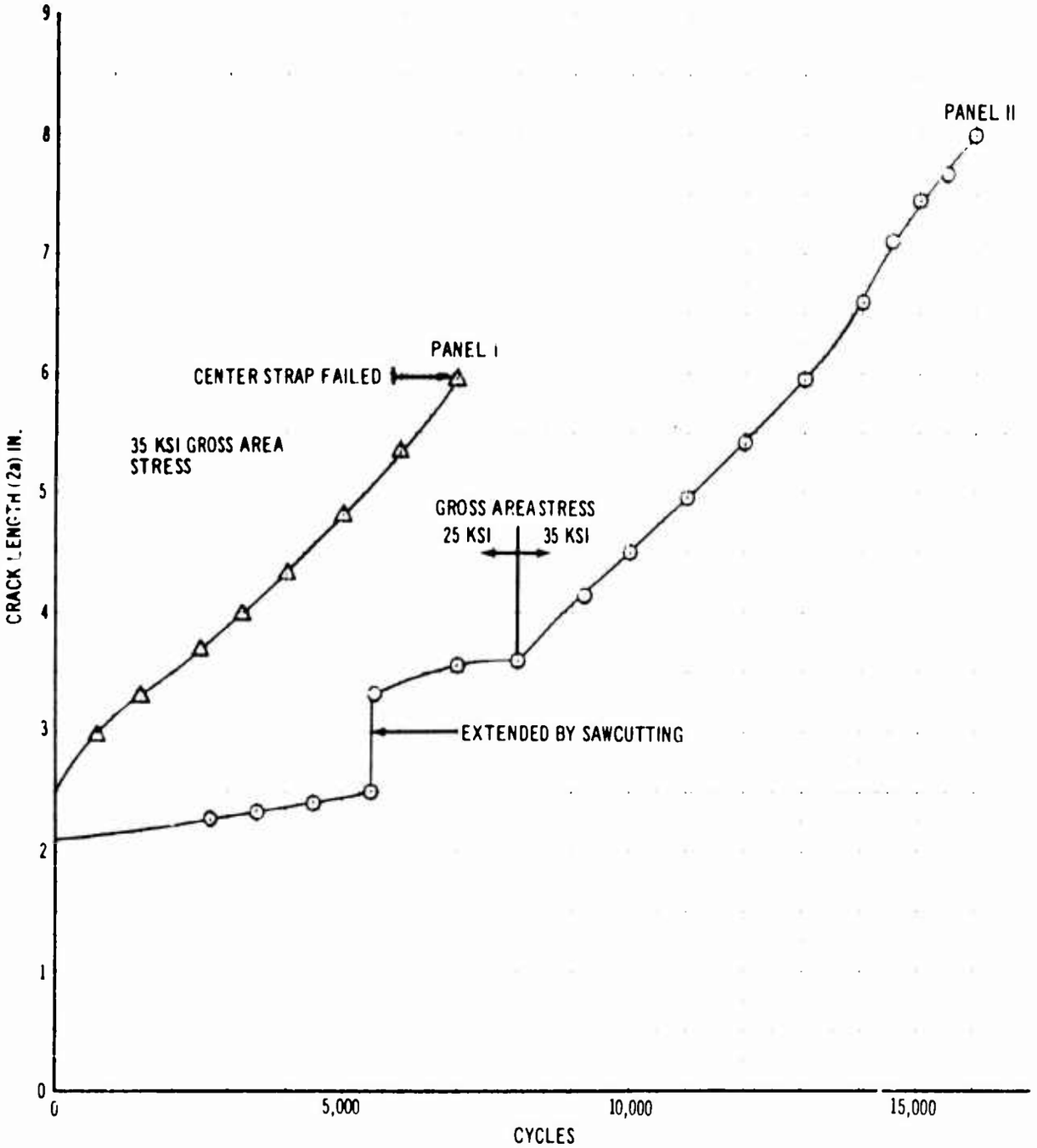


Figure 3-27. Crack Growth History – Panels I and II

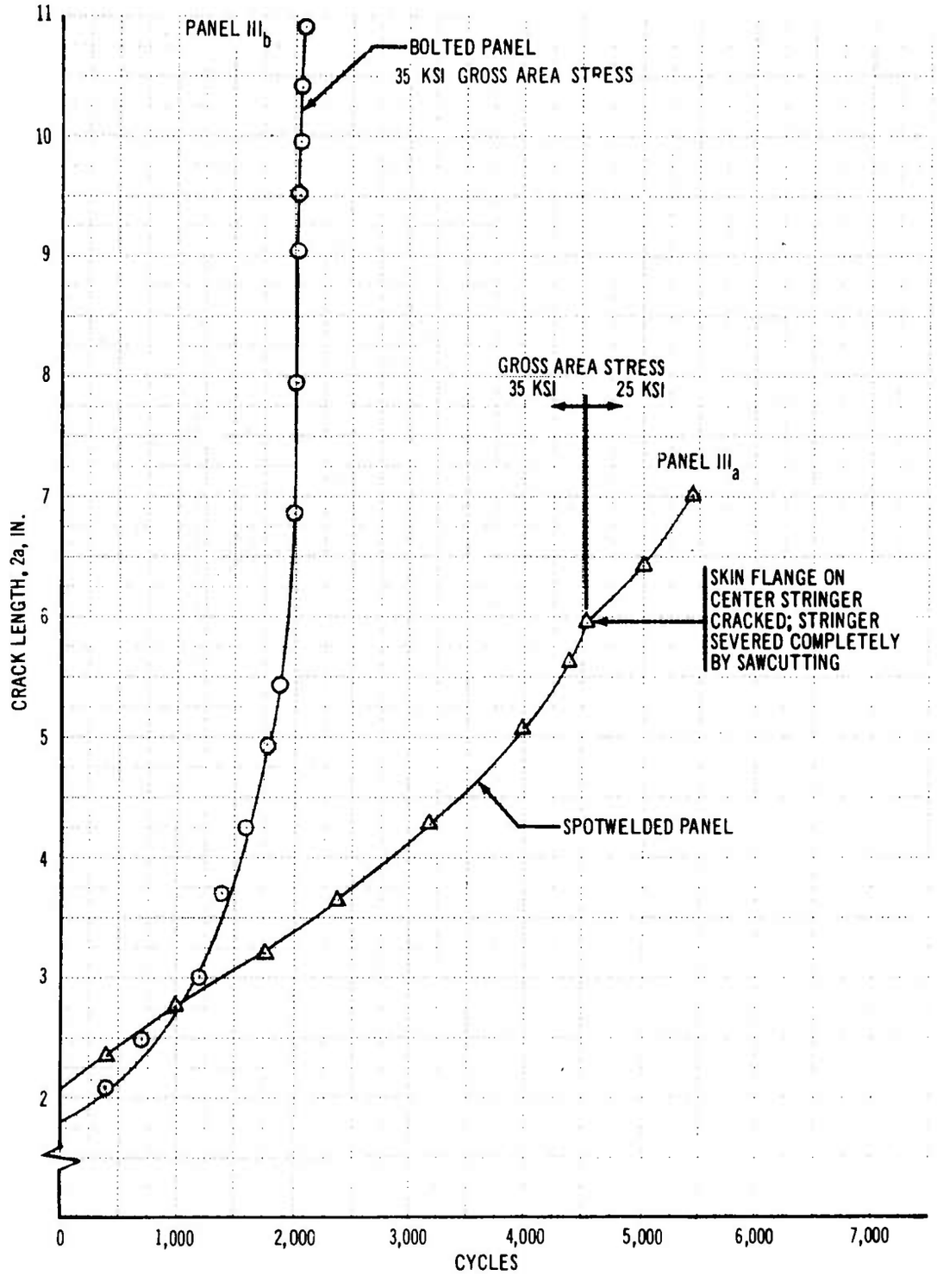


Figure 3-28. Crack Growth History – Panels IIIa and IIIb

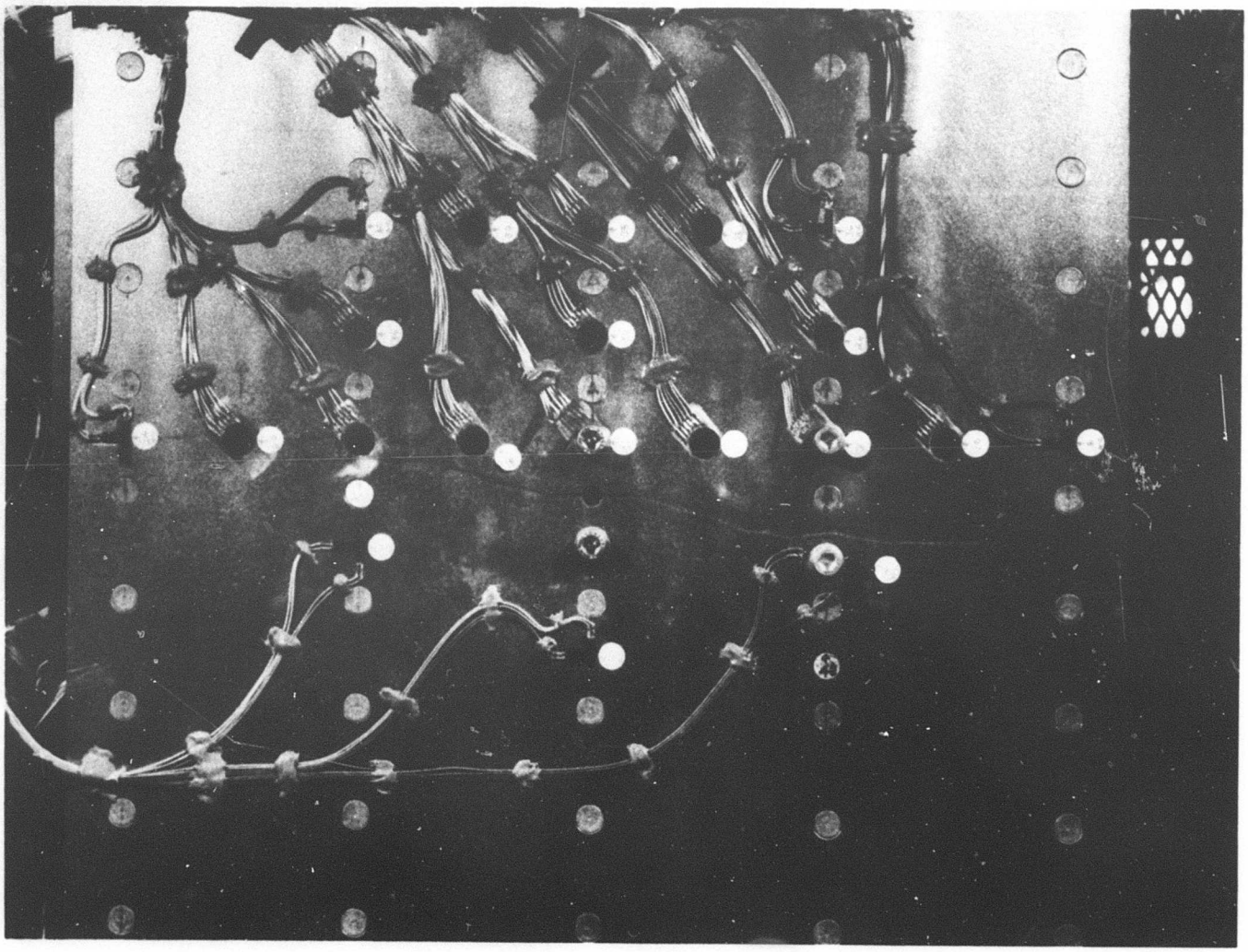


Figure 3-29. Panel IIIb Damage

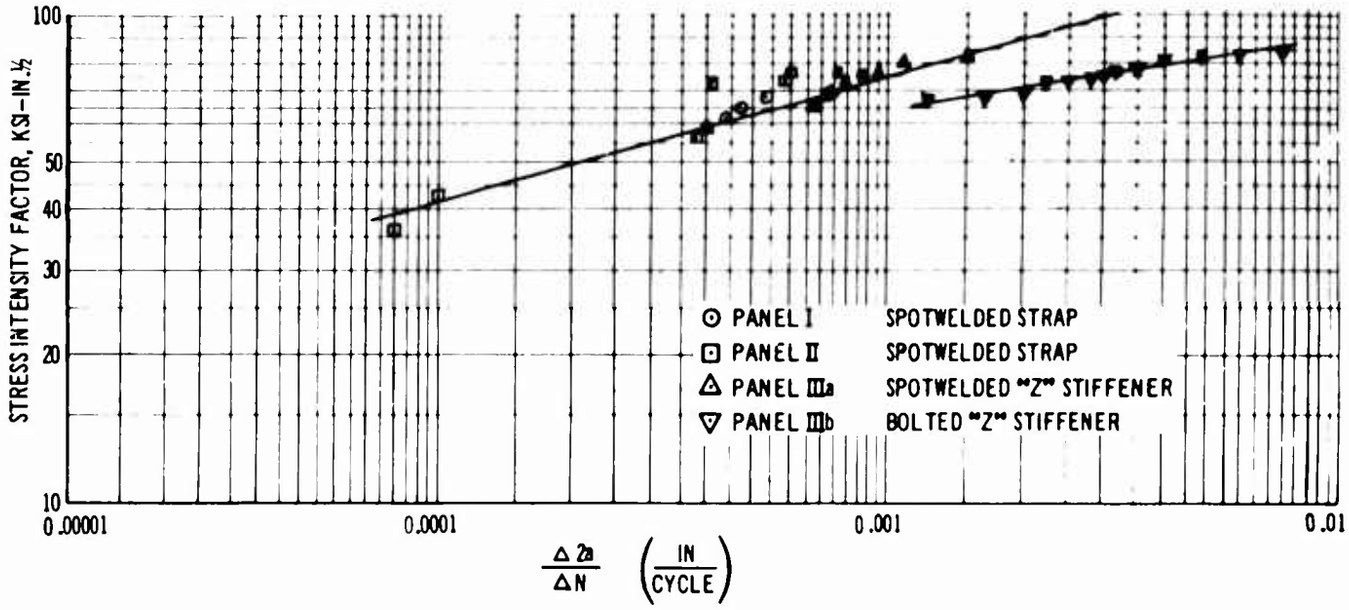


Figure 3-30. Crack Growth Rates Data – Panels I thru IIIb

other panels. Additional testing is required to determine the effects of prior fatigue history on crack growth rates.

The crack growth history of Panel IVa is shown by Fig. 3-32. The center stringer was severed completely and an initial skin crack was installed by sawcutting. The panel was cycled at a maximum gross area stress of 20 ksi in extending the crack to the adjacent stringers to obtain crack growth rate data shown by Fig. 3-33.

The center stringer of panel IVb was cut at a fastener location and the panel was cycled at a maximum gross area stress of 40 ksi. After 5,600 cycles, a crack was produced on one side of the fastener hole location at the cut in the stringer. During the next five cycles, a previously undetected crack at the first fastener hole from the end of the cut stringer grew to a length of 10 in.

The crack growth history of the tests conducted on Panel V are shown in Fig. 3-34 and Fig. 3-35 gives the crack growth rate data. The panel was designed to evaluate the effect of placing some of the stiffening area in straps between the stringers. The total stiffening ratio was the same as used for the other zee-stiffened panels. The first test was conducted with a sawcut in the skin only at the center stringer. At 7,200 cycles of 35-ksi maximum gross area stress, one crack tip grew into a fastener hole at the adjacent strap. No additional growth occurred on that side during the remainder of the test. The other side of the crack grew between the fasteners, but growth was retarded at each stiffening member. Testing was discontinued at a total crack length of 9.87 in. The panel was repaired, a stringer was completely cut, and a sawcut was installed in the skin for the next test. The panel was cycled at a maximum gross area stress of 25 ksi. At 4,800 cycles both crack tips had grown into fastener holes at the adjacent straps. After approximately 1,000 additional cycles at 25 ksi had produced no detectable growth from either end of the crack, the maximum stress level was increased to 40 ksi. A crack was initiated at the fastener hole on the left side after 373 cycles at the higher stress level and extended to a fastener hole at the adjacent stringer after 460 cycles. No additional growth was initiated at the other fastener hole and the test was discontinued. The panel was again repaired and a sawcut was made in the skin and skin flange of the stringer at a fastener location. The panel was cycled at a maximum gross area stress of 40 ksi. At a crack length of 10.9 in., the partially severed stringer failed.

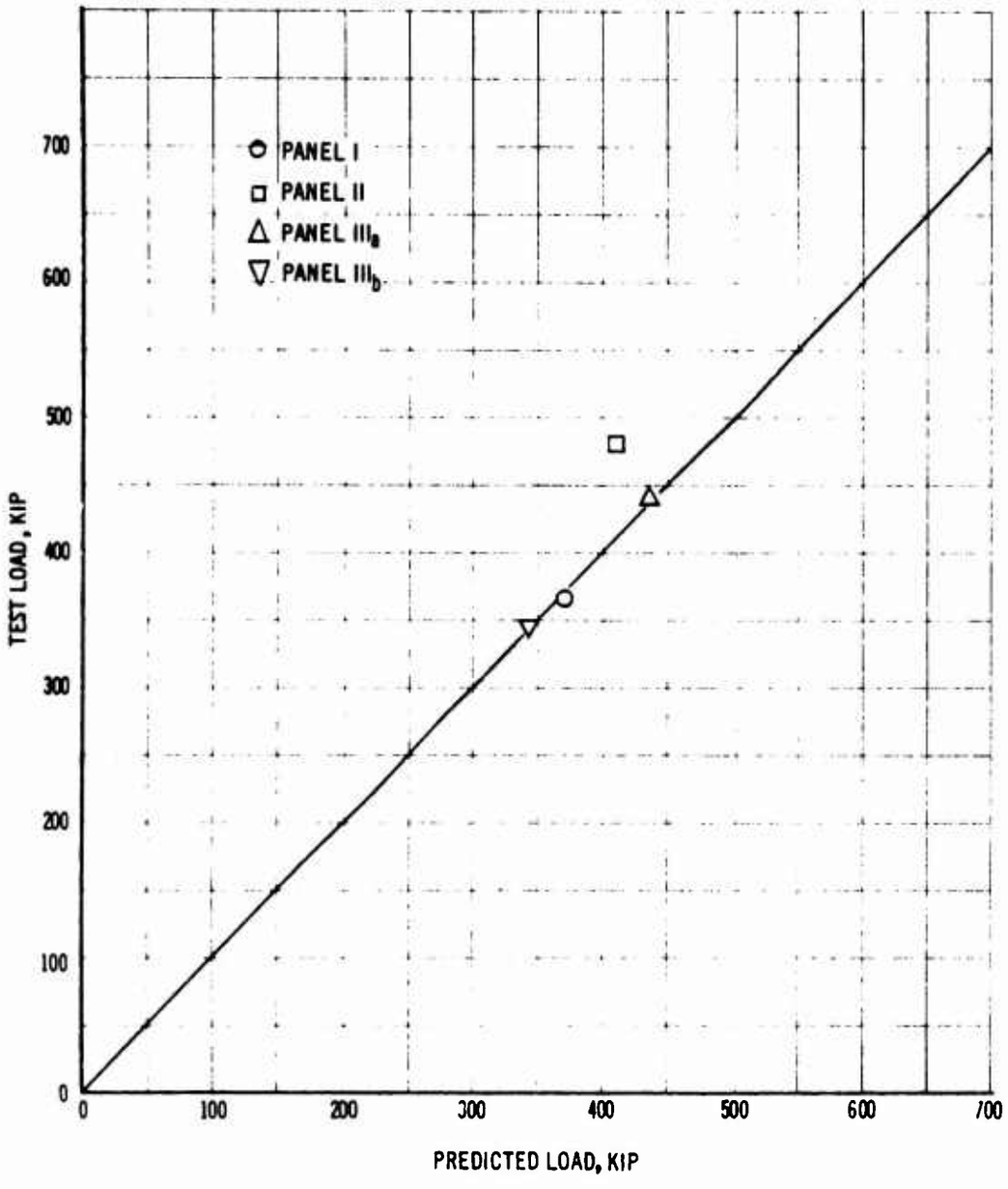


Figure 3-31. Test Versus Predicted Ultimate Fracture Loads

The ultimate strength tests have demonstrated that analysis methods can accurately predict the residual strength of damaged composite structure. The good correlation of growth rate data presented as a function of stress intensity factor indicates that reliable predictions of remaining life of damaged structure can be made.

3.2.7 Fail-Safe Tests — Wing Box

3.2.7.1 Program Objectives

The purpose of this test program is to demonstrate the ability of the full-scale wing structure to sustain design fail-safe loads after failure of various structural members.

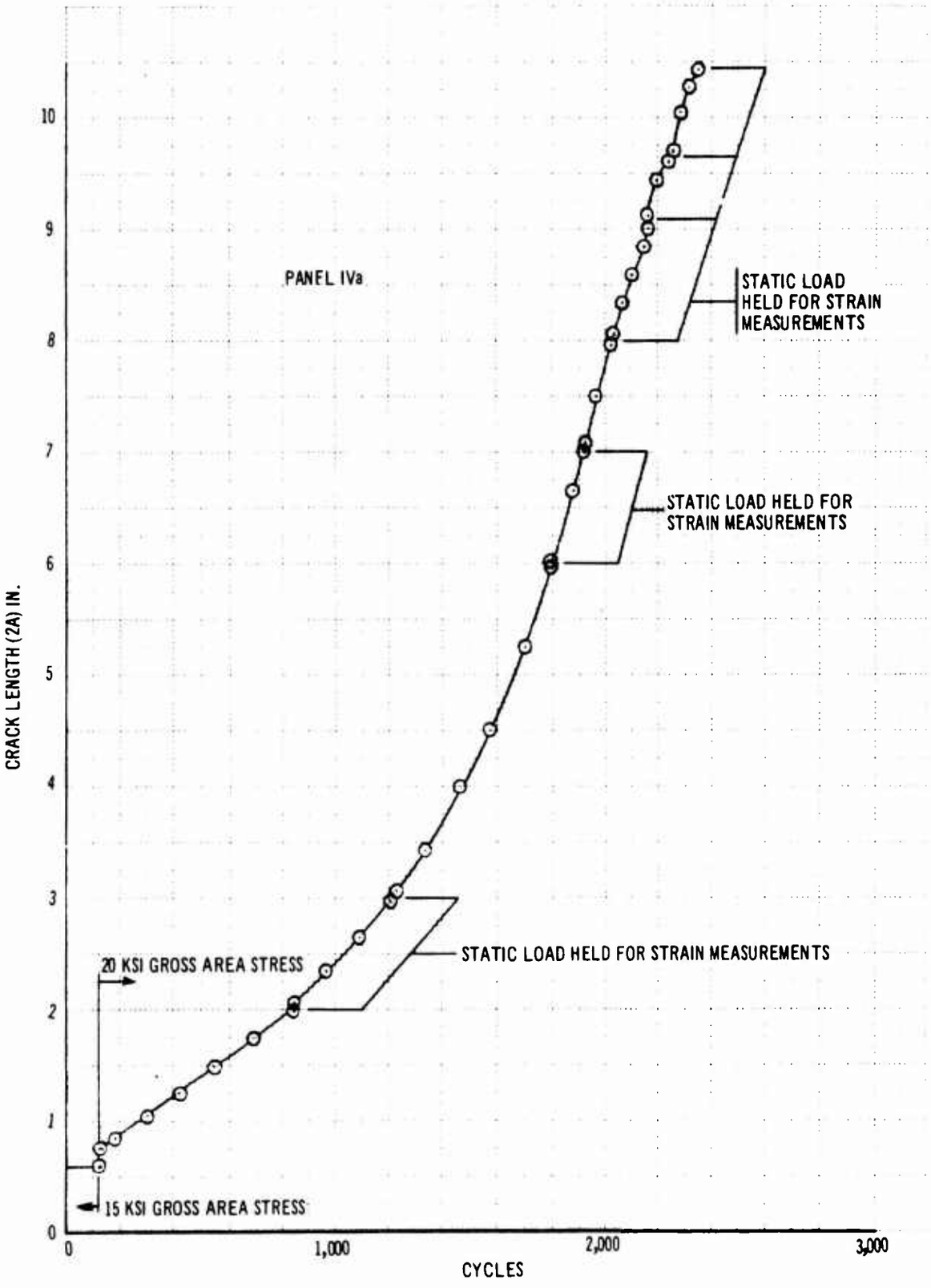


Figure 3-32. Crack Growth History – Panel IVa

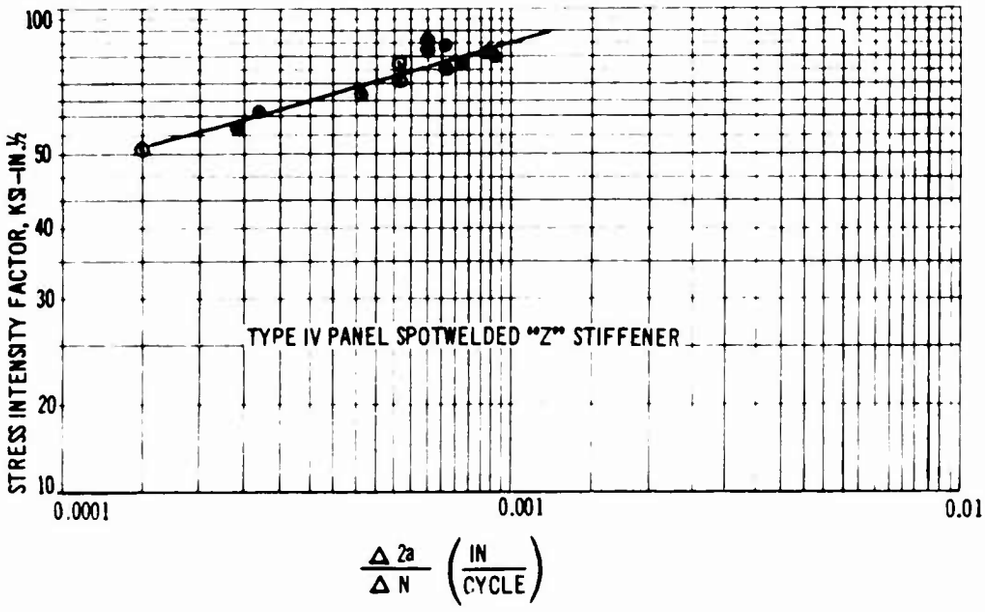


Figure 3-33. Crack Growth Rate Data – Panel IVa

3.2.7.2 Description of Test Section
After completion of the full-scale Ti 8-1-1 wing box test program described in Par. 3.2.4, a new Ti 6Al-4V fail-safe designed lower surface was installed on the box. This test program will utilize the existing test jig modified for fail-safe loading requirements. The fail-safe lower surface consists of three extruded zee-stiffened panels fabricated from Ti 6-4 Condition IV material joined by longitudinal splice stringers as shown in Fig. 3-36. Taper-Lok fasteners are used for skin splicing and attachment of skin and stringers. The structural arrangement of the test surface is representative of the B-2707 outboard wing tension structure which uses both Taper-Lok fasteners and squeezed rivets. The skin and stringers are instrumented so that stress levels and load transfer characteristics may be determined for the various test conditions.

3.2.7.3 Test Program
Crack growth and fail-safe verification loading tests will be conducted for various types of structural damage. A summary of damage to be tested for is given by Table 3-G. The testing procedure for each indicated location is given in the following paragraphs. A starter crack is installed in the structure and extended by cyclic loading producing either a one factor stress condition or stresses associated with an average flight. The crack length and stress distribution are continually monitored while the crack is being extended to the required test length. At various intervals of crack extension a static fail-safe load of 0.8 design limit load is applied. After completion of testing at one location the damage area is repaired and testing of a different damage configuration is started.

All testing is done at room temperature. The ultimate fracture strength of Ti 6-4 is higher at elevated temperatures than at room temperature. Also the ratio of ultimate fracture strength to operating stress level is larger for the elevated temperature conditions. For these reasons, room temperature tests result in more critical fracture conditions than elevated temperature tests and thus represent the critical test condition.

3.2.7.4 Initial testing of the center panel is in progress. A 2-in. saw cut at a fastener hole was extended to 10 in. in 12,000 cycles of simulated airplane loading of 30 Ksi to -15 Ksi. Crack extension from 10 to 12.88 in. was obtained from a fail-safe loading of 61 Ksi gross stress. The crack has been extended to 20.5 in. by fatigue cycling.

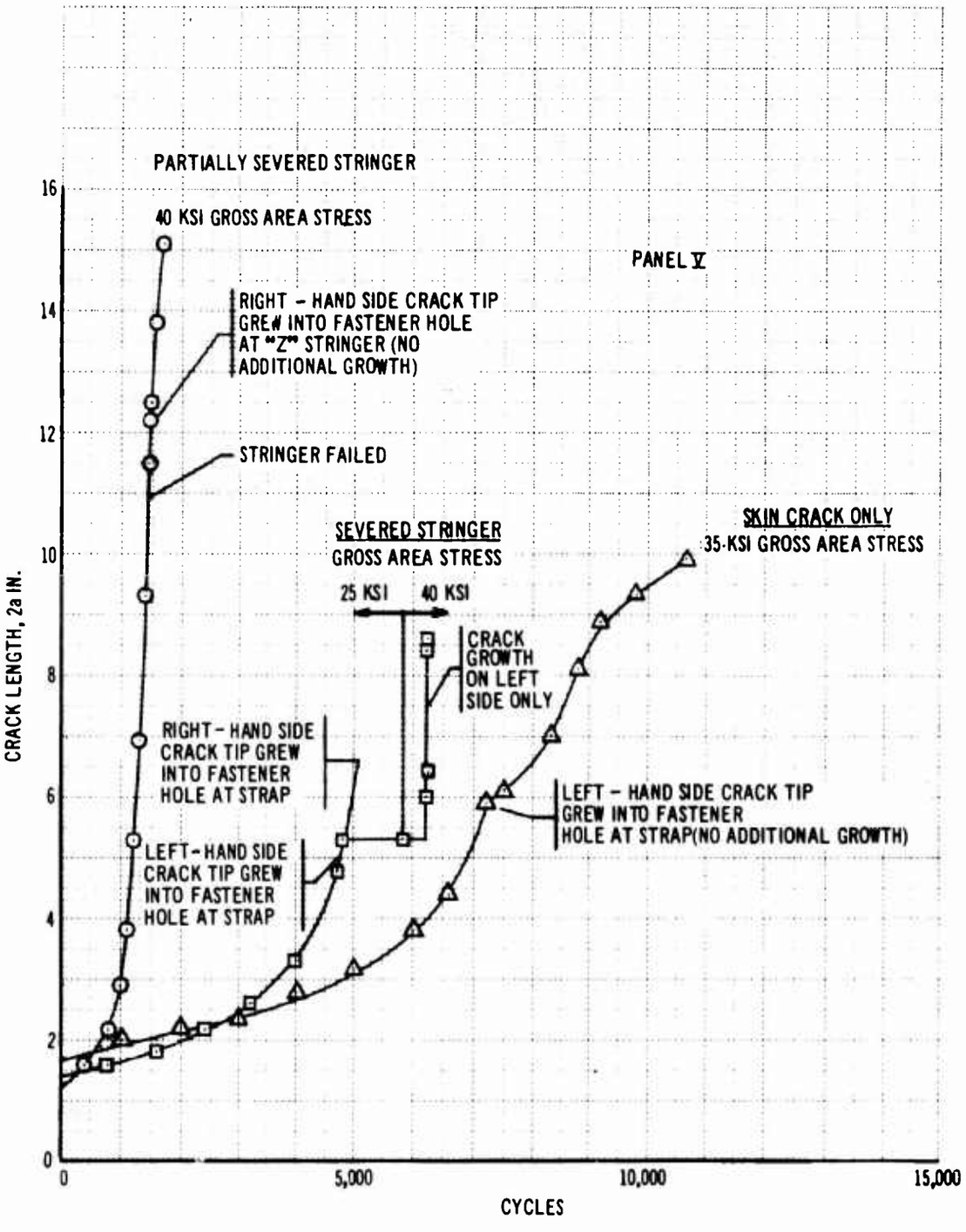


Figure 3-34. Crack Growth History – Panel V

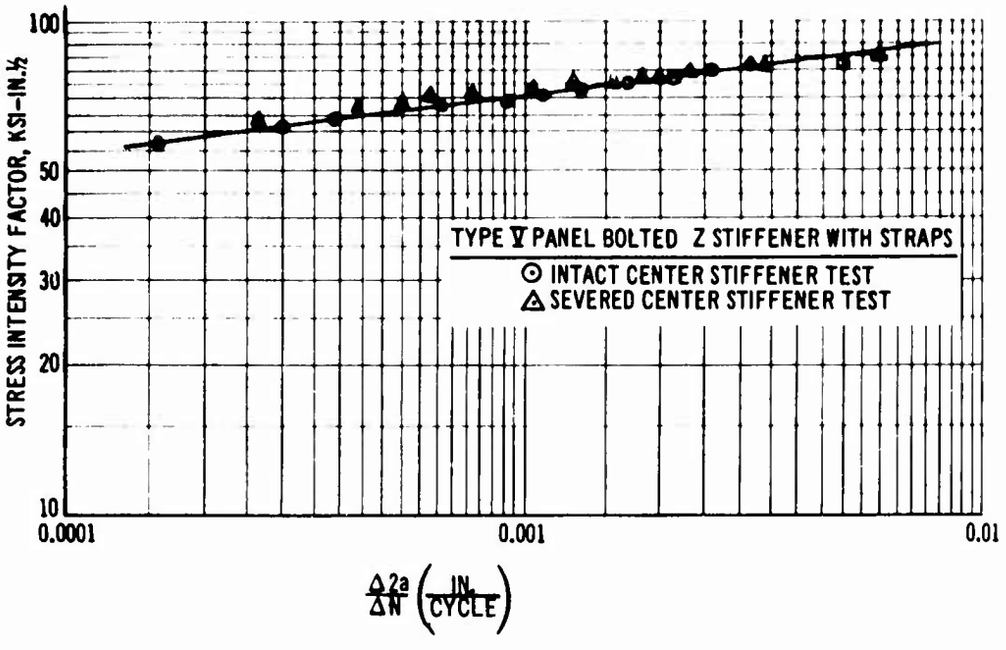


Figure 3-35. Crack Growth Rate Data – Panel V

3.2.8 Wing Spar Test

A test program has been conducted on a full-scale section of a wing spar to evaluate design concepts and analysis methods.

The test spar was a Ti 8-1-1 0.090 gage stiffened web beam having both formed and extruded stiffeners. Upper and lower chords were identical such that the beam was vertically symmetrical. One end of the beam contained an access door designed for shear loadings. The spar was supported at the ends by pin joints and one end was free to translate in the horizontal direction to allow thermal expansion. Test loads were applied at the centerline of the spar and reacted at the ends. Radiant heat lamps were used for heating during elevated temperature tests. The spar and test setup is shown in Fig. 1-7.

The first test demonstrated the feasibility of using spar access doors for ground maintenance without requiring special jacking procedures. A one-factor dead weight spar load was applied and while the spar was under load the access door was removed and reinstalled without difficulty.

The next series of tests were conducted at room temperature to obtain data on stress distributions for increment loadings up to limit design load. The access door was installed with the bolts tightened per recommended torque values for this test.

Following this test the spar was loaded to approximately 90 percent of limit load with the access door bolts installed finger tight.

Elevated temperature tests were conducted to determine thermal gradient stresses in the spar and to evaluate mechanical stress distribution in combination with thermal gradient stresses. In these tests the spar chords were heated to 500°F and a maximum temperature gradient of 350°F was obtained between spar chords and the spar web. Thermal strains were obtained initially for an unloaded condition and then for a loaded condition. Following this initial survey of thermal and mechanical strains an additional elevated temperature test was conducted. A 40,000-lb center load was applied to the spar and after strain measurements were obtained the spar chords were heated to 500°F. After obtaining the desired temperature on the test section, the load was increased to 100,000 lb. The load was then reduced to 40,000 lb and the heat turned off. The spar was allowed to cool to room temperature before final load removal. Strain and temperature data were taken at various intervals throughout the test.

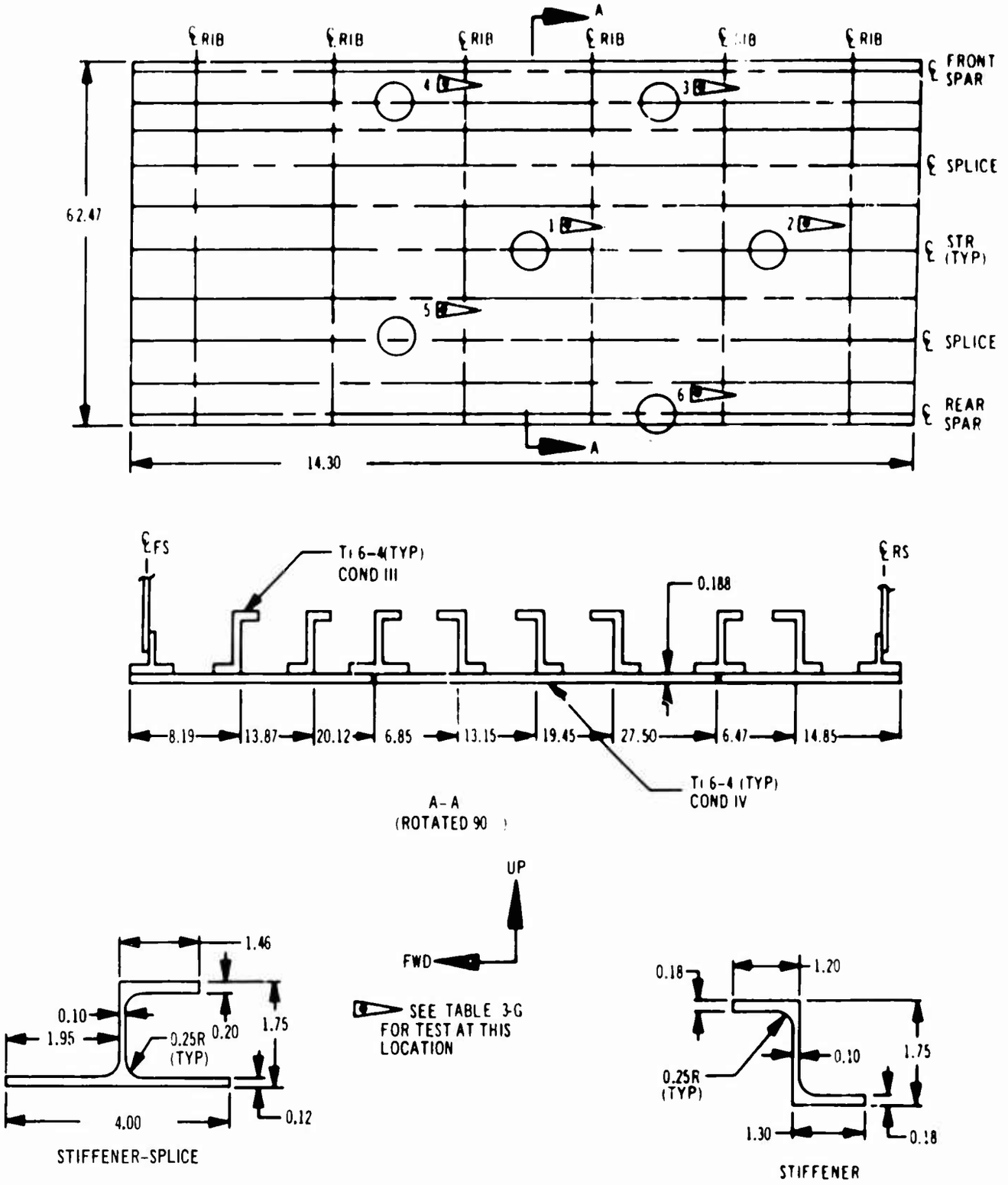


Figure 3-36. Lower Surface – Fail-Safe Test Box

Table 3-G. Fail-Safe Test Outline

CRACK GROWTH TESTS

Crack Location Ref Fig	Damage Configuration
1	Cracked skin with stringer intact
2	Cracked skin with broken stringer
3	Cracked skin with broken stringer
4	Cracked skin with stringer intact
5	Broken splice stringer with crack in one skin panel
6	Broken spar chord with cracked skin

An ultimate load destruction test was then conducted. At 89 percent of expected ultimate load the spotwelds fastening the web to stiffeners in one area of the spar failed. A repair was made by using bolts for the web to stiffener attachments. The beam was then loaded to destruction and failed at 112 percent of predicted ultimate load. Figure 3-37 shows the beam at approximately 85 percent of ultimate load.

The test results provided data for web and stiffener requirements, thermal strains, and ultimate web strengths for typical stiffened web beams. In general, the test results verified analysis methods for web strength and showed modification necessary for web stiffener analysis. Removal and reinstallation of access doors in spar members under one-factor dead weight load was demonstrated as not being a ground maintenance problem.

3.2.9 Corrugated Rib Test
A test program is to be conducted on corrugated rib panels to verify design allowables for shear and compressive strength.

The ribs have Ti 6Al-4V duplex annealed sine-wave corrugated webs welded to flat plate Ti 6Al-4V duplex annealed chords. A typical test rib is shown in Fig. 3-38. Details are given in Fig. 3-39. Web gages of 0.025 and 0.050 gage are included. The 0.025 gage panels were chem milled from 0.050 material.

Ribs of each web gage will be tested for shear alone, compression alone, and combined shear and compression. Initial tests will be for the single load conditions. In the combined loading tests a predetermined shear load will be applied and then compressive loading applied to failure. Panels will be tested for several different applied shear loadings.

Test data from this program will be used to verify design allowables for shear and compression and provide data for interaction relation of shear and compression. The panels are available for this program and testing is scheduled to begin in the near future.

3.3 FUSELAGE TESTS
The fuselage test program has included a large number of component specimens including compression panels, shear panels, and fail-safe panels. An extensive fail-safe development and verification test program has been conducted on a full-scale fuselage section. The cabin window design concept has been verified by ultimate load, fatigue, and fail-safe tests. A crew compartment section was designed and is being manufactured for testing in the follow-on period. This section will be used to verify the cab structure and windshields for pressure, thermal loading conditions, bird strikes, fatigue and fail-safe conditions.

Tests have been conducted at room and elevated temperatures where appropriate. Details of the individual tests are given in the following paragraphs.

3.3.1 Compression and Shear Tests
Test programs have been conducted to establish design allowables and substantiate analysis methods for fuselage compressive and shear structure. The results of these programs are given in Pars. 3.2.1 and 3.2.2.

3.3.2 Passenger Cabin Window Tests
A fatigue and fail-safe test program has been conducted to substantiate the fail-safe design concept of the multipane passenger cabin window. The test assembly was a structurally complete unit consisting of primary and fail-safe panes with supporting structure and skin panels similar to those of the Phase I design.

Details of the window are shown in Fig. 3-40, and the window and test fixture assembly by Fig. 3-41. The original window panes were designed as chemically-tempered glass with a

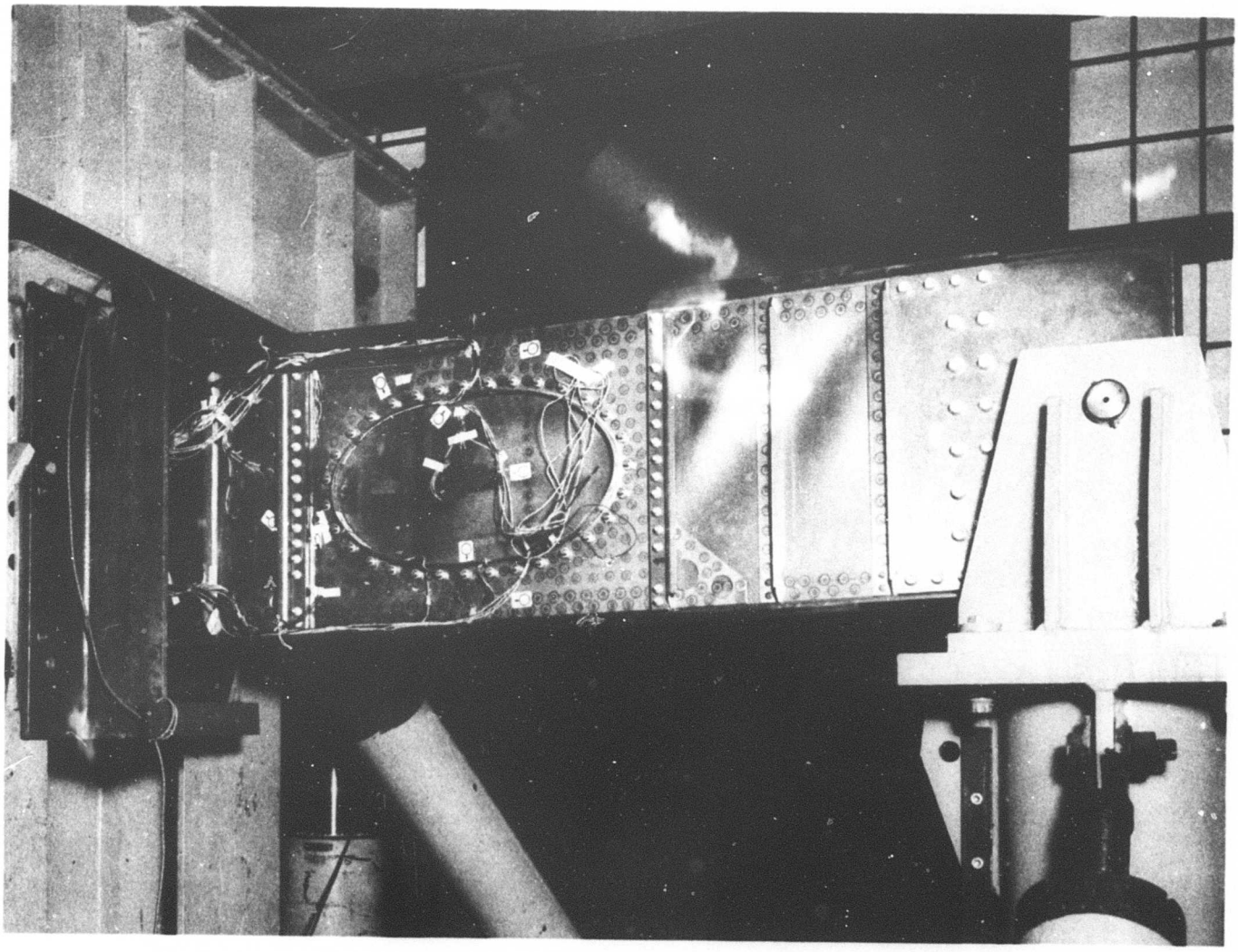


Figure 3-37. Wing Spar – Ultimate Load Test

test substitution of full-tempered soda-lime glass for the outer failsafe pane. The latest design for the passenger cabin windows (See Airframe Design Report — Part B, V2-B2707-6-2) uses a chemically tempered primary pressure pane with a fully tempered soda-lime failsafe pane. The glass combination for the units tested are identical with present design.

All testing was conducted at room temperature. For the exposure temperatures of the window unit, the coefficient of thermal expansion of glass and titanium are approximately the same. Therefore, relative elevated temperature conditions can be simulated with room temperature testing.

3.3.2.1 Ultimate Load and Fail-Safe Tests The ultimate load and fail-safe tests were conducted per the test outline given in the following sections. In the fail-safe tests the primary pressure pane was mechanically fractured such that the design pressure loading of 12 psi was dynamically imposed on the fail-safe pane. Tests simulate both small and large object damage. The required pressure differential across the primary pressure pane was verified by measurement of pressure between the window panes. There was no significant increase in the pressure between the window panes. The same outer fail-safe panel was used for the damage tests and the later fatigue tests. An ultimate pressure loading of 36 psi (3-factor pressure) was applied to the

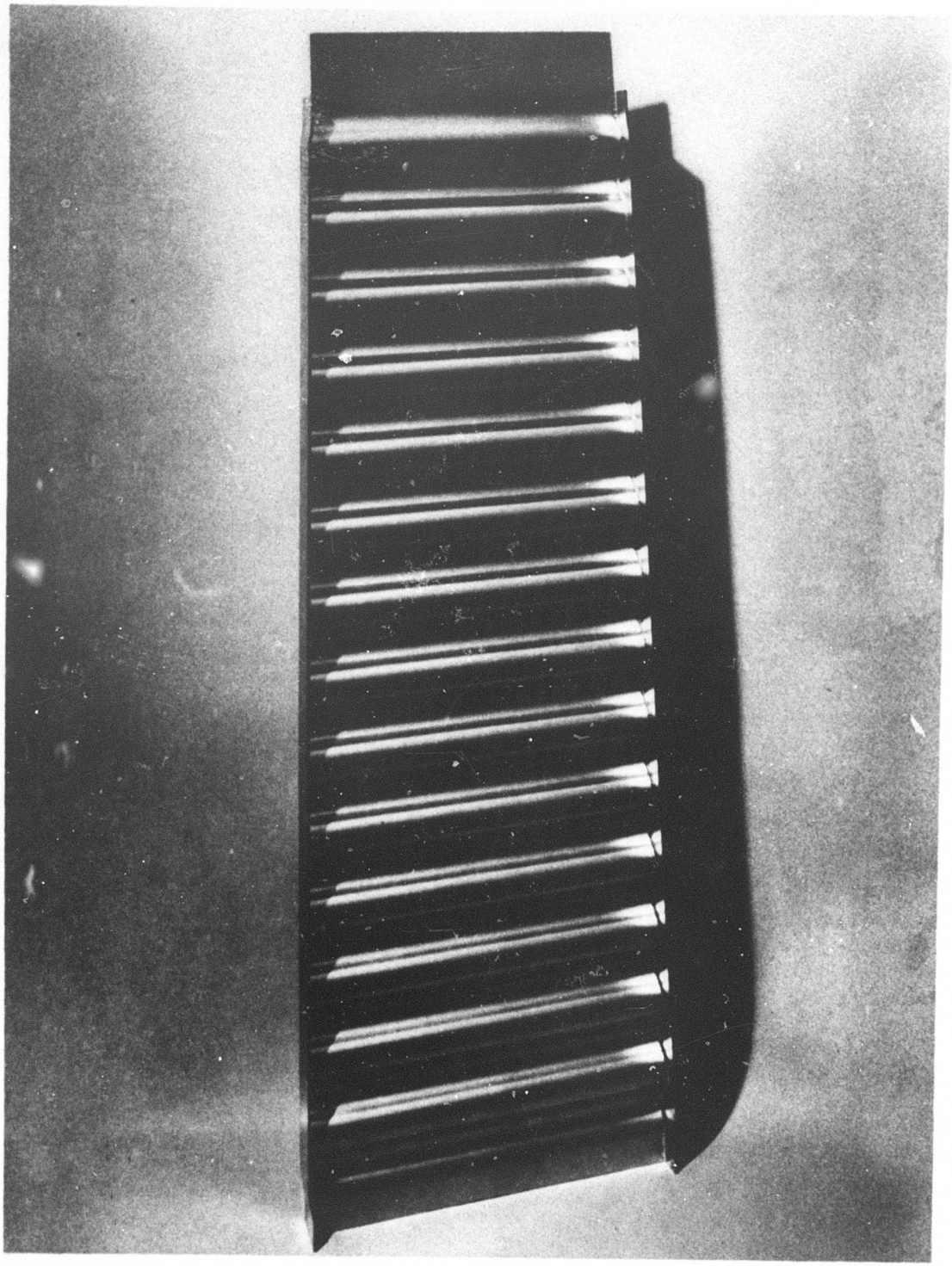


Figure 3-38. Corrugated Web Rib

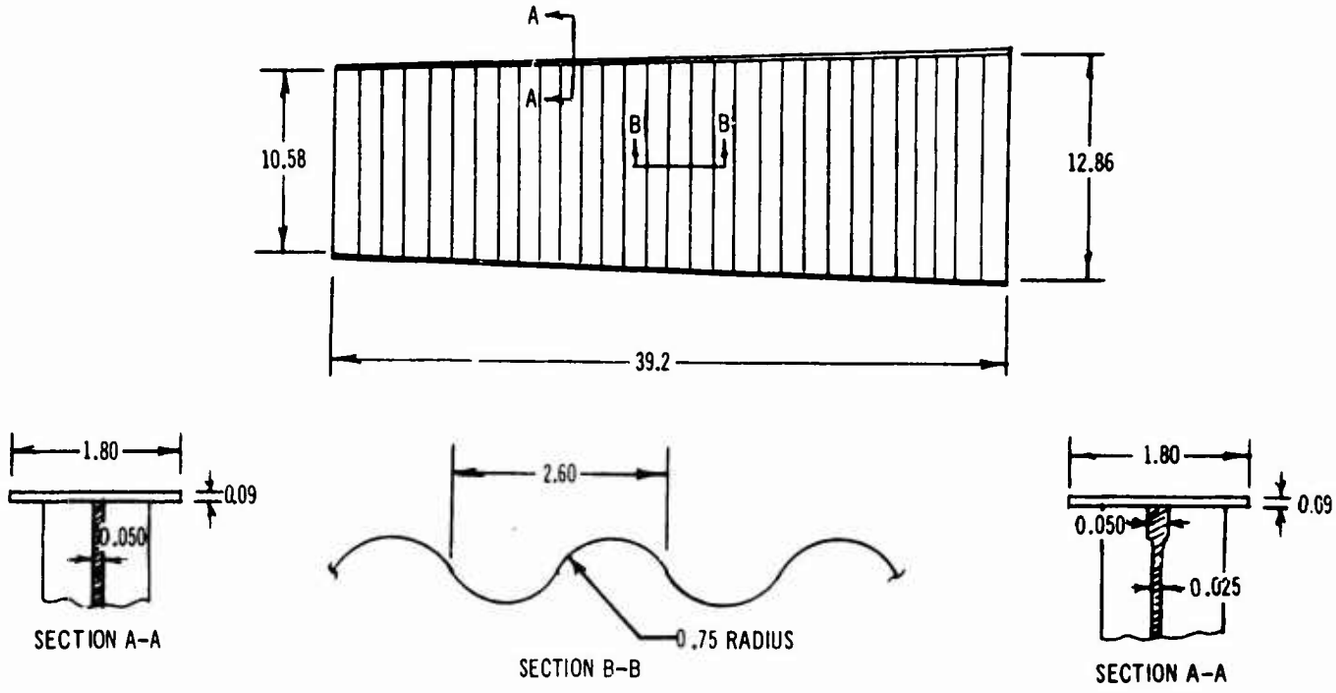


Figure 3-39. Panel Details

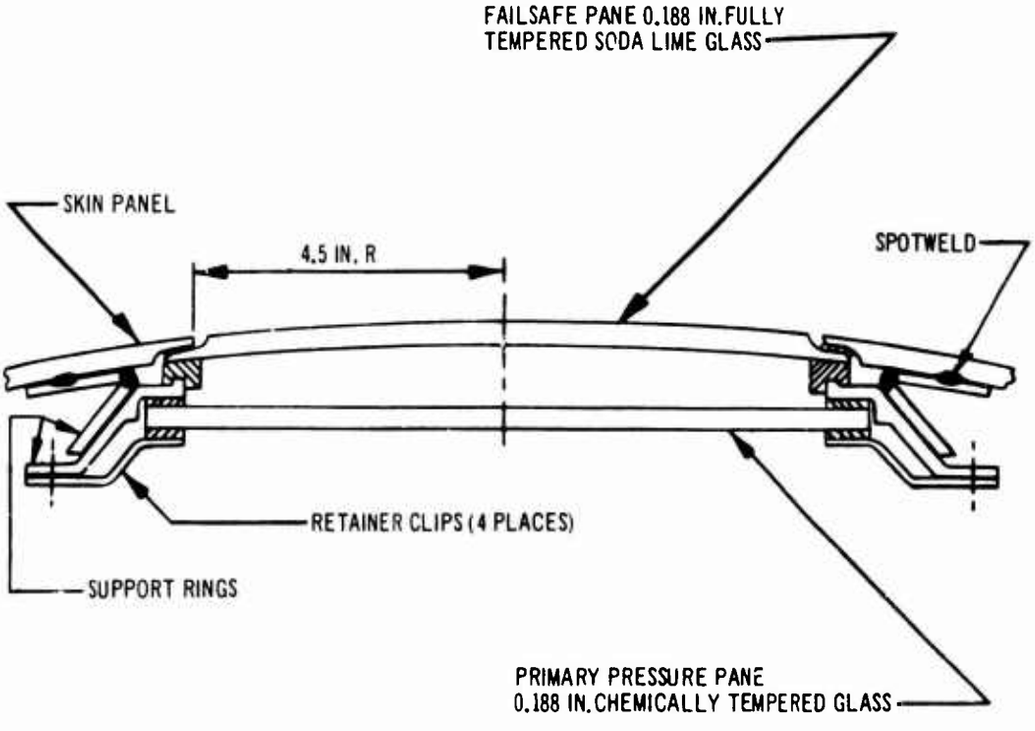


Figure 3-40. Passenger Cabin Window Details

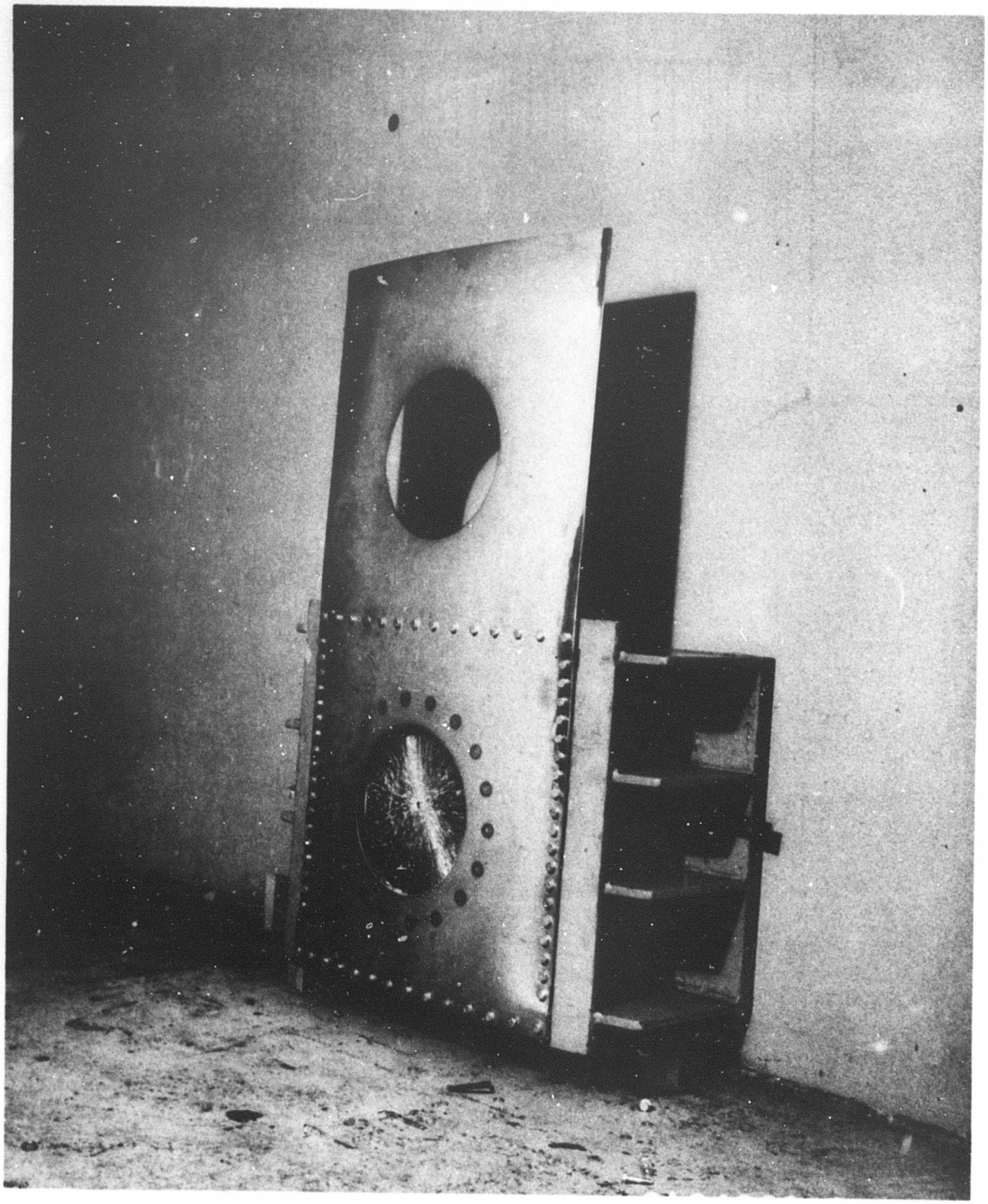


Figure 3-41. Test Fixture Assembly

primary pressure pane without incident. Fracture of the primary pressure panes for small and large object damage are shown in Figs. 3-42 and 3-43.

The small object damage testing was accomplished as follows:

a. Pressurize test box to 12 psig and maintain pressure for five minutes.

b. Instantaneously fail primary pressure pane.

c. Maintain pressure on fail-safe pane for two hours.

d. Increase pressure on fail-safe pane to 24 psig (2-factors pressure) and maintain pressure for one minute.

e. Remove pressure and inspect window for damage.

The ultimate load and large object damage testing procedures were as follows:

a. Pressurize test box to 36 psig with primary pressure pane intact and maintain pressure for five minutes.

b. Reduce pressure to 12 psig and maintain pressure for five minutes.

c. Instantaneously fail primary pressure pane.

d. Maintain pressure on fail-safe pane for one-half hour.

e. Increase pressure on fail-safe pane to 24 psi (2 factors pressure) and maintain pressure for one minute.

f. Remove pressure and inspect for damage.

3.3.2.2 Fatigue and Ultimate Strength Tests. Fatigue tests have been conducted on the passenger cabin window unit containing a damaged primary pressure pane. In the first test a scratch representative of readily detectable damage was installed on the inner surface of the primary pressure pane and the window unit was subjected to 1,050 pressure cycles at 12 psig maximum pressure without incident. To represent a severe surface damage condition, a second scratch approximately three times the depth of the first was installed and an additional 1,050 pressure cycles were applied. An additional test was conducted in which the scratch was on the outer surface of the primary pressure pane. This scratch was of the severe type and approximately twice the length of those of the first two tests. An additional 1,050 pressure cycles were applied without incident. The surface scratches for the three conditions tested are shown in Fig. 3-44. After completion of the cyclic load tests, an ultimate load test was conducted on the damaged pane. The damaged window pane failed at the ultimate design pressure loading of 36 psig.

3.3.2.3 Summary Passenger Cabin Window Tests. Test results are shown in the following paragraphs:

a. A 3 factor design ultimate load was sustained without failure.

b. Fail-safe tests for both small and large object damage were satisfactorally accomplished.

c. Fatigue tests on a deeply scratched pane were conducted without incident.

d. Follow on test demonstrated the scratch damaged pane good for ultimate design load.

The ultimate load, fail-safe, and fatigue tests substantiate that the window design meets the design objectives of the passenger cabin windows (See Airframe Design Report — Part C Structural Criteria, V2-B2707-7). The damaged primary pane fatigue tests far exceeded expectation. The number of pressure cycles applied was considerably greater than normal operating service would require for window panes as severely damaged as those of the test part.

3.3.3 Fuselage Fail-Safe — Flat Panels. Three tests were conducted on a panel representative of upper fuselage structure to evaluate the crack growth characteristics of light-gage structure under various fatigue damage conditions. Future tests are planned to verify body fail-safe design criteria.

The panel, 23-in. wide, had five formed hat section stiffeners riveted at 5 in. spacing. Skin and stiffeners were made of .045 gage Ti 6-4 Condition I. Two additional panels are being fabricated for further verification of fuselage structure. These panels are 36-in. wide with seven formed hat section stiffeners riveted at 5-in. spacing to 0.040 gage Ti 6-4 Condition I material.

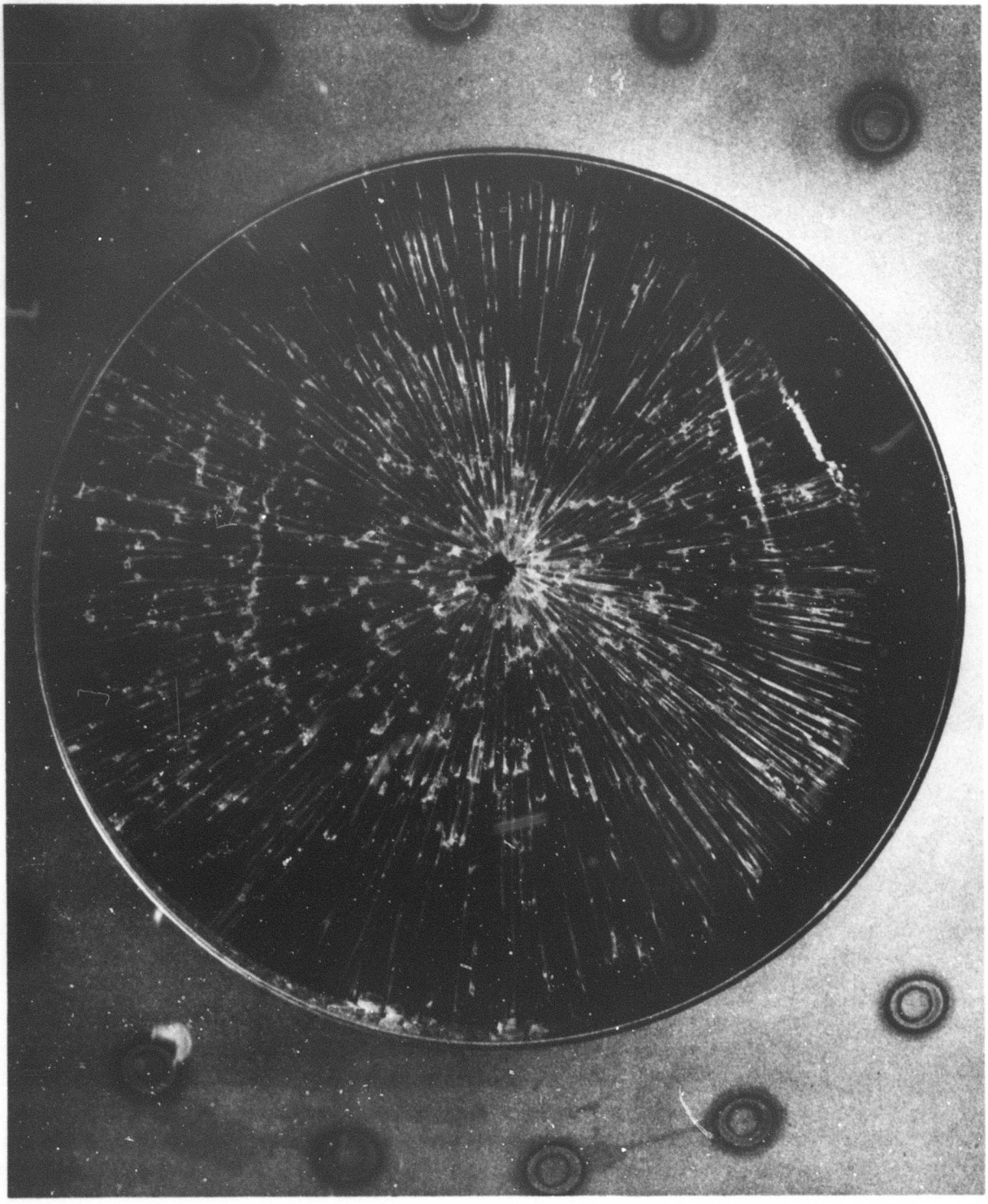


Figure 3-42. Small Object Damage

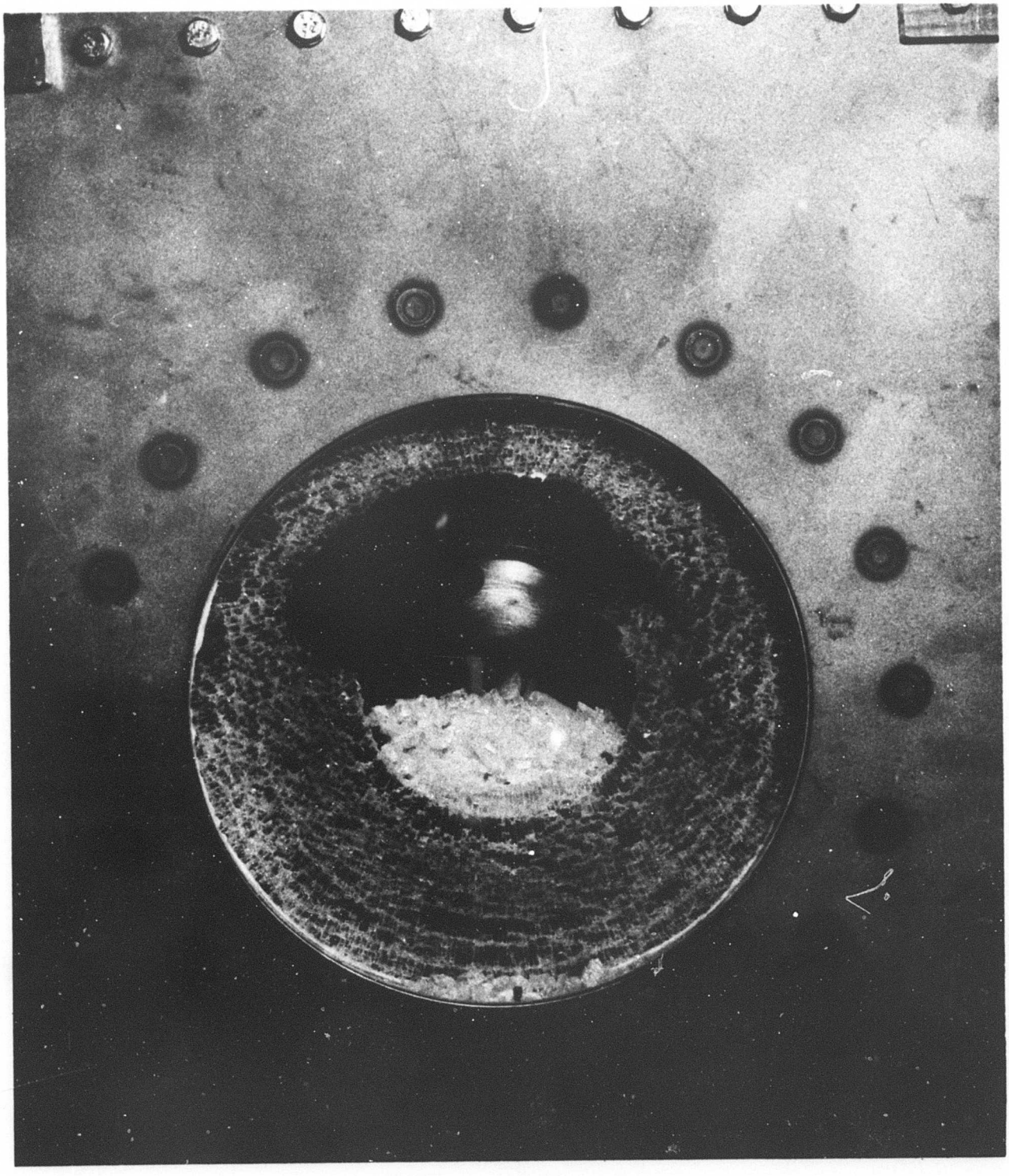


Figure 3-43. Large Object Damage

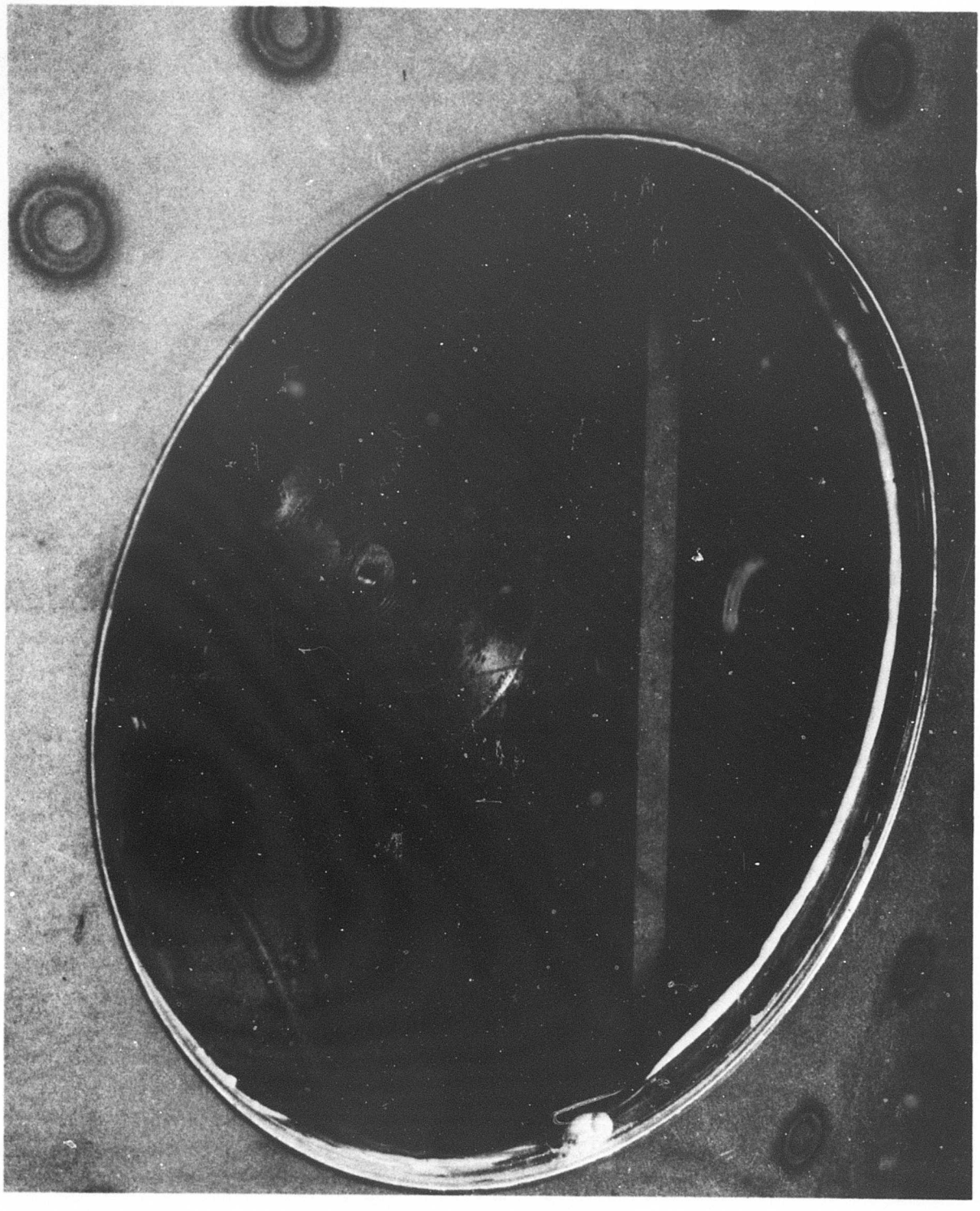


Figure 3-44. Surface Damage for Fatigue Tests

The 23 in. panel was cycled with an initial sawcut to produce a fatigue crack. Strain gage readings and crack growth data were taken during crack extension. After obtaining the required data, the panel was repaired and another test was conducted.

The crack growth histories of the panel tests are shown by Fig. 3-45. In the first test the panel was cycled at a maximum gross area stress of 35 ksi with an initial sawcut in the skin only. One crack tip grew into a fastener hole at the adjacent stiffener. The other crack tip extended between fasteners to the centerline of the fasteners. At this point the crack was arrested with no additional growth occurring for 26 cycles. Testing was discontinued at this time and the panel was repaired for additional testing.

The second test was conducted with an initial sawcut in the skin and a completely severed stiffener. The crack length was extended from 1.15 in. to 11.13 in. in 100 cycles at a maximum gross area stress of 40 ksi. Crack growth did not become unstable during the extension. When the crack was 8.35-in. long, a 38 ksi static loading produced no evidence of crack extension. The leftside crack tip ran into a fastener hole at the adjacent stringer at 93 cycles and did not resume growth during the remainder of the test. The righthand end of the crack grew between the fastener at the adjacent stringer and began to grow at an increasing rate. The test was stopped and the panel was repaired for the next test in which only the attached flange of the stiffener was cut in addition to the skin sawcut. After 1,500 cycles at 40 ksi maximum gross area stress the damaged stringer failed, producing approximately 0.35 in. of additional crack growth. The crack was extended by fatigue cycling to a length of 18 in. without unstable growth, at which time the leftside crack tip had grown into a fastener hole at a stringer. The rightside exhibited slow crack growth when a 40-ksi static load level was applied. With this indication of unstable growth, testing was discontinued. Figure 3-46 shows the final crack configuration of the third test conducted on the panel. The crack growth rate histories shown in Fig. 3-47 are based on the stress intensity factor method. Modifications have been made to the basic stress intensity concept to account for stiffener effects. These curves indicate that by using the stress intensity concept, reasonable predictions can be made for growth rates and remaining life of damaged structure.

3.3.4 Fuselage Full-Scale Fail-Safe Test

3.3.4.1 Program Objectives
The purpose of this program is to evaluate and develop fail-safe design parameters using a full-scale test section representative of actual fuselage structure. Results of the initial testing are incorporated into structural designs for verification testing.

The skin panel bounded by the stringers and frames of a frame-reinforced stiffened cylinder will bulge outward when subjected to internal pressure. In addition, there is curvature of the stringer in the longitudinal direction resulting from the restraint provided by the frames. The resultant strains associated with these differences in deflection affect the crack growth of the specimen. Existing technology does not provide analytical means for reliable scaling of geometry, pressure, and crack propagation characteristics. To obtain reliable crack growth and ultimate fracture strength data, it is necessary to test full-scale sections which allow use of actual operating stress levels.

3.3.4.2 Description of Test Specimens
The test section shown in Fig. 1-1 has a radius of 63.5 in. and is 107 in. in length. The skin-stringer panels are attached to frames spaced at 19 in. The section is constructed so that two panel sections may be removed and replaced. The removable section has been incorporated into the design so that various configurations of skin and stringer panels and tear stopper designs may be tested. The permanent section is Ti 8-1-1 DA skin and stringers. Stringer to frame connections are accomplished by various types of clips as well as direct frame to stringer attachments. The different type of frame connections were used to obtain evaluation data on methods of attachment.

The removable panel test section configurations are shown in Figs. 3-48 through 3-50. The first test panel had 0.045 Ti 8-1-1 DA skin spotwelded to zee and hat section stringers. The second panel had 0.025 fail-safe straps spotwelded on 0.032 Ti 8-1-1 DA skin. The stringers were zee sections spaced at 4.7 in. The third panel was a composite panel having 0.050, 0.060, and 0.032 Ti 8-1-1 DA skins. The 0.032 skin panel had 0.025 and 0.032 gage fail-safe straps. This panel had hat section stringers spaced at approximately 5.5 in. All panels were representative of actual fuselage structure.

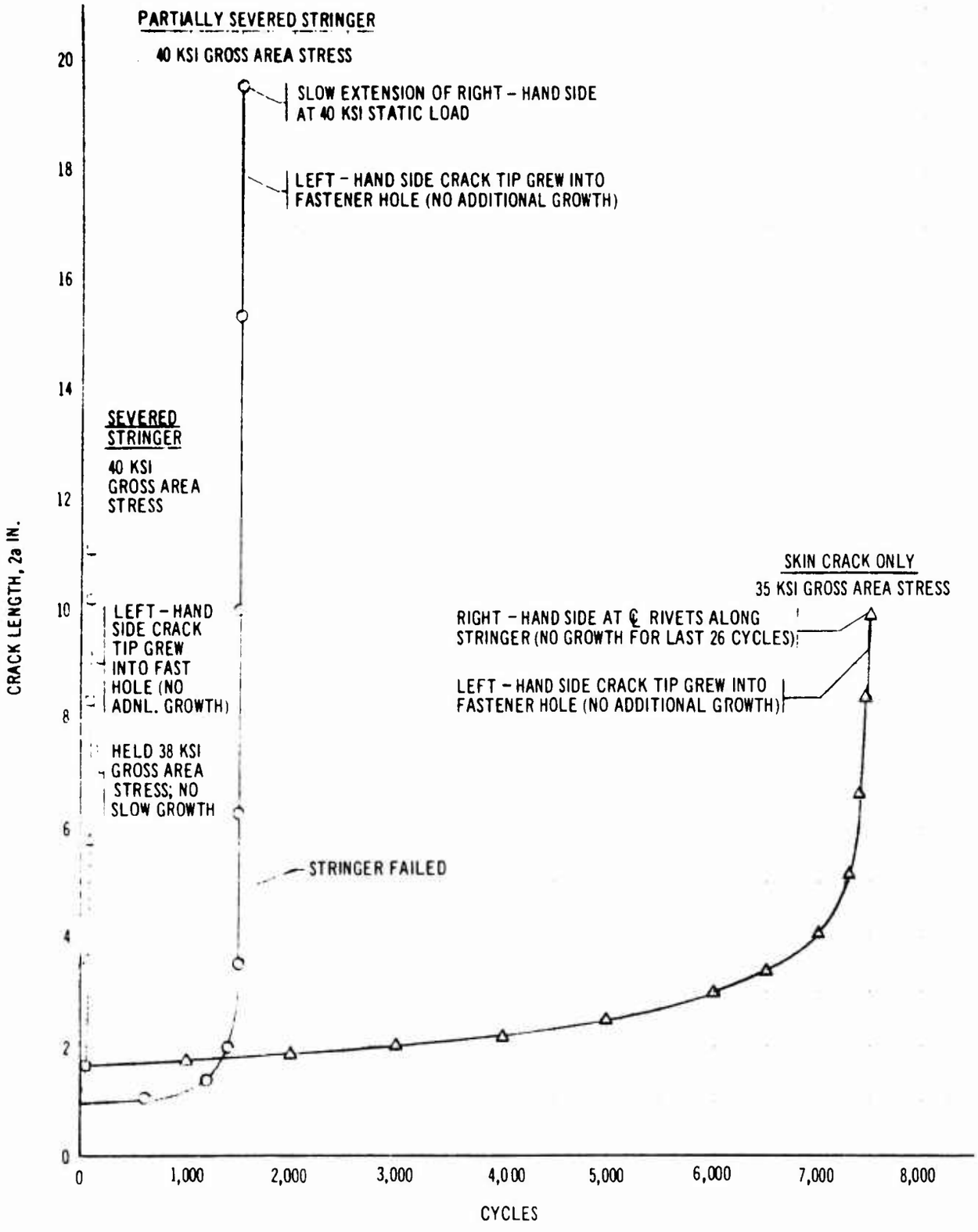


Figure 3-45. Crack Growth History

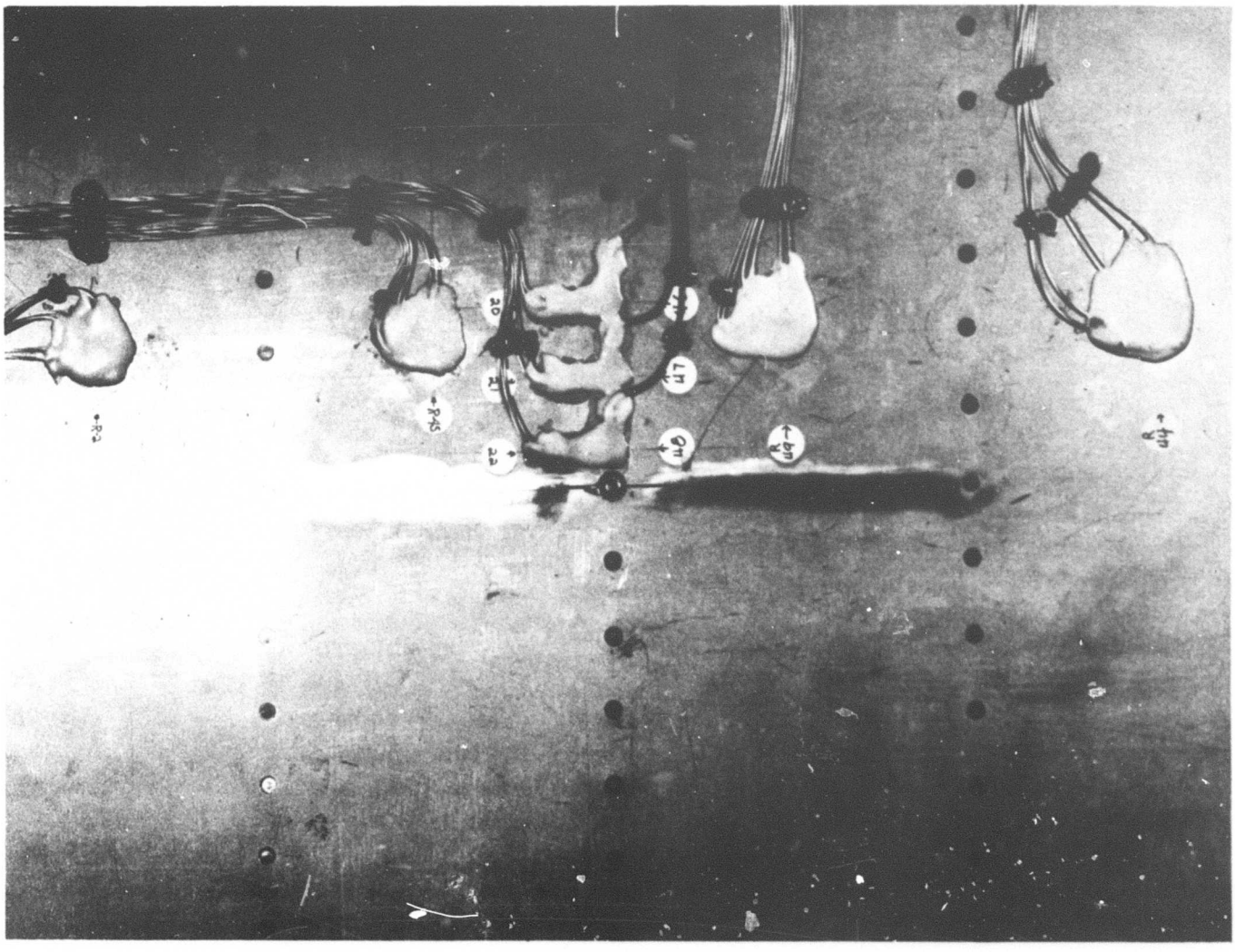


Figure 3-46. Test Panel Final Crack Configuration

3.3.4.3 Testing Procedure and Results
Initial room temperature crack growth tests have been conducted on panels with and without fail-safe tear straps. Elevated temperature tests will be conducted during the verification test program.

The effects of solution environments have been investigated by conducting tests with the test area of the panel submerged in tap water and submerged in a 3-1/2 percent NaCl solution. Puncture tests have been conducted to simulate instantaneous structural damage. An outline of tests conducted on each panel is given in Table 3-H with the types of test shown in Fig. 3-51.

In the crack growth tests a starter crack is installed in the panel and the test section is cycled at 12-psi maximum pressure to produce fatigue crack growth. Rubber seals are installed inside the section in the region of the crack to retain the internal pressure. Strain gage data and crack growth measurements are recorded periodically during crack extension. Upon completion of each test, the damaged area is repaired before con-conducting the next test.

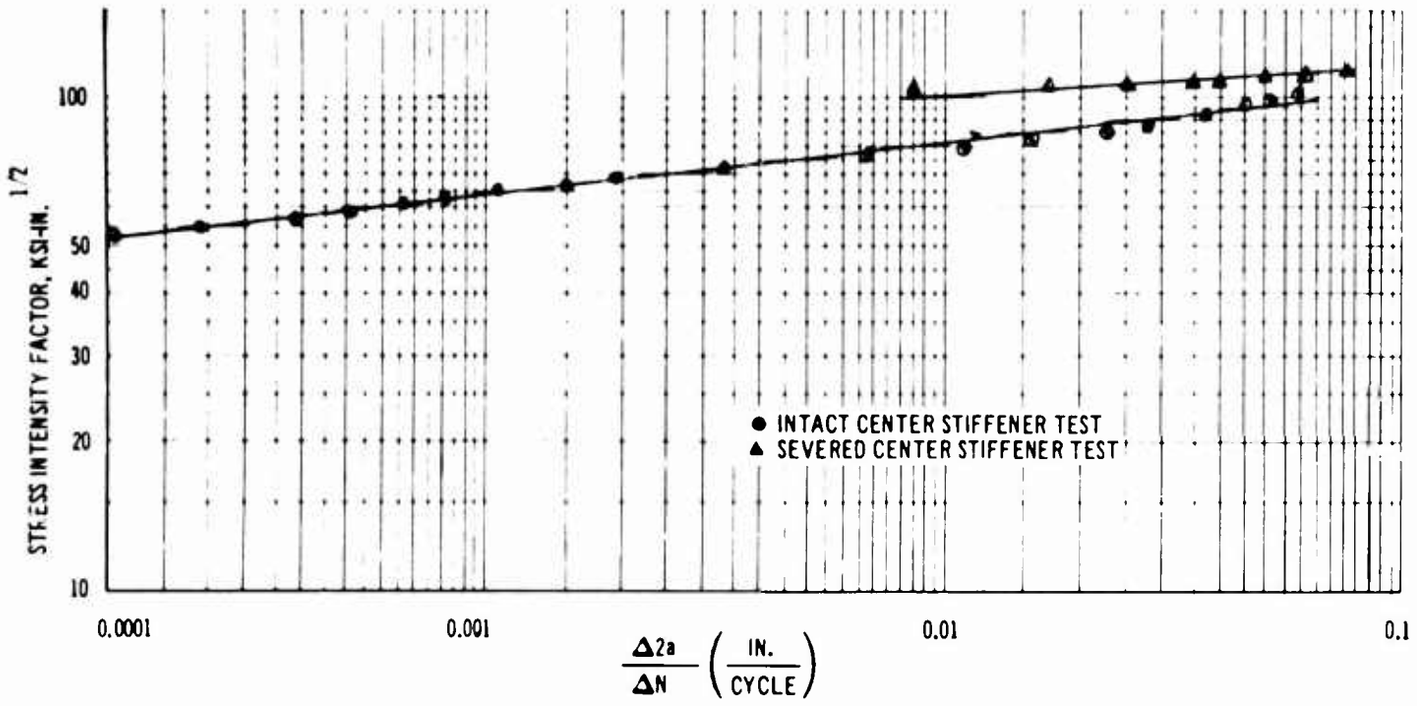


Figure 3-47. Crack Growth Rate Data

For the puncture test, the section is pressurized to 12 psig and after the pressure has stabilized, a 12-in. wide steel blade is fired at the section to produce instantaneous damage. Pressure is maintained on the test section to prevent sudden decrease in pressurization with penetration of the blade.

Crack growth histories of tests conducted on Panel I are shown in Fig. 3-52. In the first test a 6-in. longitudinal crack was cut in the skin midway between adjacent stringers and between the center frames. Crack growth data was obtained while the crack was extended to a total length of 37.9 in. At this point rapid growth seemed imminent with 12 psig internal pressure; however, the panel sustained 5 psi for 10 minutes without noticeable growth. Final crack length is shown in Fig. 3-53.

The second test investigated the effect of cracks along a row of fasteners at a skin splice. An initial sawcut 7 in. in length was installed along the edge of the first row of spotwelds at the skin splice. After 1,118 cycles has produced only negligible crack growth, additional sawcuts were installed off both ends of the initial sawcuts. (Fig. 3-51). At 1,850 cycles two more sawcuts were installed off the ends of the existing cuts extending the damage length to 17.7 in. After 4,055 cycles the initial 7-in. sawcut had propagated to a length of 8.0 in. and no growth had occurred at the other sawcuts and testing was discontinued.

The third test was initiated with an 8-in. sawcut along the spotwelds at a stringer. After 650 cycles two 1.5-in. sawcuts were installed off the ends of the initial cut. (Fig. 3-51). At 1,200 cycles the initial 8-in. crack had extended to 9.4 in. with no indication of growth from the added end cracks. At this time each of the end cracks were lengthened to 3 in. In the next 11 cycles the crack propagated into a single crack 18.75 in. long. Additional cycling caused the crack tips to begin centering themselves between the stringers, producing a situation similar to

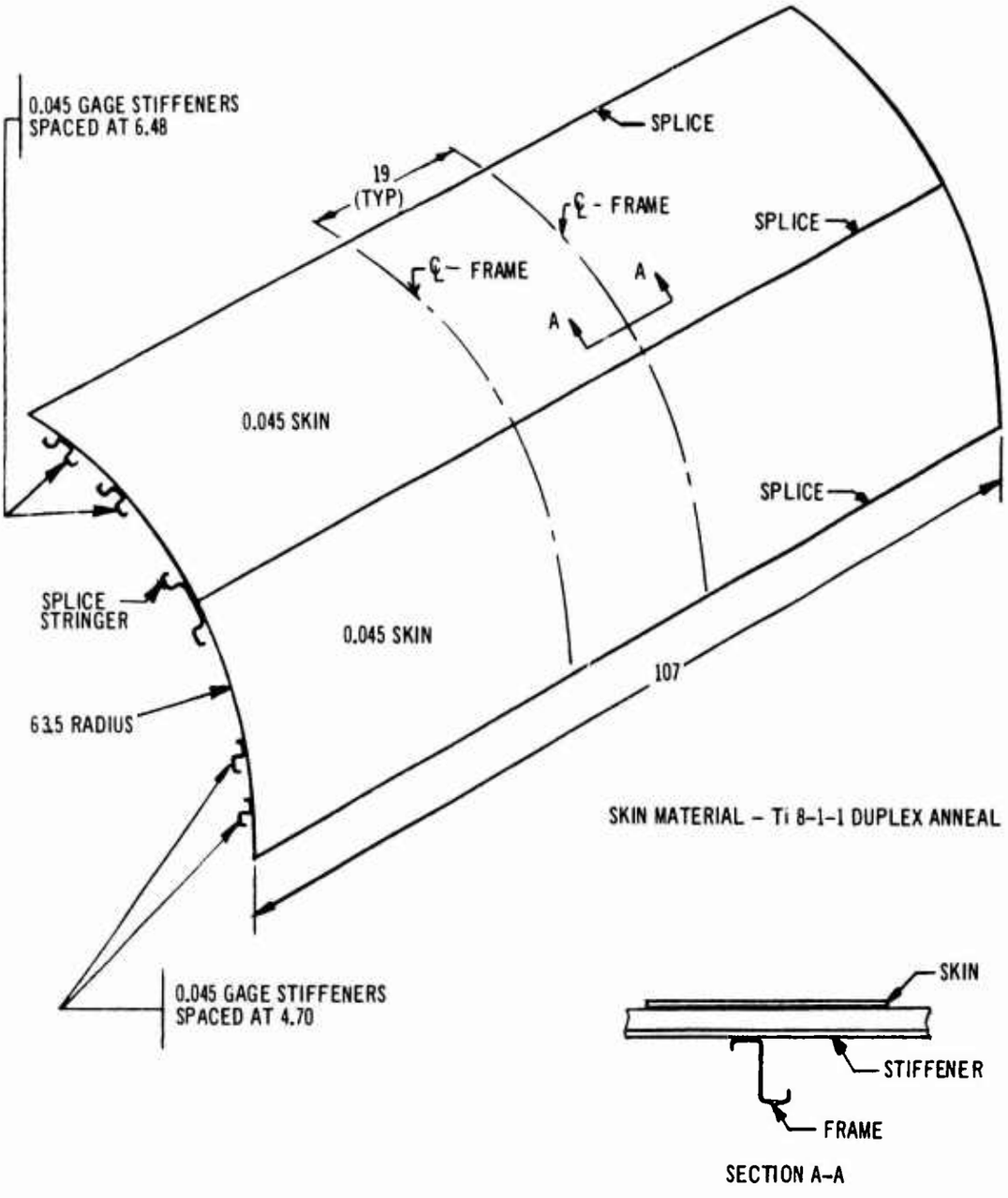
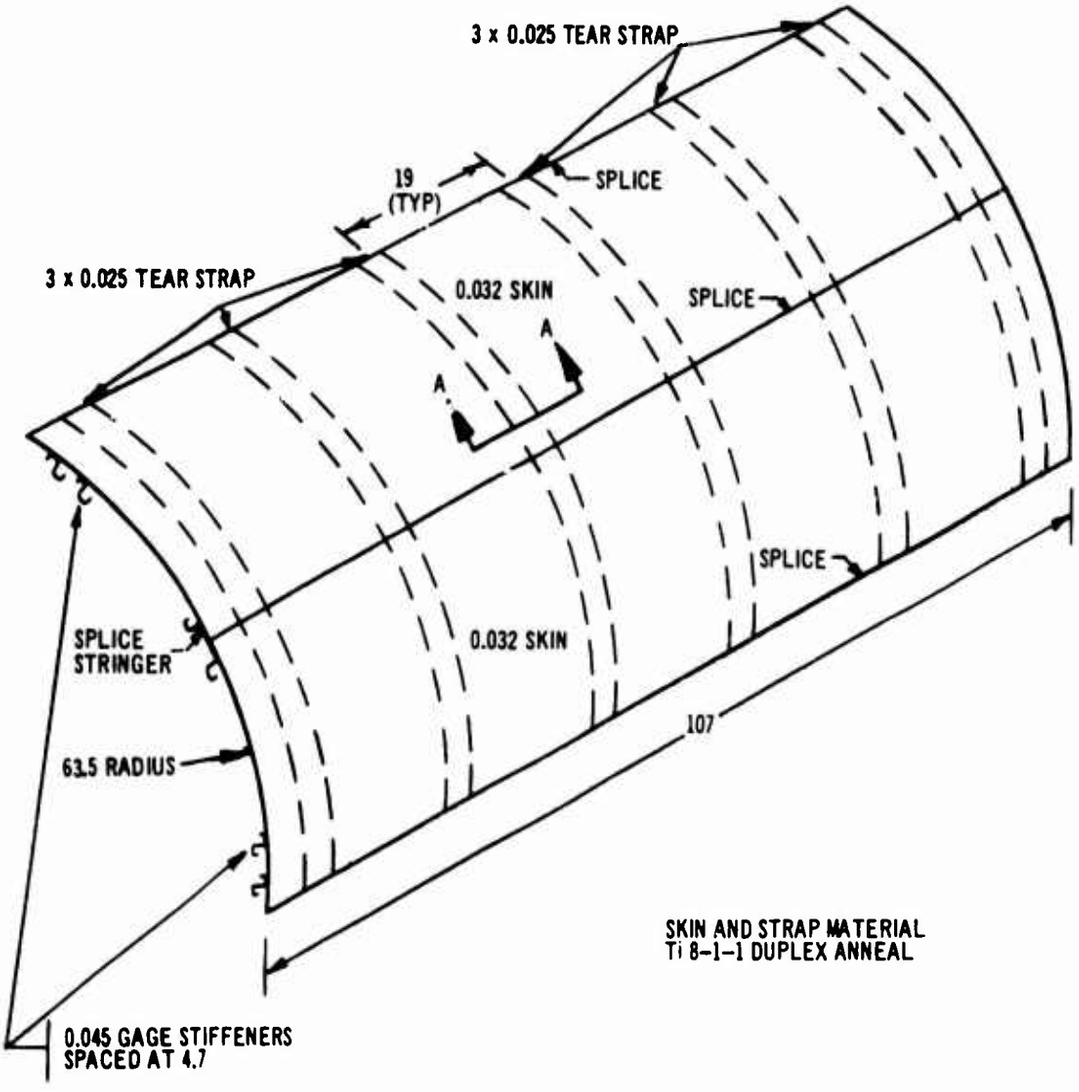


Figure 3-48. Fail-Safe Test Panel - I



SECTION A-A SEE FIG 3-50 FOR SECTION DETAIL

Figure 3-49. Fail-Safe Test Panel – II

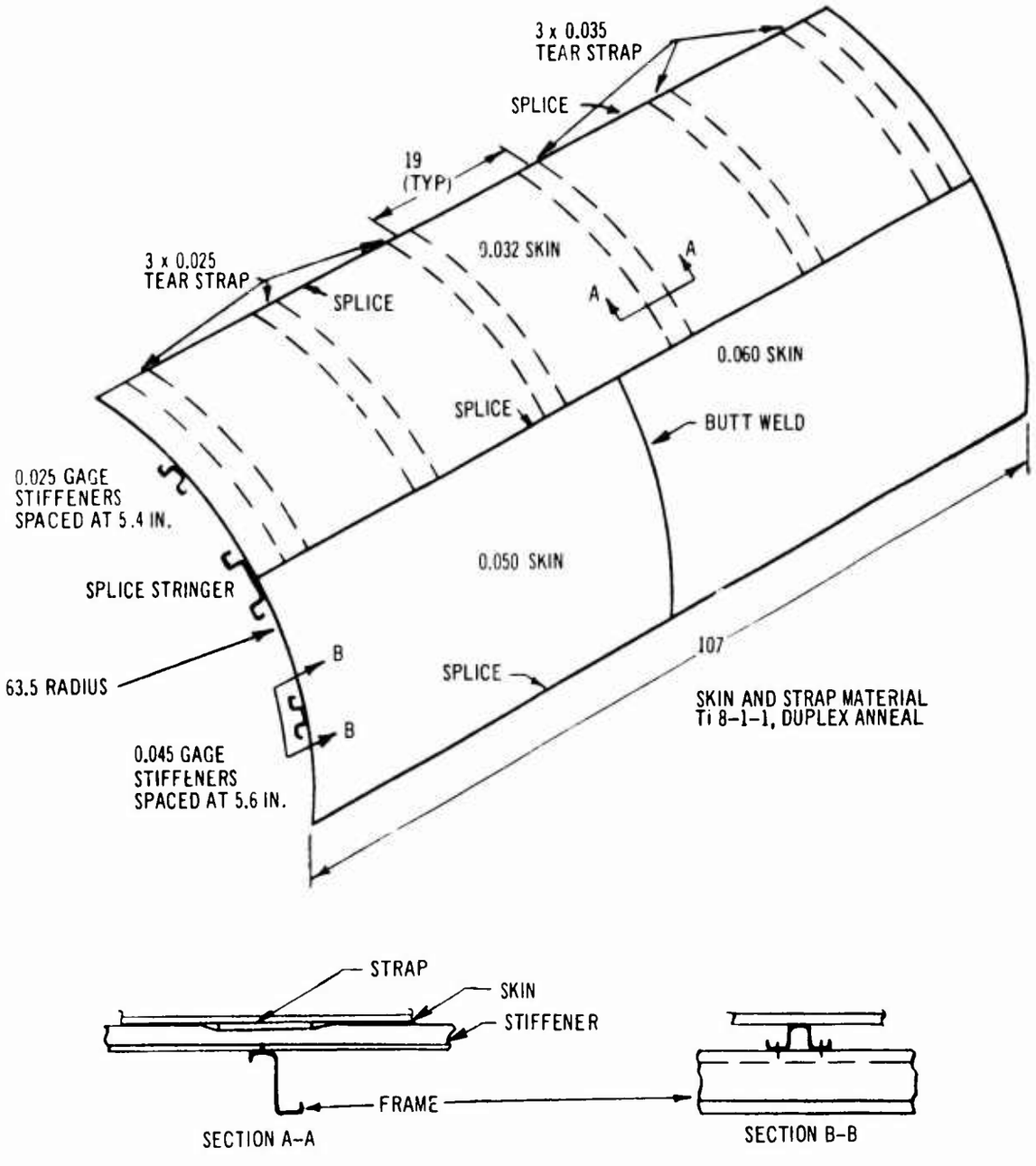


Figure 3-50. Fail-Safe Test Panel – III

Table 3-H. Test Outline

Panel	Test No.	Skin Gage and Material	Type Test	Tear Strap
1	1	0.045 T18-1-1 Du. Anneal	Crack Growth - Center Panel	None
	2	0.045 T18-1-1 Du. Anneal	Crack Growth - Spotweld Skin Splice	None
	3	0.045 T18-1-1 Du. Anneal	Crack Growth - Stringer Attachment	None
2	1	0.032 T18-1-1 Du. Anneal	Crack Growth - Center Panel	3 x 0.025
	2	0.032 T18-1-1 Du. Anneal	Crack Growth - Either Side of Strap	3 x 0.025
	3	0.032 T18-1-1 Du. Anneal	Crack Growth - At Strap	3 x 0.025
	4	0.032 T18-1-1 Du. Anneal	Puncture - Center Panel	3 x 0.025
	5	0.032 T18-1-1 Du. Anneal	Puncture - Cut Stringer	3 x 0.025
	6	0.032 T18-1-1 Du. Anneal	Puncture - Cut Frame and Stringer	3 x 0.025
	7	0.032 T18-1-1 Du. Anneal	Puncture - Double Cut	3 x 0.025
	8	0.032 T18-1-1 Du. Anneal	Crack Growth - Center Panel	3 x 0.025
	9	0.032 T18-1-1 Du. Anneal	Crack Growth - Center Panel	3 x 0.025
	10	0.032 T18-1-1 Du. Anneal	Crack Growth - Failed Strap	3 x 0.025
3	1	0.032 T18-1-1 Du. Anneal	Crack Growth - Center Panel	3 x 0.025
	2	0.032 T18-1-1 Du. Anneal	Crack Growth - Center Panel	3 x 0.025
	3	0.060 T18-1-1 Du. Anneal	Crack Growth - Center Panel	None
	4	0.050 T18-1-1 Du. Anneal	Crack Growth - Center Panel	None
	5	0.032 T18-1-1 Du. Anneal	Crack Growth - Strap Edge	3 x 0.025
	6	0.032 T18-1-1 Du. Anneal	Crack Growth - Bolted Skin Splice	3 x 0.025 & 0.035
	7	0.050 T18-1-1 Du. Anneal	Puncture - Center Panel	None
3A	1	0.032 T16-4 Cond. I	Crack Growth - Strap Edge	Dual 1.45 x 0.025
	2	0.032 T16-4 Cond. I	Crack Growth - Strap Edge	Daul 1.45 x 0.025

Test Configuration shown in Figure 3-51

All tests conducted in air except as follows:

Test 6 Panel 2 conducted with water environment.

Test 7 Panel 2 conducted with 3.5% NaCl solution environment

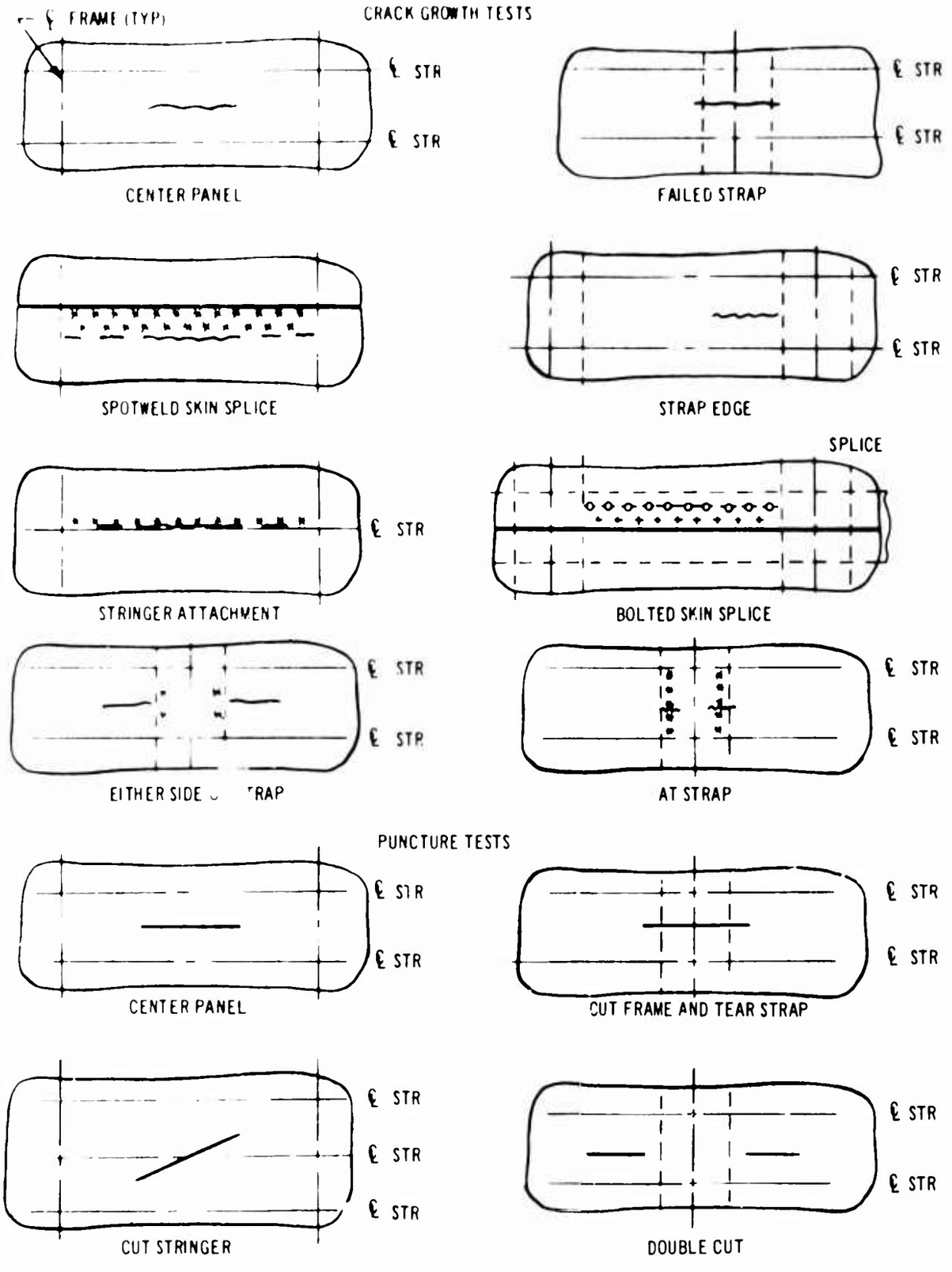


Figure 3-51. Damage Configurations

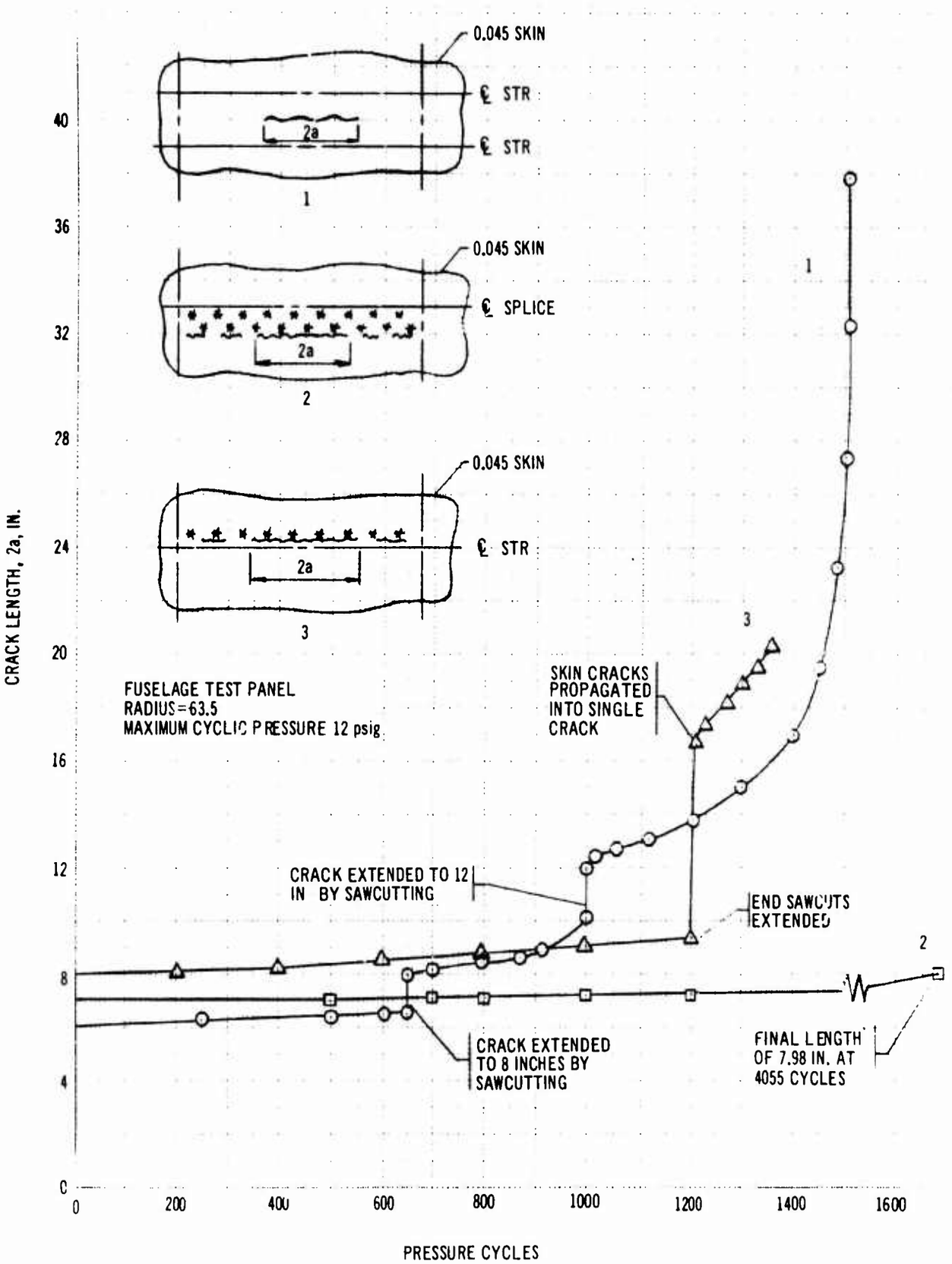


Figure 3-52. Crack Growth History – Panel I

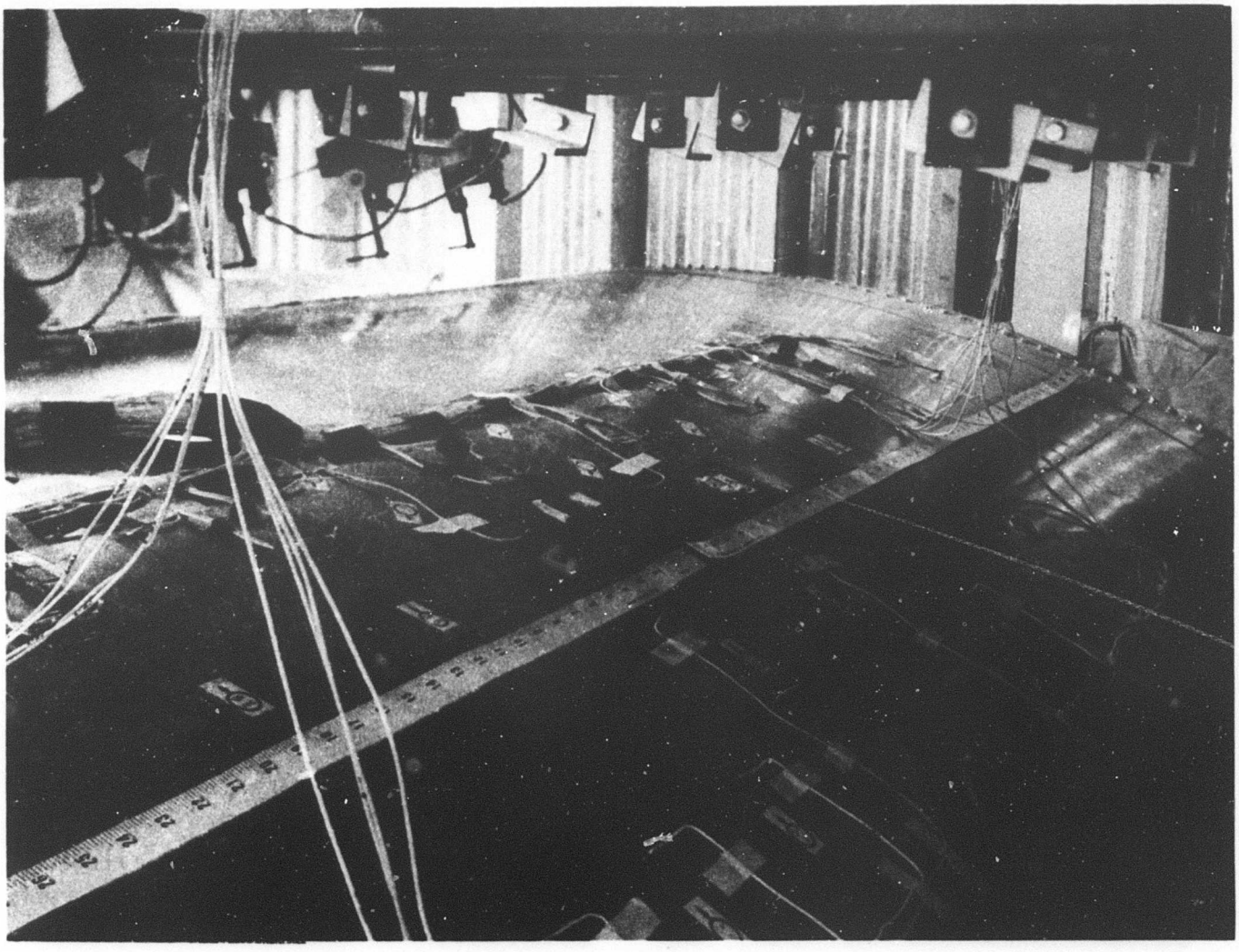


Figure 3-53. Cracked Section of Test Panel

that of the first test and testing was discontinued at a crack length of 20.3 in. These tests indicate that cracks along a row of spotwelds are a less severe condition than cracks propagating in the middle of a stringer panel.

Crack growth histories of tests conducted on Panel 2 are shown in Figs. 3-54 and 3-55. The first test demonstrated the effectiveness of the tear strap design. A crack in the center of a skin panel was propagated into the adjacent tear straps which arrested the crack growth.

The second test had an initial sawcut on either side of a tear strap. The cracks were extended by pressure cycling to a length of 6.9 and 10.8 in. in approximately 3,000 cycles. The crack tips on either side of the tear straps extended toward each other to approximately the center-line of the strap-skin spotwelds and were arrested at this point. The cracks were then extended by sawcutting to the adjacent tear straps and strain measurements were obtained for a crack extended two frame bays. Strain gage measurements indicated that at 12 psig the 0.025 x 3-in. tear strap would be marginal for the estimated fatigue cycles required to extend the crack to the adjacent tear straps.

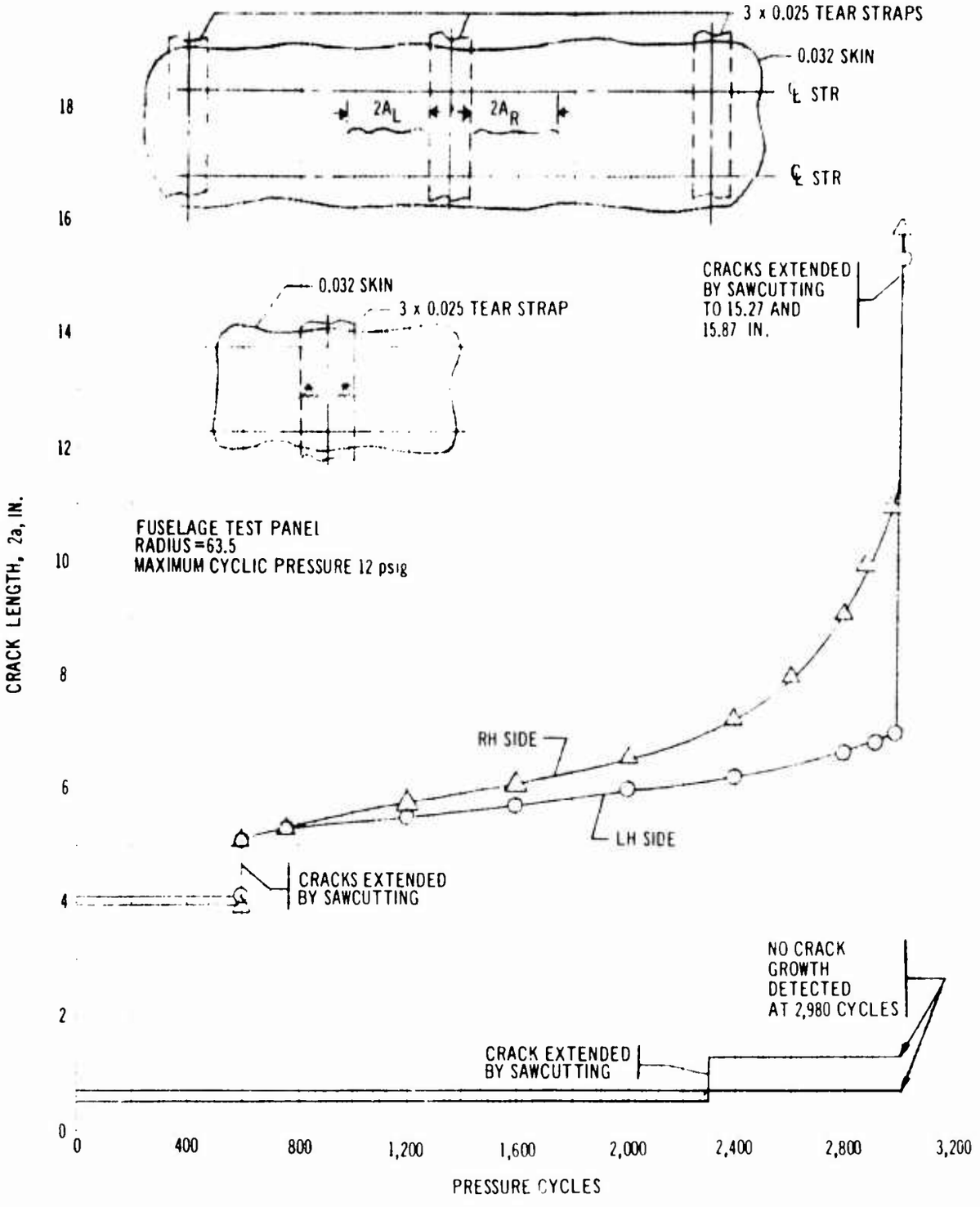


Figure 3-54. Crack Growth History – Panel II

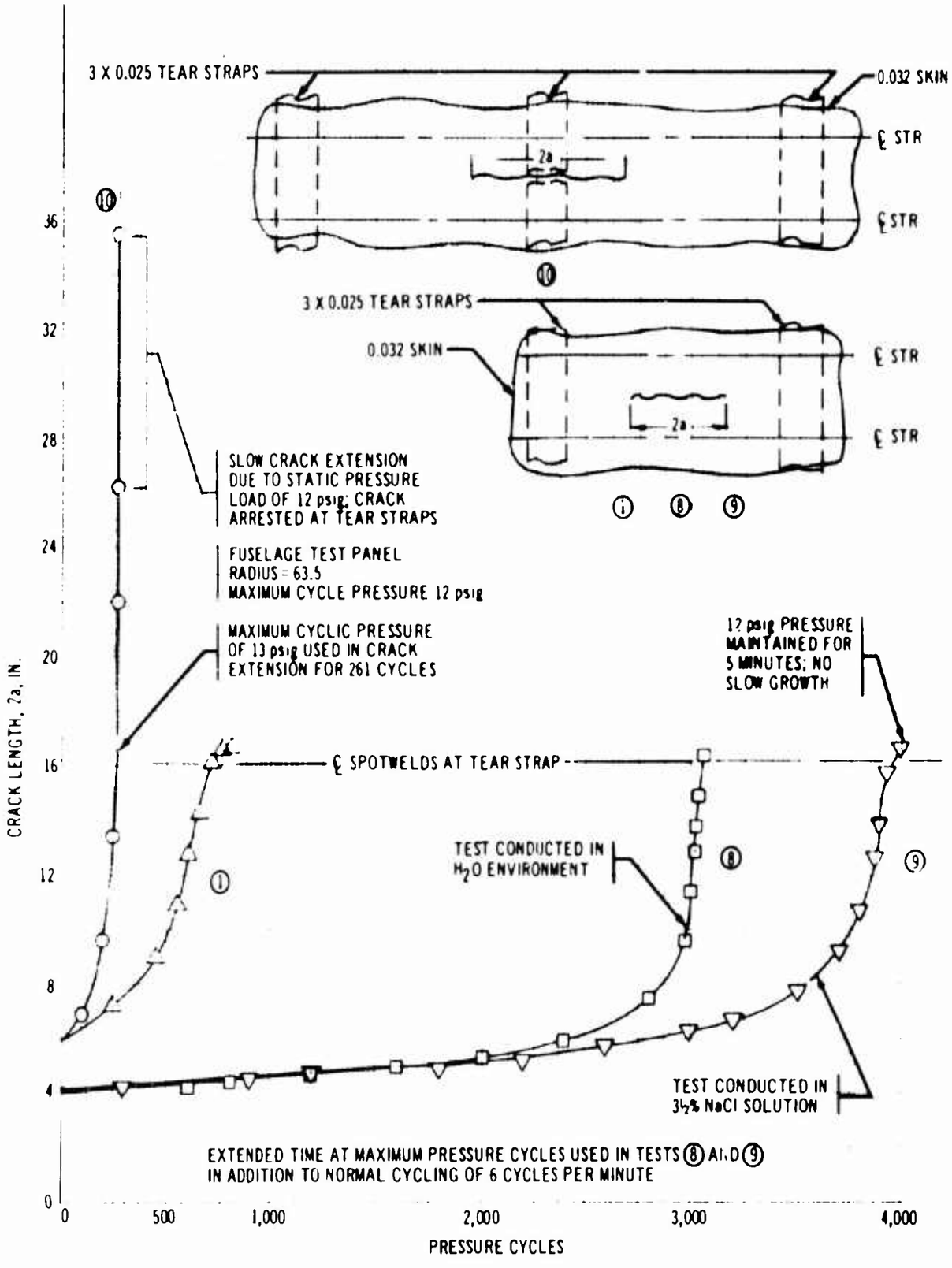


Figure 3-55. Crack Growth History – Panel II

Conducted simultaneously with the second test was a test in which sawcuts in the skin approximately 0.6-in. long were installed at the edge of two adjacent spotwelds at a tear strap location (Fig. 3-54). After 2,300 cycles produced no growth from either crack, one crack was extended to 1.2 in. At 2,980 cycles there was no evidence of crack growth and the test was discontinued.

Four puncture tests were conducted on the 0.032 gage panel for damage combinations shown in Fig. 3-51. Damage in all cases was confined to the puncture area. In the initial test, an 11-in. wide blade was used. The remainder of the tests were conducted with a 12-in. wide blade to ensure that damage would not be less than 12 in. long. Typical damage is shown in Fig. 3-56.

Tests were also conducted on the second panel to determine the effect of tap water and of 3-1/2 percent NaCl solution on crack growth. The crack growth histories are shown in Fig. 3-5. Fig. 3-57 compares the crack growth for environments of air, tap water, and 3-1/2 percent NaCl solution after the crack for each condition has obtained lengths of 7 and 10 in. Fatigue crack initiation from the starter cut was obtained by pressure cycling the test section in air. All additional crack extension testing was conducted with the exterior surface of the test area submerged in the test liquid. Two types of pressure cycles were used for crack extension: cycling at the normal rate of approximately six cycles per minute and cycling so that the maximum pressure was held for five minutes. In addition, for the 3-1/2 NaCl solution test, the maximum pressure was maintained for 25 min at selected crack lengths. The three methods were found to produce equivalent crack growth per cycle. The 25 min at maximum pressure produced no evidence of crack extension due to time at load. The crack growth rates of tests conducted in air, water, and 3-1/2 NaCl solution are shown by Fig. 3-58. It is evident that the three environments produced equivalent crack growth rates.

The next test evaluated crack growth with a severed fail-safe strap. A six-in. sawcut was centered between stringers at a frame station, completely cutting the fail-safe strap. Crack extension up to 16.5 in. was inadvertently conducted at 13 psig. The remainder of the test was conducted using 12-psig maximum pressure. When the crack had reached 26 in., the application of a constant pressure loading of 12 psig produced crack extension. Each end of the crack extended and was arrested by the tear straps. After the crack had been arrested at the straps, the maximum pressure loading was maintained for several minutes with no noticeable increase in crack length. Final crack configuration is shown in Fig. 3-59 with the crack growth history in Fig. 3-55.

Crack growth histories of tests conducted on Panel 3 are shown in Figs. 3-60 and 3-61. Six crack growth tests and one puncture test were conducted on this panel.

Two center panel crack growth tests were conducted on the 0.032-in. skin panels, one with 0.032 tear straps and one with 0.025 tear straps. The crack was arrested at the tear straps in both tests.

A crack growth test was conducted in the 0.060 gage skin without tear straps using an 8-in. starter crack centered between the stringers and the frames. After 600 cycles the crack was extended by sawcutting to 14 in. Sustained time at maximum pressure was used in addition to normal cycling. Although the growth during the extended time cycle was greater than that produced in a normal pressure cycle, it stabilized in a period of seconds after maximum pressure was applied. No indication of unstable growth occurred during the propagation of the crack to a length of 34 in. and the test was stopped.

A crack growth test was conducted in the 0.050 gage skin without tear straps. After obtaining initial crack growth data, the crack was sawcut to approximately 13 in. during the remainder of this test, several hold cycles at maximum pressure were applied. Crack stabilization was obtained for each hold cycle until reaching a crack length of 29.6 in. At this crack length, maintaining maximum pressure produced a slow growing, unstable crack and the test was stopped.

The fifth test was conducted by installing a 6-in. sawcut in an 0.032 gage skin panel with its center 5 in. from the tear strap. A combination of normal and extended time pressure cycles at 12 psig maximum were applied in extending the crack to the adjacent tear straps. The crack growth rate decreased to 0.01-in. per cycle and the crack was considered to be arrested, so the test was discontinued.

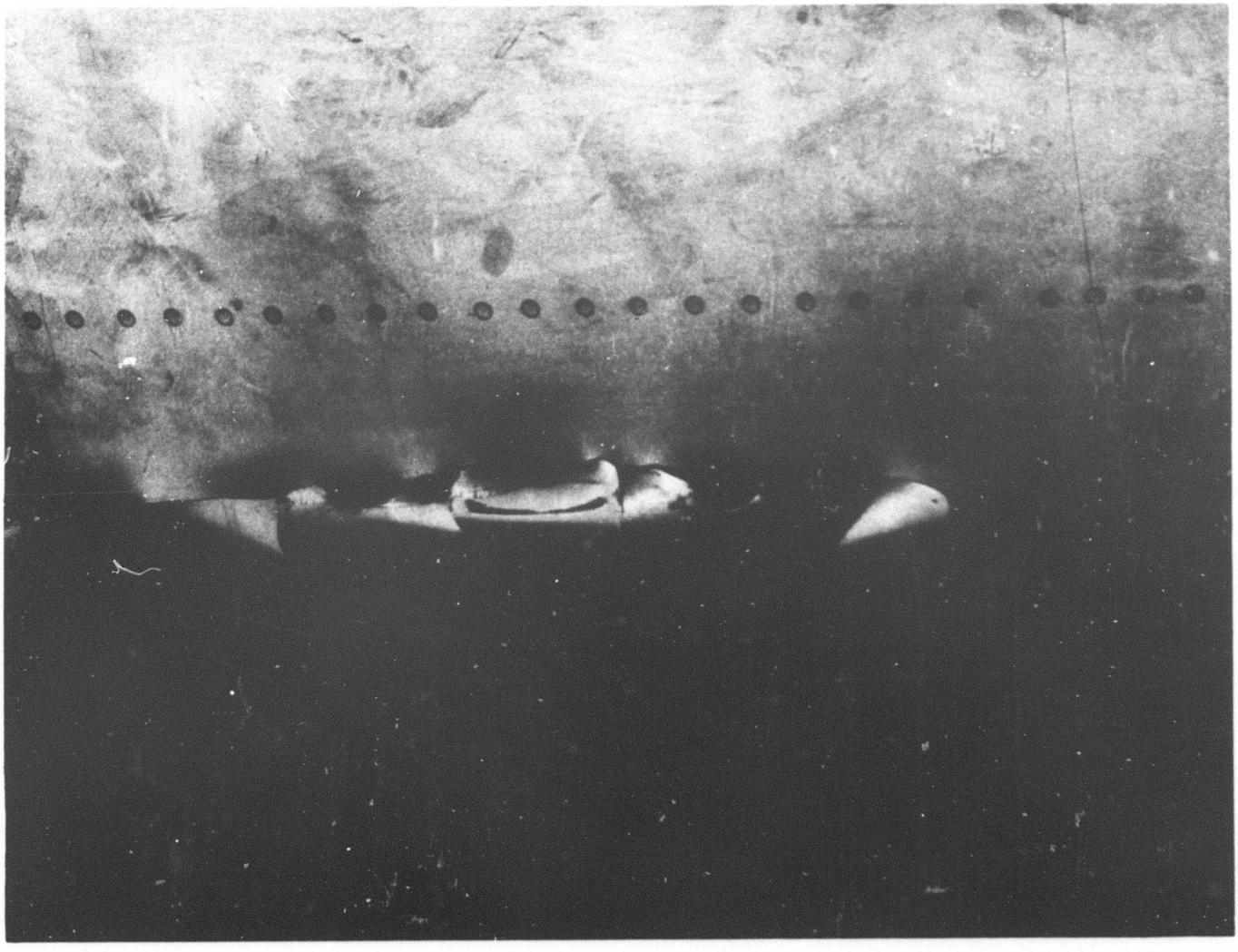


Figure 3-56. Puncture Damage

The sixth test involved a series of cracks at the first row of fasteners in the longitudinal splice of the 0.032 skin. After the application of 1,200 pressure cycles produced no evidence of growth from any of the cracks, the center crack was extended from 3.9 in. to 6.3 in. An additional 900 pressure cycles produced no evidence of growth from any of the cracks and the test was stopped.

An instantaneous damage test was conducted on the 0.050 gage skin without tear straps. The 12-in. blade punctured the skin between stringers and frame locations. Damage was confined to the puncture area.

The third test panel was modified to evaluate a dual tear strap configuration shown in Fig. 3-62. Two crack growth tests were conducted in the 0.032 gage skin. Figure 3-63 shows the crack growth histories. The dual straps involved in one test were riveted to the skin, while the dual straps in the other test were riveted and bonded. In each test a starter crack was installed in the skin with one tip located about 1/2 in. from the edge of one of the dual tear straps. Crack growth was arrested by the riveted and bonded tear straps as the crack tips propagated just past the edge of the first tear straps. For the riveted only straps, crack growth was arrested when the crack tips extended beyond the centerline of the fasteners.

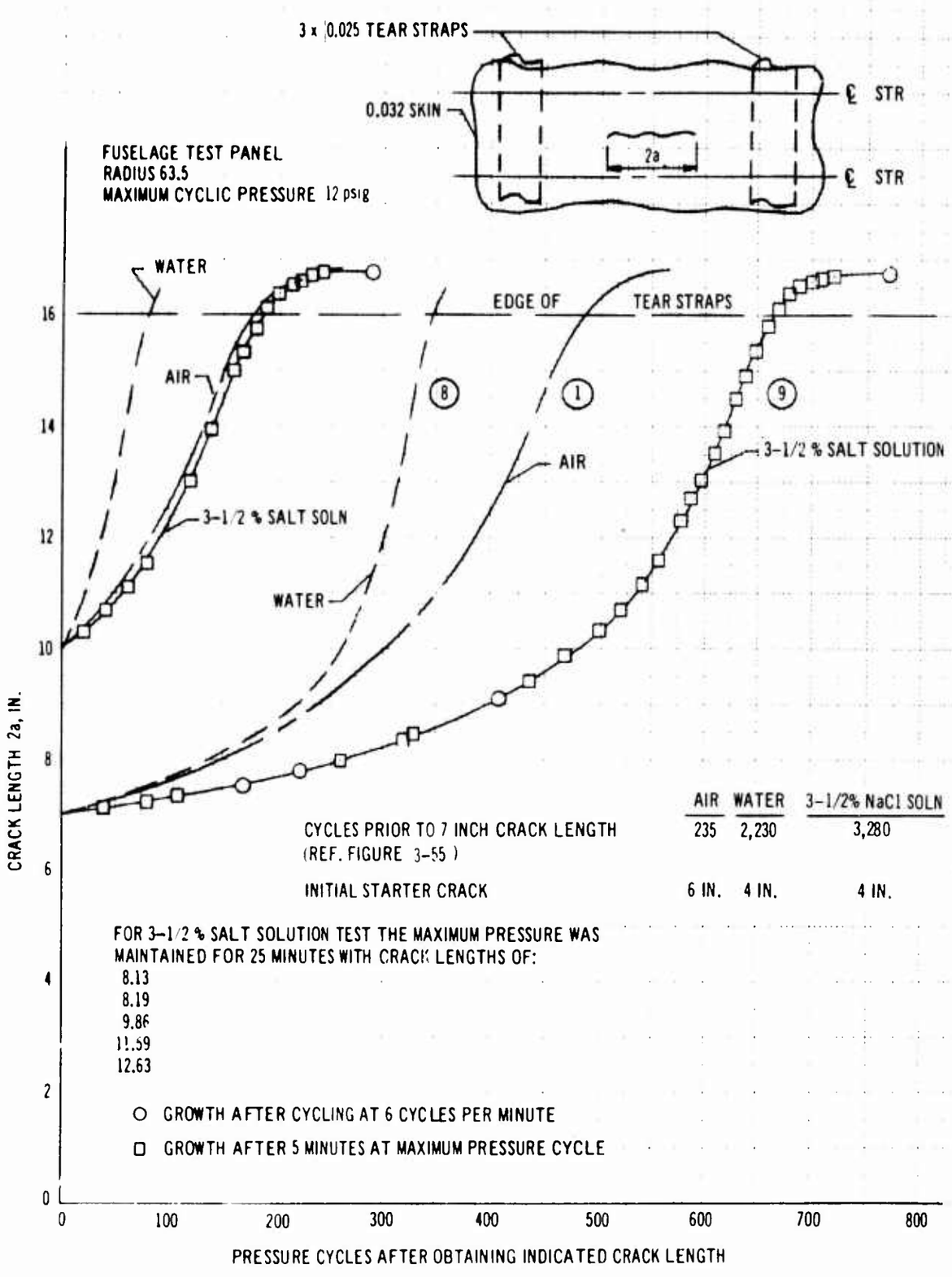


Figure 3-57. Crack Growth History – Environment Tests

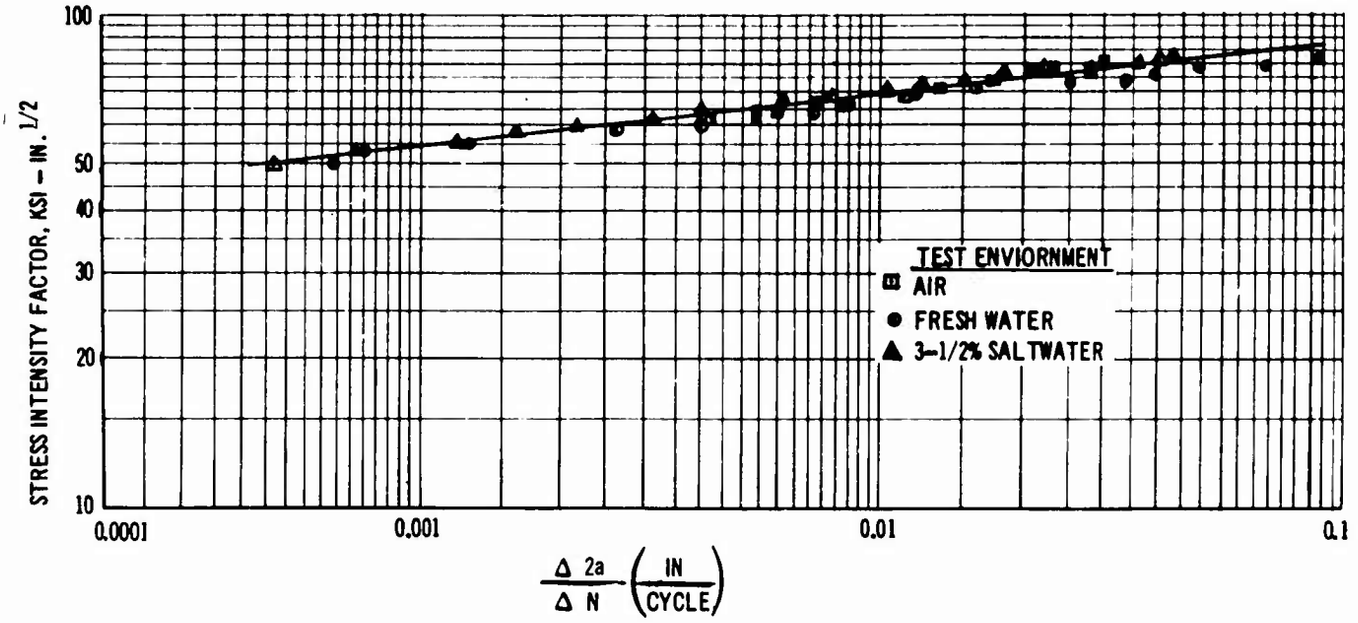


Figure 3-58. Crack Growth Rate Data – Environment Tests

Crack growth data of the three center panel cracks in Ti 8-1-1 0.032 gage skin have been compared. The crack growth histories of these tests are shown in Fig. 3-64. Crack growth rate versus stress field intensity factor is shown in Fig. 3-65 Good growth rate correlation is obtained using the stress intensity factor approach. The growth rate curve was based on test crack lengths and the measured skin stress distribution shown in Fig. 3-66. The difference in the number of pressure cycles required to obtain a given crack length for Crack A and Crack C is attributed to variations of material properties and normal test scatter. The more rapid growth of Crack B is attributed to the higher skin stress level in this test area as shown in Fig. 3-66.

The test results from the first three panels have been used to design a fail-safe verification test panel as shown in Fig. 3-67. The tests to be conducted on this panel are shown in Fig. 3-68. Crack growth tests will be conducted at room and elevated temperatures to verify panel fail-safe design for light-gage structure with dual tear straps and heavier gage structure without tear straps. Testing will include instantaneous damage tests.

Test results have demonstrated that fail-safe straps can be used effectively to arrest cracks in light-gage titanium fuselage structure. It was further demonstrated that in light-gage structure with tear straps, the crack would propagate slowly between arrestor straps with no indication that a crack would extend across a tear strap into the next panel. In heavier gage structure without fail-safe straps, it has been demonstrated that the number of cycles required to extend the crack to a critical length is ample to allow detection by inspection.

3.3.5 Cab Section Verification Hardware Test

3.3.5.1 Program Objectives

The purpose of the test program is to determine the effect of internal pressure loading, temperature, and combined temperature and internal pressure loading on the windshield and structure of the full-scale crew compartment of the B-2707 (Fig. 3-69). Tests will also be conducted to demonstrate the fatigue life and fail-safe characteristics of the crew compartment and to demonstrate the bird strike resistance of the crew compartment windshields and supporting structure.

In addition to the structural testing, the crew compartment cab will be utilized in environmental control studies to determine cooling air flow rates and paths.

3.3.5.2 Description of Test Article

The test article consists of a crew compartment similar to that proposed for the airplane and

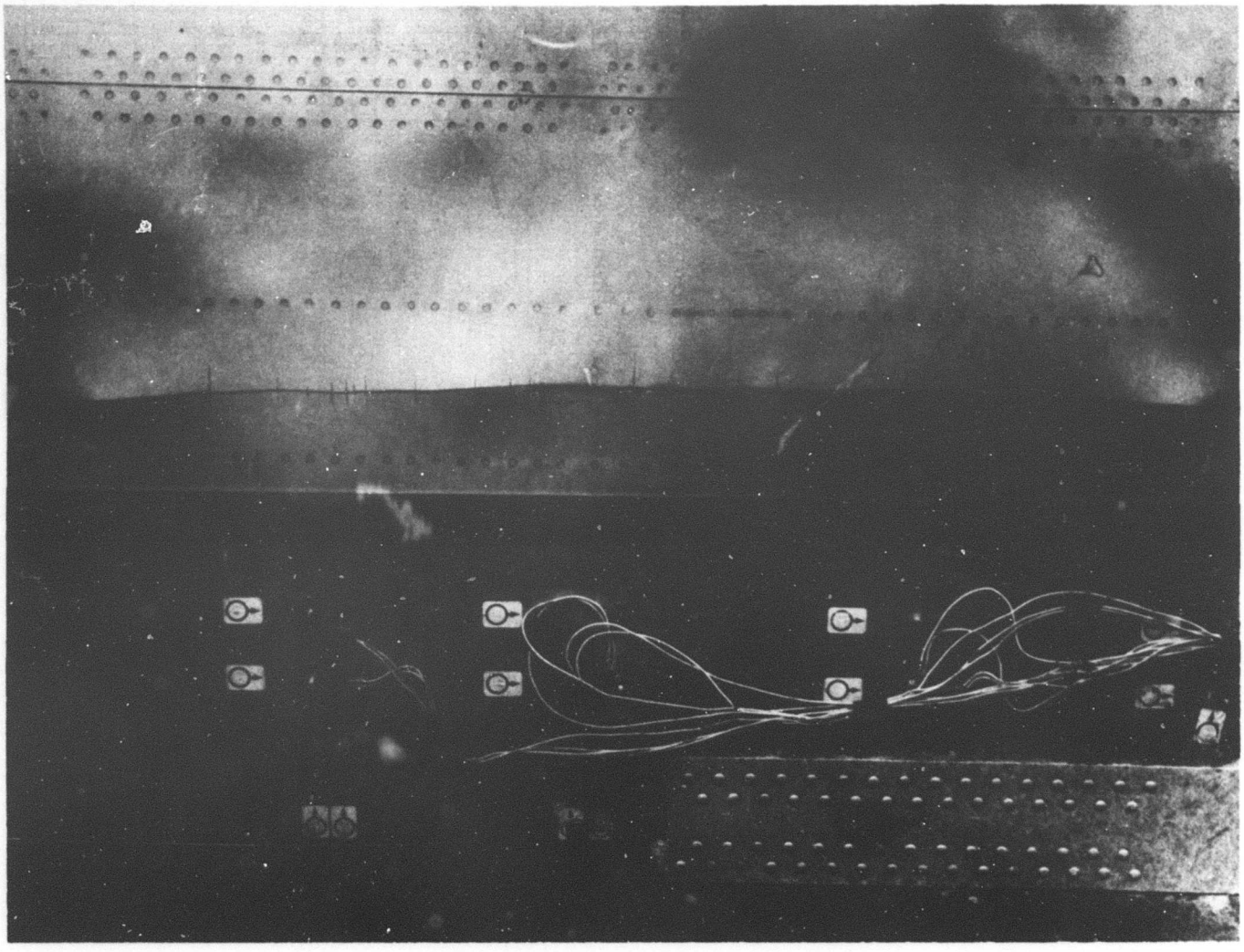


Figure 3-59. Cracked Section of Test Panel

includes all of the structure and windows above the floor from the forward pressure bulkhead to approximately 27 in. aft of the windows. The basic structural material used throughout the test cab is Ti 6Al-4V. The upper cab is mounted on a simplified lower lobe constructed of stainless steel and the entire section is cantilever supported from its aft end. Strain gages, deflection gages, and thermocouples will be employed throughout the cab to monitor stress, deflection, and temperature at critical points.

3.3.5.3 Test Program

a. Thermal and Proof Pressure Test
The windows and external surfaces of the test specimen will be heated to the appropriate temperatures and proof pressure tested to 16.68 psig in increments of 4, 8, 12, and 16.68 psig. Stress and deflection will be recorded and the effects on structure observed at each pressure increment.

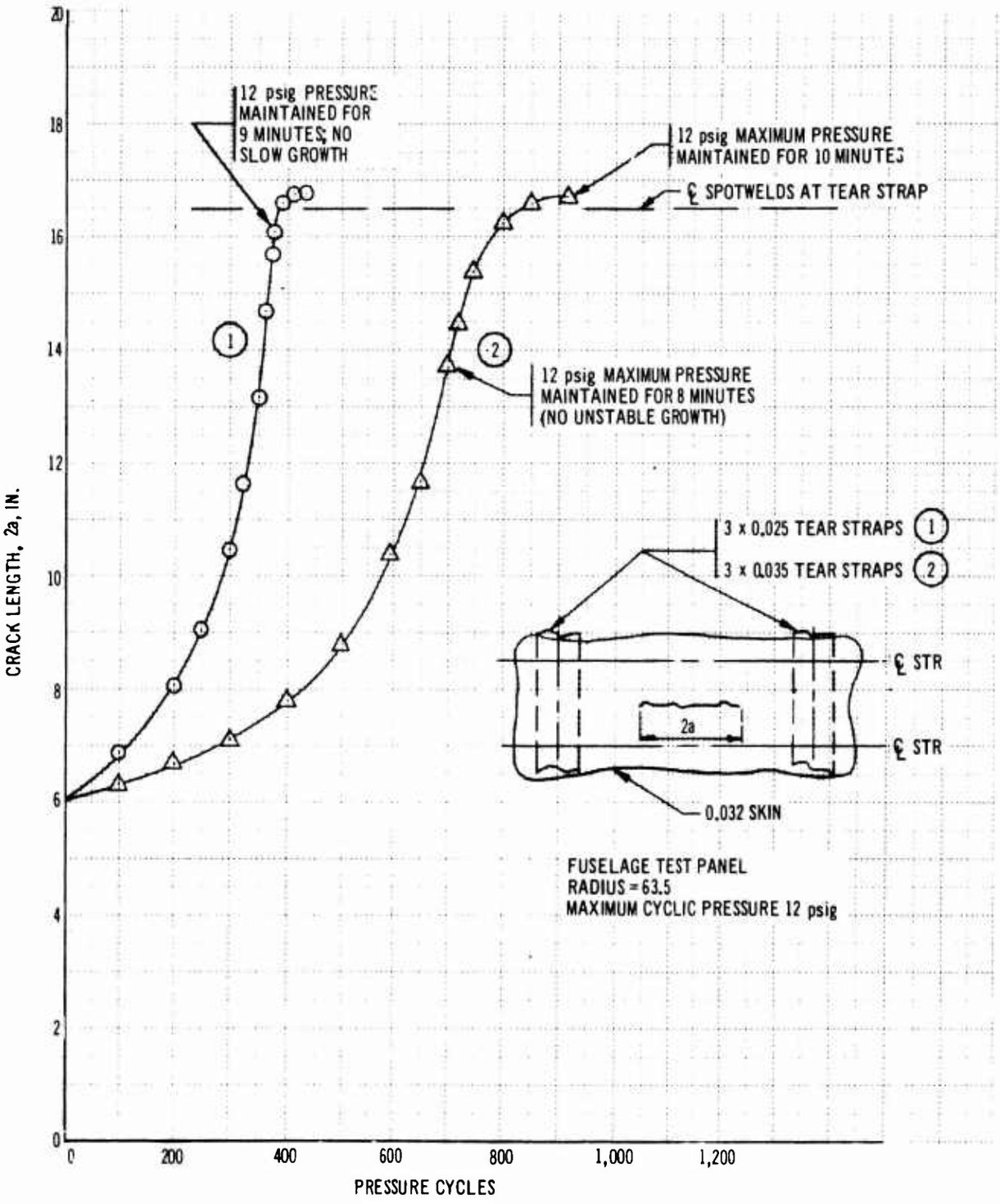


Figure 3-60. Crack Growth History – Panel III

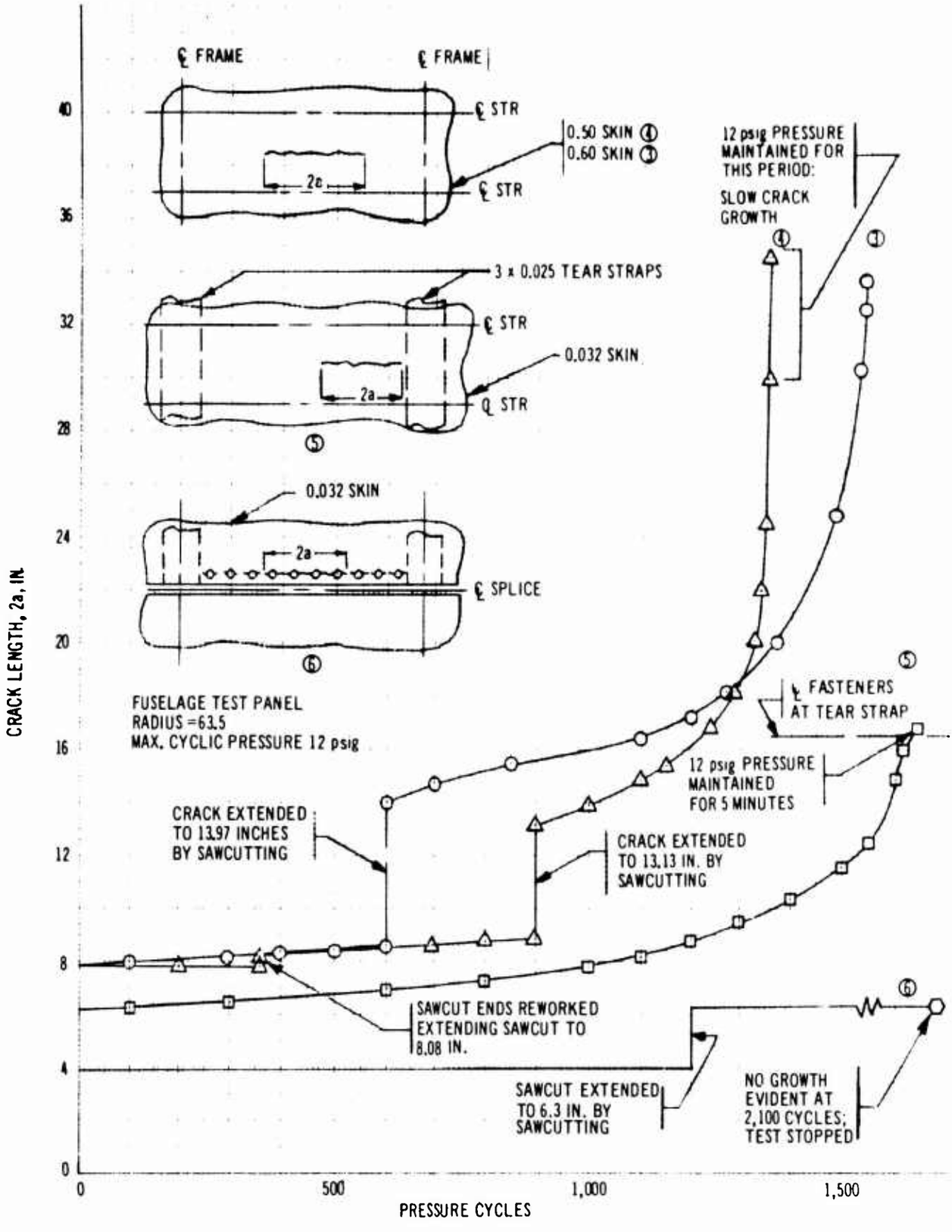


Figure 3-61. Crack Growth History – Panel III

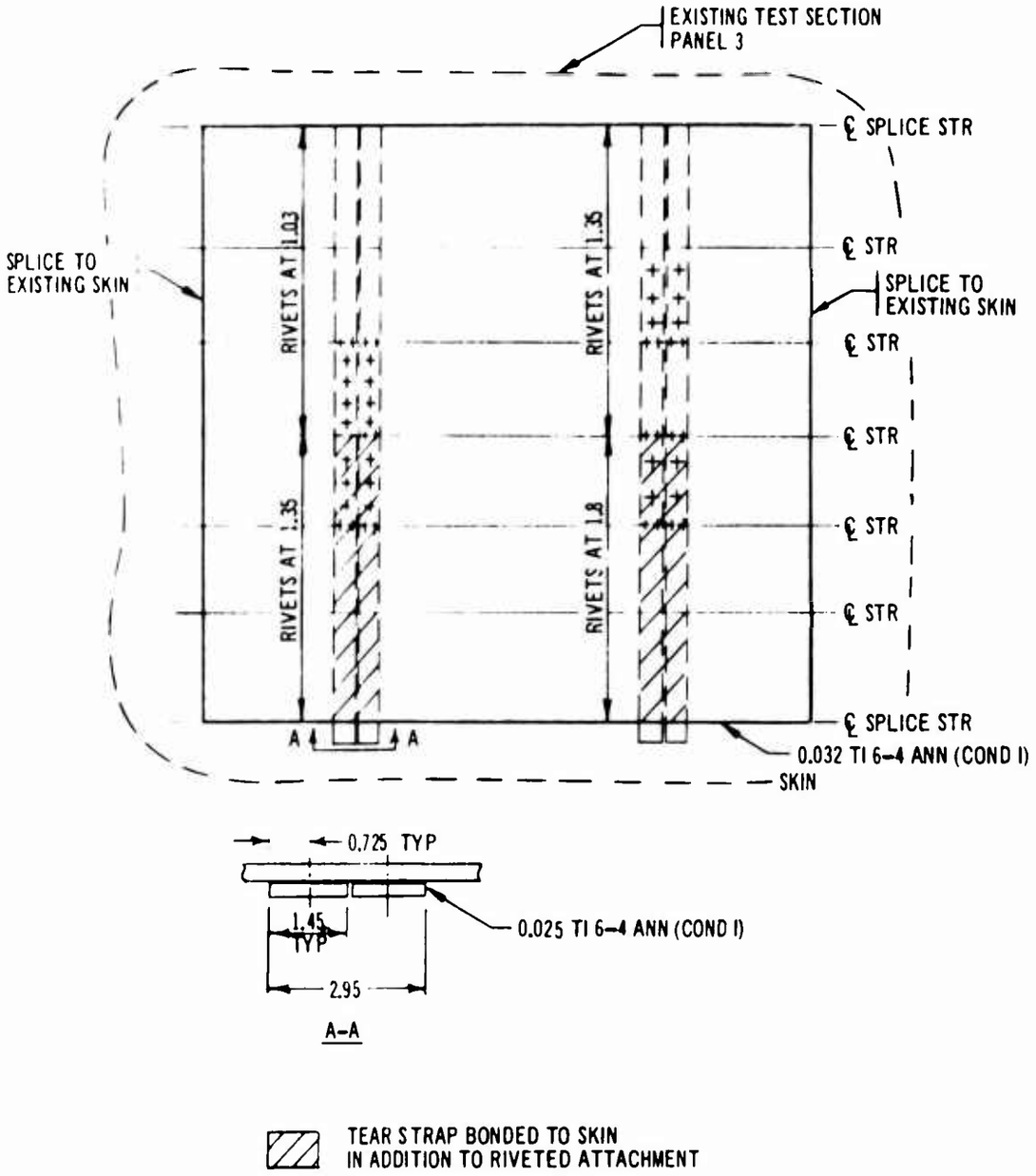


Figure 3-62. Dual Strap Panel Configuration

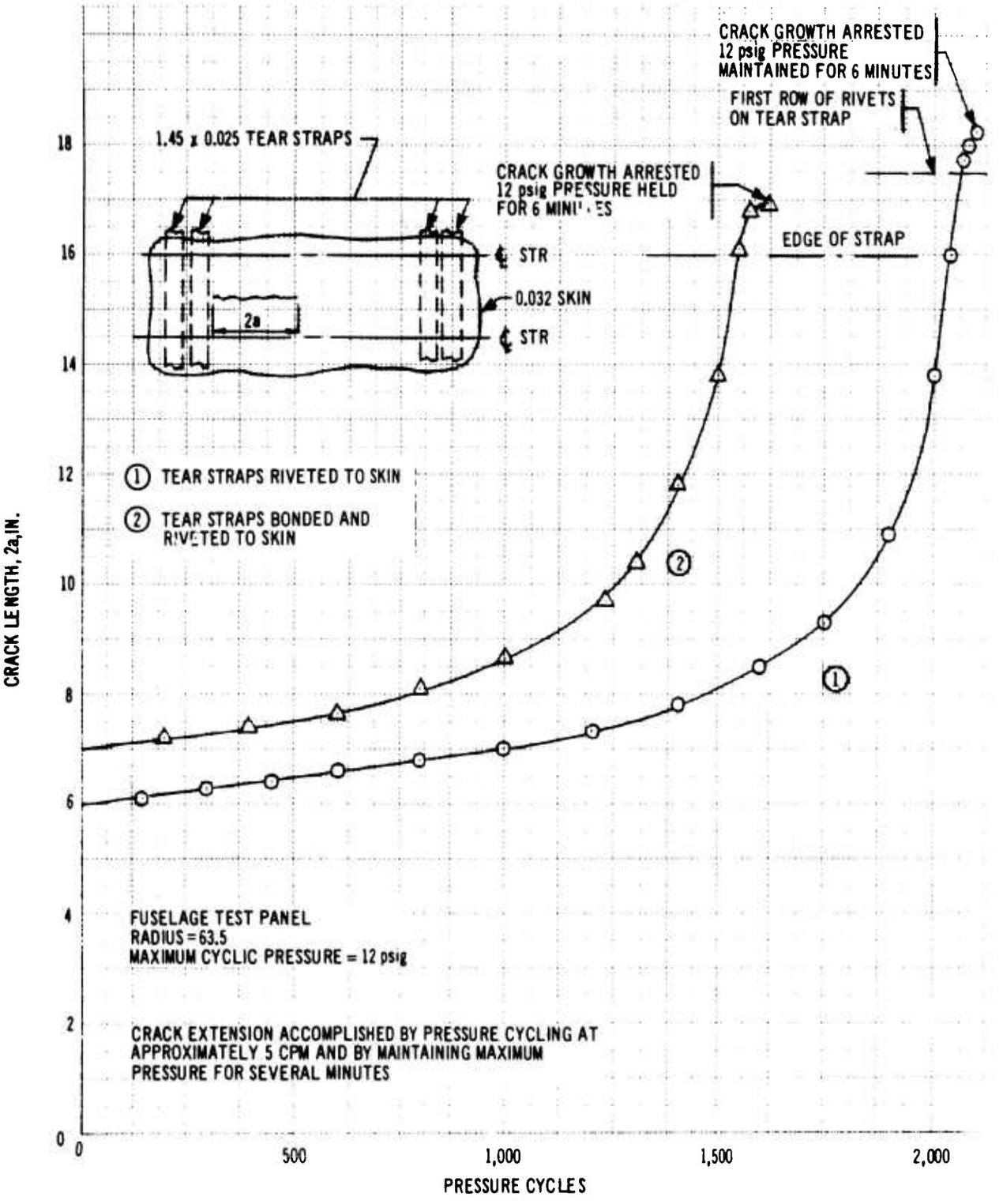


Figure 3-63. Crack Growth History – Dual Strap Test Panel

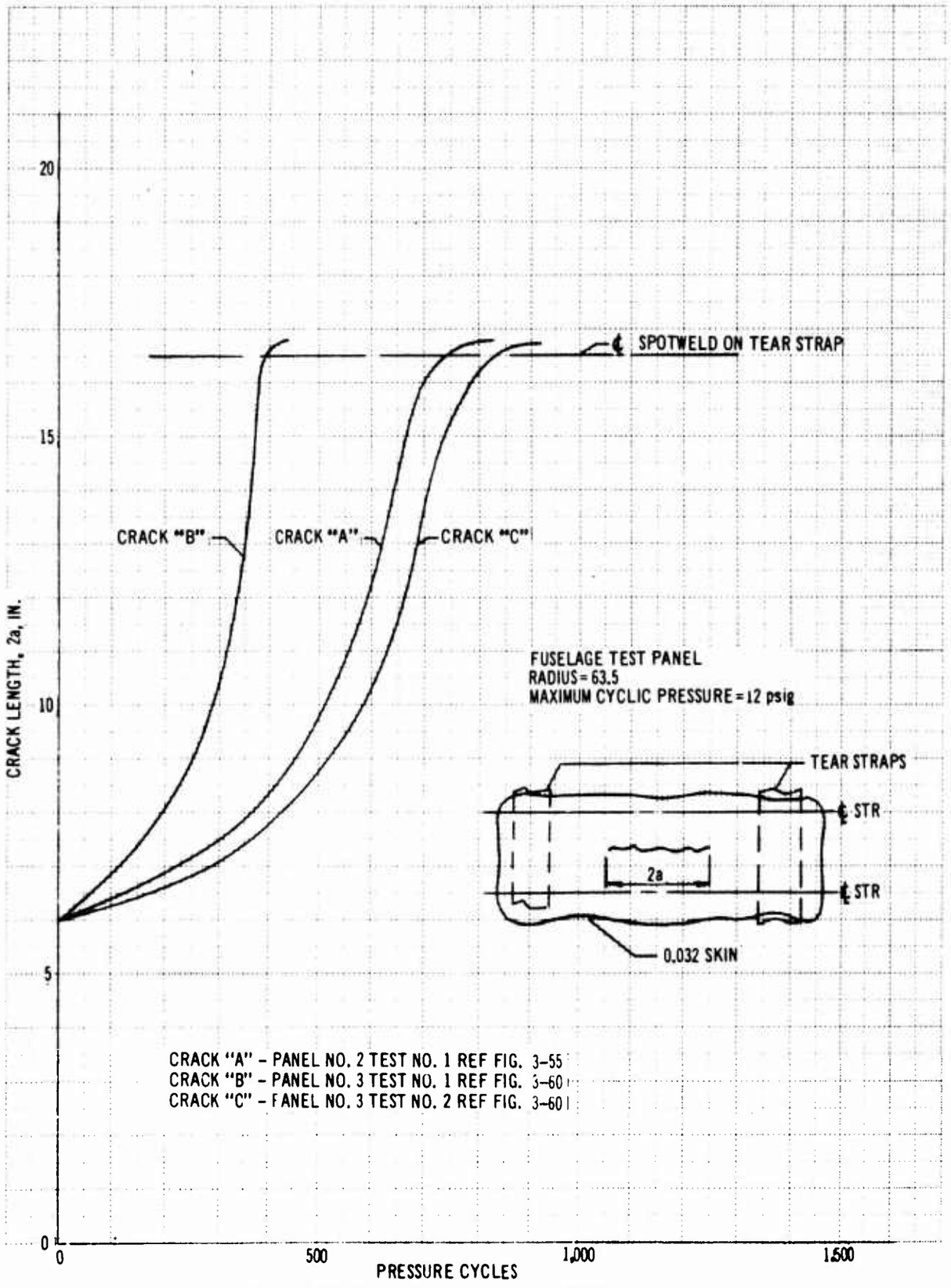


Figure 3-64. Crack Growth History – .032 Gage Test Panels

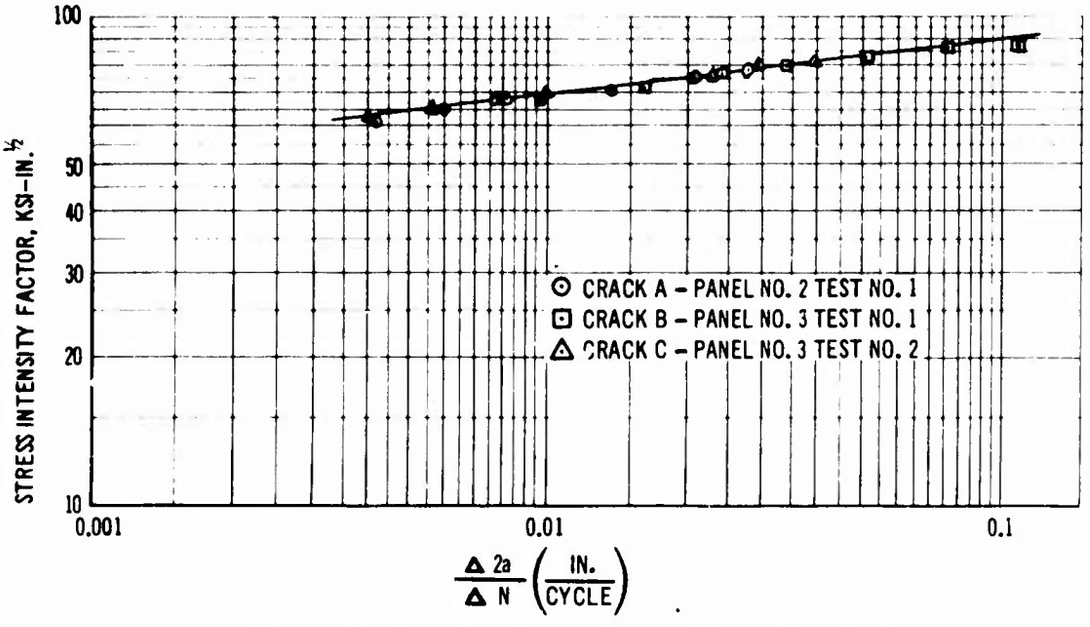


Figure 3-65. Crack Growth Rate Data – .032 Gage Test Panels

b. Cyclic Pressure Test

The crew compartment will be pressure cycled at room temperature from 0 to 11.12 psig with inspections scheduled at the end of 500 cycles, 1,500 cycles, 2,500 cycles, and every 2,500 cycles thereafter. Stress and deflection will be recorded at every 500 cycles and the effects on structure observed during each inspection layup.

c. Room Temperature Pressure Test

The crew compartment will be pressure tested at room temperature to 25 psig in increments of 5, 10, 15, 20, 23, and 25 psig. Stress and deflection will be recorded and the effects on structure observed at each pressure increment.

d. Thermal and Static Pressure Test

The compartment will be pressurized to 11.12 psi and heat applied to structure and window surfaces to 200°F, 300°F, 400°F, 450°F, and 530°F on five successive runs. The 200°F, 300°F, and 400°F temperatures will be maintained 2 hr each, the 450°F temperature will be maintained 45 min and the 530°F temperature maintained for one min. Stress, deflection, and temperature will be recorded and the effects on structure observed.

e. Thermal and Fail-Safe Window Test

To simulate a window-out condition, the outer pane of the left forward side window will be removed and the crew compartment pressurized to 11.12 psig (Fig. 3-69). Heat will be applied to the structure and window surfaces to 200° F, 300° F, 400° F, and 450° F on four successive test runs and temperature maintained for 30 min at each temperature. Stress, deflection, and temperature distribution will be recorded and the effects on structure observed. The outer pane will be replaced and the main pressure pane bypassed permitting the 11.12 psig pressure to be carried by the outer pane. Heat will be applied in the same manner listed above. The above two tests will be repeated for the left aft side window. Similar fail-safe tests will be conducted for the left forward windshield except the temperature runs will be 2 hr at 200°F, 300°F, and 400°F, 45 min at 450°F and one min at 530°F.

To simulate a visor-off condition, the crew compartment will be pressurized to 11.12 psi and heat will be applied to the left forward windshield to 200°F and 300°F for 2 hr, 400°F for 5 min, and 530°F for 1 min on 4 successive runs. Stress, deflection, and temperature will be recorded and effects on the structure observed.

f. Bird Strike Tests

The left forward windshield will be tested for bird-strike resistance with the windshield heating off and with the effects of the maximum thermal environment. The outside surface of the crew compartment will be heated to 450°F and the

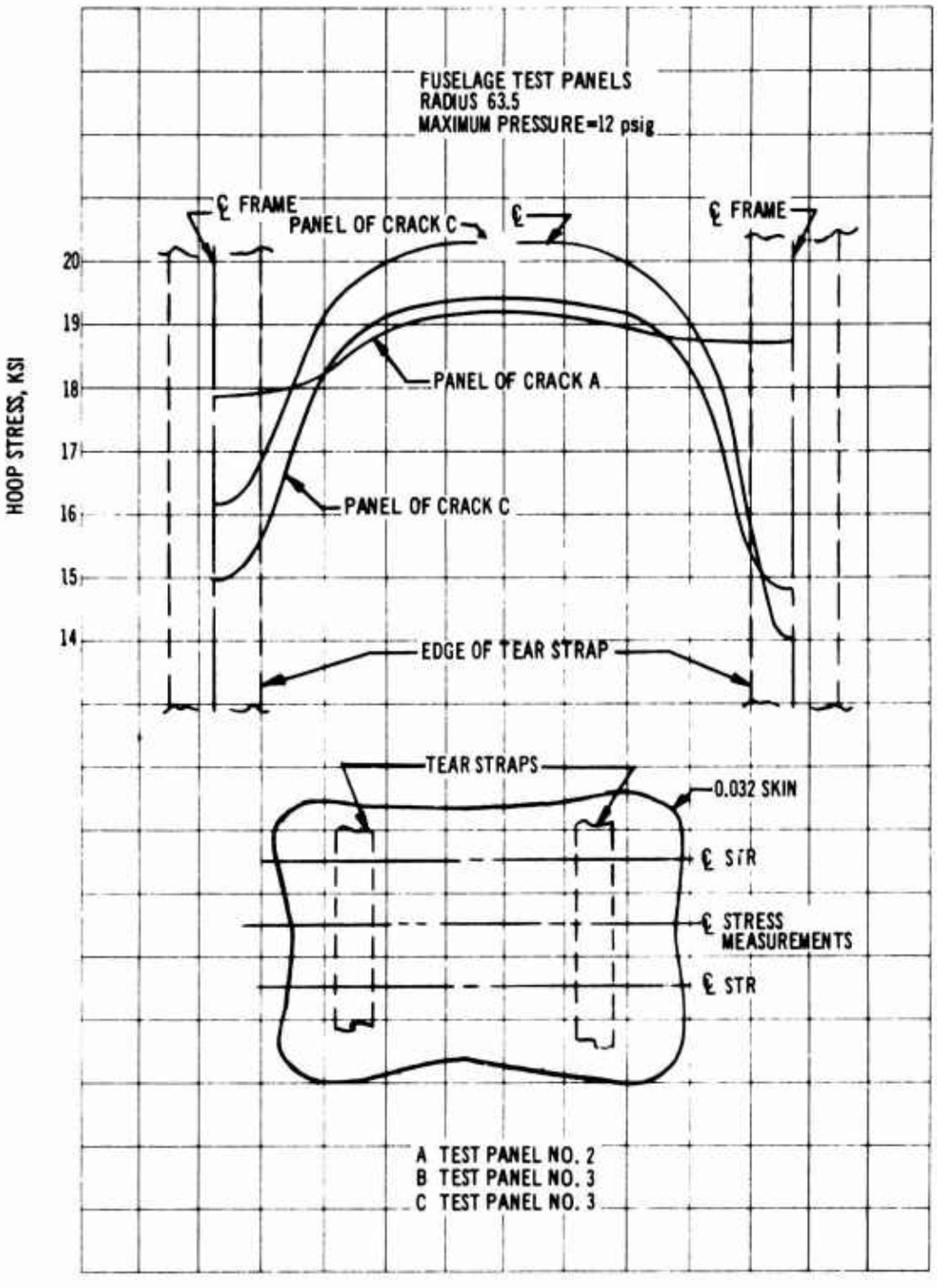


Figure 3-66. Test Panels Stress Distribution

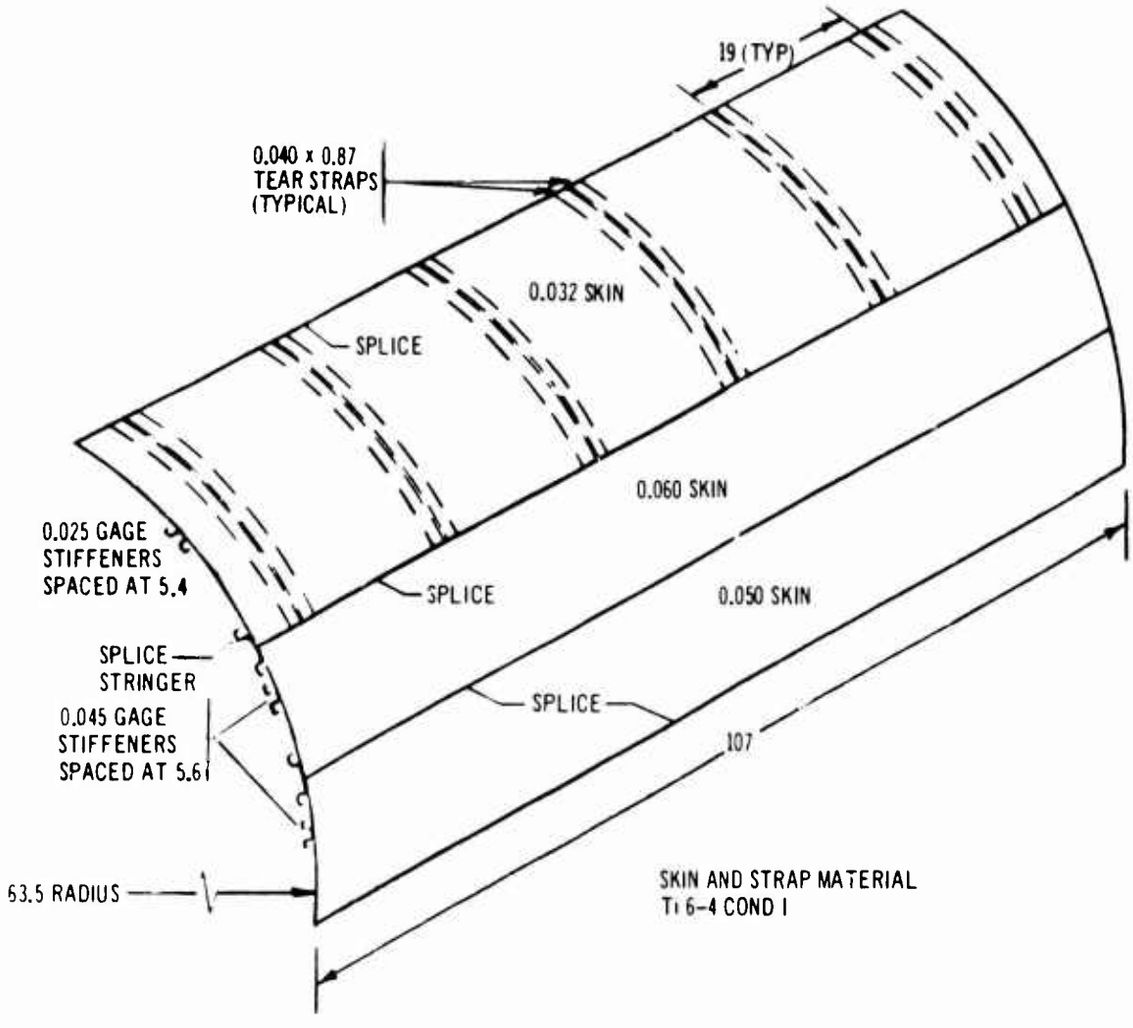


Figure 3-67. Verification Test Panel Configuration

interior cab air temperature maintained at 70°F. The outer window will have an outer and inner surface temperature of 350°F. The inner window will have an outer surface temperature of 150°F and an inner surface temperature of 115°F. The windshield assembly will be struck by freshly killed four pound birds with an impact velocity of 450 mph. The impact areas will be the center and upper outboard corner of the windshield with two strikes in each area. High-speed movies will be taken of the bird impact.

3.4 EMPENNAGE TESTS

Two box structures representative of skin-stringer construction and honeycomb panel construction were subjected to mechanical and thermal loads. The primary concern was accurate determination of surface buckling which could result in aerodynamic drag penalties. The tests and specimens are described in the following paragraphs.

3.4.1 Thermal Buckling Test of Skin-Stringer Box

Because of the detrimental effects of surface buckles and waviness on aerodynamic drag, a structural box was designed to study the effect of heat on the structural response of typical lightweight titanium skin stringer structure. The box has been tested extensively in support of analytical techniques for predicting surface waviness. Methods of analysis have evolved which

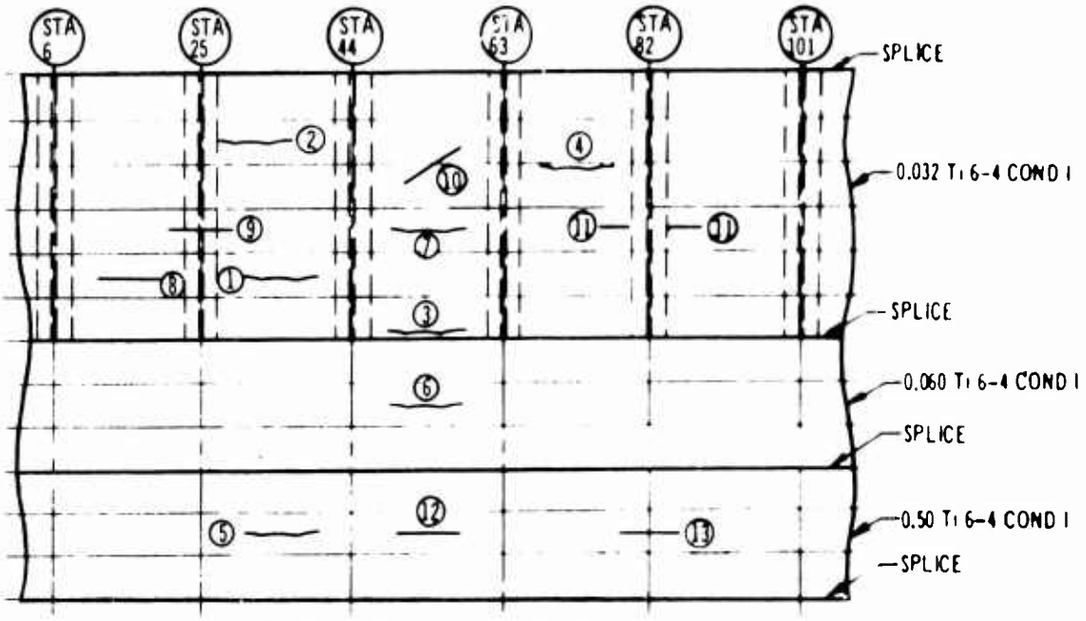


Figure 3-68. Verification Test Outline

allow accurate determination of the buckling stresses, the buckling temperatures, and the surface waviness of conventionally stiffened titanium skin panels. The variables that can be accounted for are skin thickness, skin area, stringer area, stringer spacing, rib area, rib spacing, rib stiffness, shear tie spacing, shear tie stiffness, externally applied uniaxial or biaxial stresses and temperature differences between skin and stringer or skin and rib. Charts have been constructed which show those combinations of these parameters that are required for either no buckling or a calculated degree of buckling. The derivation of the theory and correlation with test results are explained in detail in Boeing Document D6-16240, Ref. 21

3.4.1.1 Description of Test Box and Test Procedure

The test box (Fig. 3-70) was 80 in. long, 30 in. wide and 9 in. deep. The upper and lower surface panels were designed to be representative of the type and size of construction intended for the outer portion of the empennage and wing surfaces where the end loading is approximately 7,000 lb/in. Subassemblies (Ti 8-1-1) were fastened by diffusion spotwelds and final assemblies were bolted with close tolerance steel bolts in Class I holes. The upper panel was stiffened with 0.050 in. stringer at 3.0 in. spacing. The skin material was chem-milled from a basic 0.120 sheet to 0.030 in. thickness between the stringers. The lower panel was a constant thickness 0.064 sheet stiffened by 0.060 stringers at 3.90 in. spacing. The ribs had conventionally stiffened webs and were spaced at 18.0 in.

The surface panels were subjected to compressive end loads by applying bending moments to the box through extensions. Direct transverse loads were also applied. Heat was applied by radiant lamps programmed to follow rates which simulated normal supersonic flight conditions. The panels were forced into buckling patterns by several combinations of longitudinal and transverse loads and several combinations of longitudinal loads and heat cycles. During the heat cycles surface waviness, stress, and temperature were recorded continuously against a time scale. Figure 3-71 shows the lower surface under a compression loading of 2,600 lbs/in. and the instrument used for recording surface waviness. The effect of disconnecting all but the end shear tie between each rib and skin was examined and found to reduce

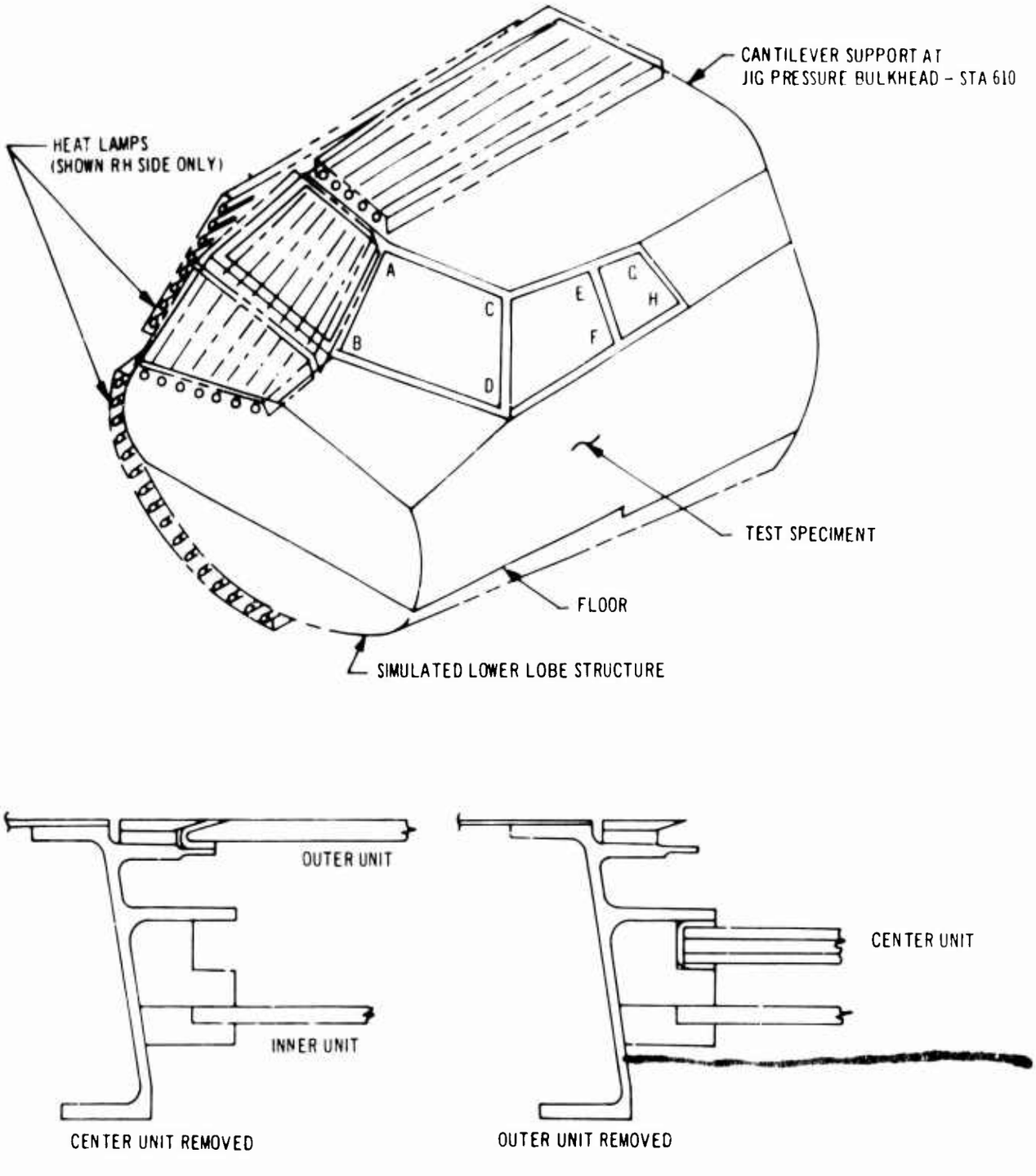


Figure 3-69. Cab Test Section

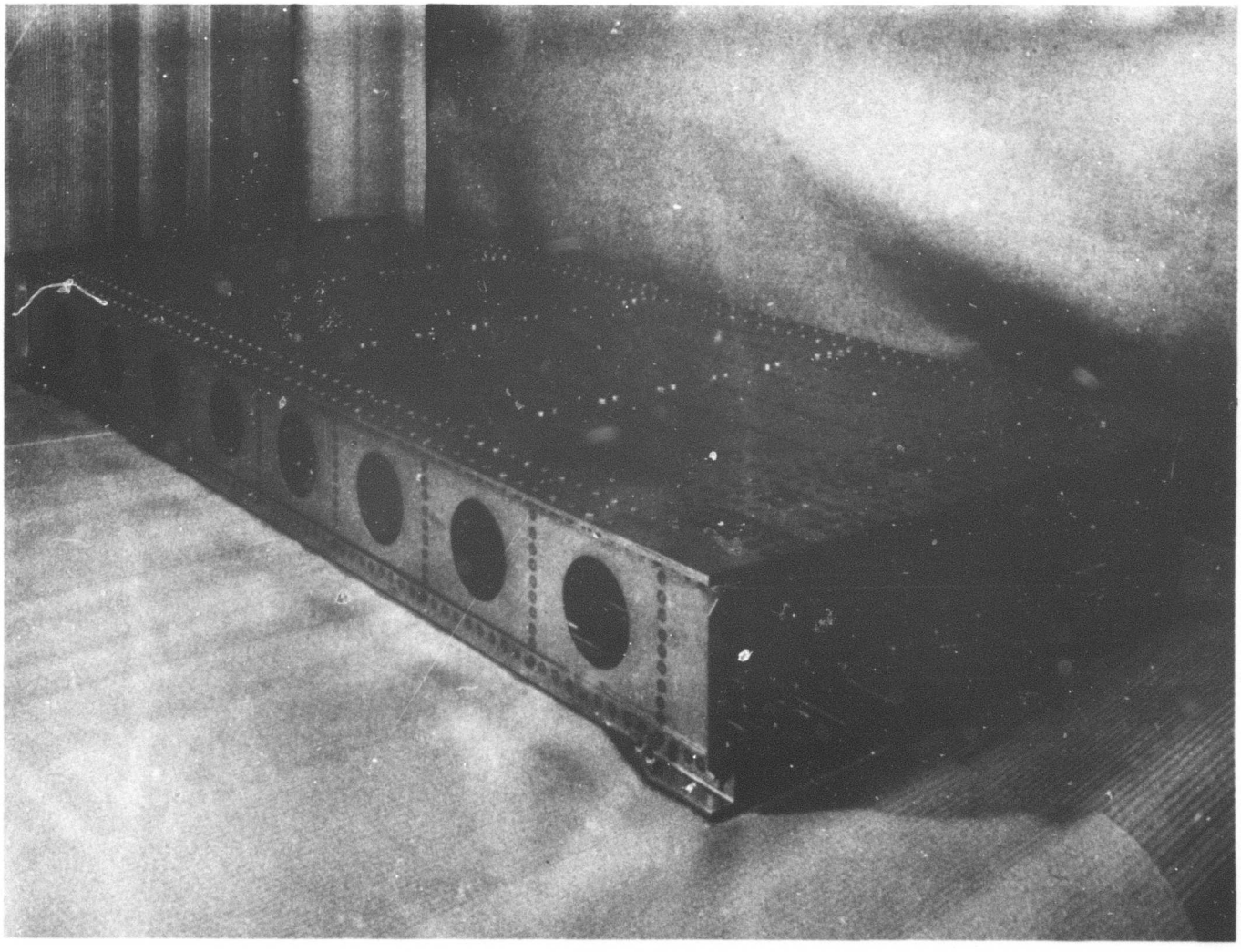


Figure 3-70. Thermal Buckling Box

the restraint of the ribs on the expansion of the the skin by approximately 45 percent at the upper surface and 23 percent at the lower surface as indicated by both measured and calculated stress levels in the rib chords. The effect of internal pressure up to 4 psi on the buckling patterns was found to be negligible.

The following analytical techniques were derived for predicting the surface waviness.

a. Calculation of the temperature distribution using the Boeing Thermal Analyzer Program, Ref. 3.

b. Calculation of the thermal stress distribution.

c. Calculation of the buckling stresses.

d. Calculation of the buckling temperature.

e. Calculation of the surface waviness on the basis that a temperature increase above the buckling temperature produces an elongation in the panel that causes a sine wave buckle shape.

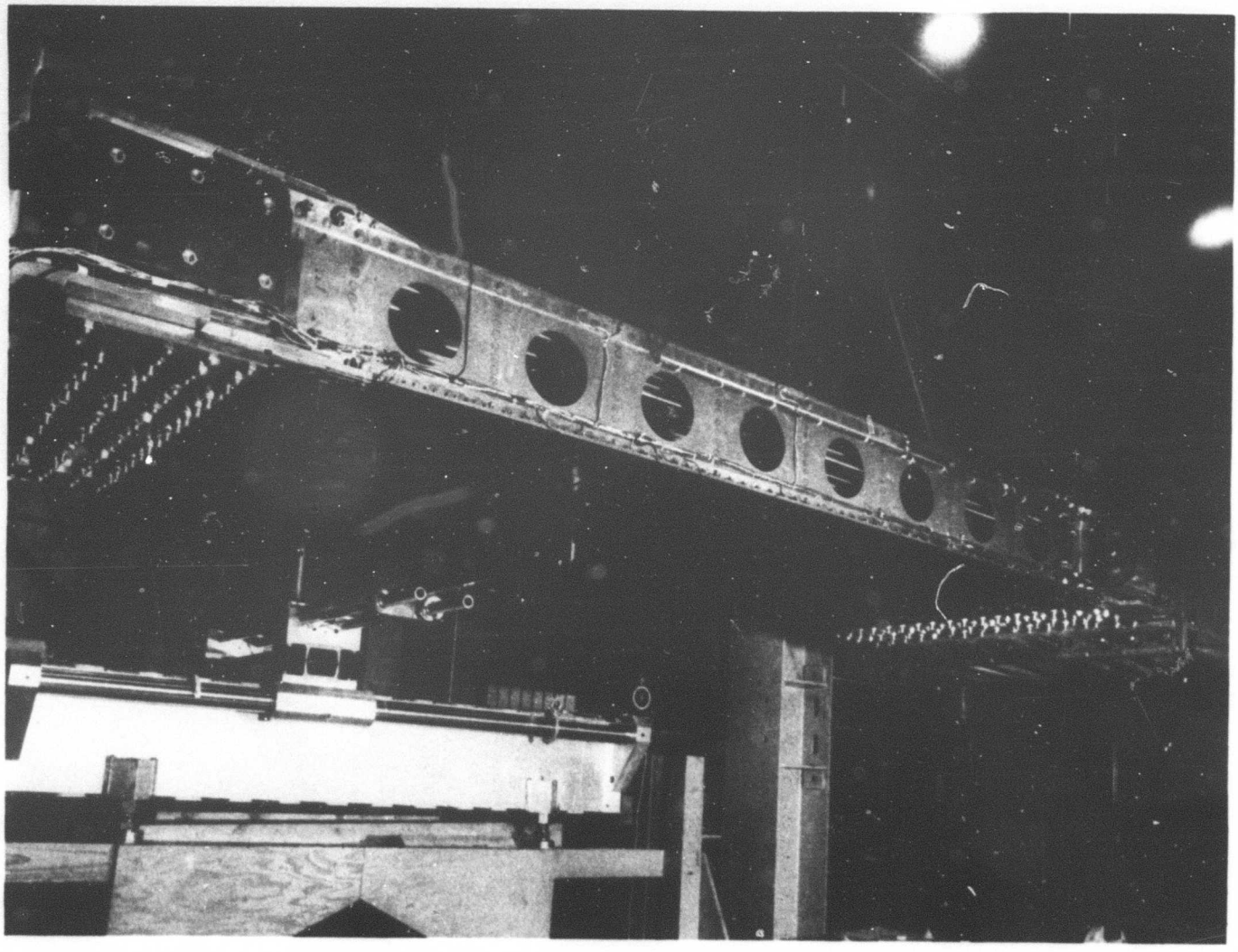


Figure 3-71. Thermal Box Test Setup

Each of these steps was correlated to the corresponding test result so that the theory used could be amended for closer agreement. Adjustment to the theory was found to be necessary in the following areas.

a. The calculation of transverse stresses had to be corrected empirically for the additional flexibility of the shear tie joints.

b. The calculation of the axial buckling stresses had to be based on buckling coefficients derived from this and previous tests. The assumption of a simply supported edge condition was overly conservative.

c. The calculation of biaxial buckling stresses had to be based on an interaction buckling curve derived from the test program.

Figure 3-72 shows the correlation between the amended theory and the test results for one of the test conditions.

3.4.2 Thermal Buckling Honeycomb Panel

A light-weight honeycomb panel has undergone extensive testing for surface waviness under a variety of environmental conditions. The results indicate a decided surface smoothness advantage over skin-stringer construction. Normal methods of calculating panel deflection under thermal

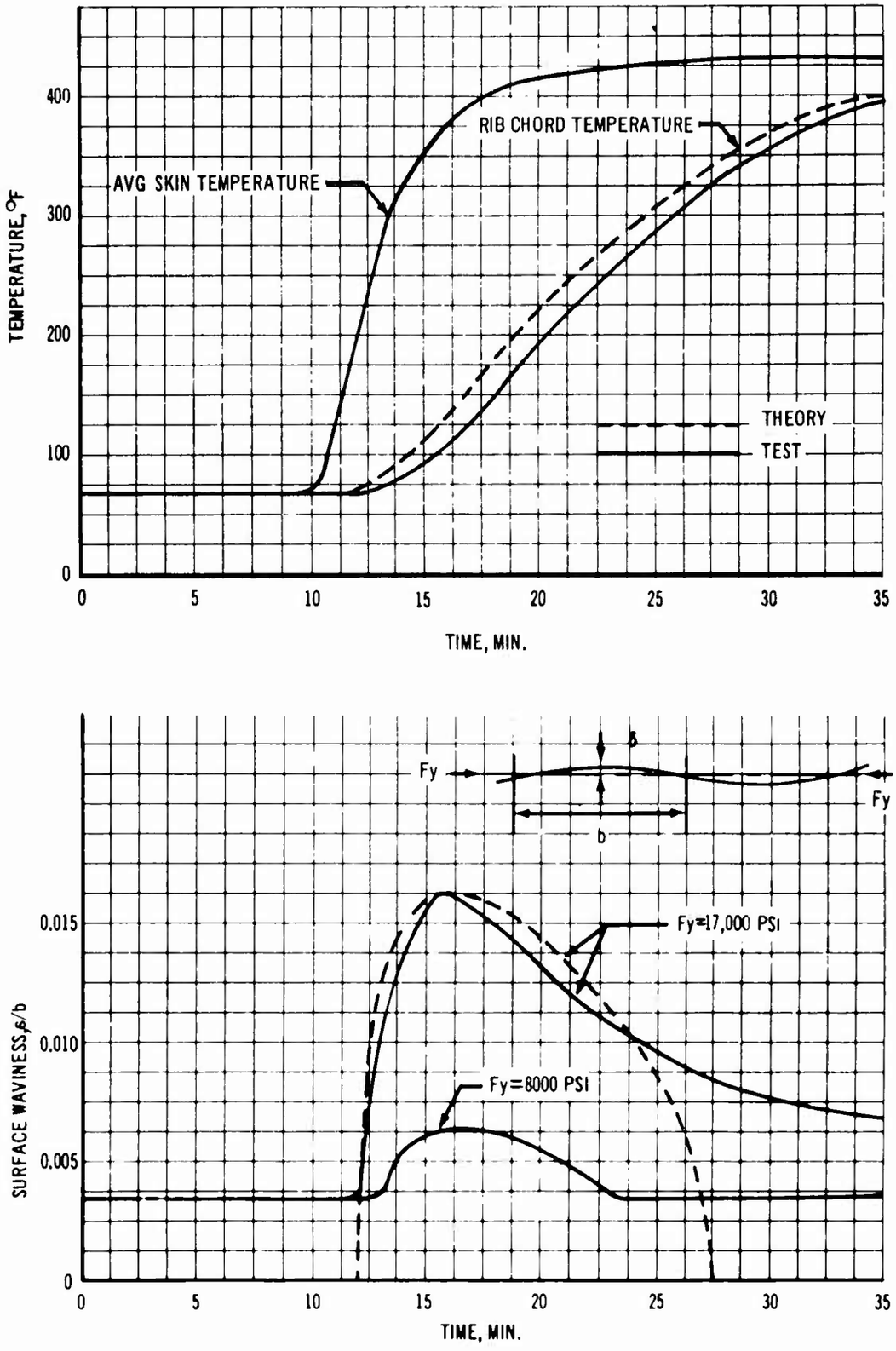


Figure 3-72. Correlation of Theory and Test – Skin-Stringer Panel

gradients and transverse pressures were found to be accurate and in the case of in-plane load conditions these were conservative except where local buckling developed.

3.4.2.1 Description of Honeycomb Panel and Test Procedure

The honeycomb panel was mounted on the thermal buckling box in place of the upper stringer panel. The core material was 3/4 in. thick HRH 324 tapered to zero thickness at the spar and rib locations. The outside skin was 0.050 titanium 8-1-1 sheet chem-milled down in two steps to 0.021 at full core depth. The inner skin was 3-ply polyimide fiber glass reinforced in steps to 6-ply where it met the outer skin. The panel (Fig. 3-73) carried strain gages and thermocouples so that stress and temperature distribution could be measured.

The panel was tested in the same manner as the skin and stringer panels. Fig. 3-74 shows the panel being tested under the radiant heat lamps.

Initial tests revealed that local distortion took place at the panel edges. This was attributed primarily to lack of flexural stiffness in the panel edges and insufficient torsional stiffness in the rib chords. As it is intended that this type of panel will be used in conjunction with corrugated ribs, the rib chords and web stiffeners of the test box were replaced by more rigid members



Figure 3-73. Honeycomb Test Panel

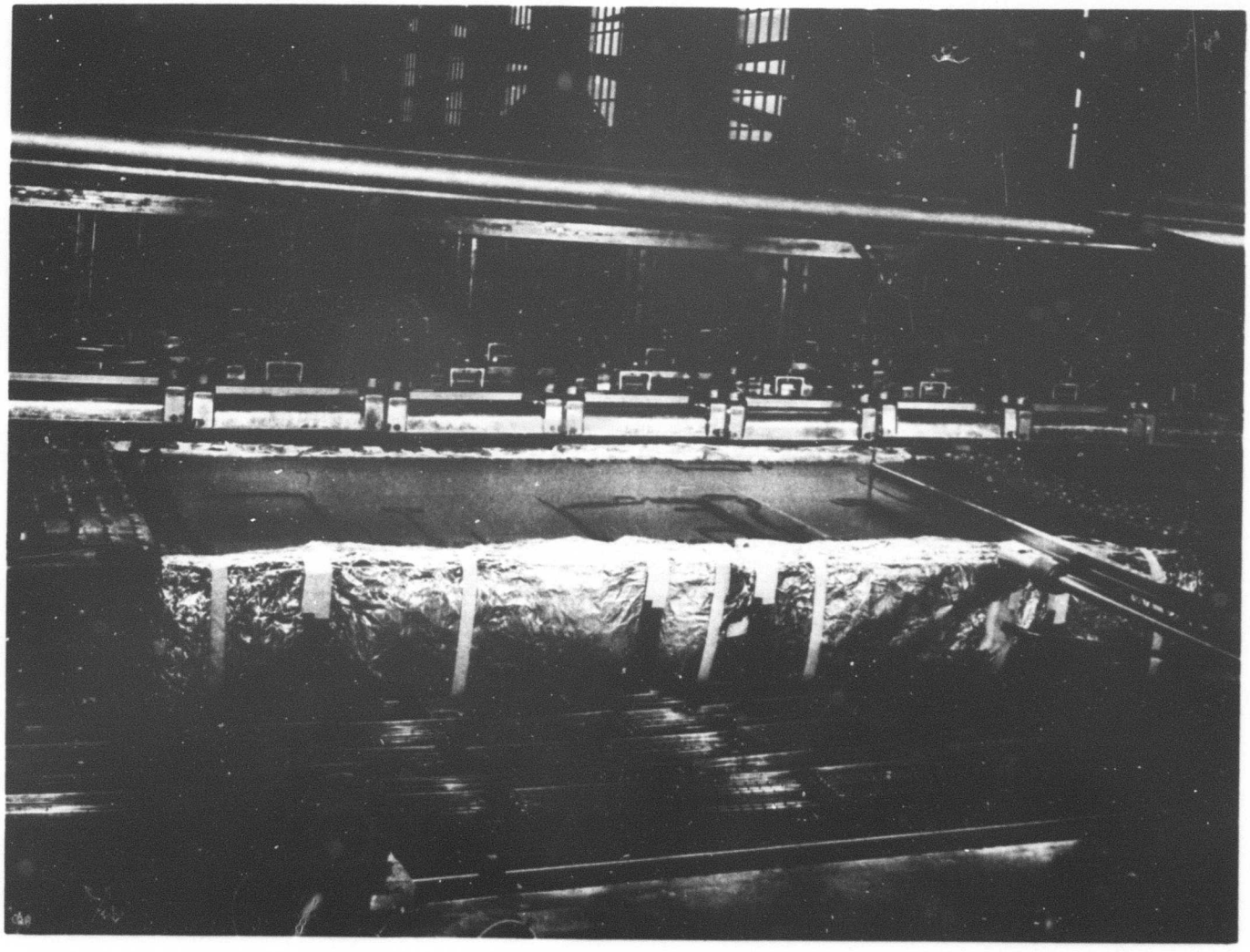


Figure 3-74. Radiant Heat Test of Honeycomb Panel

calculated to give the same torsional stiffness at the panel connections as would be obtained from a corrugated rib. In addition thin titanium doublers were added to the inner surfaces of the tapered edges of the panels.

Improvements in buckling load capability were obtained as a result of the reinforcement. Local buckling however was not prevented along the spar-chord edges under transverse loads, and the maximum stress level obtained at the center of the panel under transverse loads prior to local buckling was approximately 45,000 psi. Local buckling occurred at the one critical rib location and the maximum stress level obtained at the panel center under longitudinal loads was approximately 65,000 psi. Considerable data was collected before the final test, on panel deflection, stresses, and temperatures under varying combinations of longitudinal load, transverse load, internal pressure, and heat. It was noted that thermal deflection was prevented at high longitudinal loads when the loads preceded the thermal gradient but not if the thermal gradient preceded the load.

Figure 3-75 shows the temperatures and surface waviness measured for one of the test conditions compared with those measured on a stringer panel for comparable load conditions. The superiority of the honeycomb panel over the skin-stringer panel with respect to surface waviness is clearly indicated.

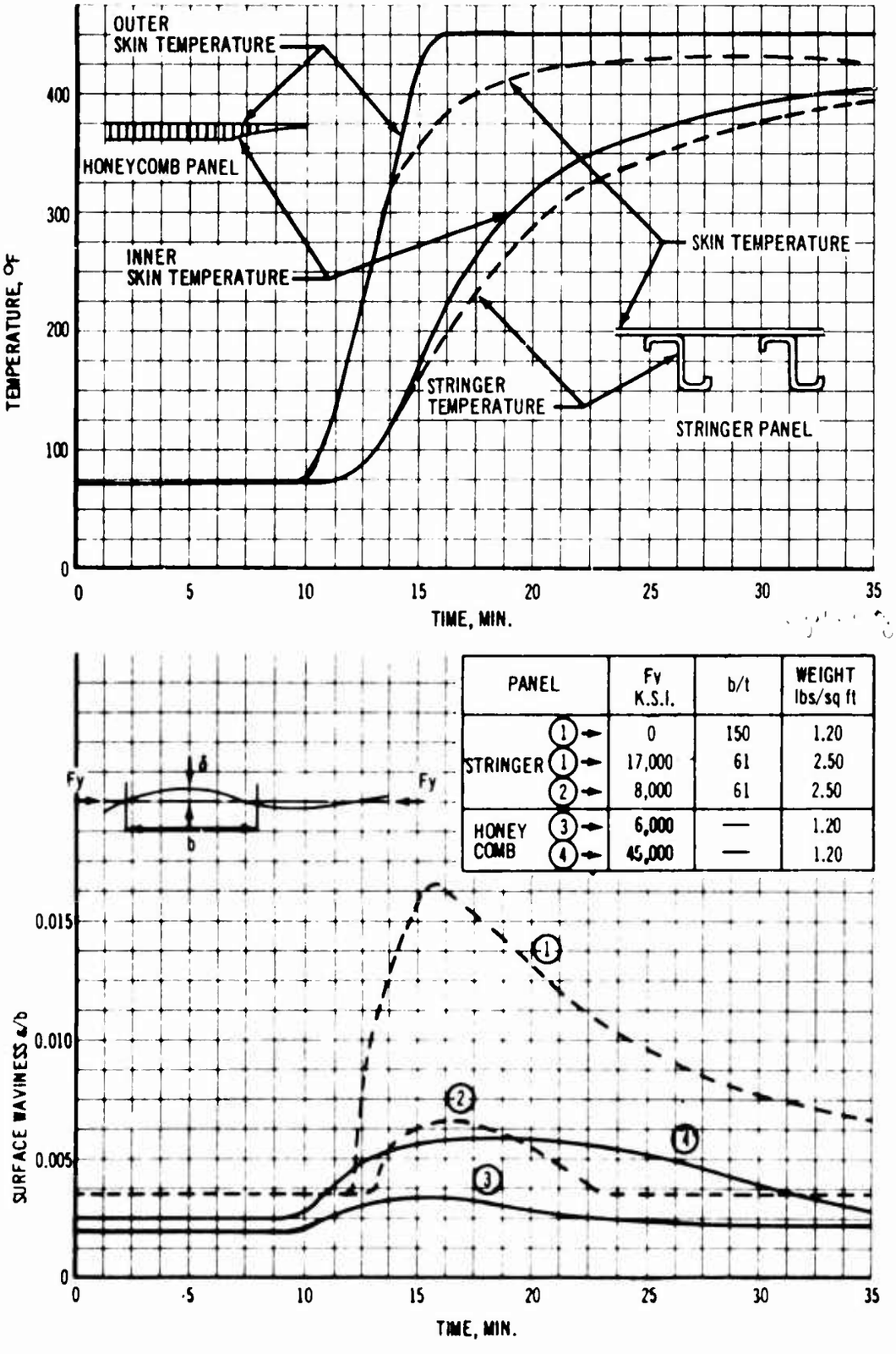


Figure 3-75. Temperature and Waviness of Lightweight Panels

3.4.3 Empennage Test Structure

A large assembly representing empennage structure is being fabricated for testing in late 1966. It consists of a solid honeycomb core leading edge, corrugated ribs supporting honeycomb surface panels and a primary box. The box is fitted with a honeycomb panel spliced to a skin stringer panel at mid-spar. The purpose of this test program is to examine the response of the individual panels as an assembly when subjected to biaxial in-plane loads, surface pressures, and heat typical of normal and design flight conditions. The honeycomb panels have been designed to exhibit general buckling in place of the local buckling which occurred in previous tests. Figure 3-76 shows a sketch of the assembly. Document D6A10235-1 (Ref. 4) shows the design loads and stress analysis of the assembly.

3.5 PROPULSION POD TESTS

3.5.1 Centerbody Pressure Test

In the process of an orderly development of the variable-geometry engine inlet system, a program was initiated to design, fabricate, and test a complete, full-size, expandable inlet centerbody. The centerbody was fabricated of annealed Ti 6Al-4V to demonstrate manufacturing capability and to properly assess the effects of structural deflections under load on the inlet performance. The centerbody design was sized from an earlier airplane configuration, having a local inlet Mach number of 2.55.

Fabrication of the centerbody and its pressure tank facility have been completed and the initial test is imminent. Testing will be conducted in a specially constructed pressure tank. The tank is divided into three compartments to permit simultaneous application of different pressures which simulate the varying pressure loadings on the engine centerbody resulting from aerodynamic shock waves within the engine inlet. Tests will be conducted at both room temperature and 550°F, utilizing preheated air. The test program will encompass seal leakage, seal wear, measurement of structural deflections, and evaluation of load distributions within the centerbody structure. Test conditions will cover the entire airplane Mach number range.

Test results from this program will be utilized to assess the performance of the centerbody seal design and the ability of the seals to sustain repeated cycling without excessive wear or structural failure. Strain gage data will permit evaluation of structural load paths and optimization of material distribution. Deflection data will be used to adjust configuration contours for optimum inlet performance. Test results will be applied to the design of the full-scale inlet test program scheduled for the Advanced Engineering Drawing Change Propulsion Wind Tunnel facility during Phase III.

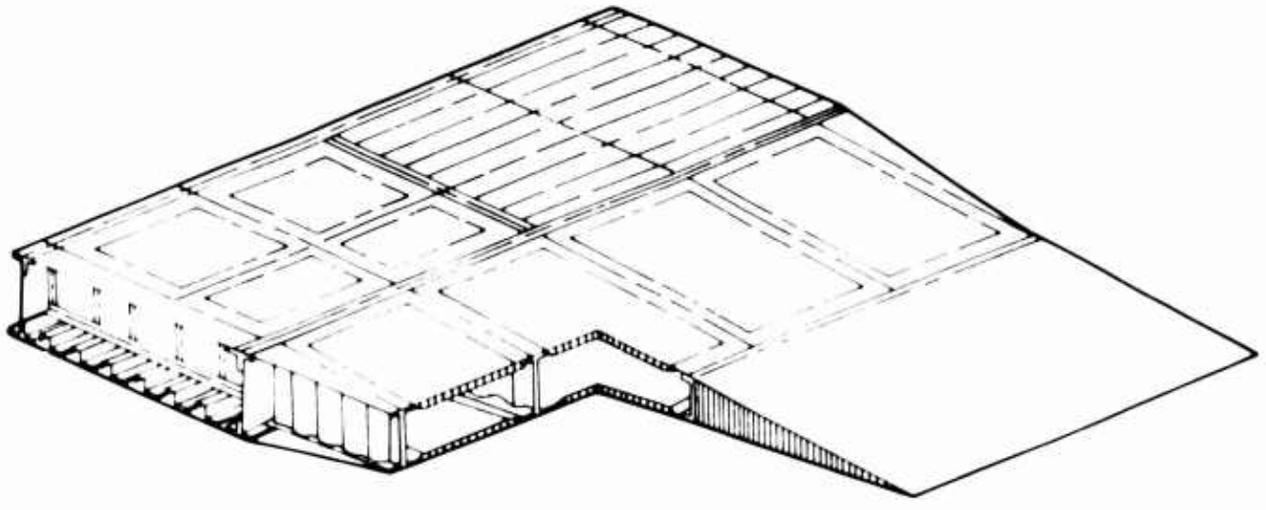


Figure 3-76. Empennage Test Structure

3.6 FATIGUE TESTS

This program has been conducted to provide an accurate assessment of the fatigue quality of the various titanium structures for the B-2707. Data from these tests have been used to establish fatigue design criteria that will provide the extended service life necessary on the B-2707. Data are presented for simple coupon tests through large scale specimen tests and for basic structure through complex joints. A general assessment shows the Ti 6Al-4V alloy to be adequate for the 50,000-hr service life requirement so long as close attention is given to the detail design and assembly methods.

3.6.1 Summary

This section presents a summarization of results for the titanium fatigue test programs conducted in support of the design. Those programs which were completed or in work are described. Design criteria and finalized S-N curves are presented in Section 5 of V2-B2707-6-2. Additional development fatigue test data is presented in the Materials and Process, Document V2-B2707-8.

3.6.2 Wing Structure Fatigue Tests

3.6.2.1 Full-Scale Tests

A program of fatigue tests of full-scale segments of wing structural configurations is in work. These tests are used to evaluate variables such as structural geometry, materials, fastening techniques, and load and temperature effects. The test results provide data on the suitability of structural concepts and are the basis for establishing initial S-N curves for fatigue analysis.

All test panels are either Ti 8-1-1 or Ti 6Al-4V alloys and as large as possible commensurate with desired test stress levels and test machine capability. This large size enables a more realistic representation of actual structural behavior to be achieved than can be realized from simple specimen testing. A basic wing skin stiffener test panel is shown in Fig. 3-77. This configuration has a width of 15-in., 0.125 skin and three zee section stiffeners. Figure 3-78 shows a spotwelded panel with a 0.375 thick skin and two zee stiffeners. The fatigue life of spanwise splices was investigated with the configuration shown in Fig. 3-79. An access door panel is in work to evaluate initial design concepts. This configuration is shown in Fig. 3-80. Two stiffener runout panels, containing four different runout designs, are in fabrication. Figure 3-81 shows the primary details. To provide initial design data on the effects of local chordwise loads on basic wing structure, two panels of the configuration shown in Fig. 3-82 are being fabricated. Both panels will be tested with the same spanwise load, but only one will have the chordwise load.

The panels tested to date have all been at room temperature with constant amplitude loadings. Extension of the program will include elevated temperature and spectrum loading. In addition most panels will be subjected to a thermal soak at 500° F prior to testing.

The test results to date, and the panels currently in fabrication or ready for test, are summarized in Table 3-J.

3.6.2.2 Small Specimens

A large number of tests have been conducted with representative specimens of the wing and stringer basic structure configuration. The specimen shown in Fig. 3-83 is composed of two strips connected with fasteners or spotwelds. One of the members is narrower than the other in the test section and represents the stringer skin attachment leg of a skin-stringer basic wing structure. Although producing somewhat longer life than the large specimen described in Par. 3.6.2.1, this configuration provides good correlation with large scale specimens at a much reduced cost and is used in establishing design criteria and configuration. The specimens are tested in a Riehle-Los or similar test machines (Fig. 3-84) at both elevated temperatures and room temperature. A large number of these specimens have been used to evaluate the effects of many variables on fatigue performance, including fastener types and installation, materials and finishes. Test results are presented in Figs. 3-85 through 3-91 and Tables 3-K and 3-L. Additional baseline specimens (220) are being tested as a part of a program in work and will be used to optimize the structure arrangement, fasteners, fastener installation, testing methods, and exposure effects. Test data available from this program is presented in Figs. 3-92 through 3-94. Other data pertinent to fastener selection is shown in Figs. 3-95, 3-96, and 3-97, and summarizes the performance of various fastening methods. These data show the squeezed fastener to be superior to all other methods tested. The data shown for pad attachments and simulated skin fracture (Figs. 3-96 and 3-97) also illustrate the major

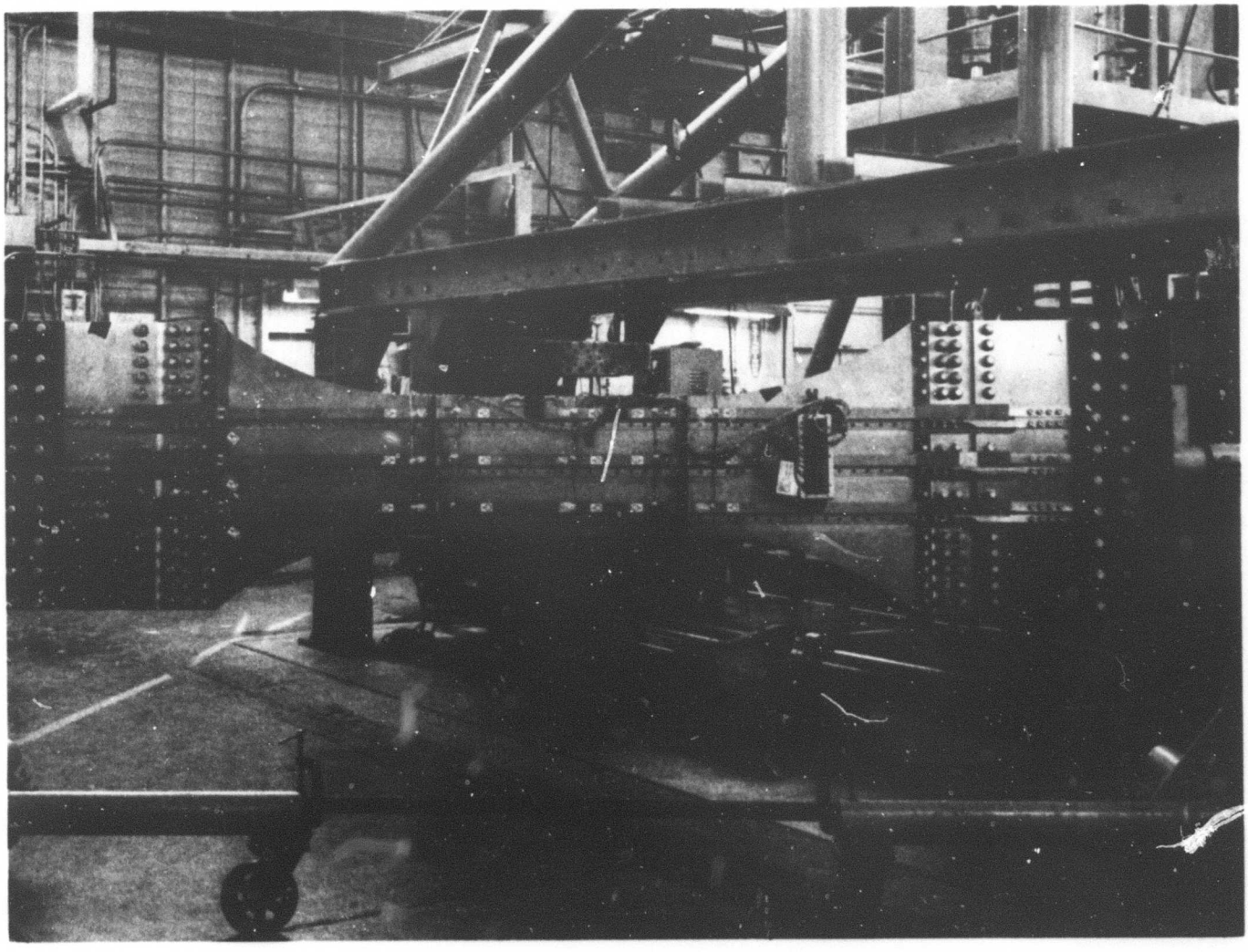


Figure 3-77. Wing Skin and Stiffener Panel

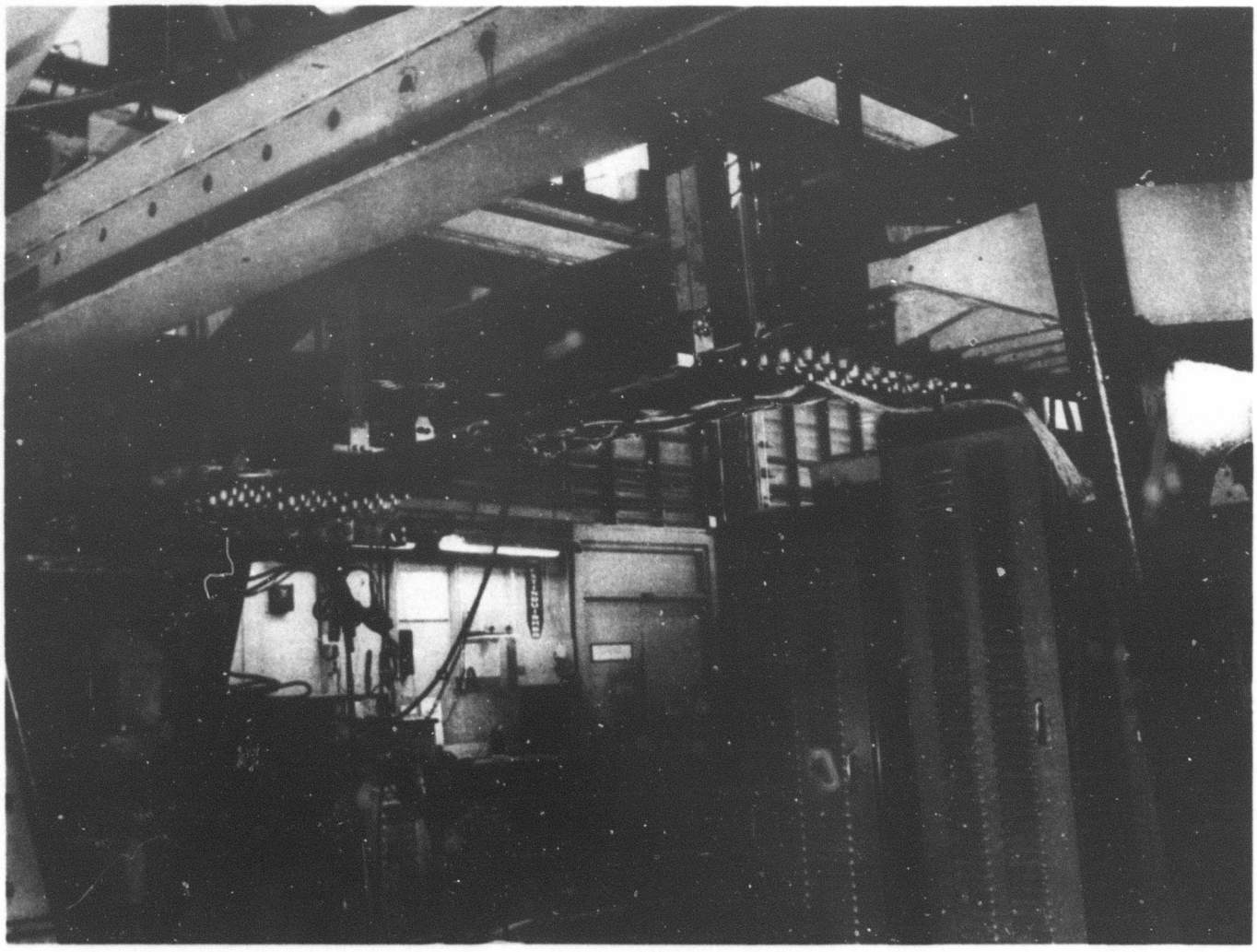


Figure 3-78. Spotwelded Wing Panel

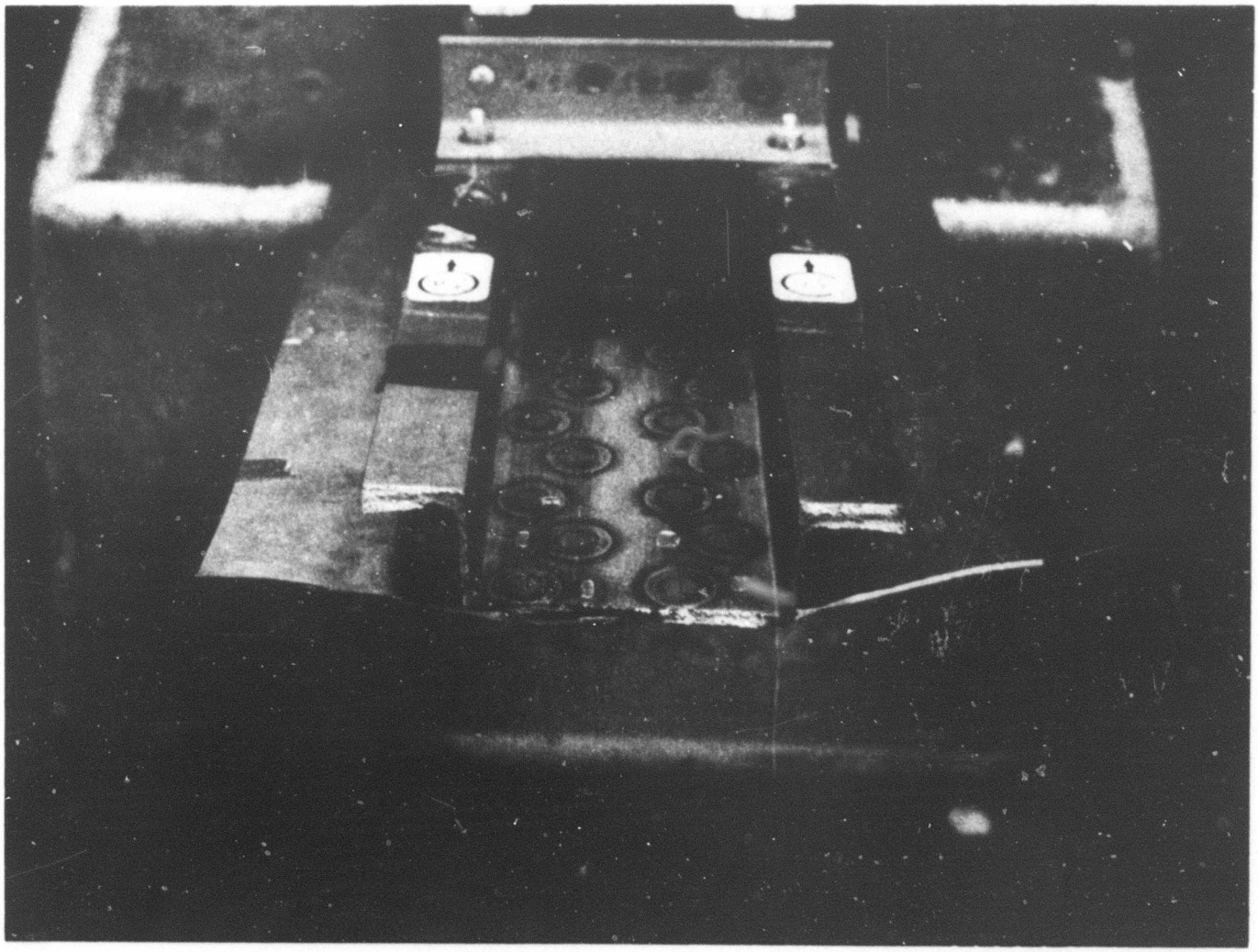


Figure 3-79. Spotwelded Wing Spanwise Splice Panel

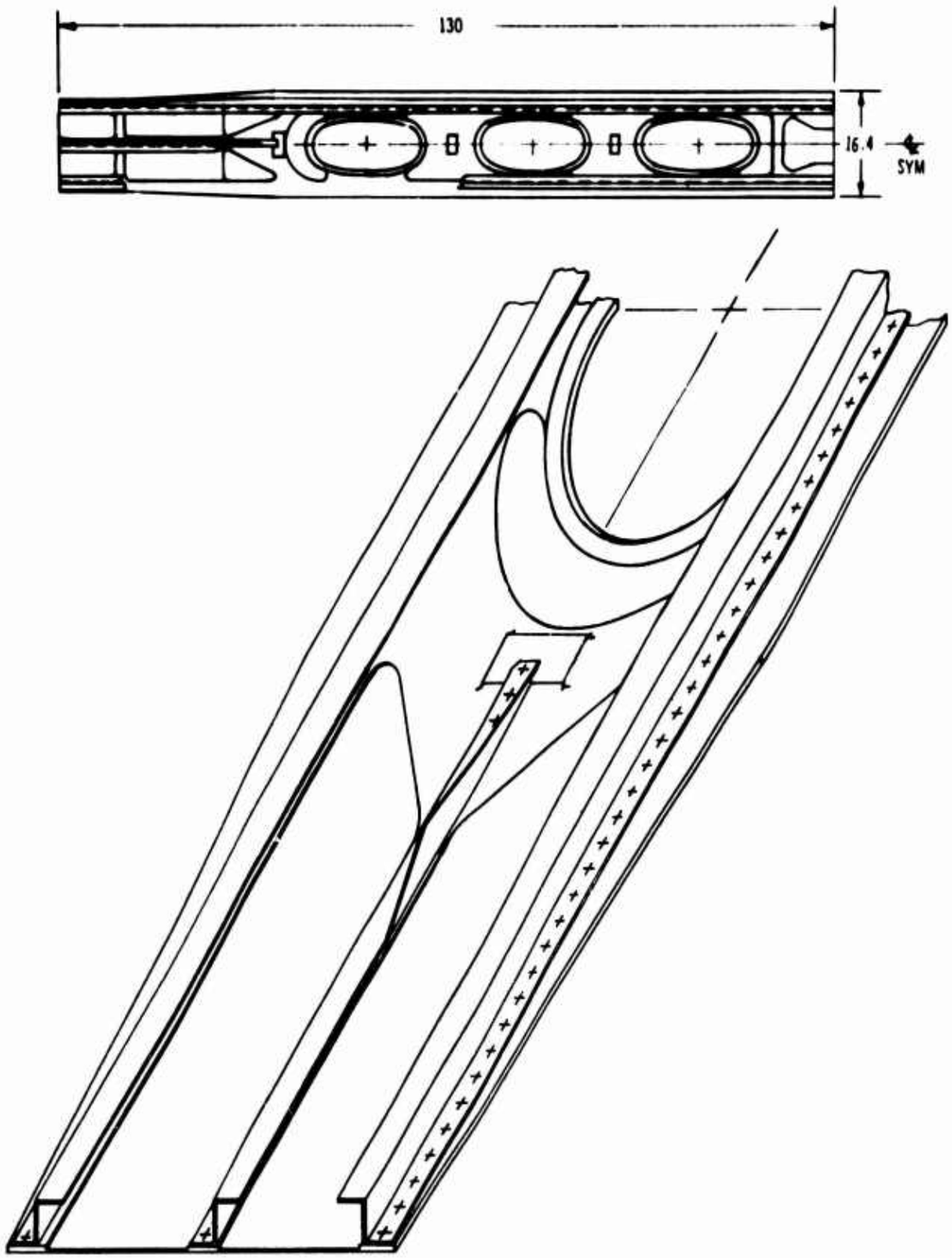


Figure 3-80. Access Door Fatigue Test Panel

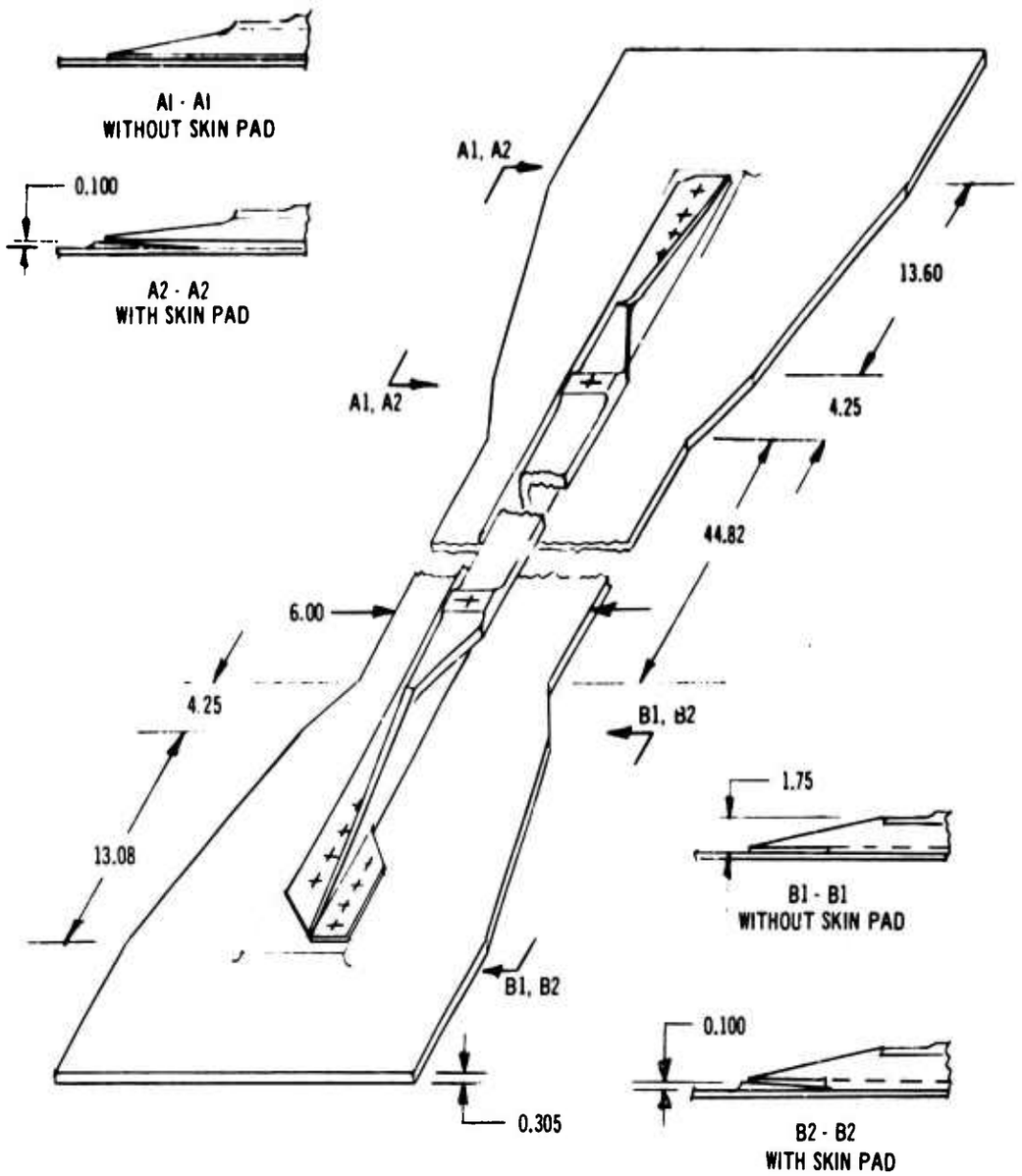


Figure 3-81. Stiffener Runout Fatigue Test Panels

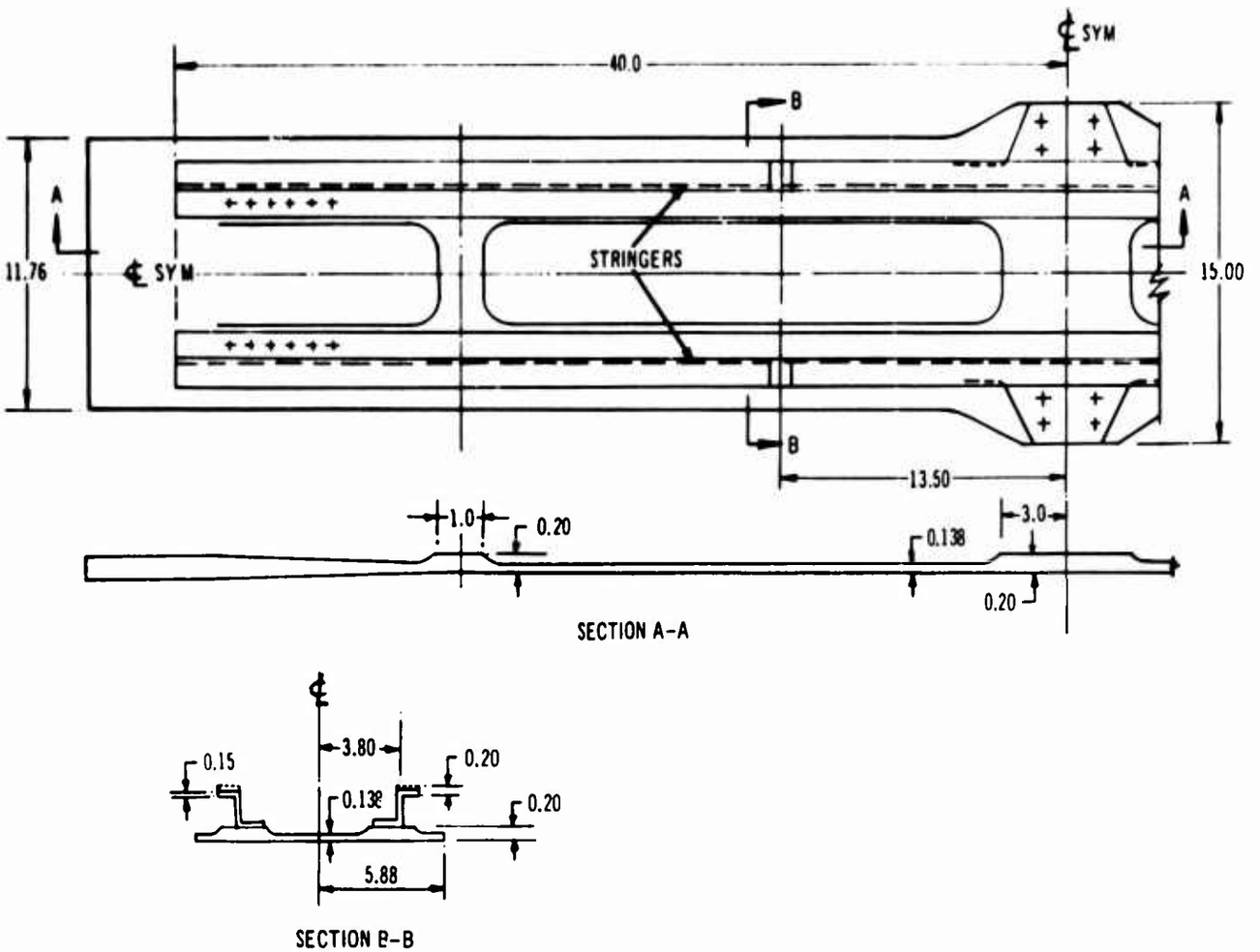


Figure 3-82. Flap Track Attachment Fatigue Test Panel

Table 3-J. Wing Structure Fatigue Tests

Configuration	Material	Fasteners	Pretest Exposure		Stress KSI		Cycles to First Crack
			°F	Hr	f_{max}	f_{min}	
Basic Structure 0.125 skin and 3 Stiffeners	8-1-1	Spotwelds	---	---	60	3.6	42,000
					60	3.6	51,000
		Hi-Loks	---	---	50	-10	43,000
					40	2.4	77,000
		Taper-Loks	---	---	60	3.6	57,000
		A-286 Rivets	500	500			In Work
	6-4	Hi-Loks	---	---	60	3.6	30,000
		Taper-Loks	500	500			In Work
		A-286 Rivets	500	500			In Work
			---	---			In Work
0.375 skin and 2 Stiffeners	8-1-1	Spotwelds	---	---	50	-10	43,000
Spanwise Splice, 2 Skins and Splicing Stiffener	8-1-1	Spotwelds	---	---	60	3.6	39,000
		Hi-Loks	---	---	60	3.6	29,000
Access Door Panel	6-4	A-286 Rivets	500	500			In Work
Stiffener Run-Outs	6-4	Taper-Loks	500	500			In Work
							In Work
Flap Track Attachment	6-4	Taper Loks & A-286 Rivets	500	500	Axial Load		In Work
					Biaxial Load		In Work
Wing Box Transition and Grip Design	8-1-1	A-286 Rivets	---	---			In Work
	6-4	A-286 Rivets	---	---			In Work
Double Shear Laminated Butt Joints	8-1-1	NAS Bolts	---	---	35	2.1	39,000
			---	---	35	2.1	34,000
	8-1-1 With Steel Splice Plates	NAS Bolts	---	---	35	2.1	41,000
			---	---	30	1.8	44,000
		Taper-Loks	---	---	35	2.1	448,000
			---	---	45	2.7	265,000

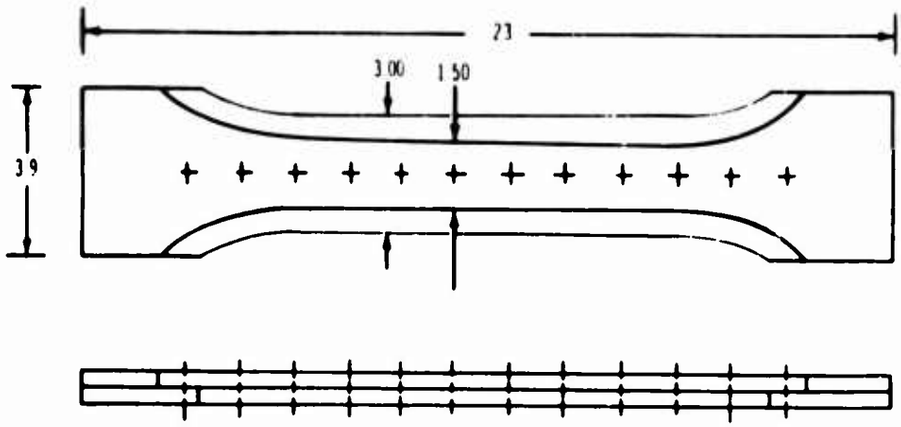


Figure 3-83. Baseline Fatigue Specimen

problem with spotwelded structure, and, the greatly reduced fatigue life from any transfer of load. Although many attempts were made to overcome this reduction in fatigue life through process variations, coining, and peening, no satisfactory solution was found. Data on small specimen tests conducted during this investigation will be found in Par. 3.6.4.

Earlier testing with a similar specimen was used for evaluating spotwelding processes and spotweld stress relief methods. This specimen consisted of two identical pieces, both continuous for the full length of the specimen and, connected with twelve spotwelds spaced along the specimen length as shown in Fig. 3-98.

More than 100 of these inline spotwelded specimens were tested. Variables included sheet thickness, grain direction, spotweld spacing, spotweld treatment, and processing. Typical results are shown in Table 3-M and illustrate the large variation in fatigue life that was obtained with various spotwelding processes.

3.6.3 Fuselage Structure Fatigue Tests

3.6.3.1 Full-Scale Specimens
A program of fatigue tests of full-scale segments of fuselage structural configurations is in work. The variables being evaluated and usage of test results are analogous to those for the wing program discussed in Par. 3.6.2.1.

The test specimens which represent the fuselage basic panel design utilized two hat section stiffeners attached to a skin panel. Design details, such as fail-safe straps, are included as required to represent the design. The earlier panels utilized spotwelding for the attachments and later panels use mechanical fasteners. A panel typical of the spotwelded specimens with tear straps is shown in Fig. 3-99. The short fatigue life of this type of panel compared to the similar panels without tear straps led to the design of a panel having a bonded and riveted tear-strap and a riveted dual tear strap. Panel configurations similar to the above but incorporating a joint will evaluate various methods of splicing the skin and stiffeners at the midspan of the panel. Splice designs being investigated include a minimum cost panel with no pad-up in the joint, a panel with chem-milled pad-up, and a panel with tapered doubler utilized to reduce basic stress levels at the joint. This program includes panels with elevated temperature exposure prior to the room temperature fatigue testing and will be extended to include elevated temperature and spectrum load testing.

The results of completed tests are summarized in Table 3-N.

3.6.3.2 Small Specimens
A number of small specimens were tested to aid development of fuselage design details. The results are summarized in Table 3-P and Figs. 3-100 and 3-101. Information from these tests has been incorporated into the full-scale specimens shown in the previous paragraphs.

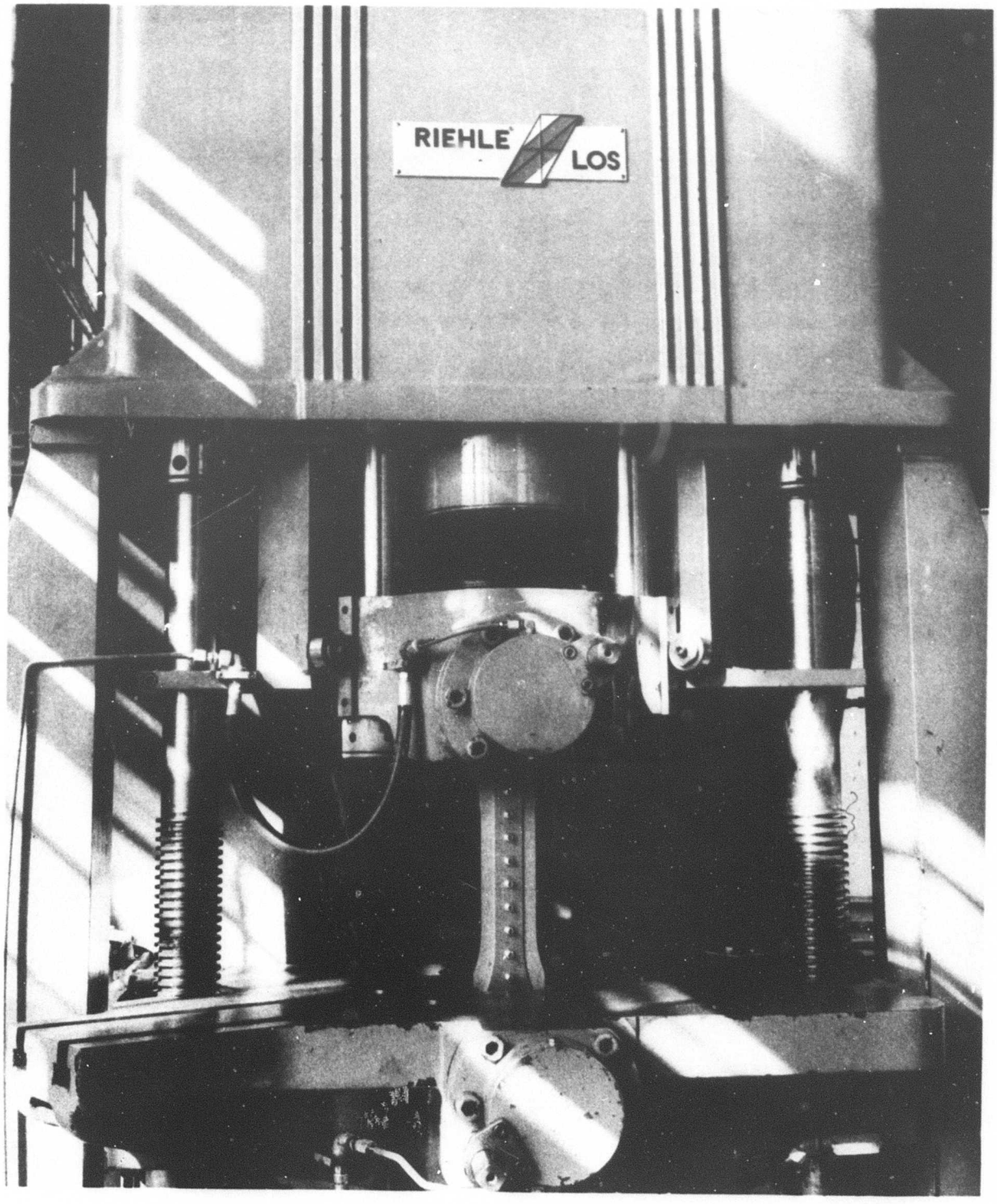


Figure 3-84. Baseline Fatigue Specimen in Test Machine

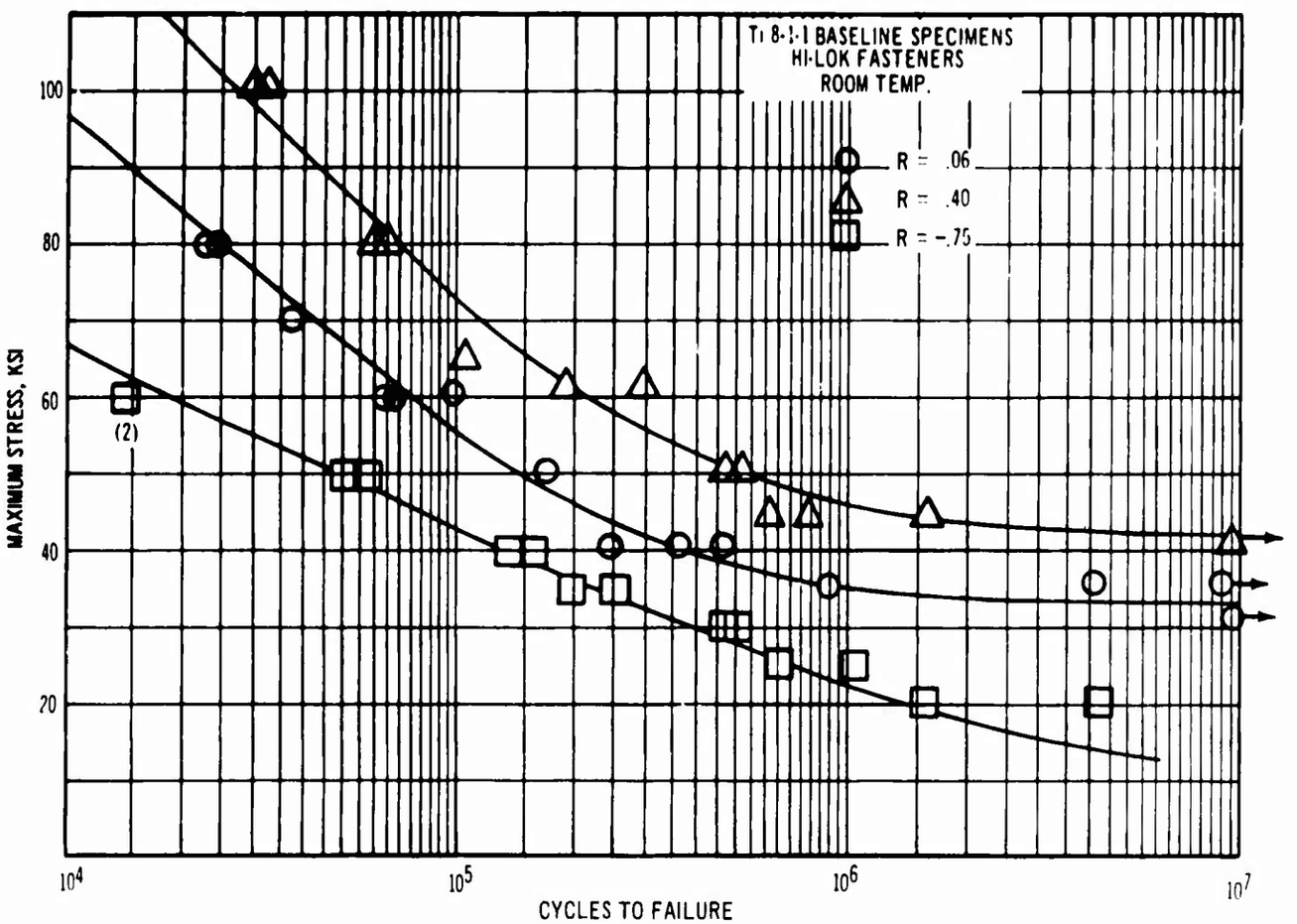


Figure 3-85. Effect of R Ratio on Hi-Lok Baseline Fatigue Life

Table 3.K. 8-1-1 Taper-Lok Baseline Specimens

Test Temp	Pretest Environment Hr at °F	Prior Static Load KSI at °F	Maximum Stress, KSI (R = 0.06)	Cycles To Failure, $X10^{-3}$
Room	None	None	60	108
Room	None	None	60	122
Room	None	None	60	177
Room	None	None	60	201
Room	None	None	60	229
Room	None	None	60	159
Room	None	None	60	127
Room	None	None	60	170
Room	None	None	60	140
Room	None	None	60	270
Room	None	None	60	243
Room	None	None	60	85
Room	None	None	60	74
Room	None	None	61.2	238
Room	None	None	61.2	215
Room	None	None	61.2	381
Room	None	None	61.2	133
500°F	None	None	50	192
500° F	None	None	60	140
500° F	None	None	40	448
500° F	None	None	35	1,028
Room	500 at 500	None	40	1,413
Room	500 at 500	None	50	90
Room	500 at 500	None	50	1,021
Room	500 at 500	None	60	148
Room	500 at 500	None	60	271
Room	500 at 500	None	60	57
500° F	500 at 500	None	50	112
500° F	500 at 500	None	60	49
500° F	500 at 500	None	60	74
500° F	500 at 500	None	40	534
Room	500 at 500	85 at 500	60	94
Room	500 at 500	85 at 500	60	165
Room	500 at 500	95 at 70	60	191
Room	500 at 500	95 at 70	60	232
Room	500 at 500	115 at 70	60	158
Room	500 at 500	115 at 70	60	180
500° F	500 at 500	85 at 500	60	94
500° F	500 at 500	85 at 500	60	102
500° F	500 at 500	115 at 70	60	92
500° F	500 at 500	115 at 70	60	118

Table 3-L. 6-4 Baseline Specimens With A-286 Squeezed Rivets

Test Temp	Pretest Environment Hr at °F	Squeeze Force, Kips	Maximum Stress, KSI (R = 0.06)	Cycles To Failure x 10^{-3}
Room	None	32	60	246
Room	None	32	60	191
Room	None	32	60	422
Room	None	32	60	397
Room	None	32	60	352
Room	None	32	60	399
Room	None	32	60	198
Room	None	32	60	1,540
Room	None	25.5	60	178
Room	None	25.5	60	201
Room	None	32	80	37
Room	None	32	45	981
Room	500 at 500	32	60	254
Room	500 at 500	32	60	234
Room	500 at 500	32	60	354
Room	500 at 500	32	60	478
Room	1000 at 500	32	60	599
500° F	500 at 500	32	60	249
500° F	500 at 500	32	60	134
500° F	500 at 500	32	50	301
500° F	500 at 500	32	45	In Test

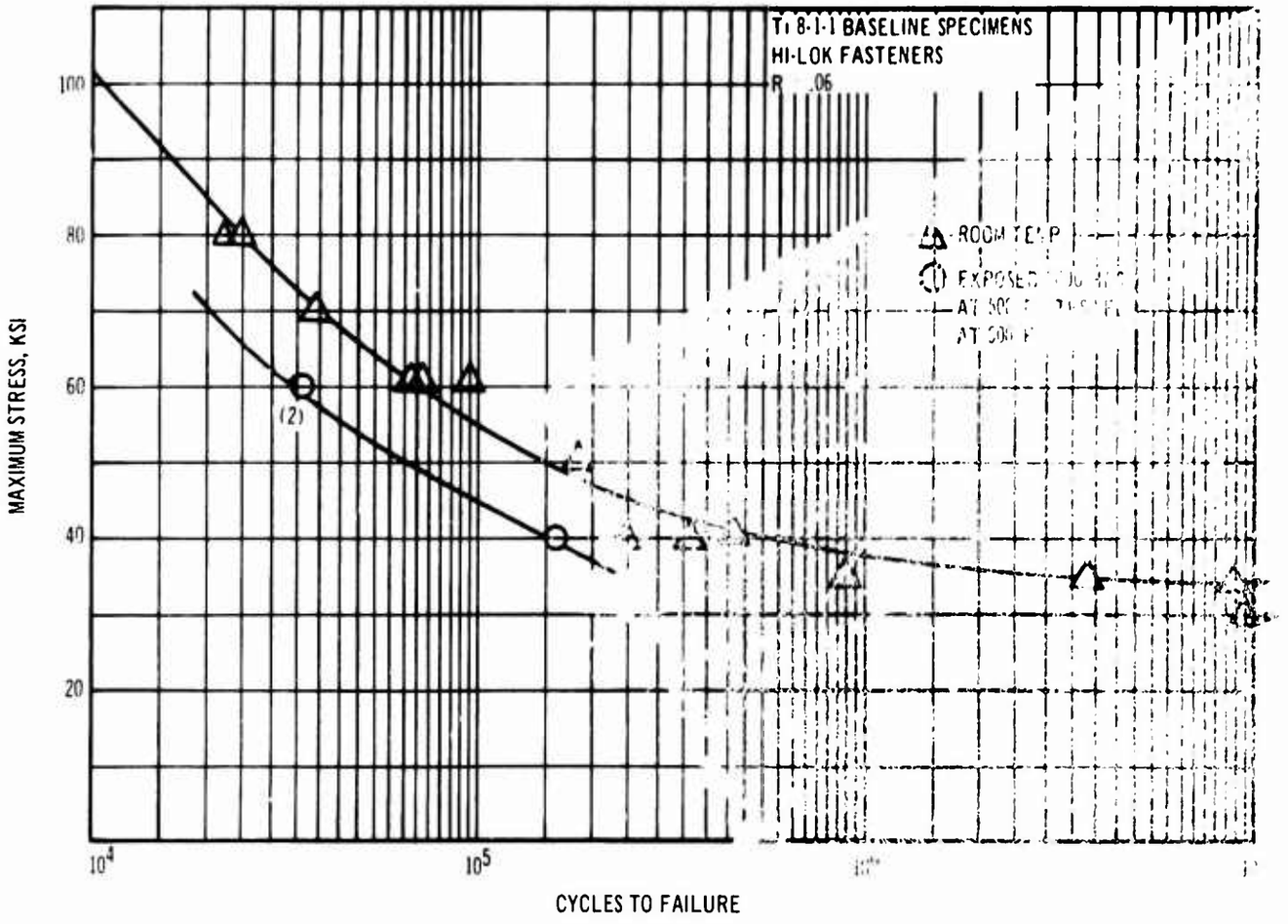


Figure 3-86. Temperature Effect on Hi-Lok Ba.. ire Fatigue Life

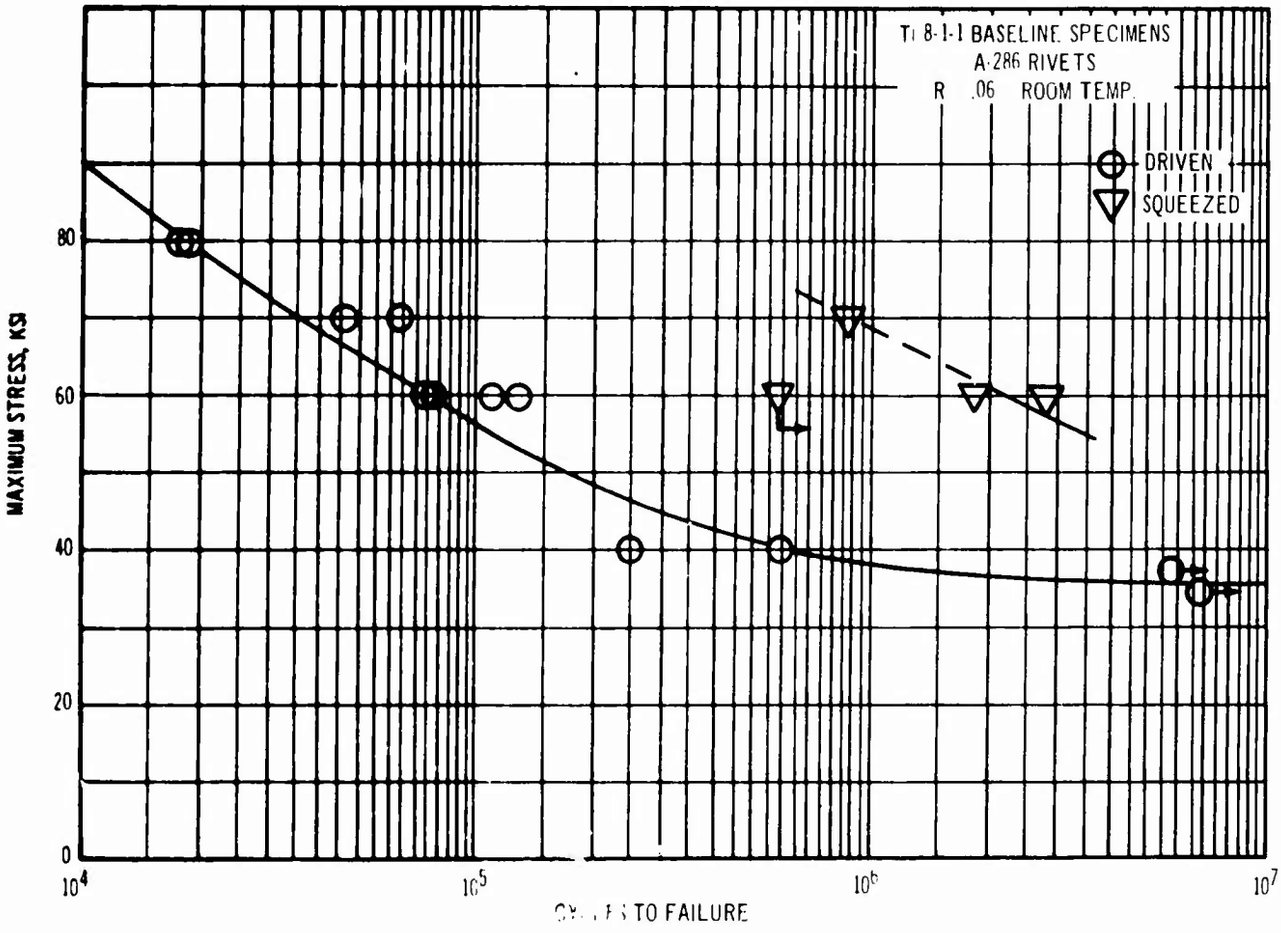


Figure 3-87. Fatigue Life Improvement From Squeeze Riveting

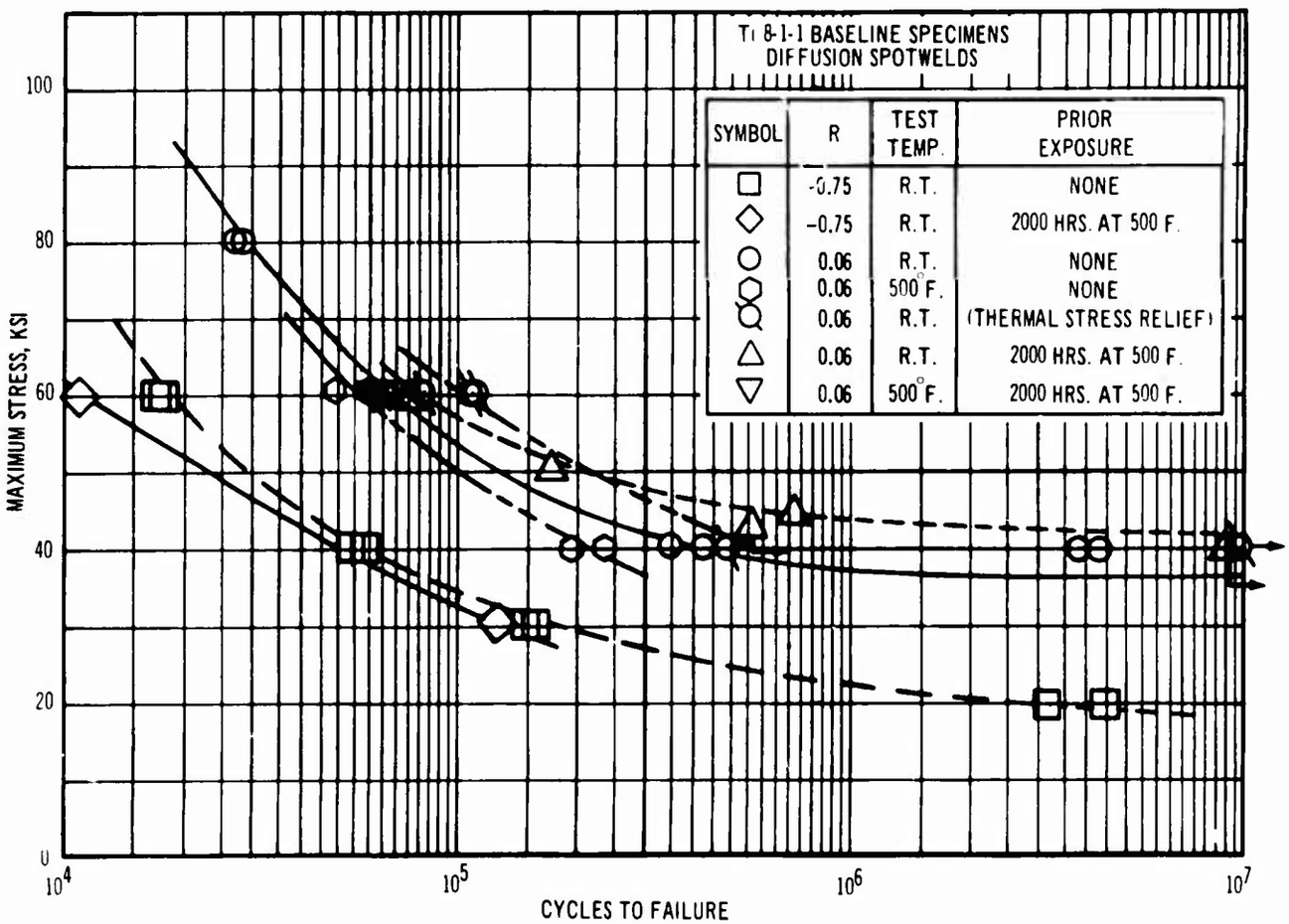


Figure 3-88. Fatigue Test Results for Spotwelded Baseline Specimens

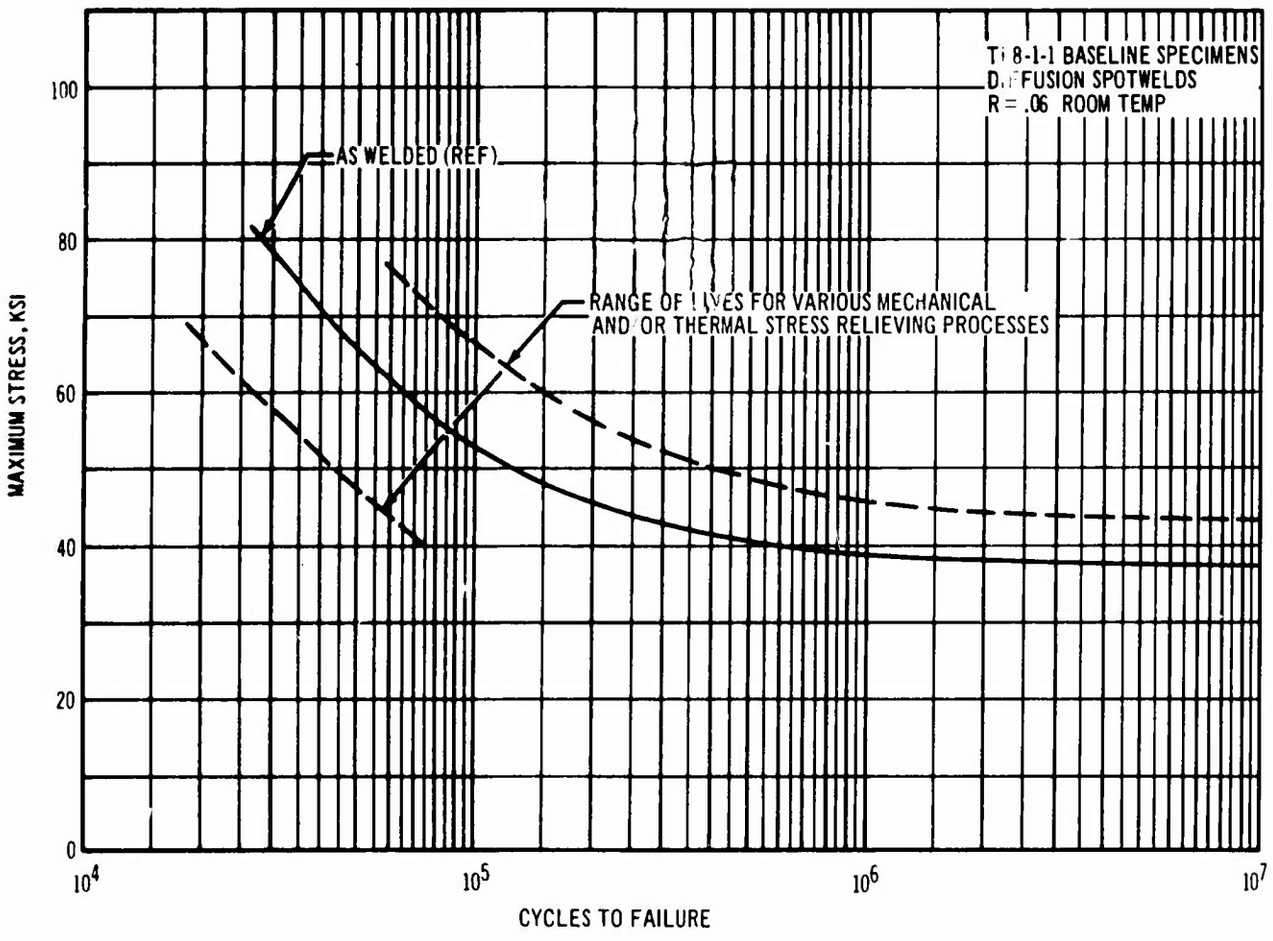


Figure 3-89. Effect of Stress Relief on Spotwelded Baseline Specimens

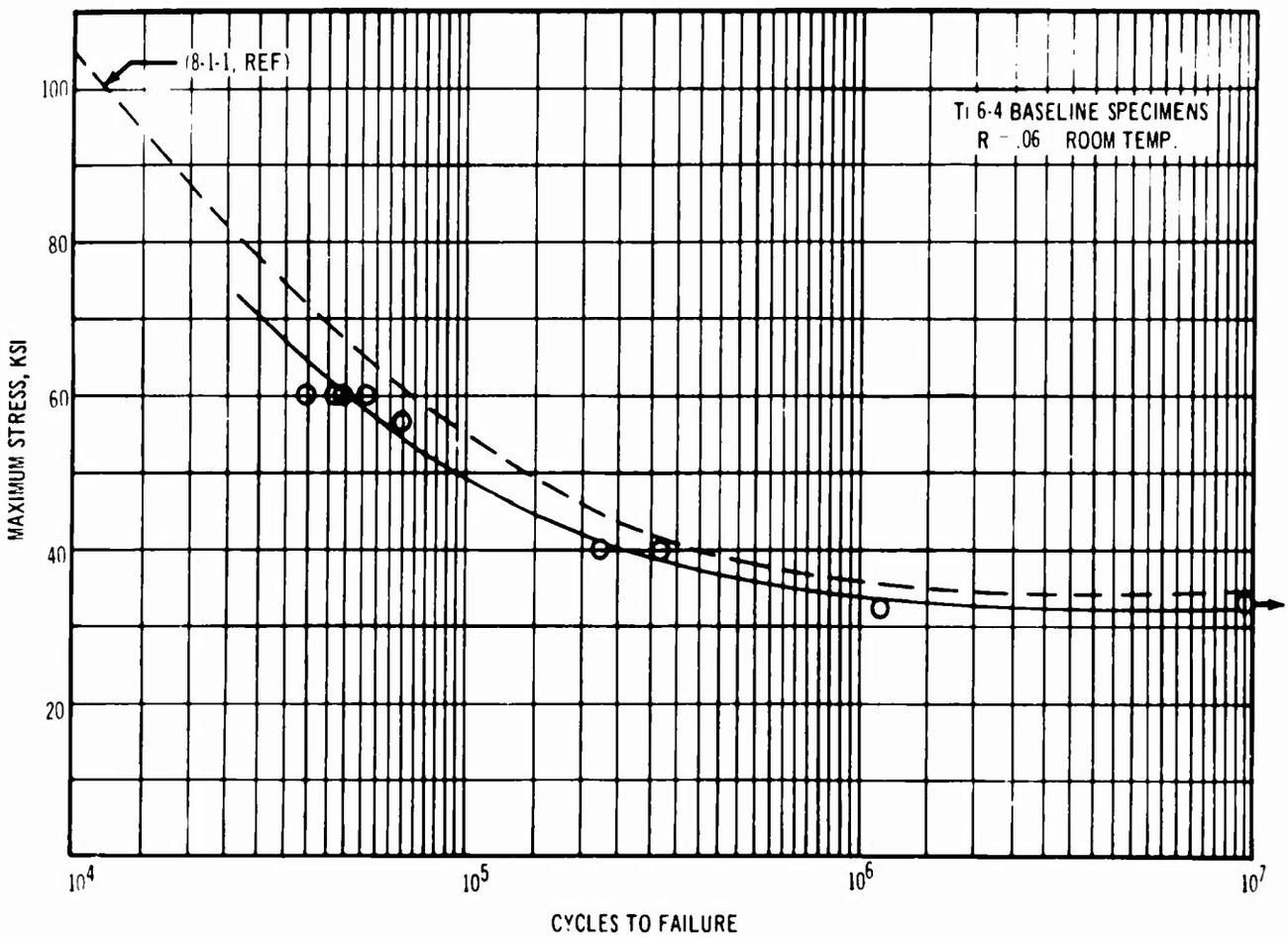


Figure 3-90. Effect of Material on Baseline Fatigue Life

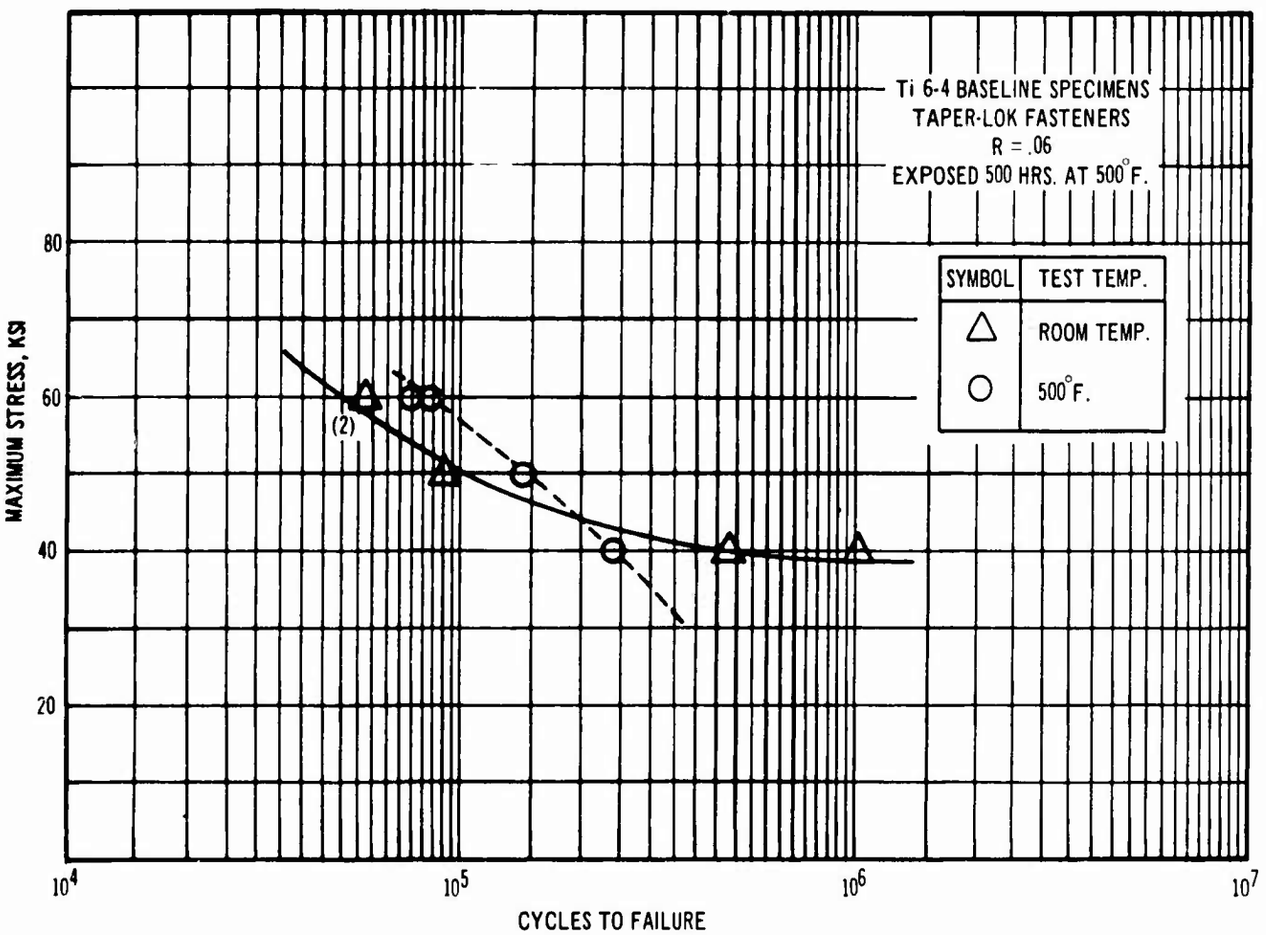


Figure 3-91. Effect of Temperature on Taper-Lok Baseline Fatigue Life

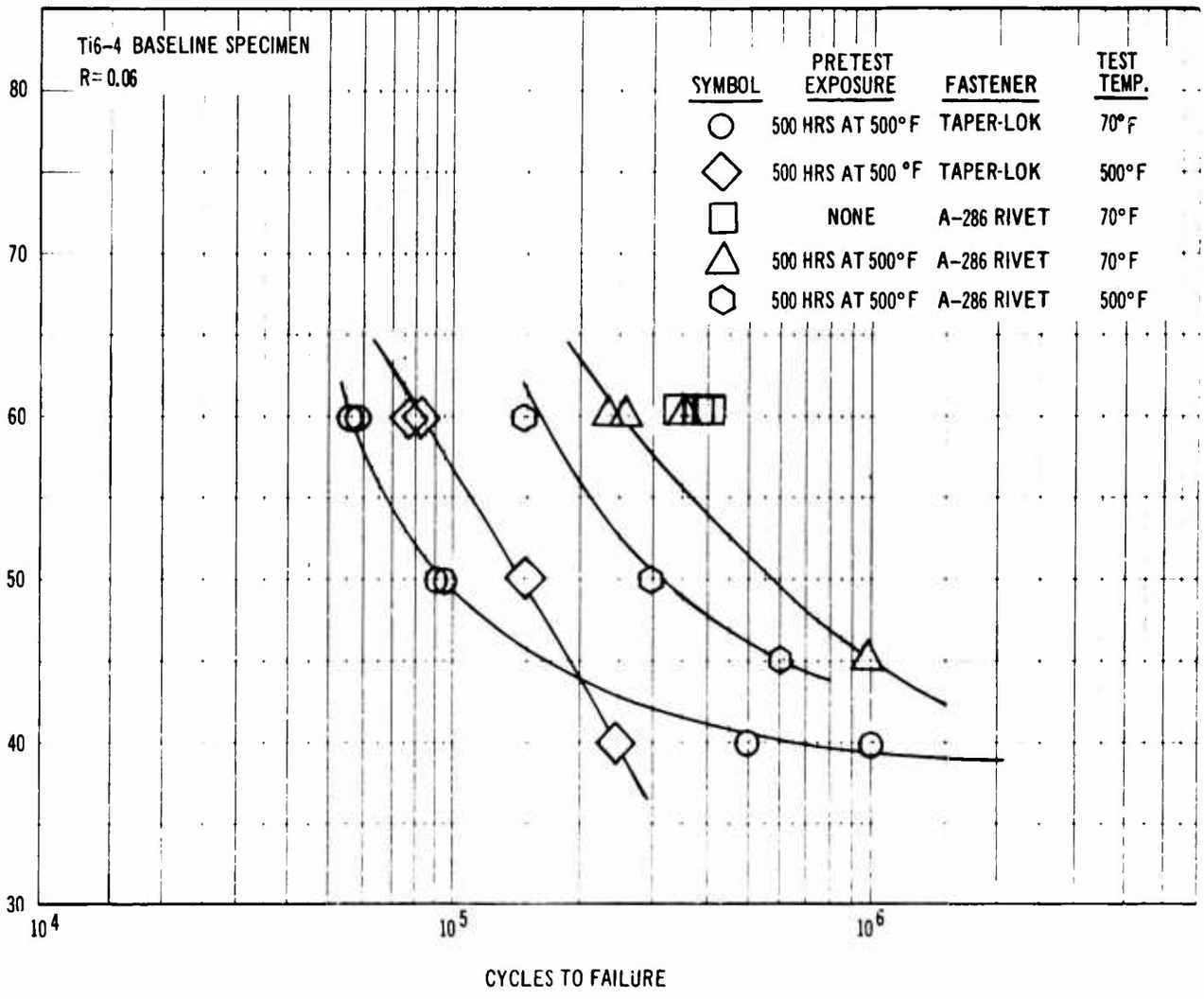


Figure 3-92. 6-4 Baseline Specimen Test Results

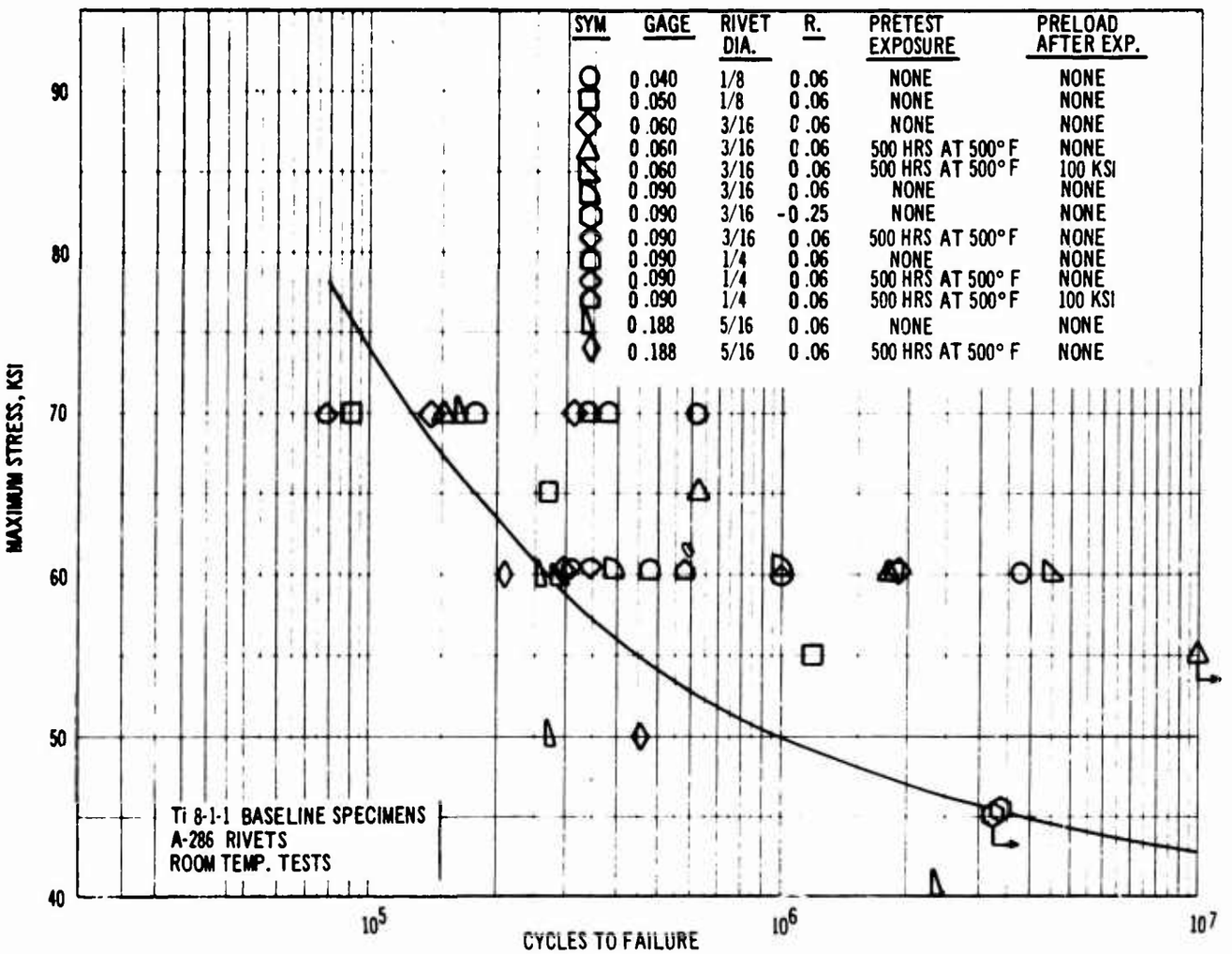


Figure 3-93. Gage Effects on Baseline Specimen Fatigue Life

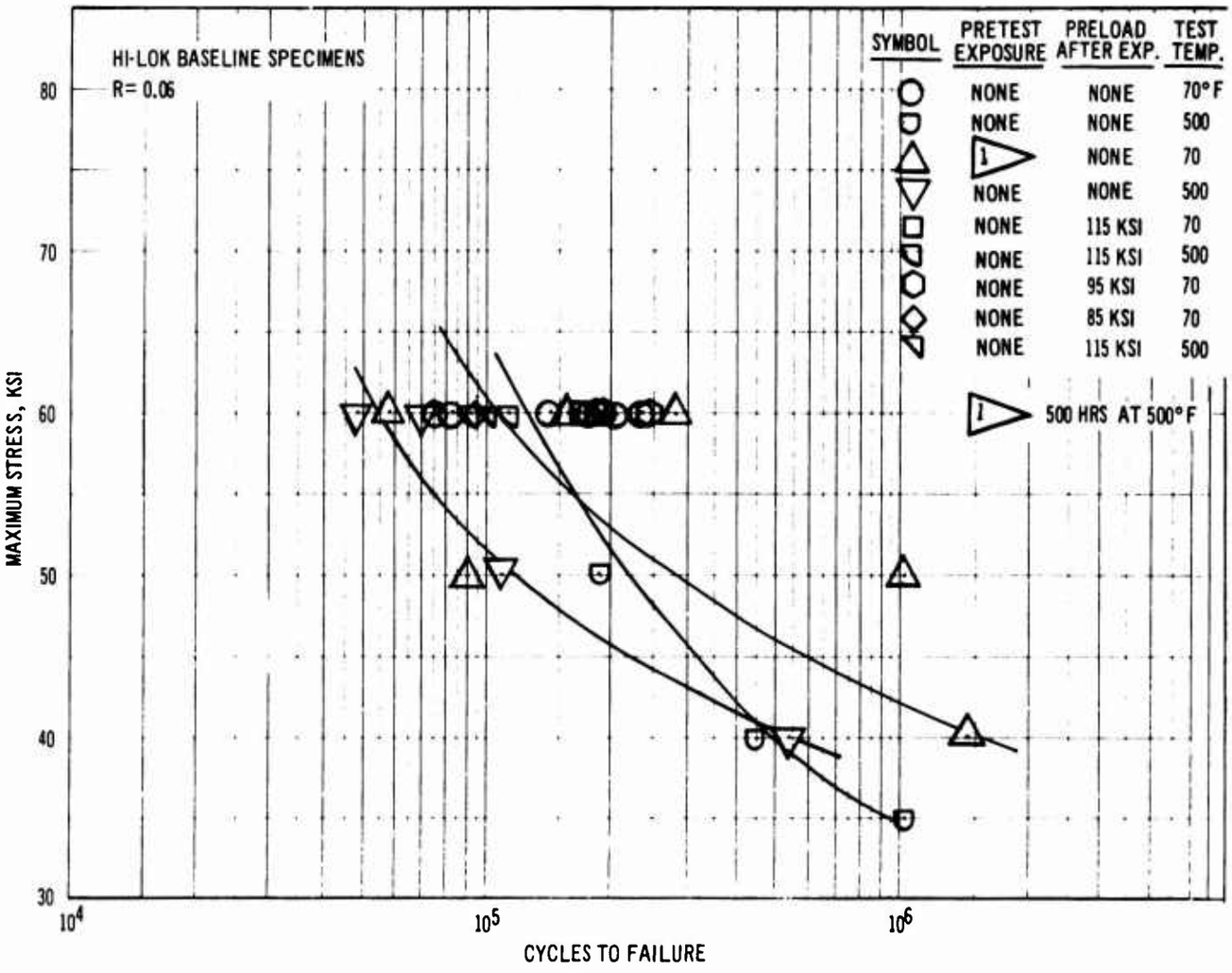


Figure 3-94. Exposed and Preloaded Baseline Specimen Test Results

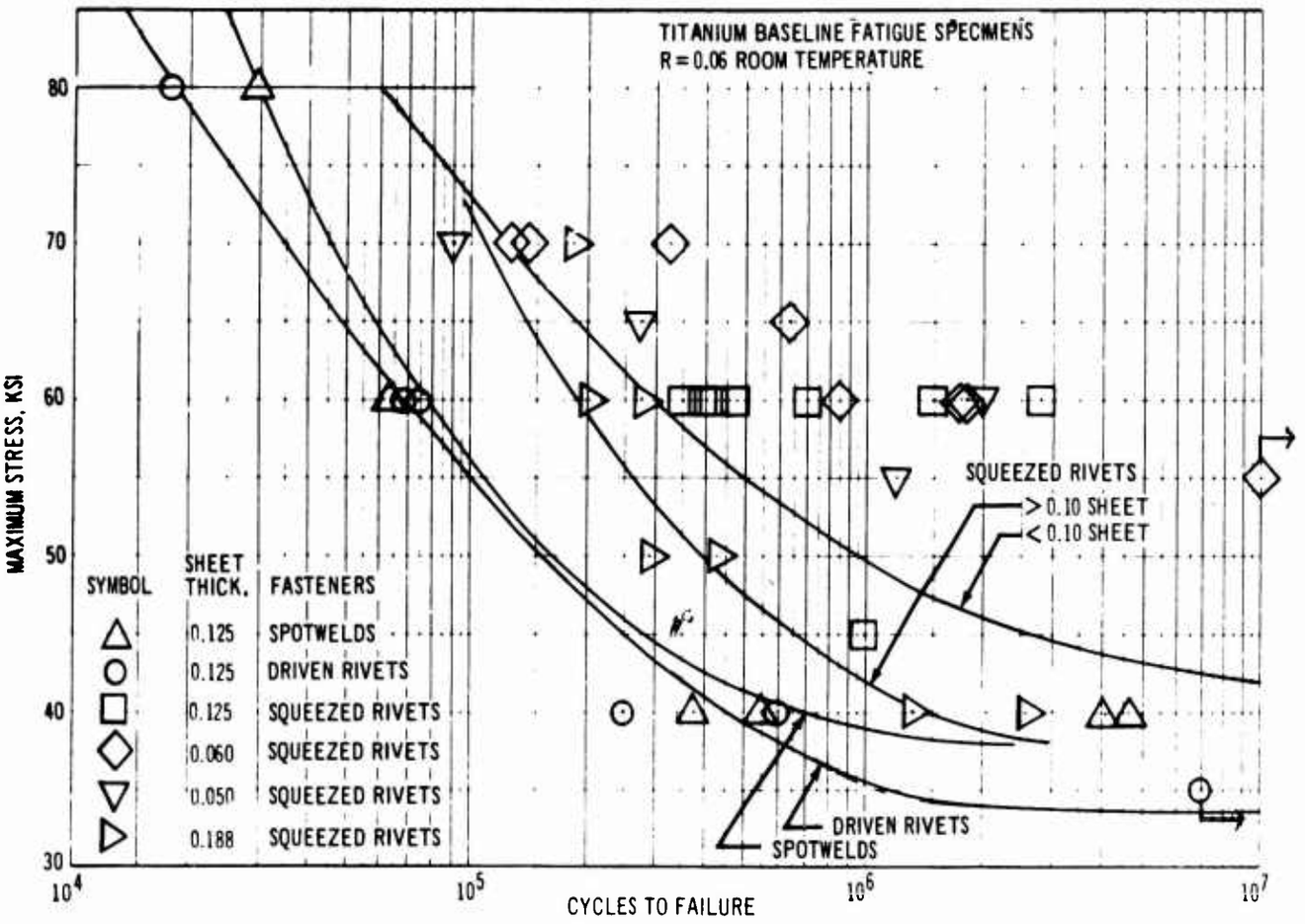


Figure 3-95. Riveted and Spotwelded Baseline Specimen Data

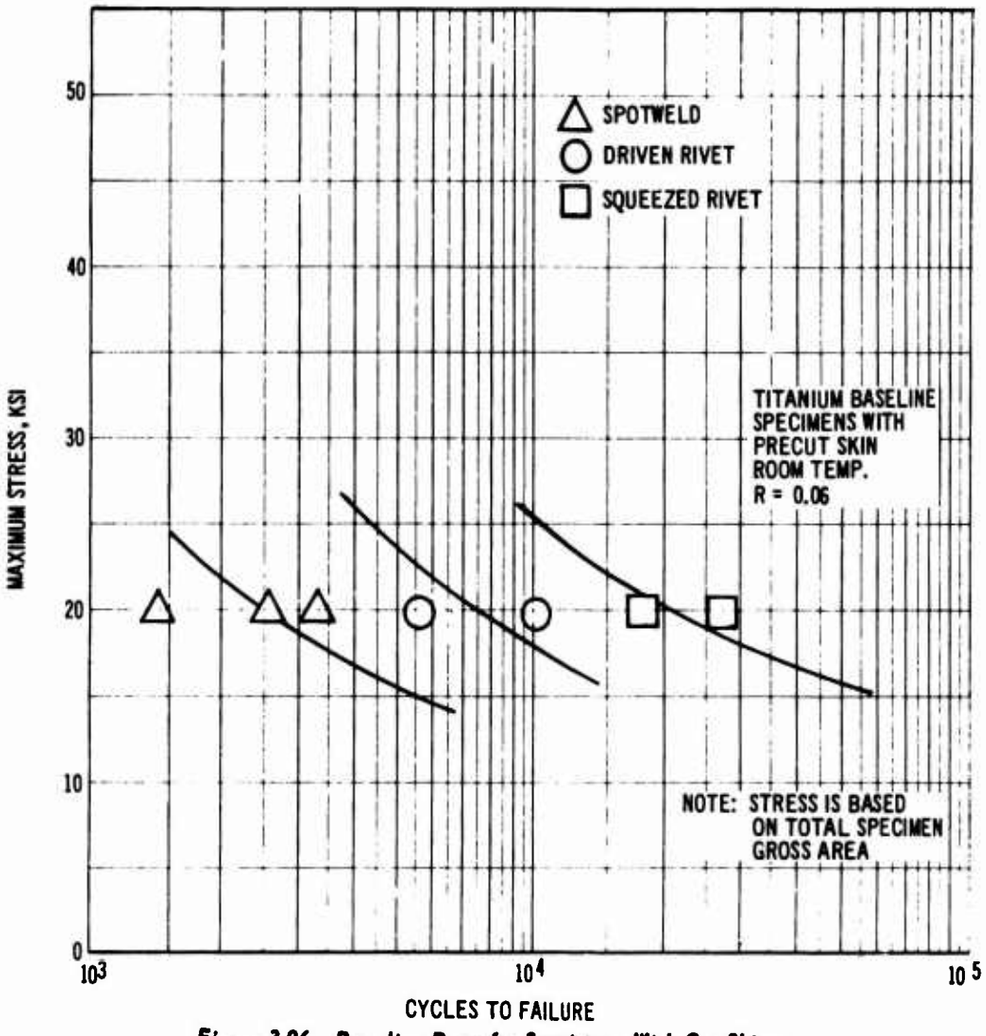


Figure 3-96. Baseline Data for Specimens With Cut Skins

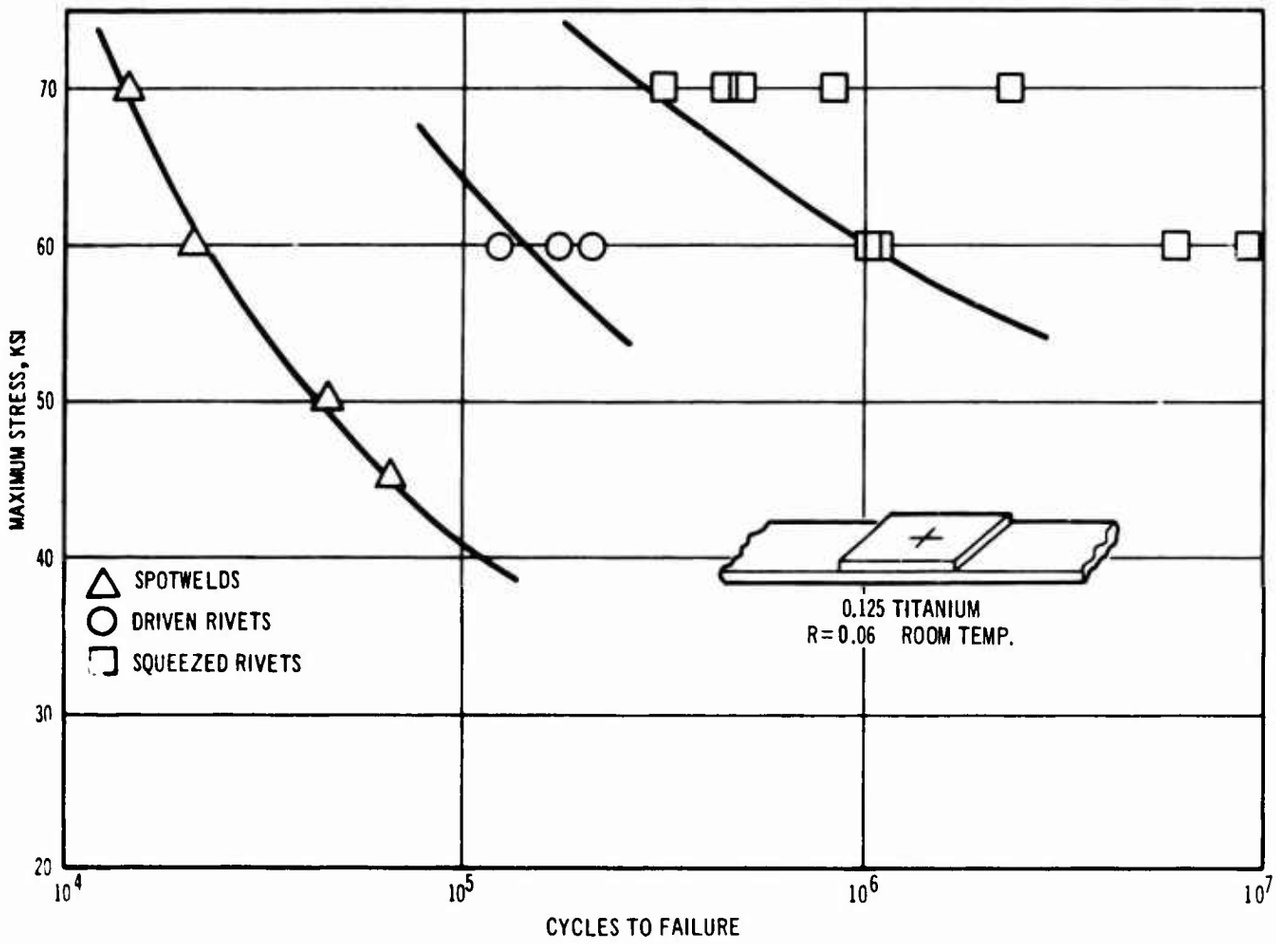
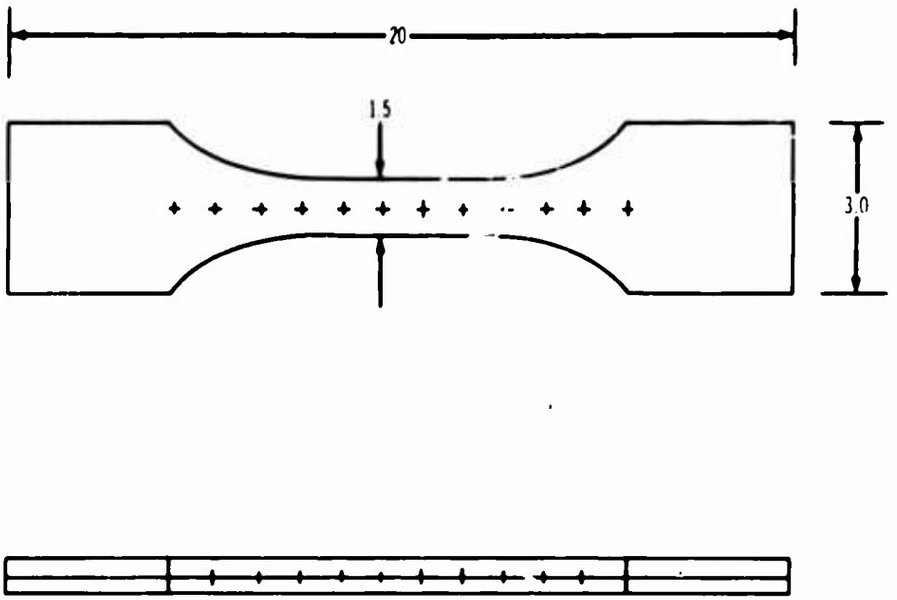


Figure 3-97. Riveted and Spotwelded Pad Attachment Fatigue Data



DIMENSIONS VARY, TYPICAL VALUES SHOWN

Figure 3-98. Inline Fatigue Specimen

Table 3-M. Spotwelded Inline Specimen Fatigue Lives

Maximum Stress, KSI (R = 0.06)	Cycles To Failure, $X10^{-3}$	Remarks
61.2	44.8	Standard Spotweld
61.2	17.9	Standard Spotweld
61.2	43.6	Hot Forged Spotweld
61.2	42.2	Standard Spotweld Coined
61.2	102.0	Standard Spotweld Coined and Machined
60.0	103.7	Standard Spotweld Coined and Machined
61.2	61.0	Standard Spotweld Coined and Machined
61.2	116.2	Standard Spotweld Coined, Machined and Stress Relieved (10 Hr at 550°F)
61.2	57.8	Standard Spotweld Coined, Machined and Stress Relieved (10 Hr at 970°F)
61.2	23.5	Standard Spotweld, Stress Relieved (15 Min at 1,450°F)
61.2	17.9	Standard Spotweld, Stress Relieved (15 Min at 1,450°F in Argon)
60.0	32.6	Standard Spotweld, Machined
61.2	60.3	Standard Spotweld, Machined and Stress Relieved (15 Min at 1,450°F in Argon)

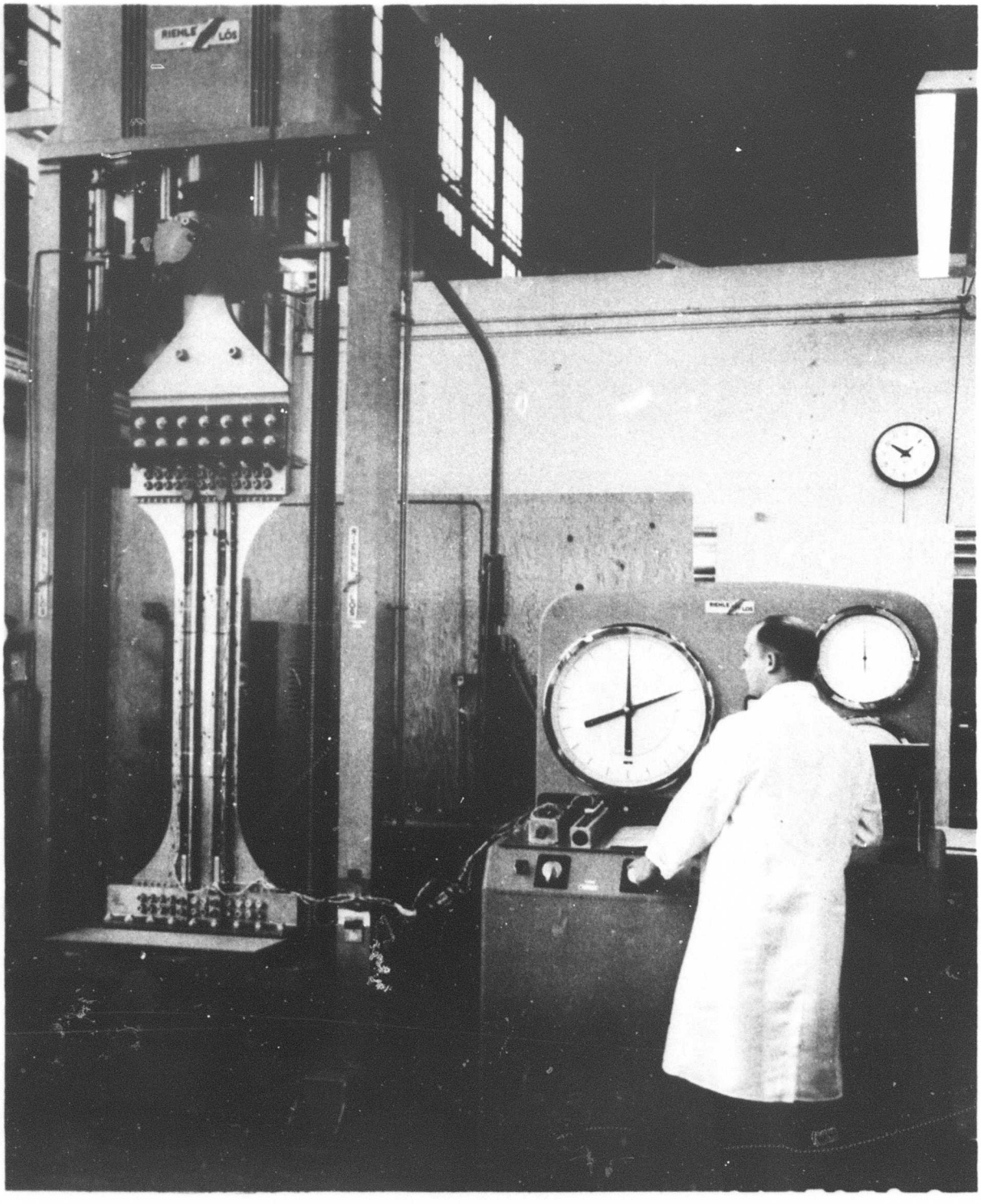


Figure 3-99. Spotwelded Fuselage Panel With Tear Straps

Table 3-N. Fuselage Structure Full Scale Fatigue Tests

Configuration	Material	Fasteners	Pretest Exposure		Stress KSI		Cycles to First Crack
			°F	Hr	f_{max}	f_{min}	
0.040 Skin, Hat Section Stiffeners Joggled Over Tear Straps	8-1-1	Spotwelds	---	---	60	3.6	5,300
					30	1.8	31,000
0.050 Skin, Hat Section Stiffeners	8-1-1	Spotwelds	---	---	60	3.6	54,000
		Driven A-286 Rivets	---	---	60	3.6	25,000
0.040 Skin, Hat Section Stiffeners Joggled Over Dual and Bonded-Riveted Tear Straps	6-4	Squeezed A-286 Rivets	500	500			In Work
Skin and Stiffener Splices:		Squeezed A-286 Rivets and Taper-Loks					
No Pad	6-4		500	500			In Work
Chem-Milled Pad	6-4		500	500			In Work
Tapered Doubler	6-4		500	500			In Work

Table 3-P. Fuselage Structure Small Specimen Tests

Configuration	Material	Fasteners	Pre-Test Exposure		Stress KSI		Cycles to First Crack
			°F	Hr	f_{max}	f_{min}	
Tapered Doubler for Stress Reduction	Ti6Al-4V	A-286 Rivets (Driven)	---	---	50	3.0	40,000
					40	2.4	107,000
					50	3.0	64,000
					40	2.4	222,000
		A-286 Rivets (Squeezed)	---	---			In Work
							In Work
							In Work
57 Skin Joints. Many Configurations	Ti8-1-1	Hi-Loks or Taper Loks	---	---	See Fig. 3-100		
84 Tear Strap to Skin Specimens	Ti8-1-1	Spotwelds, Rivets, or Bonding	---	---	See Fig. 3-101		

Five bolted and spotwelded stiffener-to-frame shear tie designs were evaluated as shown in Fig. 3-102. The Type E chosen for the airplane design develops many times the life of those used on existing airplanes (Type B and C).

3.6.4 Fatigue Tests - General

Fatigue tests of relatively small specimens have been used to evaluate design parameters and processes. These tests determine the effects of variations in hole preparation methods, processes, materials, finishes, and environments. Also, test methods are evaluated with these specimens prior to testing the larger and more expensive fatigue specimens. Many hundreds of these specimens have been tested at room and elevated temperatures both with and without prior temperature exposure. Tests were conducted in SF-10-U, Riehle-Los, Losenhausen, and Research Incorporated Fatigue testing machines. A typical test setup is shown in Fig. 3-103.

3.6.4.1 Simple Coupon Tests

The specimens are conventional notched and unnotched, butt fusion welded, and other single element coupons. It is difficult to provide accurate interpretation of the data and only general assessments are presented with the data. The program to evaluate the effects of various hole preparation techniques on fatigue life is summarized in Table 3-Q. Holes were prepared by drilling, reaming, broaching, and cold working. Specimens with and without fasteners in the holes were tested at room temperatures at a stress ratio of 0.06. These tests showed an improvement in fatigue life for broached holes over reamed holes with rivets in the holes.

Table 3-R shows the results of a test program designed to evaluate the effects of introducing compressive stresses around the hole of a Ti 8-1-1 center notched specimen. The compressive stresses were introduced by means of impact coining. This coining operation consists of using a ring die which is impacted by dropping a 10-lb hammer from various heights. The impact treatments were made to both sides of all specimens. Some specimens were exposed to elevated temperature for various lengths of time prior to testing to evaluate the effect this environment has on reducing the compressive stresses induced by the impact coining operation. All testing was conducted at room temperature at R = 0.06. The coined specimens showed greater fatigue life than the uncoined specimens although part of the improvement was lost when the specimens had prior exposure at elevated temperature. The uncoined specimens with bolts installed in the holes appeared better than any of the coined specimens.

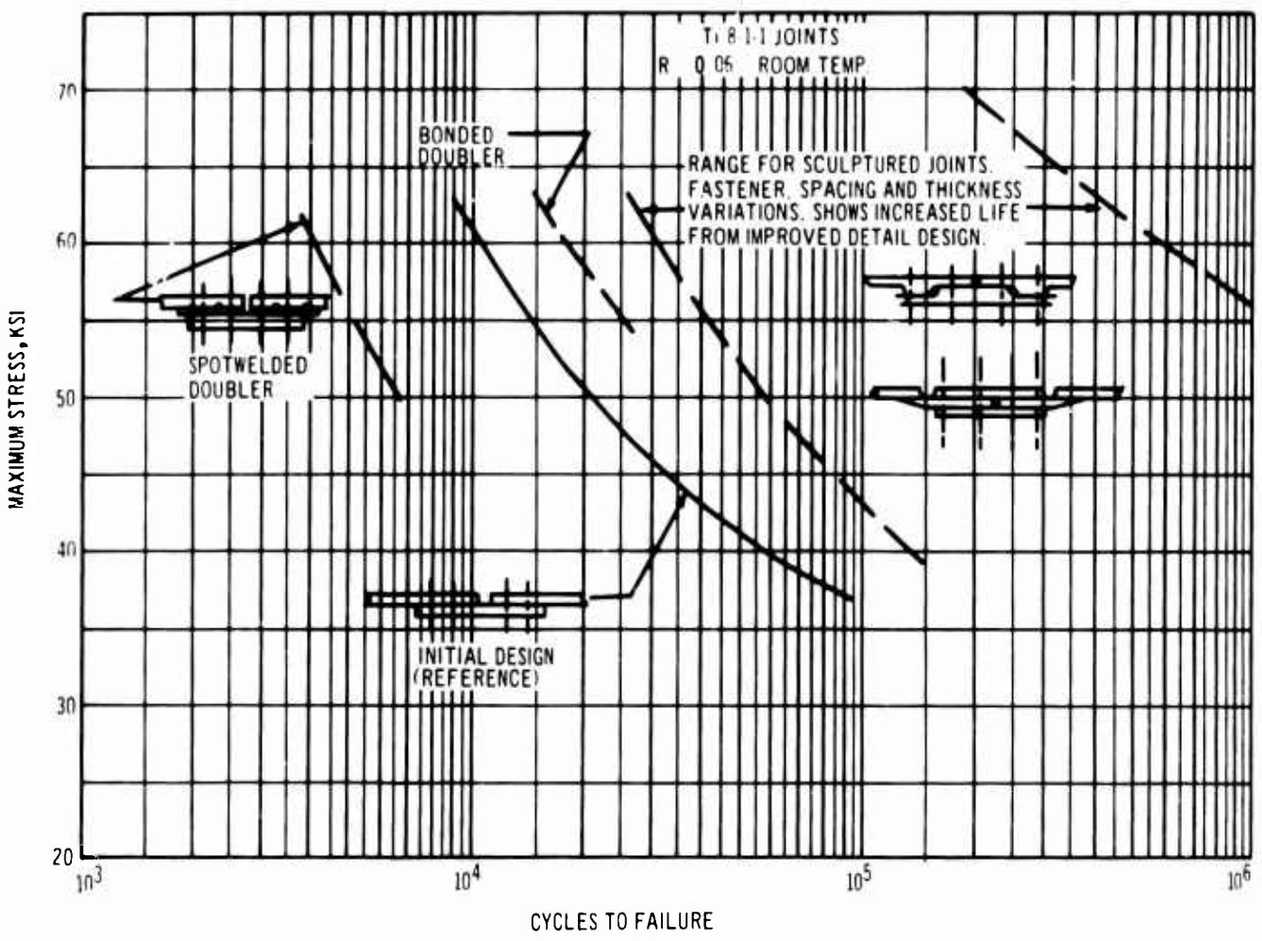


Figure 3-100. Joint Fatigue Life Increase by Improved Detail Design

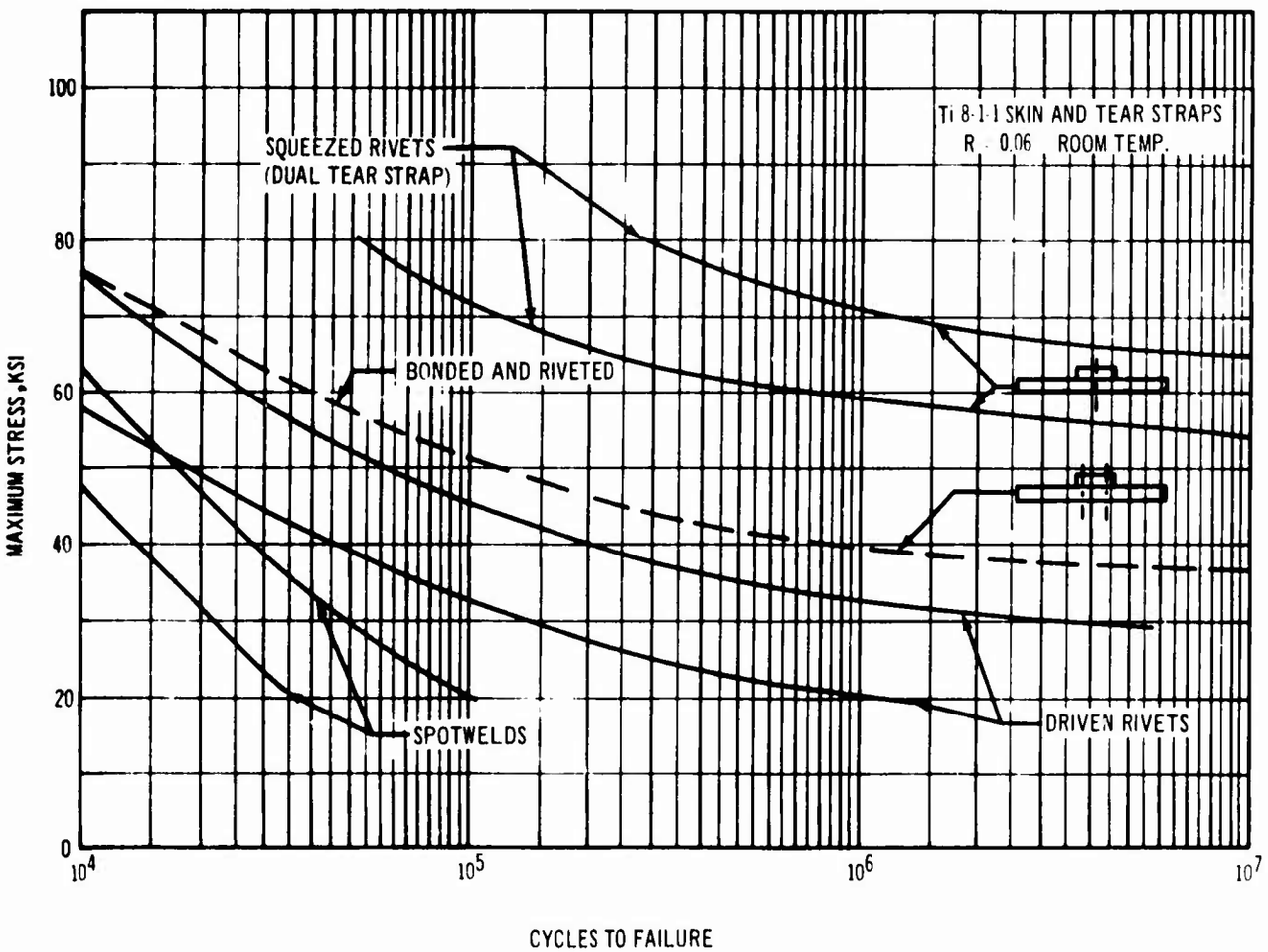


Figure 3-101. Fatigue Life Improvement for Body Tear Strap to Skin Attachment

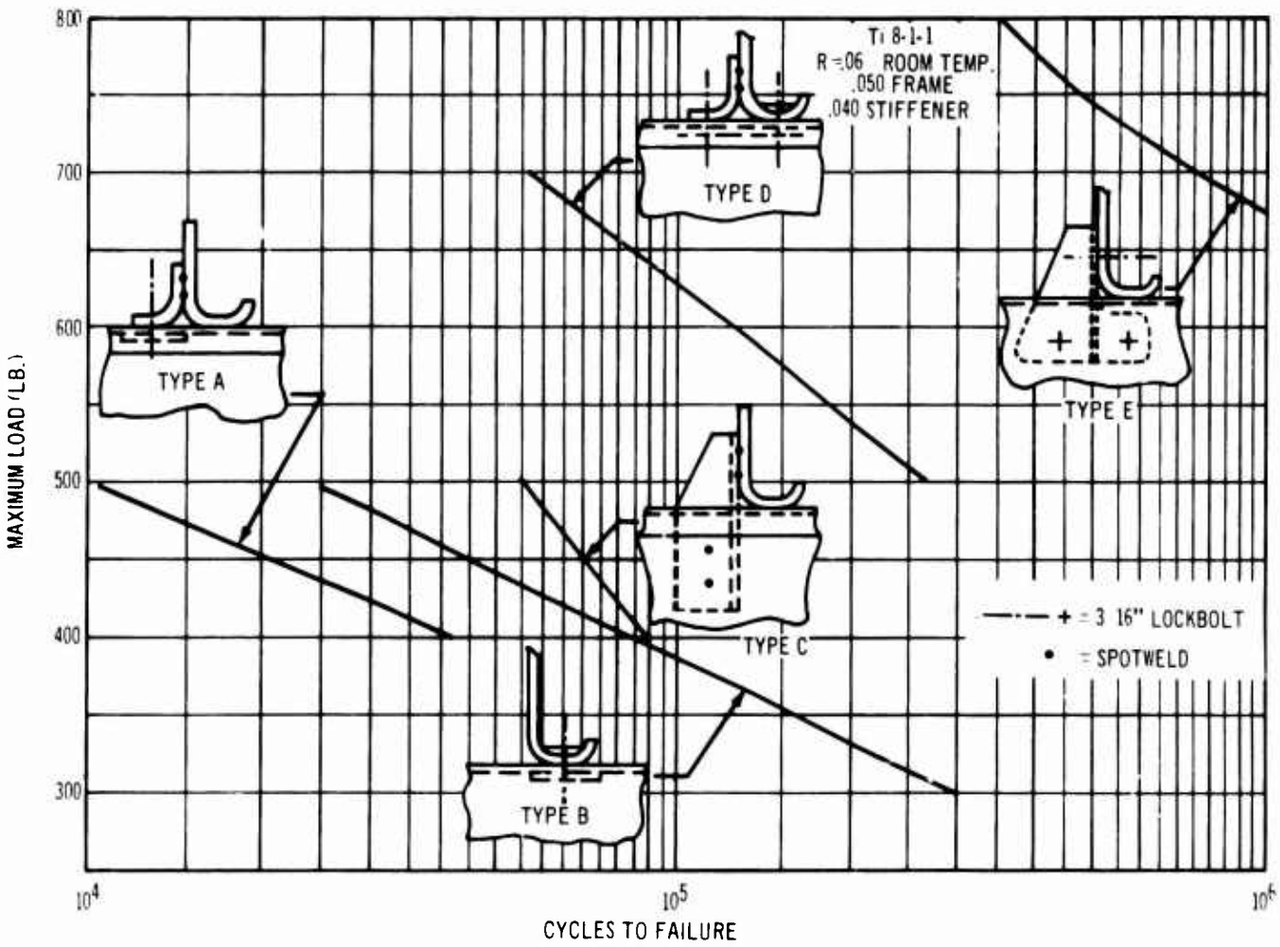


Figure 3-102. Fatigue Life of Stiffener to Frame Attachment

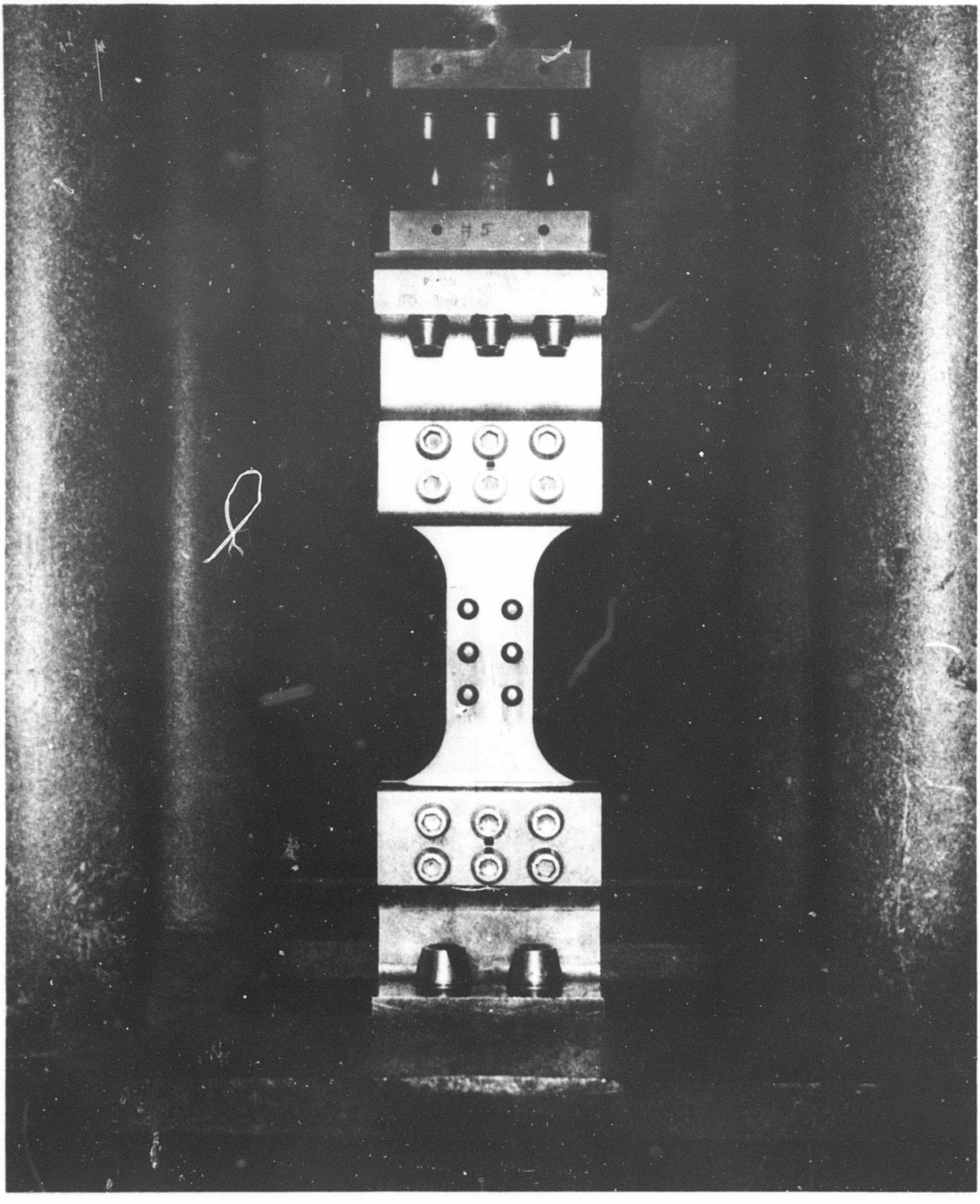


Figure 3-103. Typical Test Setup

Table 3-Q. Effects of Hole Preparation on Fatigue Life

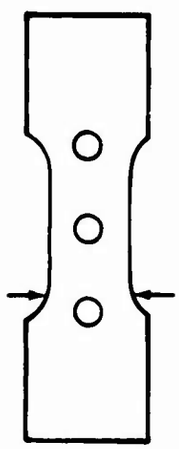
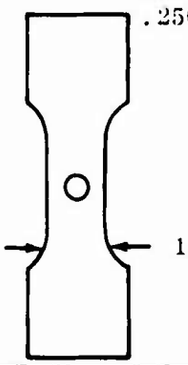
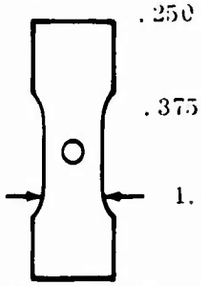
Configuration	Hole Preparation	Fastener	Max Gross Stress, KSI	Cycles To Failure, x 10^{-3}
MATL: 8-1-1 .125 GAGE  	Drill & Ream .2495/.2505 DIA	None	50 50 50 45 45 40	630 499 686 865 1020 2147 N. F.
	Drill & Broach .2515/.2525 DIA	None	55 55 55 50 50 50	826 160 153 248 793 1090
	Drill & Ream .2495/.2505 DIA	1/4 Std Head A-286 Rivet	70 70 70 70 60	162 111 799 144 2040 N. F.
	Drill & Broach .2515/.2525 DIA	1/4 Std Head A-286 Rivet	70 70 70 70 70 70	1750 1535 1252 2030 341 852
MATL: 8-1-1 .250 GAGE  	Ream .500 DIA	None	80 60 40 30 25 20	<1 5 33 227 223 25108
	Broach & Cold Work .500 DIA	None	60 50 40 35 35 30	7 16 101 156 179 617
MATL: 8-1-1 .250 GAGE  	Class I	None	60	40
	Close Ream	Bolt No Torque	60	27
	Class I	Bolt Torque 400 in lb	60	141
		Bolt Torque 800 in lb	60	138
		Taper-Lok Torque 400 in. lb	70 60 60 90 80	187 343 3142 6 84

Table 3-R. Effects of Impact Coining on Fatigue Life

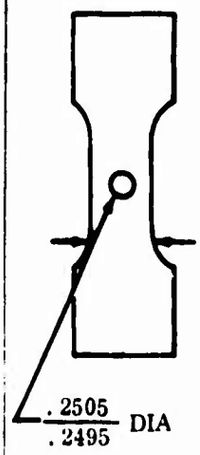
Configuration	Coining	Fastener	Pretest Exposure °F	Pretest Exposure Hr	Max Gross Stress, KSI	Cycles To Failure, x 10^{-3}
MATL: 8-1-1 .090 GAGE  (CLOSE REAM)	None	None	---	---	60	39
			---	---	50	62
			---	---	40	131
			---	---	35	2,558(N.F.)
			550	100	60	21
			550	100	50	41
			550	100	40	95
			550	500	50	38
	3/8 Dia Die 2 Ft Drop (Both Sides)	None	---	---	75	9
			---	---	70	30
			---	---	65	60
			---	---	60	79
			---	---	55	117
			550	101	65	26
	3/8 Dia Die 3 Ft Drop (Both Sides)	None	---	---	75	19
			---	---	70	52
			---	---	65	61
			---	---	60	398
			---	---	55	385(Grip)
			550	101	70	18
	7/16 Dia Die 4 Ft Drop (Both Sides)	None	---	---	80	15
			---	---	70	35
			---	---	60	55
			---	---	50	118
			550	100	70	16
			550	100	60	36
			550	100	50	95
			550	500	60	27
	7/16 Dia Die 4 Ft Drop (Both Sides) Plus .250 Dia Drill Rod Inserted in Hole During Coining Operation	None	---	---	80	19
			---	---	70	37
			---	---	60	98
			---	---	50	250
			550	100	70	23
			550	100	60	43
			550	100	50	88
			550	500	60	36

Table 3-S shows the results of a test program conducted on Ti 8-1-1 to evaluate the effect of installing the hole in center-notched specimens by either a drilling or punching operation. The specimen holes were installed in pairs and identified to distinguish the top and bottom plates during the operation. The holes were not reamed or de-burred and some of the specimens were tested with fasteners installed in the holes. All testing was conducted at room temperature and at an R = 0.06. Preparation of holes by the punching technique is satisfactory.

A program was conducted on 8-1-1 to evaluate the performance of various structural pad-up geometries. A csk Hi-Lok bolt was installed in each specimen and all testing was conducted at room temperatures and using an R of 0.06. The results, shown in Table 3-T, did not show large differences between the various lengths of pads, although the padded specimens were much better than the unpadded ones.

Center-notched specimens were tested to evaluate the effect of test temperature on fatigue life. The test results are plotted in Fig. 3-104 and show somewhat longer fatigue life at room temperature for the higher stress levels and comparable lives at the lower stress levels.

Figures 3-105 and 3-106 show the results of tests conducted on 8-1-1 center-notched specimens. These tests were conducted to evaluate the fatigue life of notched specimens subjected to a prior exposure of elevated temperature and stress. Unexposed specimens were also tested to develop a basis of comparison. The prior exposure consisted of both cyclic and steady-state stress (40 ksi) and temperature (500° F and 650°F) for periods of 2,000, 5,000, and 10,000 hours. All tests were conducted at an R of 0.06 and at room temperature, 500° F, and 650° F. The effect of the exposure did not appear to be significant for this type of specimens. The lives of the specimens fatigue tested at elevated temperature were less than those of the specimens tested at room temperature.

A program is in progress to evaluate the effect of various temperature and load parameters on the fatigue resistance of two heat treats of Ti 6Al-4V. Both center-notched and riveted doubler specimens are used. Specimens are exposed to a loading and temperature spectrum derived from the flight environment. One test flight takes 90 min, of which 60 min are at elevated temperature. Specimens are subjected to this environment for 10,000 flights and 20,000 flights and then fatigue tested at room temperature. The results are compared with those of unexposed specimens. Other specimens are continued to failure under the flight loading. Identical specimens are tested to evaluate the effects of various means of reducing test time. The same loading spectrum was condensed in time from the 90 min to 30 sec, and specimens tested at both room temperature and 500°F. These results are shown for center-notched Ti 6Al-4V mill-annealed specimens in Table 3-U. Additional specimens of the same configuration were tested with R = 0.06 and a maximum stress of 60 ksi to evaluate loading frequency and temperature effects. Results are shown in Table 3-V. Examination of the results in both tables shows that both spectrum life and constant amplitude life at 500°F were less than that at room temperature. The effects due to differences in loading frequency were negligible and less than the scatter in test results.

Table 3-W summarizes a test program conducted using 8-1-1 fusion-welded specimens. The tests were conducted to evaluate the fatigue life of fusion-welded specimens subjected to a prior exposure of elevated temperature and stress. The pretest environment is the same as that previously described in Fig. 3-105 and Fig. 3-106 less 10,000-hour specimens. Two specimen configurations were employed in the test program: butt-fusion welded specimens with the weldment transverse to the direction of loading and in-line fusion welded specimens with the weldment parallel to the direction of loading. All tests were conducted at an R of 0.06 and at room temperature, 500°F, and 650°F. There was no pronounced effect due to the prior exposure. The fatigue lives at elevated temperature were less than those at room temperature.

In addition to these welded specimens, more than 100 small butt-welded specimens have been fatigue tested. The large number of variables evaluated precludes a condensed summarization of individual test results. The primary variables and examples of each are as follows:

a. Material (Ti 8-1-1 mill annealed, duplex annealed and triplex annealed, Ti-6-6-2 solution, treated and aged).

b. Thickness (.040 in. to 1.00 in.)

Table 3-S. Comparison of Drilled and Punched Hole Fatigue Life

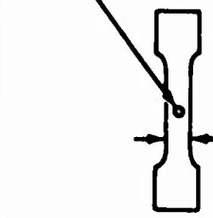
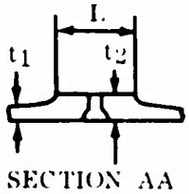
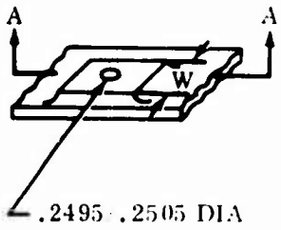
Configuration	Test Temp, °F	Fastener	Hole Preparation	▷ Top	▷ Bottom	Max. Gross Stress, KSI	Cycles To Failure, x 10^{-3}
MATL: 8-1-1 .050 GAGE $\frac{.201}{.190}$ DIA HOLE (HOLES FORMED IN PAIRS, DO NOT REAM OR DE-BURR  ▷ TOP OR BOTTOM PLATE DURING DRILLING OR PUNCHING OPERATION.	R.T.	None	Drill	X		40	78
			Drill		X	40	69
			Drill	X		30	1,570(N.F.)
			Drill		X	35	2,542(N.F.)
			Punch	X		40	44
			Punch		X	40	30
			Punch	X		30	2,111(N.F.)
			Punch		X	30	84
			Punch	X		35	345
			Punch		X	35	63
		Bolt	Punch	X		60	349
		Bolt	Punch		X	60	262
		Lock Bolt	Punch	X		60	266
		Lock Bolt	Punch		X	60	107
		Rivet	Punch	X		60	136
		Rivet	Punch		X	60	565

Table 3-T. Pad Geometry Effect on Fatigue Life

Configuration	Test Temp, °F	Pad Geometry t_1	Pad Geometry t_2	Pad Geometry L	Pad Geometry W	Fastener	Maximum Stress, KSI (R=.06)	Cycles To Failure, x 10^{-3}
Ti 8-1-1  SECTION AA  .2495 - .2505 DIA	R.T.	.080	.080			1/4 CSK Hi-Lok Bolt	80	19(Grip)
	R.T.	.080	.080				70	86
	R.T.	.080	.080				60	178
	R.T.	.080	.080				55	358
	R.T.	.080	.080				55	336
	R.T.	.080	.120	1.00	1.00		80	165
	R.T.	.080	.120	1.00	1.00		80	236
	R.T.	.080	.120	1.00	1.00		75	1,707
	R.T.	.080	.120	1.00	1.00		70	1,980
	R.T.	.080	.120	1.00	1.00		60	970(Grip)
	R.T.	.080	.120	2.00	1.00		80	157
	R.T.	.080	.120	2.00	1.00		80	211
	R.T.	.080	.120	2.00	1.00		75	241
	R.T.	.080	.120	2.00	1.00		70	2,338(N.F.)
	R.T.	.080	.120	2.00	1.00		60	13,245
	R.T.	.080	.120	5.00	1.00		80	174
	R.T.	.080	.120	5.00	1.00		75	233
	R.T.	.080	.120	5.00	1.00		70	1,241
	R.T.	.080	.120	5.00	1.00		65	321
	R.T.	.080	.120	5.00	1.00		65	4,564

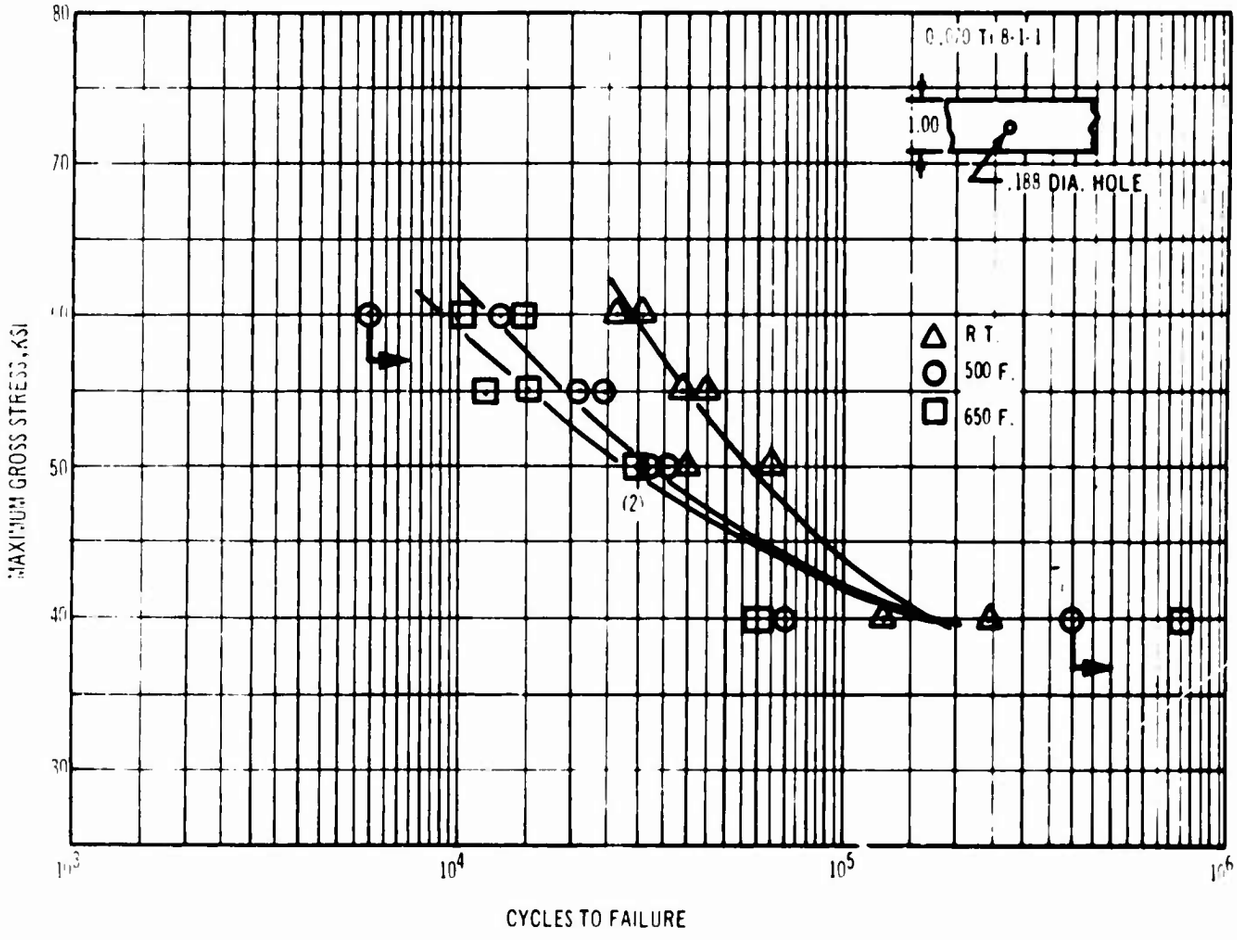


Figure 3-104. Temperature Effect on Center Notched Fatigue Life

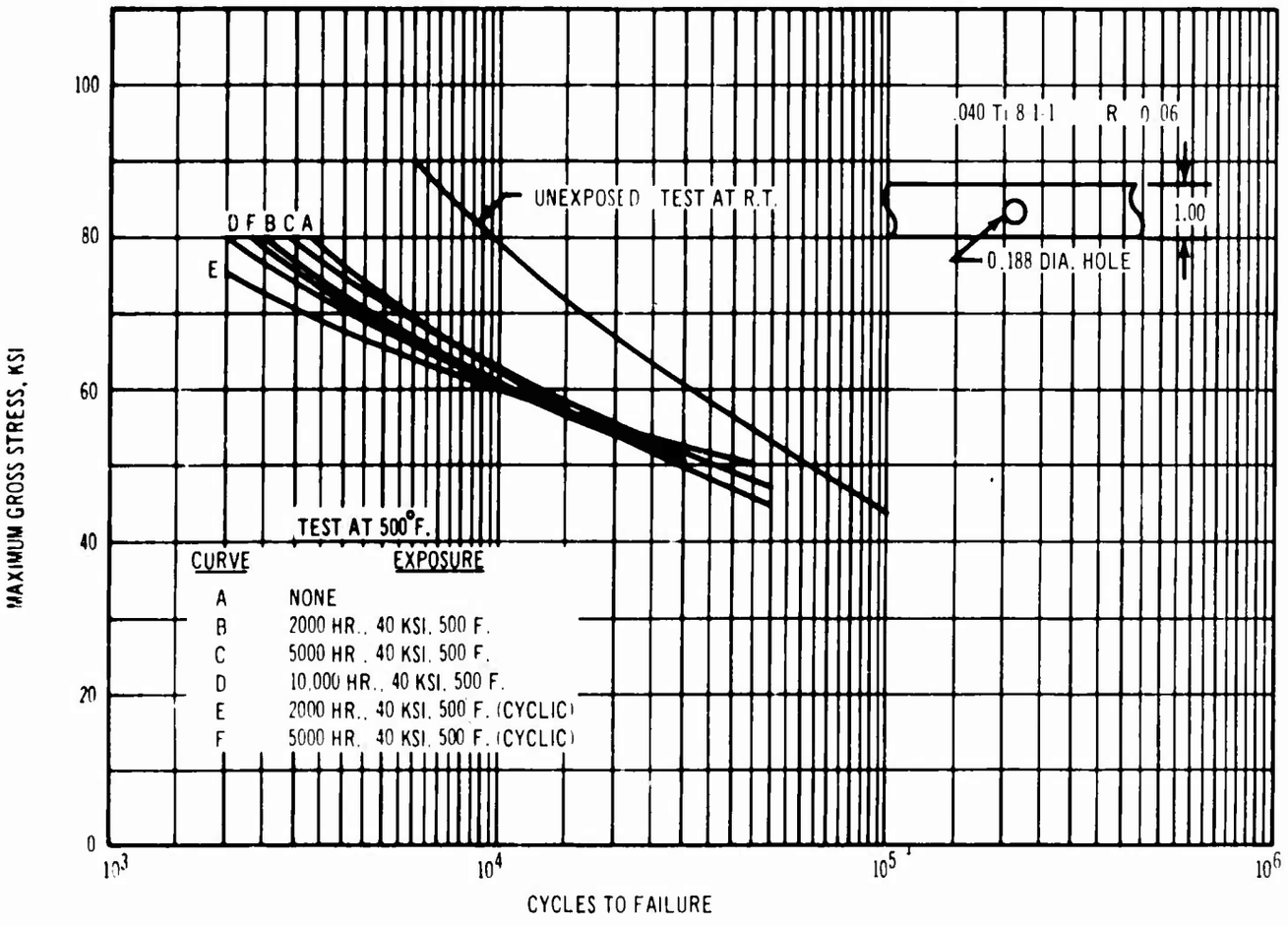


Figure 3-105. 500°F Exposure Effects on Center Notched Fatigue Life

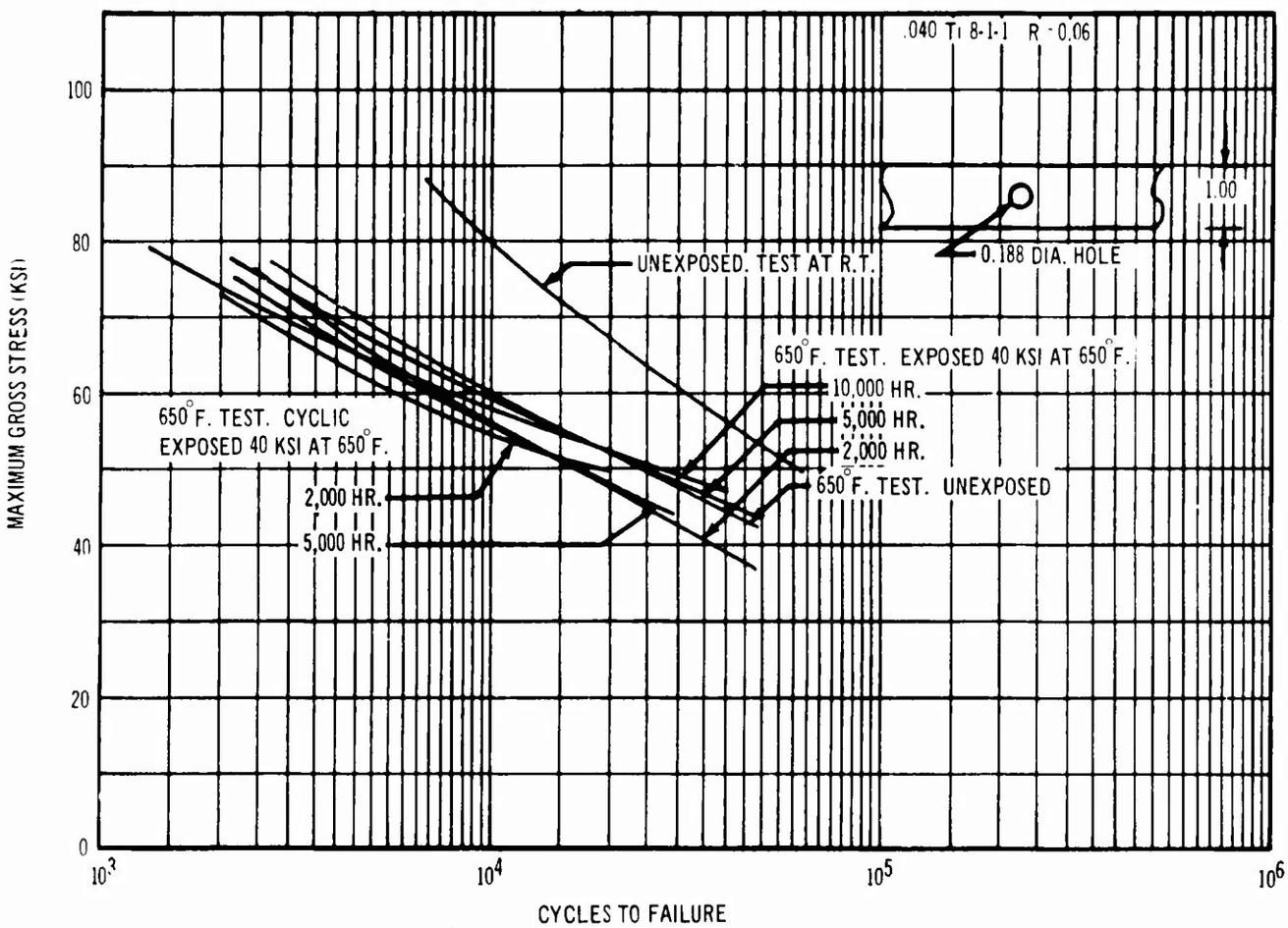


Figure 3-106. 650°F Exposure Effects on Center Notched Fatigue Life

Table 3-U. Center Notched Specimen Spectrum Life

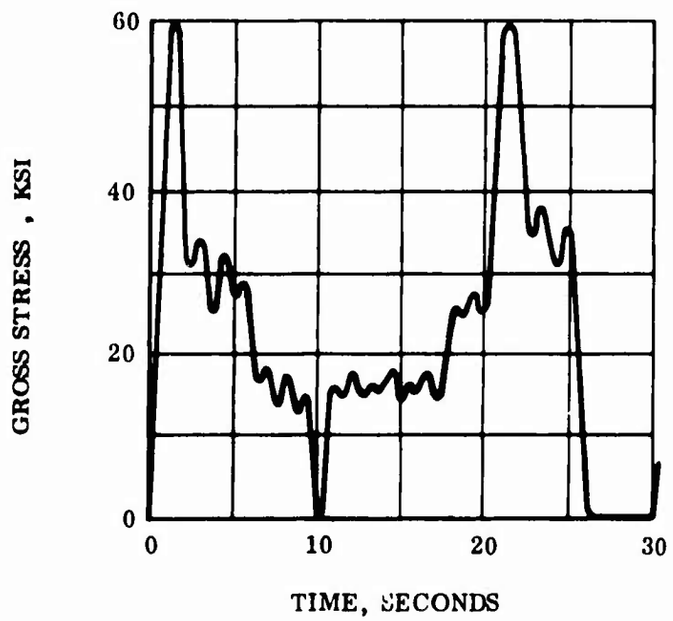
Loading Spectrum	Test Temp, °F	No. of Spectra To Failure
	70	11,440 6,972 4,620
	500	5,364 3,696 3,396

Table 3-V. Effects of Load Frequency on Center Notched Specimens

Test Temp, °F	Load Frequency, CPS	Maximum Gross Stress, KSI (R= 0.06)	Cycles To Failure, x 10^{-3}
70	0.33	60	16.8 24.9 36.6
500			11.7 10.8 11.0
70	3.3	60	26.2 42.0 15.5
500			10.2 9.9 9.2
70	33	60	24.3 27.1 42.6
500			13.1 10.6 10.7

c. Weld method (T.I.G., electron beam, flash).

d. Post-weld treatment (mechanical and thermal stress relief).

e. Prior exposure (time at load and temperature).

f. Test environment (load and temperature).

g. Specimen configuration (transverse and longitudinal welds).

3.6.4.2 Simple Fabricated Specimen Tests
The simple fabricated specimen tests are essentially an extension of the coupon specimen test to include the effect of fastening parameters and to provide an improved evaluation of basic structure and joint design.

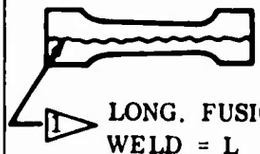
Spot welded double-strap butt-joint specimens were used to evaluate the effects of prior exposure, load, time, and test temperature. Results are

Table 3-W. Fusion Welded Specimen Fatigue Test Results

Configuration	Pre-Test Exposure					Test Temp, °F	No. of Spec.	Maximum Stress, KSI	Average Cycles To Failure, $X10^{-3}$
	1	2	°F	Hr	Stress, KSI				
MATL: Ti 8-1-1 GAGE: 040 R = 0.06	T					R.T.	2	120	10.4
	T					R.T.	2	100	36.1
	T					R.T.	2	90	114.4
	T					R.T.	3	80	114.8
	T					500	2	120	2.5
	T					500	2	105	2.3
	T					500	2	90	23.7
	T					500	3	80	60.3
	T					650	2	120	1.4
	T					650	2	105	4.9
	T					650	2	90	14.4
	T					650	3	80	39.0
	L					R.T.	2	120	23.6
	L					R.T.	1	110	25.0
	L					R.T.	2	100	46.0
	L					R.T.	3	80	316.0
	L					500	2	120	2.5
	L					500	2	105	9.2
	L					500	2	90	29.6
	L					500	2	80	54.0
	L					650	2	120	1.0
	L					650	2	105	2.2
	L					650	3	90	16.0
	L					650	2	80	40.2
	T	SS	500	2,000	40	R.T.	4	90	19.6
	T	SS	500	2,000	40	500	4	110	3.5
	T	SS	500	2,000	40	500	4	85	36.2
	T	CT	500	2,000	40	R.T.	2	90	66.5
	T	CT	500	2,000	40	500	2	110	4.0
	T	CT	500	2,000	40	500	2	85	29.0
	L	SS	500	2,000	40	R.T.	4	90	91.0
	L	SS	500	2,000	40	500	4	110	10.2
	L	SS	500	2,000	40	500	4	85	110.0
	L	CT	500	2,000	40	R.T.	2	90	64.0
	L	CT	500	2,000	40	500	3	110	9.0
	L	CT	500	2,000	40	500	3	85	56.5
	T	SS	650	5,000	0	R.T.	2	90	94.0
	T	SS	650	5,000	0	650	2	110	3.6
	T	SS	650	5,000	0	650	2	85	22.2
	L	SS	650	5,000	0	R.T.	2	90	104.0
	L	SS	650	5,000	0	650	2	110	1.4
	L	SS	650	5,000	0	650	2	85	53.0



1 TRANS. FUSION WELD = T



1 LONG. FUSION WELD = L

2:

SS = STEADY STATE ENVIRONMENT

CT = CYCLIC TENSION ENVIRONMENT

Table 3-W. (Continued)

Configuration	Pre-Test Exposure					Test Temp, ° F	No. of Spec	Maximum Stress, KSI	Avg. Cycles To Failure, x 10^{-3}
	1	2	° F	Hr	Stress, KSI				
SEE PREVIOUS PAGE	T	SS	650	2,000	40	R. T.	4	90	20.4
	T	SS	650	2,000	40	650	4	110	1.7
	T	SS	650	2,000	40	650	4	85	16.8
	T	CT	650	2,000	40	R. T.	2	90	150.4
	T	CT	650	2,000	40	650	1	110	2.0
	T	CT	650	2,000	40	650	2	85	27.9
	L	SS	650	2,000	40	R. T.	4	90	34.8
	L	SS	650	2,000	40	650	4	110	1.0
	L	SS	650	2,000	40	650	4	85	15.4
	L	CT	650	2,000	40	R. T.	2	90	218.0
	L	CT	650	2,000	40	650	3	110	5.7
	L	CT	650	2,000	40	650	3	85	30.2
	T	CT	500	5,000	40	R. T.	2	90	40.1
	T	CT	500	5,000	40	500	1	110	6.0
	T	CT	500	5,000	40	500	1	95	18.0
	T	CT	500	5,000	40	500	2	85	35.9
	L	CT	500	5,000	40	R. T.	1	100	179.0
	L	CT	500	5,000	40	R. T.	1	90	108.0
	L	CT	500	5,000	40	R. T.	1	80	2,490(N. F.)
	L	CT	500	5,000	40	500	2	95	48.8
	L	CT	500	5,000	40	500	1	85	52.0
	L	CT	500	5,000	40	500	2	110	5.0
	T	SS	500	5,000	40	R. T.	2	90	18.8
	T	SS	500	5,000	40	500	2	110	6.3
	T	SS	500	5,000	40	500	2	85	14.4
	L	SS	500	5,000	40	R. T.	2	90	41.2
	L	SS	500	5,000	40	500	2	110	11.5
	L	SS	500	5,000	40	500	2	85	148.0
	T	SS	650	5,000	40	R. T.	2	90	7.0
	T	SS	650	5,000	40	650	2	110	1.4
	T	SS	650	5,000	40	650	2	85	6.3
	L	SS	650	5,000	40	R. T.	2	90	24.1
	L	SS	650	5,000	40	650	2	110	1.4
	L	SS	650	5,000	40	650	2	85	13.6
	T	SS	500	5,000	0	R. T.	2	90	62.0
	T	SS	500	5,000	0	500	2	110	5.0
	T	SS	500	5,000	0	500	2	85	11.2
	L	SS	500	5,000	0	R. T.	2	90	110.0
	L	SS	500	5,000	0	500	2	110	11.4
	L	SS	500	5,000	0	500	2	85	44.7

presented for 92 specimens in Figs. 3-107 and 3-108. These tests show only minor effects from the thermal exposure.

The effect of sheet gage and spot spacing on the fatigue life of arc spotwelded lap joints is shown in Fig. 3-109. All test points fall within a fairly narrow scatter band.

Fatigue lives of spotwelded lap joints having different types of spotwelds and post-weld treatments are summarized in Table 3-X. All specimens were tested at room temperature and R = 0.06 Coining of the spotwelds had no apparent effect. The standard spotwelded specimens with post-weld treatment had better lives than those unexposed, but may have been due to configuration and gage differences.

A comparison of the fatigue lives of double-strap butt-joints having standard spotwelds, T.I.G. spotwelds and spot brazing is shown in Fig. 3-110. The specimens with T.I.G. spotwelds and those spotbrazed with .002 in. Ag-Li foil had comparable lives which were less than those for specimens with standard spotwelds.

The influence of the type of braze foil used for spotbrazed lap joints is shown in Fig. 3-111. The specimens with the thin gold spray were inferior to those with the other four foil materials.

Because of the low fatigue life for spotwelded specimens with load transfer, single and double shear joints were designed to equalize the strain between members. The joints were made with either spotwelds, seamwelds or spot brazing.

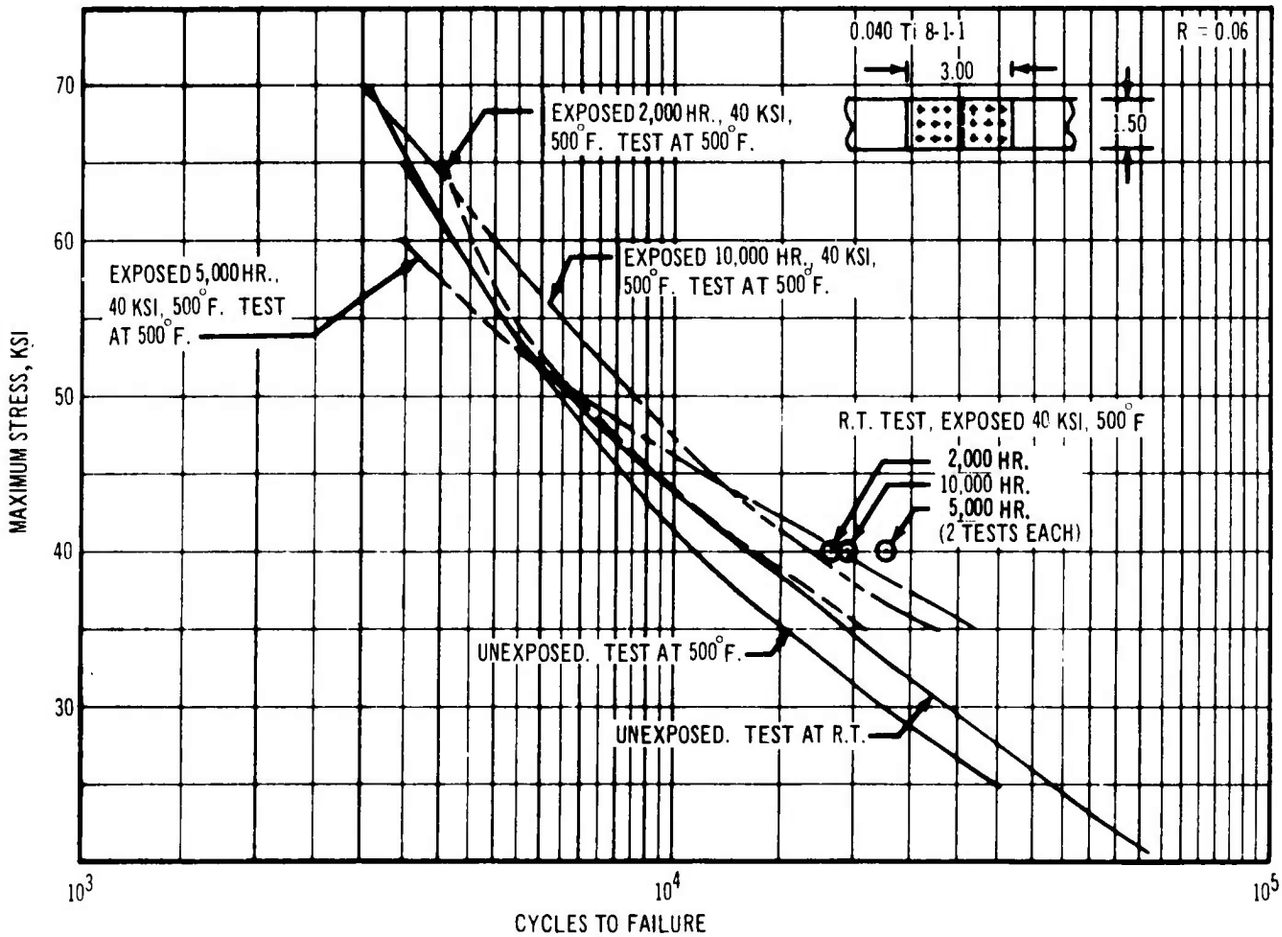


Figure 3-107. 500°F Exposure Effects on Spotwelded Fatigue Life

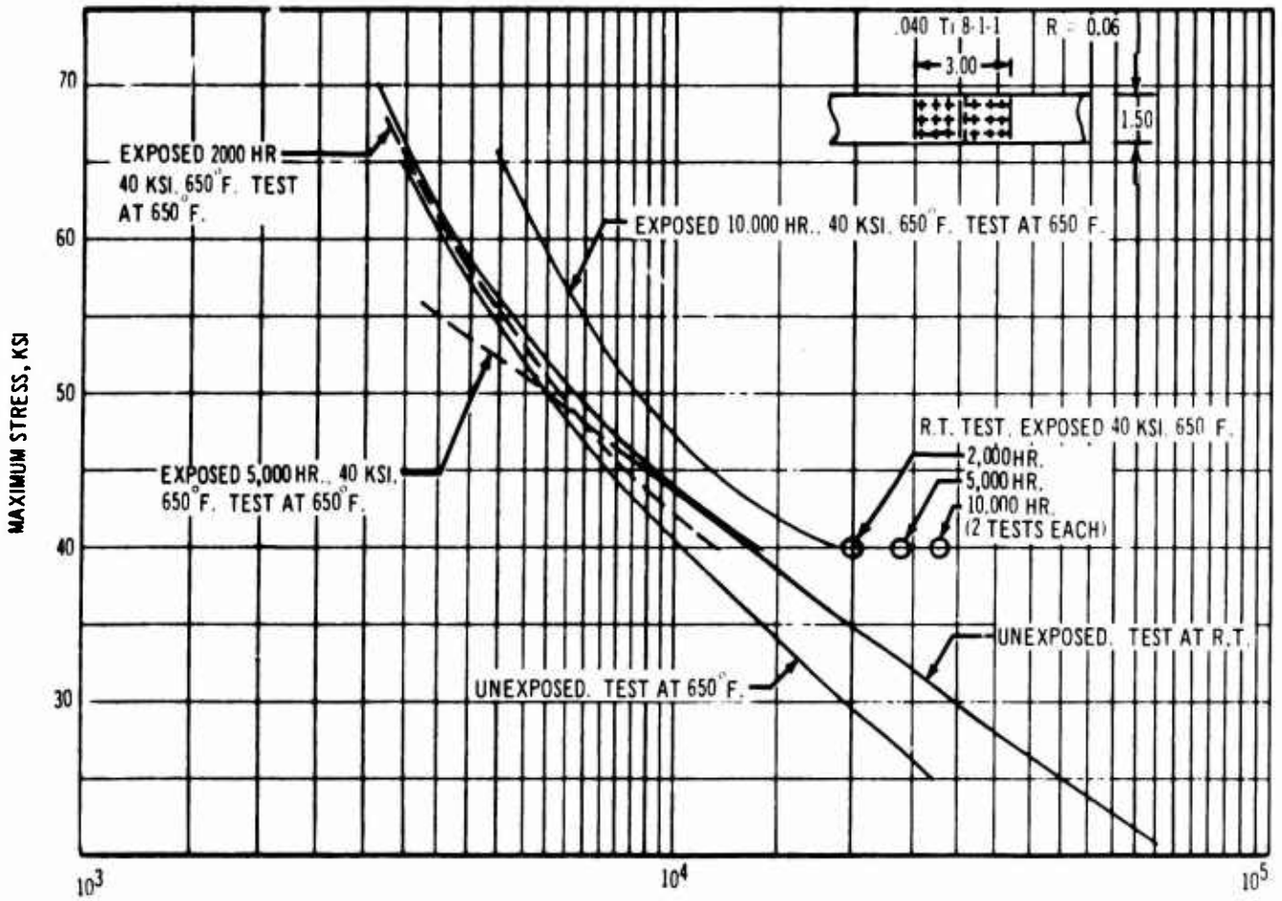


Figure 3-108. 650°F Exposure Effects on Spotwelded Fatigue Life

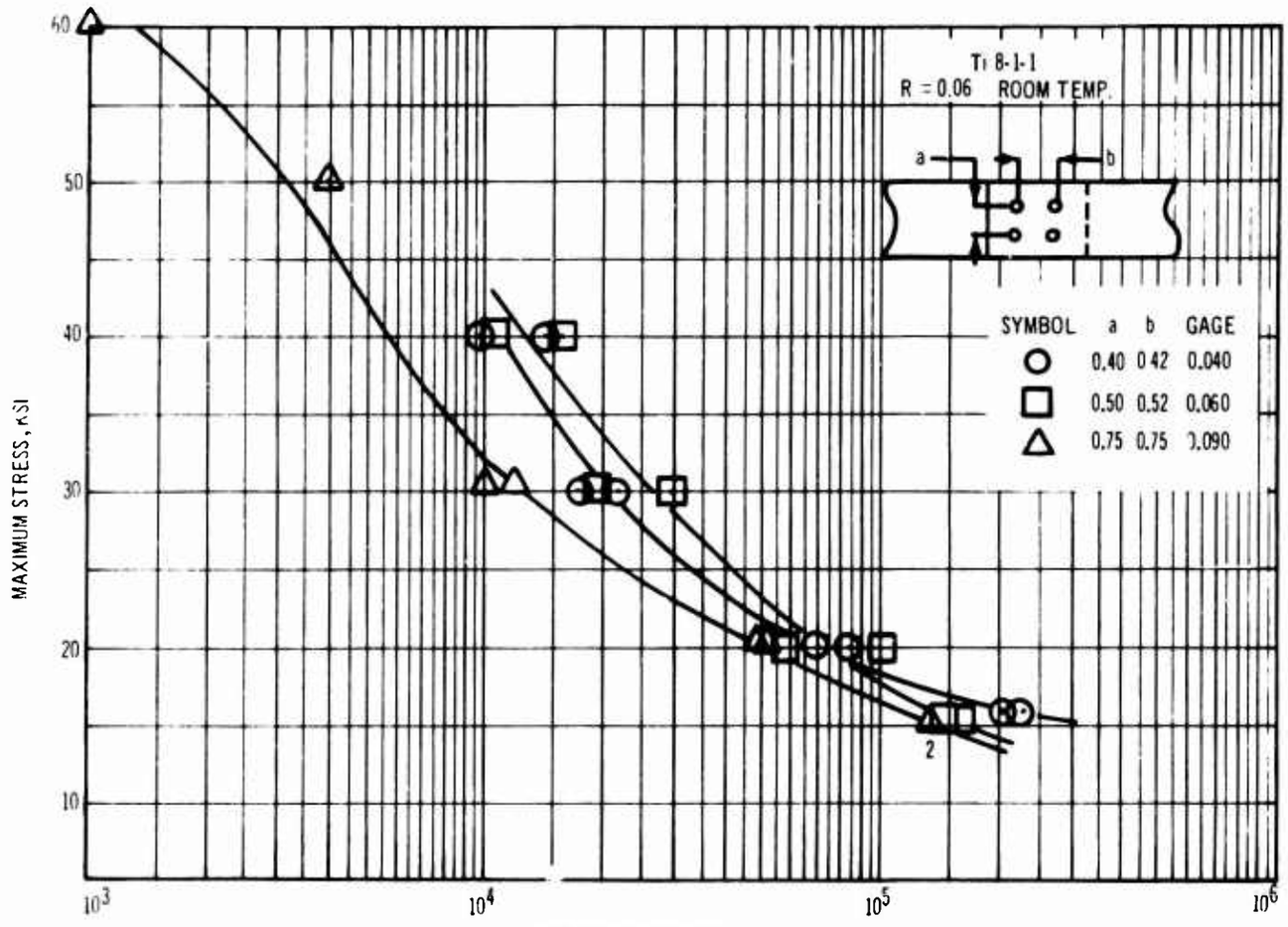
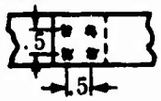
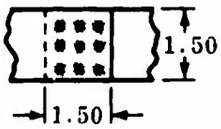


Figure 3-109. Arc Spotwelded Lap Joint Fatigue Life

Table 3-X. Spotwelded Joint Fatigue Lives

Configuration	Nominal Gage In	Post-Weld Treatment	Spotweld Type	Max Gross Stress, KSI	Cycles To Failure, x 10^{-3}
MATL: Ti8-1-1 	0.035/0.035	None	Standard	60 40 30 20	6 13 23 94
MATL: Ti8-1-1 	0.060/0.060	1,296 Hrs at 550° F	Standard	45 40 30	44 52 136
	0.050/0.050	None	Non-Forgeout	50 40 35 30	8 18 23 52
	0.050/0.050	Impact Coined	Non-Forgeout	40 35 30 25	19 30 43 56

Test results are presented in Fig. 3-112, and, when compared with standard joints, show some improvement in life although still unacceptable for fatigue critical areas.

Specimens with a single fastener installed through a sheet with a doubler are used to evaluate the effect on fatigue life of fastener and fastener installation variables. The beneficial effects of interference fits are illustrated in the test information summarized in Table 3-Y. Similar specimens with Hi-Lok fasteners were tested to evaluate the effects on fatigue life of cold working at the intersection of the sheet surface and hole surface. Cold working was accomplished by using a special die and a drop hammer. No particular benefit was shown by this method and the work was discontinued. Data is shown in Table 3-Z.

Mechanically fastened double-strap butt-joints were fatigue tested at room temperature to evaluate the effects of the type of fastener, the bolt torque (for threaded fasteners), the fastener pattern, and prior exposure. Table 3-AA summarizes the program.

The bolted joints generally had longer lives than the riveted joints, and the life was improved by increased nut torque or fastener interference.

The influence of three types of fasteners on lap joint fatigue life is shown in Fig. 3-113. The Hi-Loks and Taper-Loks showed comparable lives and both were better than the slug rivets.

Bolted and riveted lap joints were fatigue tested to provide data on the significance of burrs left on fastener holes. Some specimens were deburred while others were left with various heights of burrs. Testing was at room temperature at an R of 0.06. The results presented in Table 3-BB show a detrimental effect of the burrs for the bolted joints but not for the riveted joints.

Tests of single-shear butt joints, utilizing a splicing channel to reduce lateral deflections, were conducted to evaluate fastener types. These tests are summarized in Fig. 3-114 for machined skins and Fig. 3-115 for unmachined skins. Results show Taper-Loks and bolts to be the best, followed by driven rivets and then spotwelds.

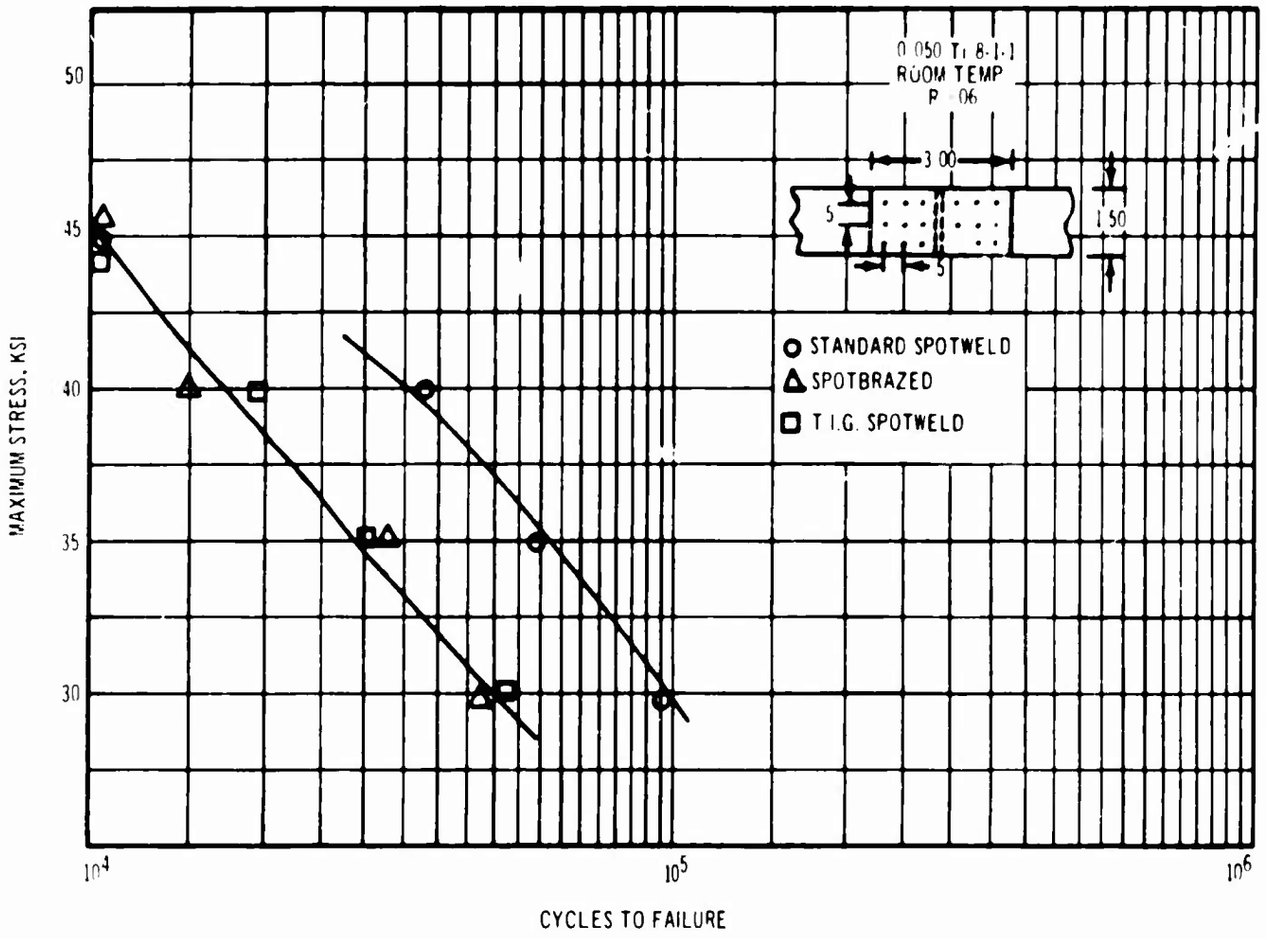


Figure 3-110. Welded Butt Joint Fatigue Life

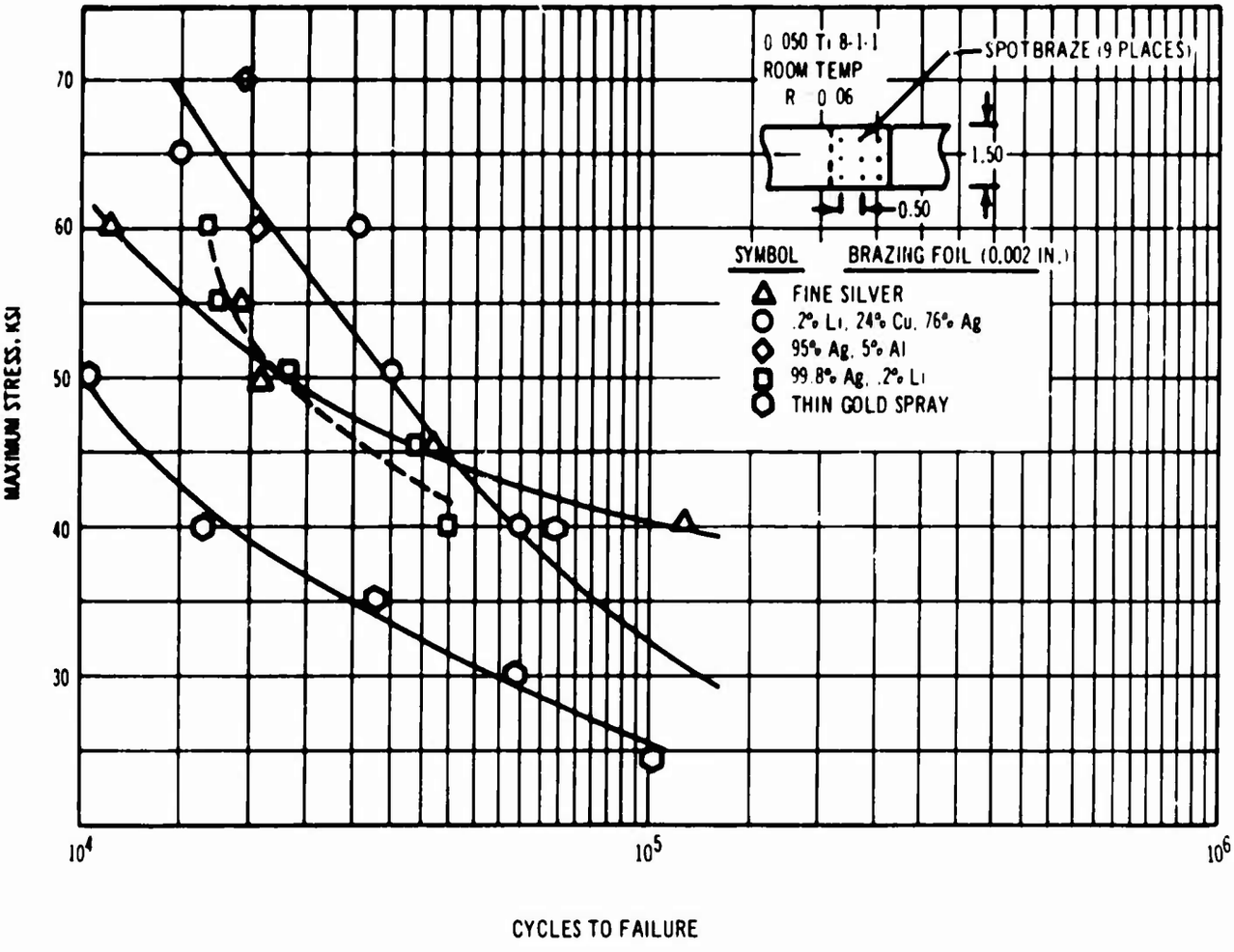


Figure 3-111. Effect of Spotbraze Foil on Fatigue Life

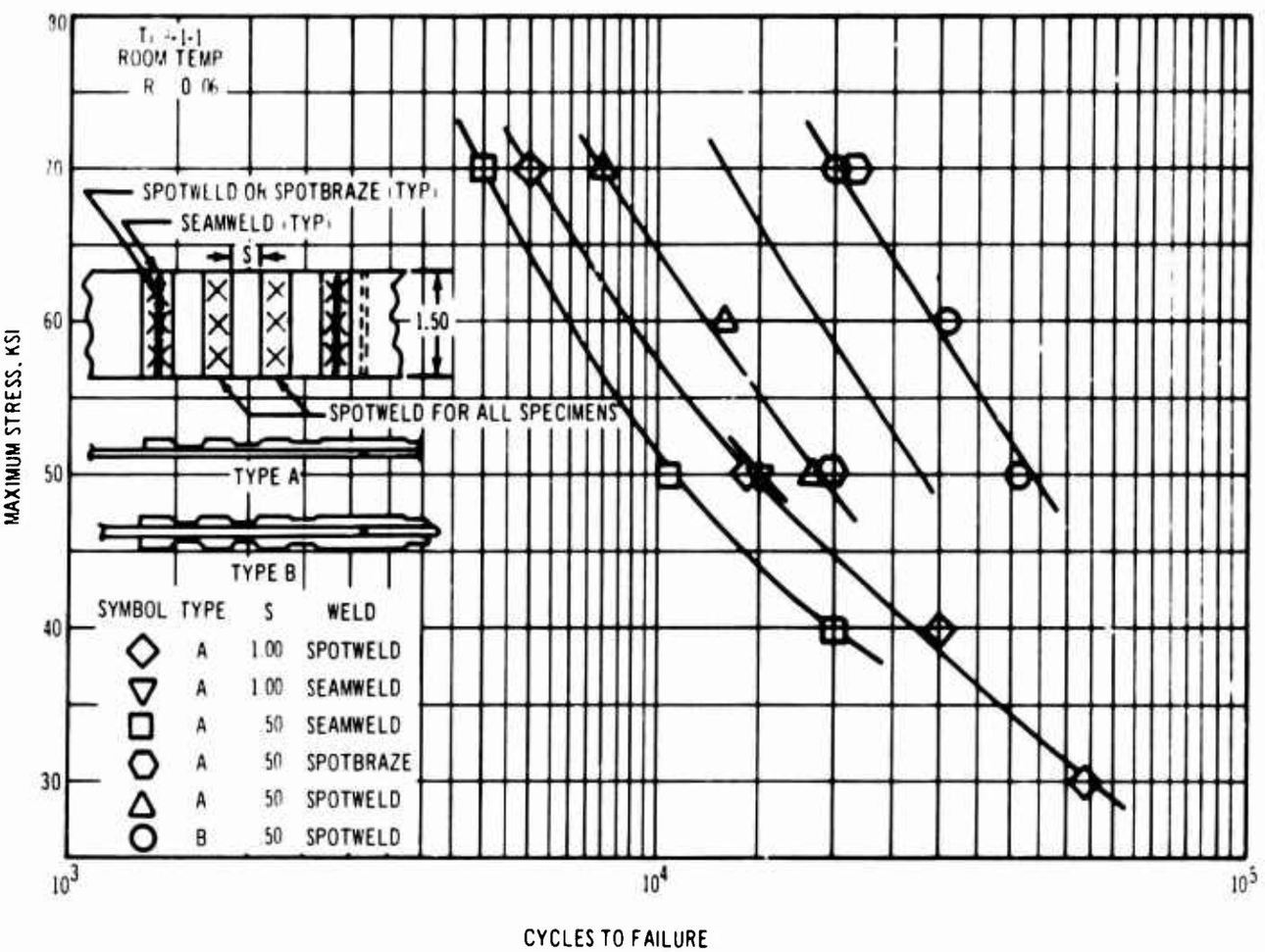


Figure 3-112. Fatigue Life of Strain Design Joints

Table 3-Y. Riveted Doubler Specimen Fatigue Lives

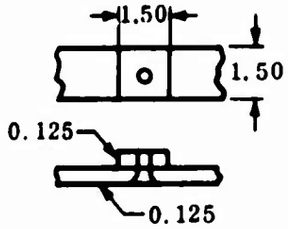
Configuration	Test Temp	Fastener	Hole Clearance	Squeeze Kips	Max Gross Stress, KSI	Cycles to Failure, $X10^{-3}$
MATL: T18-1-1 R-.06  	R. T.	1/4 CSK A-286 Rivet	-0. 0002	31	70	144
	R. T.		-0. 0002	31	70	326
	R. T.		-0. 0002	31	70	187
	R. T.		-0. 0002	32	70	64
	R. T.		-0. 00023	32	70	79
	R. T.		-0. 00023	32	70	141
	R. T.		-0. 00023	31. 5	70	619
	R. T.		-0. 00043	31. 5	70	411
	R. T.		-0. 00043	31. 5	70	778
	R. T.		-0. 00043	31	70	538
	R. T.		-0. 00030	31	70	304
	R. T.		-0. 00030	31	70	142
	R. T.		-0. 00030	30. 7	70	103
	R. T.		-0. 00043	30. 7	70	403
	R. T.		-0. 00043	30. 7	70	229
	R. T.		-0. 00043	30. 3	70	207
	R. T.		-0. 0004	30. 3	70	352
	R. T.		-0. 0004	30. 3	70	218
	R. T.		+0. 002	31	70	2, 013 (N. F.)
	R. T.		+0. 002	31	70	1, 293
	R. T.		+0. 002	31	70	1, 284
	R. T.		+0. 002	31	70	1, 183
	R. T.		+0. 002	31	70	677
	R. T.		+0. 002	31	70	1, 031
	R. T.		-0. 002	31	70	210 (grip)
	R. T.		-0. 002	31	70	880
	R. T.		+0. 002	31	70	809
	R. T.		+0. 002	31	70	891
	R. T.		—	(Gun Driven)	—	20 specimens are in Test

Table 3-Y. (Continued)

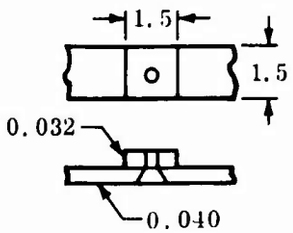
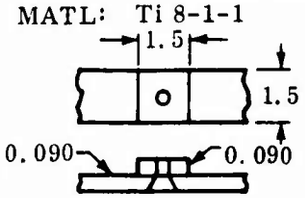
Configuration	Test Temp	Fastener	Hole Clearance	Squeeze Kips	Max Gross Stress, KSI	Cycles to Failure, $X10^{-3}$
MATL: Ti 6-4 	R. T.	5/32	+0.002	MANUAL	70	204
	R. T.	A-286	+0.002		70	225
	R. T.	CSK	+0.0035		70	140
	R. T.	Rivet	+0.002		70	133
	R. T.		+0.001		70	440
	R. T.		+0.002		60	1,037 (N. F.)
	R. T.		+0.002	14	70	1,168 (N. F.)
	R T.		+0.003	14	70	101
	R. T.		+0.001	14	70	402
	R. T.		+0.002	14	70	1,198 (N. F.)
	R. T.		+0.002	14	70	159
	R. T.		+0.003	14	70	107
	R. T.		+0.0015	14	70	261 (grip)
	R. T.		+0.004	14	70	299 (grip)
	R. T.		+0.003	14	70	429
	R. T.		+0.003	14	70	800
	R. T.		+0.004	14	70	144
	R. T.		+0.003	14	70	527
MATL: Ti 8-1-1 	R. T. and 500°F	1/4 CSK Ti6Al-4V Rivet	0(Nom.)	32	12 Specimen no Exposure 24 Specimens 500 hr at 500°F 6 Specimens 1000 hr at 500°F } In Test	

Table 3-Z. Effect of Hole Cold Work on Fatigue Life

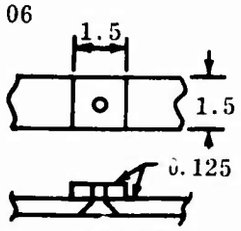
Configuration	Impact Location	50 lb Impact Hammer				Max Gross Stress, KSI	Cycles to Failure, $X10^{-3}$
		Strap		Skin			
		Times Dropped	Height	Times Dropped	Height		
MATL: Ti8-1-1		—	—	—	—	60	114
ROOM TEMP	—	—	—	—	—	60	246
R=.06		—	—	—	—	60	172
		2	1 Ft	4	1 Ft	60	66
		2	1 Ft	1	2 Ft	60	91
		2	1 Ft	1	2 Ft	60	84
		2	1 Ft	1	2 Ft	60	120
		2	1 Ft	1	2 Ft	60	258
		2	1 Ft	1	2 Ft	60	197
		1	2 Ft	1	2 Ft	60	123
NOTE: IMPACT		1	2 Ft	1	2 Ft	60	794
PRIOR TO ASSEMBLY		1	2 Ft	1	2 Ft	60	199

Table 3-AA. Mechanically Fastened Butt Joint Fatigue Life

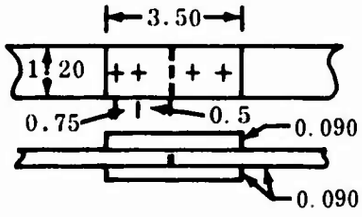
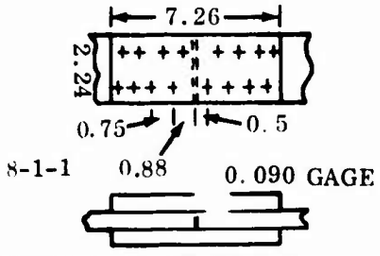
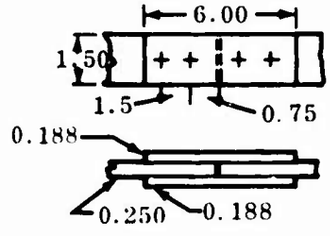
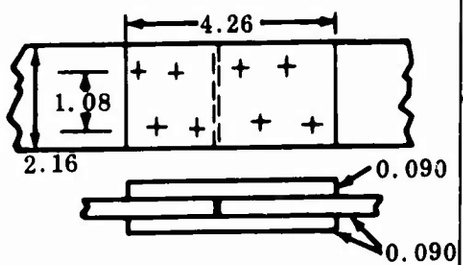
Configuration	Fastener	Torque, In-Lb	Pre Test Exposure °F	Pre Test Exposure HRS	Max Gross Stress, KSI	Cycles To Failure, x 10^{-3}
MATL: Ti8-1-1 0.090 GAGE  	External Wrenching Bolt	100	---	---	70	16
		100	---	---	65	21
		100	---	---	60	72
		100	---	---	50	180
		200	---	---	85	57 (Grip)
		200	---	---	75	95
		200	---	---	65	136
		200	---	---	65	71 (Grip)
		200	550	100	65	270
		200	550	500	65	41 (Grip)
	Hex Head Bolt (Steel)	90	---	---	70	11
		90	---	---	60	45
		90	---	---	50	197
		180	---	---	80	116
		180	---	---	70	112
		180	---	---	60	41 (Grip)
		180	550	100	80	182
		180	550	100	70	253
		180	550	500	70	250
 	Std Head Rivet	Does Not Apply	---	---	50	40
			---	---	50	35
			---	---	45	127
			---	---	40	144
			550	100	45	78
			550	100	40	167
			500	500	50	35
MATL: Ti8-1-1  	Taper-Lok (Steel)	400	---	---	70	59
			---	---	60	169
			---	---	55	336
	NAS Bolt	400	---	---	70	25
			---	---	60	175
			---	---	55	110
	Taper-Lok (Titanium)	350	---	---	80	16
			---	---	70	49
			---	---	60	214
			---	---	50	278

Table 3-AA. (Continued)

Configuration	Fastener	Torque, In-Lb	Pre Test Exposure °F	Pre Test Exposure HRS	Max Gross Stress, KSI	Cycles To Failure, X 10^{-3}
MATL: Ti8-1-1 .090 GAGE  	Hex Head Bolt (Titanium)	70	—	—	75	47
		70	—	—	70	100
		70	—	—	60	202
		70	—	—	50	264
		150	—	—	70	126
		150	550	100	70	176 (Grip)
		150	550	100	60	198
		150	550	500	70	126
	Pull-Type Lock Bolt (Titanium)	Does Not Apply	—	—	80	97
			—	—	70	121 (Grip)
			—	—	60	153
			—	—	50	328
			—	—	50	116
			550	100	60	268
	Stump Type Lock Bolt (Titanium)	Does Not Apply	—	—	70	91
			—	—	60	142
			—	—	60	111 (Grip)
			—	—	50	355
			550	100	60	27
			550	100	50	236 (Grip)
			550	500	60	66
			550	500	50	453
	Lock Bolt (Steel)	Does Not Apply	—	—	60	147
			—	—	50	193
			550	100	60	114
			550	100	50	210 (Grip)
	Taper-Lok (Titanium)	100	—	—	60	77 (Grip)
		100	—	—	60	92
		100	—	—	60	148
		100	—	—	70	54
		100	—	—	70	83
		100	—	—	80	15
		100	550	100	60	86
		100	550	100	70	19
	Std. Hd. Rivet	Does Not Apply	—	—	60	28
			—	—	50	92
			—	—	40	331

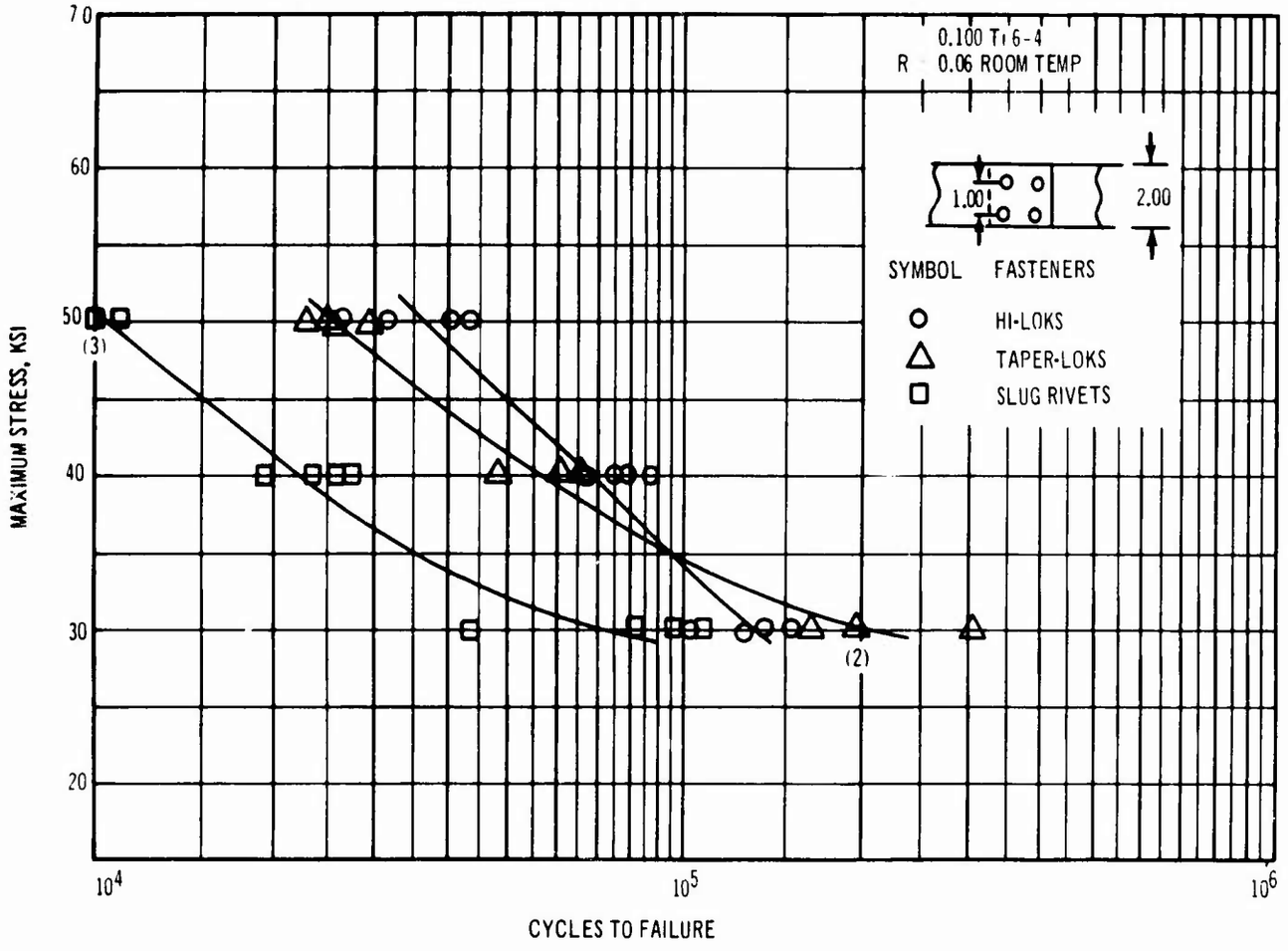
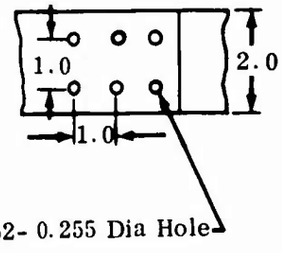


Figure 3-113. Fatigue Life of Mechanically Fastened Lap Joints

Table 3-BB. Effects of Burrs on Lap Joint Fatigue Life

Configuration	Fasteners	Burr Height At Interface, In.	Max Gross Stress, KSI	Cycles To Failure, x 10^{-3}
MAT: Ti 8-1-1 0.100/0.100 Gage  0.252- 0.255 Dia Hole R=.06	NAS Bolts	Deburred	50	19
		Deburred	50	24
		Deburred	50	18
		Deburred	35	103
		Deburred	35	86
		Deburred	35	38
		0.0035-.006	35.3	73
		0.0035-.006	35	47
		0.0035-.006	35	42
		0.0025-.003	35	63
		0.0025-.003	35	56
		0.0025-.003	35	46
		0.001-.0015	35	63
		0.001-.0015	35	54
		0.001-.0015	35	34
	A-286 Rivets	Deburred	40	101
		Deburred	40	219
		Deburred	40	151
		Deburred	35	158
		Deburred	35	156
		Deburred	35	126
		Deburred	35	176
		Deburred	35	213
		Deburred	35	147
		Deburred	30	639
		Deburred	30	1,759 (N.F.)
		Deburred	30	342
		0.002-.005	40	141
		0.002-.005	40	148
		0.002-.005	40	361
		0.002-.005	30	652
		0.002-.005	30	3,672
		0.002-.005	30	658
		0.0035-.006	35	277
		0.0035-.006	35	686
		0.0035-.006	35	292
		0.0025-.003	35	259
		0.0025-.003	35	510
		0.0025-.003	35	466
		0.001-.0015	35	473
		0.001-.0015	35	224
		0.001-.0015	35	306
		0.003-.008	35	4,000 (N.F.)

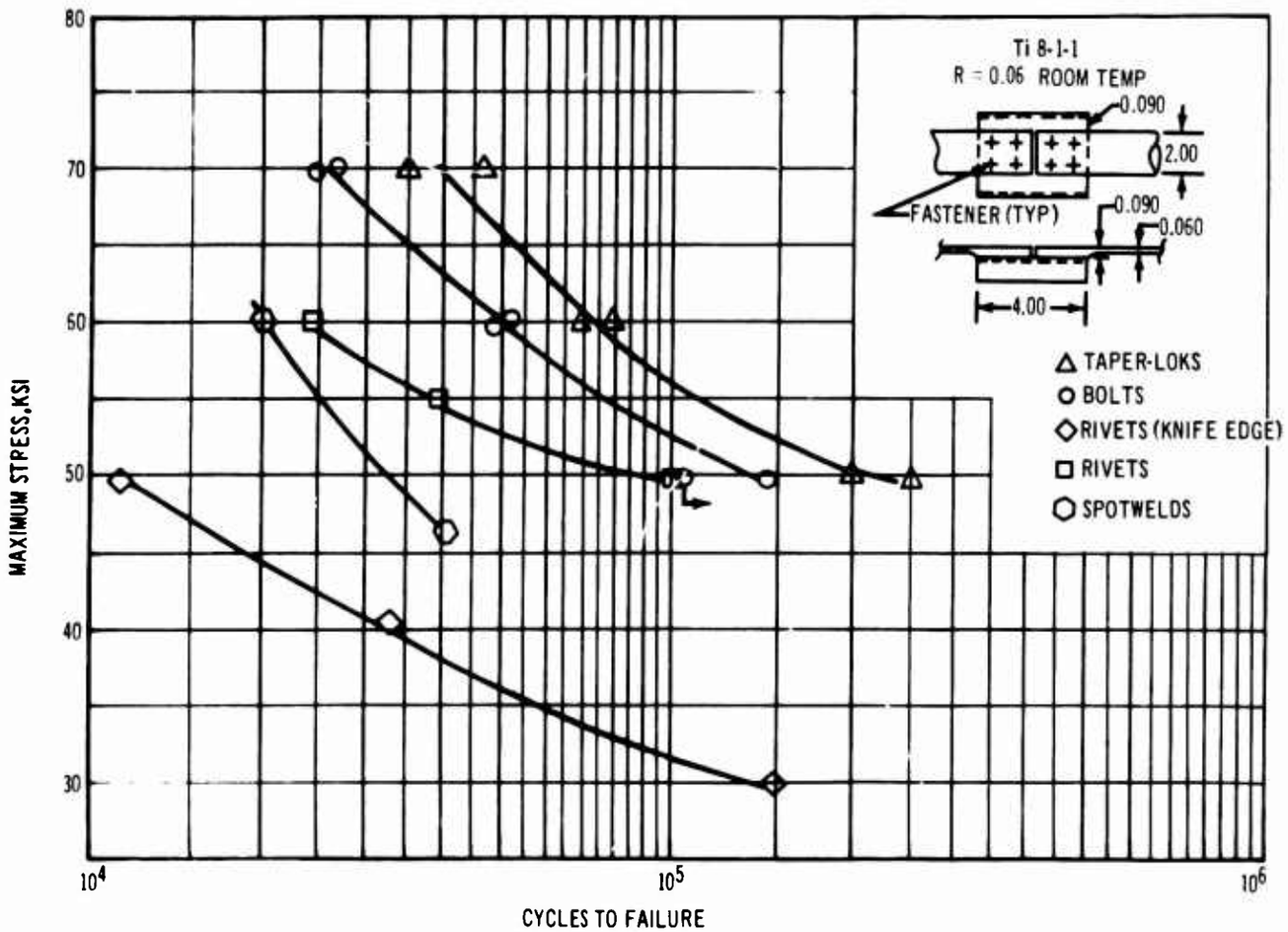


Figure 3-114. Effect of Fasteners on Padded Skin Joint Fatigue Life

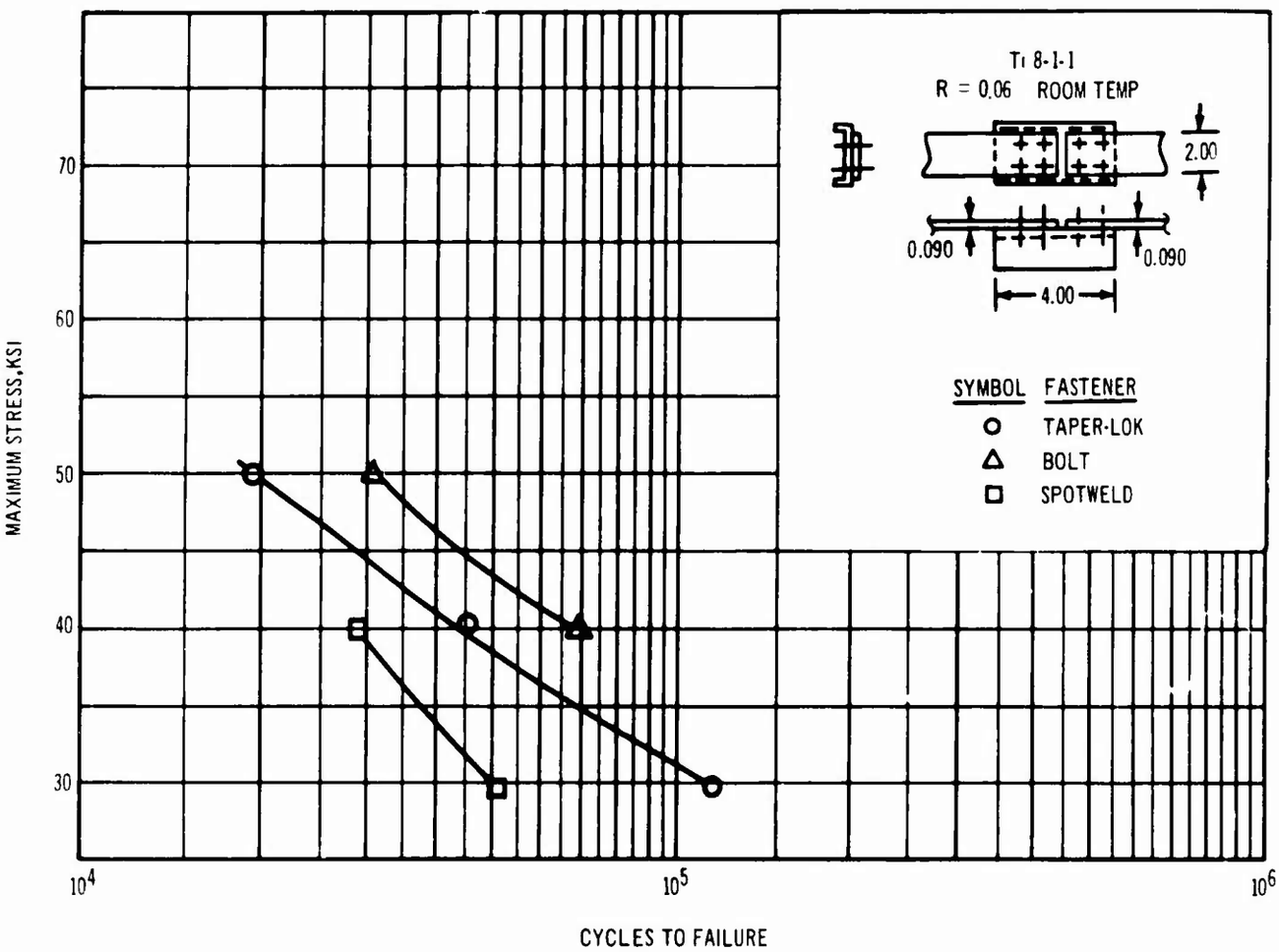
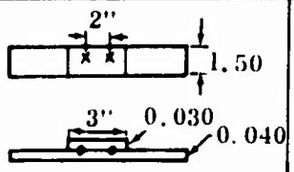
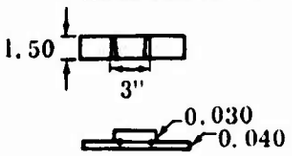
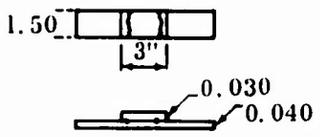
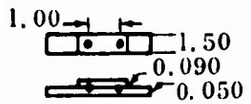
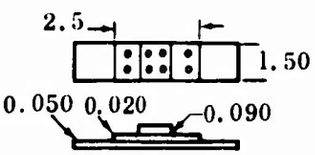
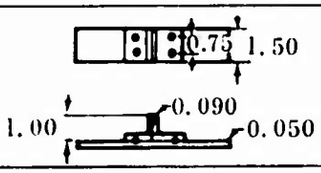
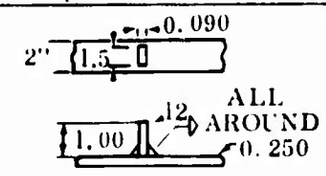


Figure 3-115. Effect of Fasteners on Unpadded Skin Joint Fatigue Life

Table 3-CC. Local Attachment Fatigue Test Results

Specimen Configuration	Test Temp, °F	Max. Gross Stress, KSI (R=.06)	Cycles to Failure, X10^{-3}	Pretest Environment	Notes
	R. T. R. T. R. T. R. T.	60 50 40 30	7 10 13 45	None None None None	Std. S/w
RESISTANCE BRAZE 	R. T. R. T. R. T. R. T. R. T. R. T.	80 70 65 60 30 65	25 65 57 89 1,769(N. F.) 109	None None None None None 100 HRS at 550°F	
SEAM BRAZE WITH NICKEL-GOLD FOIL 	R. T. R. T. R. T. R. T. R. T. R. T. 400 400	60 50 40 60 50 40 50 40	52 136 251 38 76 190 56 116	None None None 100 HRS at 450 100 HRS at 450 100 HRS at 450 100 HRS at 450 100 HRS at 450	
	R. T. R. T. R. T.	70 60 50	7 14 25	None None None	Standard Spotweld
	R. T. R. T. R. T. R. T. R. T. R. T.	70 50 40 70 60 50	5 14 ▷1 32 16 24 ▷2 47	None None None None None None	▷1 Standard Spotweld ▷2 Seam Weld
	R. T. R. T. R. T.	70 60 50	18 25 39	None None None	
	R. T. R. T. R. T. R. T.	67.5 48.2 57.8 62.5	23.5 134.5 98 40	None None None None	

Various techniques for local attachment to continuous members were evaluated in an attempt to solve the spotwelded structure fatigue problems. Test results for spotwelded, fusion welded, and brazed attachments are contained in Table 3-CC. All specimens were Ti 8-1-1 and tested with R = 0.06. Three specimens of spotwelded member runout were fatigue tested at room temperature with R = 0.06. Table 3-DD shows the results. None of these methods were adequate although some life extension was provided.

3.7 SONIC TEST

3.7.1 Summary

Fifty structural panels have been sonic tested representing both skin-stiffener and sandwich construction. Continuous testing and design improvements have resulted in structures of both types that provide lighter weight and higher sonic resistance than previously attained. Sandwich panels of less than 1.2 lb/sq ft have resisted sonic environments through 172db. Riveted skin-stiffener panels of less than 2.0 lb/sq ft have resisted sonic environments through 172db. Tables 3-EE and 3-FF summarize the panel configurations and results of the more significant testing. Highlights of the development program are as follows:

a. Tests have been conducted with random noise which closely duplicates the aircraft engine noise.

b. Agreement was obtained between panel response measured behind a J-75 engine and panel response measured in the progressive wave chamber using random noise. See Fig. 3-116 for comparison and Figs. 3-117 and 3-118 for photos of engine and horn test setups.

c. Correlation between panel geometry and sonic induced stresses is shown in Fig. 3-116 Photographs of a typical skin-stiffener panel with strain gages attached are shown in Fig. 1-8.

d. Panel tests have demonstrated an order of magnitude improvement in sonic resistance for riveted structure versus spotwelded structure. Design criteria have been developed for light-weight riveted structure and are presented in Figs. 3-119 and 3-120. Spotwelds will not be considered for any use in sonic critical areas.

e. Tests of honeycomb structure have demonstrated that minimum weight designs are adequate for sonic environments in excess of the B-2707 noise levels.

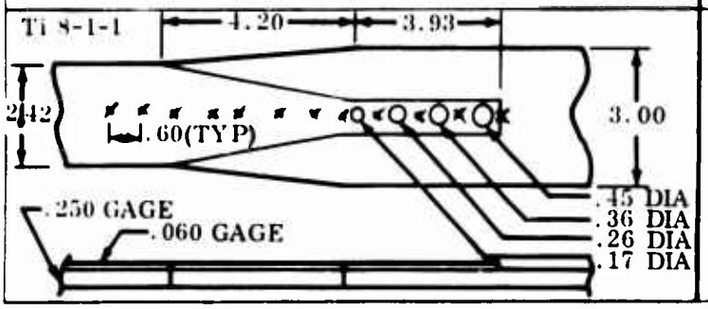
3.7.2 Sonic Test Methods

Horn testing is conducted in a progressive wave chamber with the sound generated by a 20,000 watt transducer. This transducer is capable of generating random noise with a variable frequency shape to 171db sound level. The distribution of frequencies used for the random noise testing has been established on the basis of J-75 engine testing as the SST engines will not have significantly different frequency distributions than the large J-75 engines. Limited tests were conducted on panels behind the J-75 engines and then in the horn chamber to verify panel response. Results of strain gage reading shown in Fig. 3-116 demonstrate that there is almost identical panel response for horn and engine tests.

The progressive wave chamber is an enclosed tunnel with sound waves generated at one end and terminated or absorbed at the downstream end. The test specimen is mounted flush in one of the tunnel walls. See Fig. 3-118 for a photograph of the test set-up. The sound waves strike the test specimen at a grazing incident which has been found to best represent the position of structure downstream of an engine exhaust.

Throughout the sonic testing program, continuous improvements have been made in test methods to more accurately represent airplane structure and environment. Earlier tests generally utilized a discrete frequency noise input that was established on the basis of panel response as measured by deflection. Since mid-1965 all testing has been conducted using a random noise source to better represent the jet engine environments. Also, panel response is measured on the basis of strain gage readings. The present system uses a horn noise shaped to duplicate a J-75 engine. With this environment, the same stresses are consistently measured during horn testing as those obtained during actual engine tests. The panels have been heavily instrumented with strain gages in order to record maximum sonic-induced stresses. A comparison of the stress response from actual engine noise and that from the horn source shows that proper shaping of the random input results in an accurate representation of the airplane structure damage.

Table 3-DD. Spotwelded Member Runout

Configuration	Maximum Stress, KSI (R=.06)	Cycles To First Crack, x 10^{-3}	Cycles To Failure, x 10^{-3}
	50	40	44
	40	46	61
	30	117	240

Tests have been conducted to establish the effect of various panel geometries on the relationship between sonic-induced stresses and panel geometry. For the skin stiffener panels this relationship is shown to be a function of the skin thickness and panel spacing. Fig. 3-120 shows that this relationship is clearly established and usable for design improvements.

3.7.3 Sonic Fatigue Test Interpretation

Sonic fatigue is similar to conventional structural fatigue and may be analyzed in a like manner. However, a significantly longer cyclic life is required for sonic-loaded structure than the more conventional mechanical fatigue-loaded airplane structure.

Engine sonic environment can induce more than 10^6 cycles per hour so the structure must be designed for the extremely long life portion of the S-N curve and test results must be interpreted accordingly.

Methods have been used to interpret accelerated horn type test results in terms of the sonic-intensity level that the structure would withstand on the airplane. The adjusted sound pressure level for 100 hrs life is shown in Table 3-FF with the panel test results. The 100 hr life is the approximate time that any B-2707 structure is exposed to the severest engine sonic environment. This environment occurs at start of take off run and again on landing when the engine thrust is reversed.

The method used for evaluating skin-stringer construction, 100-hr life, is similar to that proposed in Ref. 5 (ASD - TDR - 63-820) and depends upon relating test stress and cycles to the life available at that stress as shown by a conventional S-N curve.

An S-N curve for riveted titanium skins has been developed and is presented in Fig. 3-121. This curve is based on small bending specimen test results and is a fair representation of riveted skin panels although conservative. This curve is used for extrapolation of test data obtained at high-db levels and relatively short test times.

As an example, Fig. 3-116 establishes the relationship between panel geometry and sonic-induced stresses at 160db overall sound pressure. Fig. 3-122 establishes the variation in stress for any other noise level. By combining the data in these two figures with the S-N curve shown in Fig. 3-121, the relationship between panel geometry and 10 hrs, 100 hrs and 1000 hrs life at any noise level has been derived and is presented in Fig. 3-119.

Miner's cumulative damage theory was used to determine the effect of combined test time at several sound pressure levels. The equivalent sound pressure levels for 100-hr life for the panels tested is shown in Table 3-FF. The 100-hr life sound pressure level is the minimum capability of a panel because failure of representative structure usually did not occur. Failures occurred in the supports or cracked at the edge of the panel.

Table 3-EE. Summary of Panels Tested

PANEL NO.	PANEL CONSTRUCTION (TITANIUM ALLOY EXCEPT AS NOTED)				
	PANEL SIZE (in.)	SKIN GAGE	STIFFENER SPACING (in.)	FASTENER TYPE	PANEL WEIGHT LBS. / FT.^{2}
B	24x24	.052	4.33	5/32 Monel CSK Rivet	1.97
C	24x24	.050	4.33	Spotweld	1.93
D	24x24	.052	5.40	Spotweld	1.82
E	24x24	.051	4.33	5/32 Monel CSK Rivet	1.95
F	24x24	.051	5.40	5/32 Monel CSK Rivet	1.79
G	24x24	.045	3.60	1/8 A286 CSK Rivet	1.88
H	24x18	.049	5.40	5/32 Monel CSK Rivet	1.75
J	24x24	.043	5.40	1/8 A286 CSK Rivet	1.55
K	24x24	.076	5.40	5/32 Monel CSK Rivet	2.58
L	34x24	.050	5.40	5/32 Monel CSK Rivet	1.84
1	20x18	Honeycomb	Outer Skin: Polyimide-Glass .030 Gage Core: Polyimide-Glass Honeycomb Inner Skin: Polyimide-Glass .030 Gage		.91
2	20x18	Honeycomb	Outer Skin: Titanium .010 Gage Core: Polyimide-Glass Honeycomb--5# Inner Skin: Polyimide-Glass .030 Gage		1.16
3	20x18	Honeycomb	Outer Skin: Titanium .010 Gage Core: Polyimide-Glass Honeycomb--5# Inner Skin: Polyimide-Glass .030 Gage		1.08
4	20x18	Honeycomb	Outer Skin: Titanium--.060c/mto .010 Gage Core: Polyimide-Glass Honeycomb--5# Inner Skin: Polyimide-Glass .030 Gage		1.32
5	20x18	Honeycomb	Outer Skin: Titanium--.060c/mto. 010 Gage Core: Polyimide-Glass Honeycomb--5# Inner Skin: Polyimide-Glass .030 Gage		1.32
6	20x18	Honeycomb	(Same as 5)		1.32
7	20x18	Honeycomb	(Same as 5)		1.32
8	20x18	Honeycomb	(Same as 5)		1.32

Table 3-FF. Summary of Test Results

PANEL NO.	TEST DATA				ADJUSTED SOUND PRESSURE LEVEL FOR 100 hr LIFE WITH RANDOM NOISE	NOTES
	SOUND PRESSURE LEVEL	FREQ. CPS	TIME MIN	TEMP ° F		
B	162 db 165 db 168 db 168 db	237 237 237 Random	180 180 150 240	R.T.	165.3db	Cracked skin at free edge where stresses were not representative
C						Tested behind J-75 engine.
D						Tested in horn with various configurations for response comparisons
E	165 db 168 db 170 db	Random Random Random	120 120 78	450°	165.8db	Failed in supports No skin failure.
F	165 db 168 db	Random Random	120 120	450°	164.0 db	Failed in supports No skin failure.
G	165 db 168 db 170 db	Random Random Random	120 120 105	R.T.	166.1 db	Failed in supports No skin failure.
H	165 db 168 db	Random Random	120	R.T.	164.2 db	Cracked skin at free edge where stresses were not representative.
J	165 db 168 db	Random Random	120 19	R.T.	161.8 db	Cracked skin at free edge where stresses were not representative.
K						Measured strain gage response.
L						Measured strain gage response with various support methods.

Table 3-FF. (Continued)

PANEL NO.	TEST DATA				ADJUSTED SOUND PRESSURE LEVEL FOR 100 hr LIFE WITH RANDOM NOISE	NOTES
	SOUND PRESSURE LEVEL	FREQ. CPS	TIME MIN	TEMP ° F		
1	160 db 165 db 168 db 170 db	200 200 200 200	60 60 60 37	R.T.	168 db	Cracked inner skin. No bond failure.
2	165 db 168 db 170 db 172 db	280 278 275 270	60 60 60 73	R.T.	171 db	Edge failure. No bond failure.
3	165 db 168 db 170 db 172 db	300 300 300 300	60 60 60 115	R.T.	172 db	Edge failure. No bond failure.
4	160 db 165 db 168 db 170 db 171 db	Random	180 180 90	R.T.	168.3 db	Did not fail.
5	160 db 165 db 168 db 170 db	Random	180 180 180 180	450°	167 db	Did not fail.
6	170 db	Random	360	R.T.	After first 180 minutes of testing, a 2-inch diameter steel ball was dropped four feet onto the .010 gage titanium skin. Panel did not fail and had only minor extension of damage after an additional 180 minutes of testing.	
7	170 db	Random	360	R.T.	Same as 6 except ball was dropped 6 feet. No failure.	
8	170 db	Random	360	R.T.	After the first 120 minutes of testing the panel was damaged by dropping a 2 inch diameter steel ball onto the .010 gage titanium outer skin. The ball was dropped on five separate locations from a six foot height. An additional 180 minutes of testing at 170 db was accomplished without failure. At two locations the damaged area had grown approximately 1-inch.	

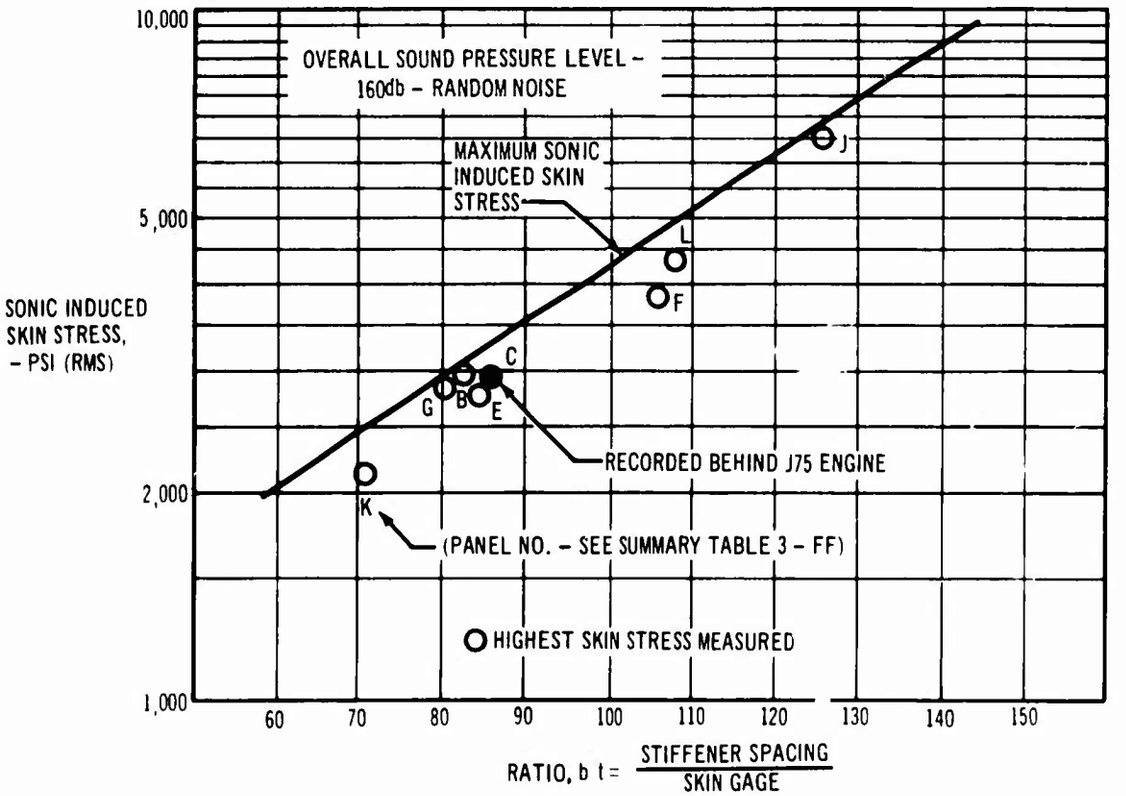


Figure 3-116. Panel Geometry Versus Sonic Induced Stress

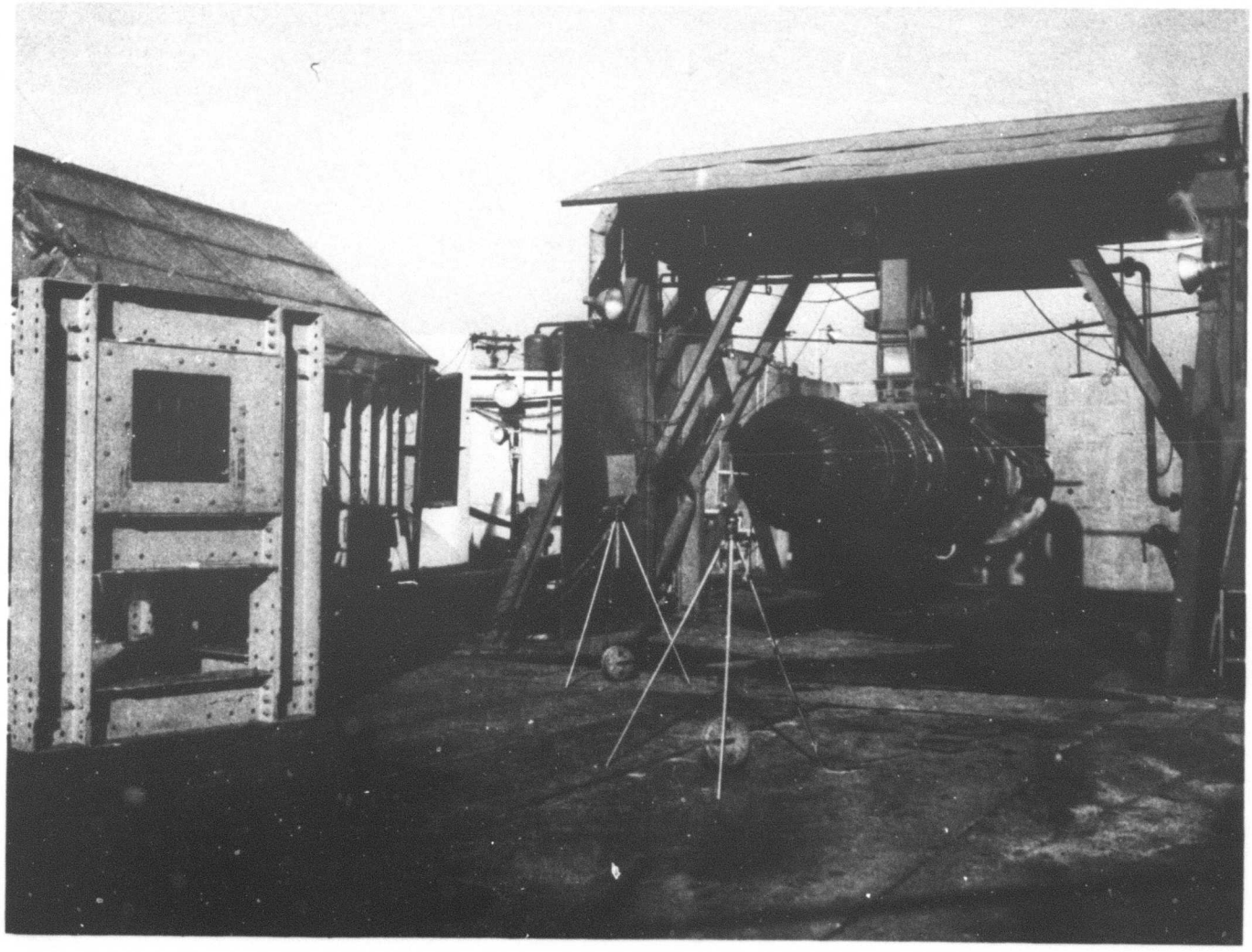


Figure 3-117. Engine Sonic Test

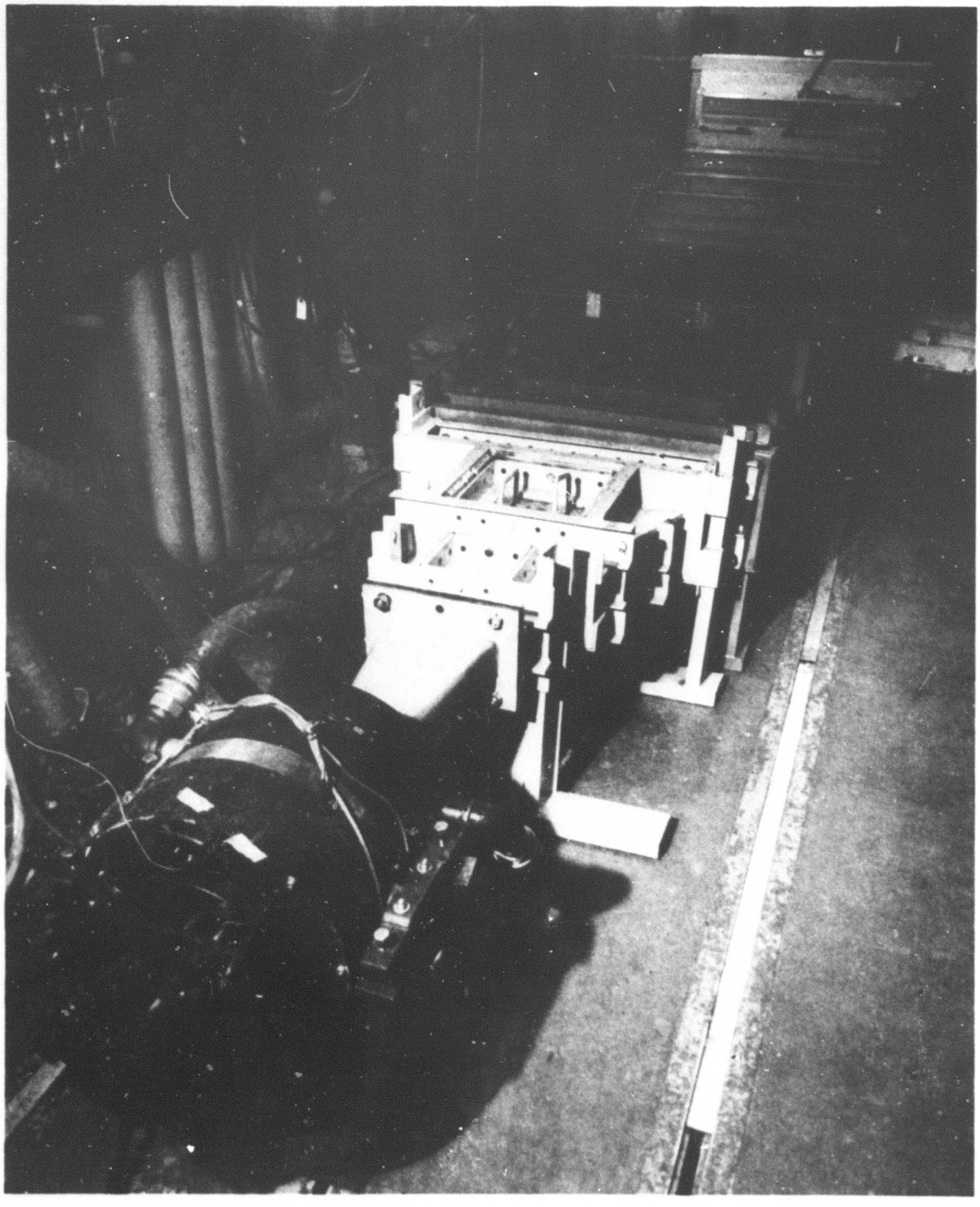


Figure 3-118. Sonic Horn Test Facility

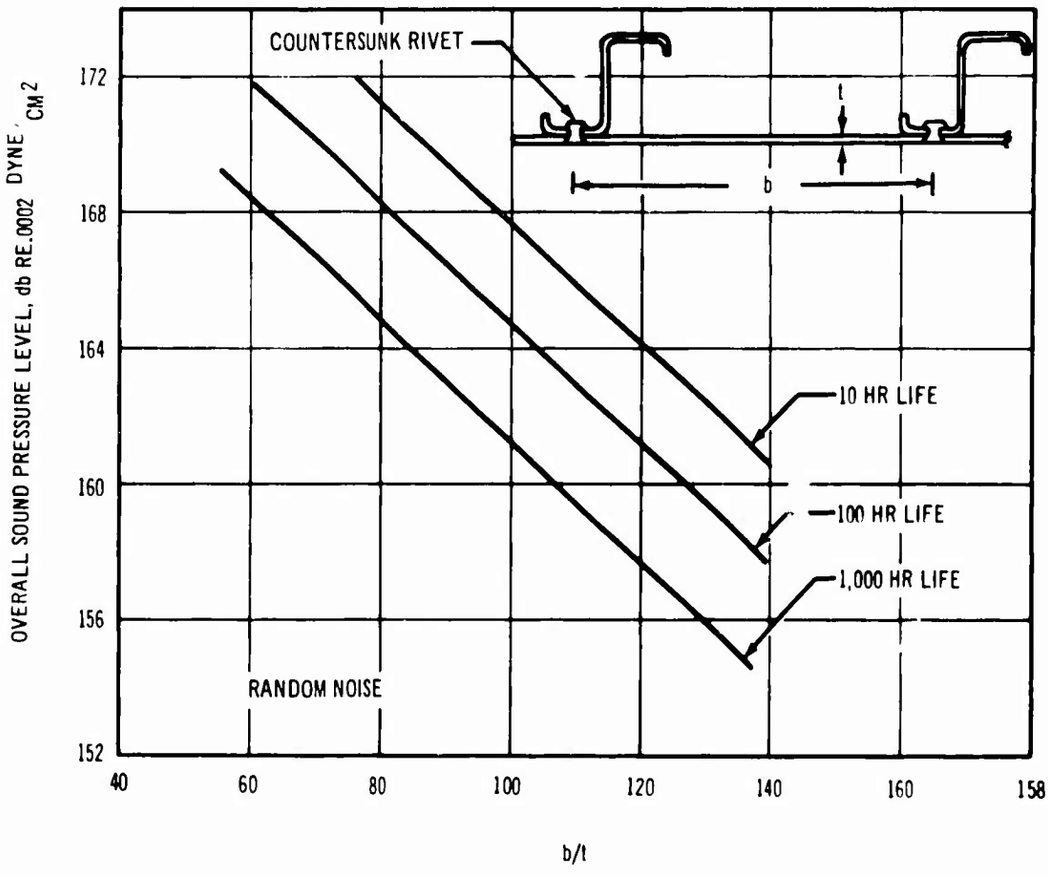


Figure 3-119. Sonic Fatigue Design Parameters

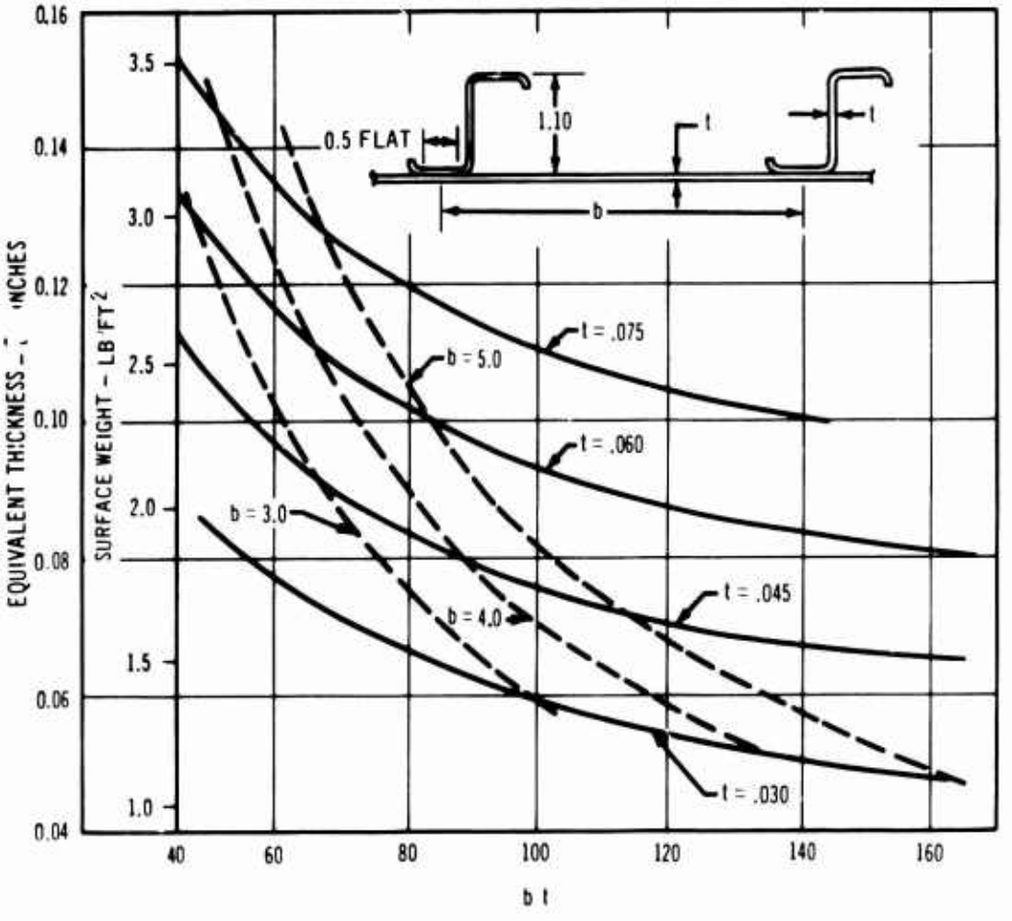


Figure 3-120. Skin Stiffener Panel Geometry

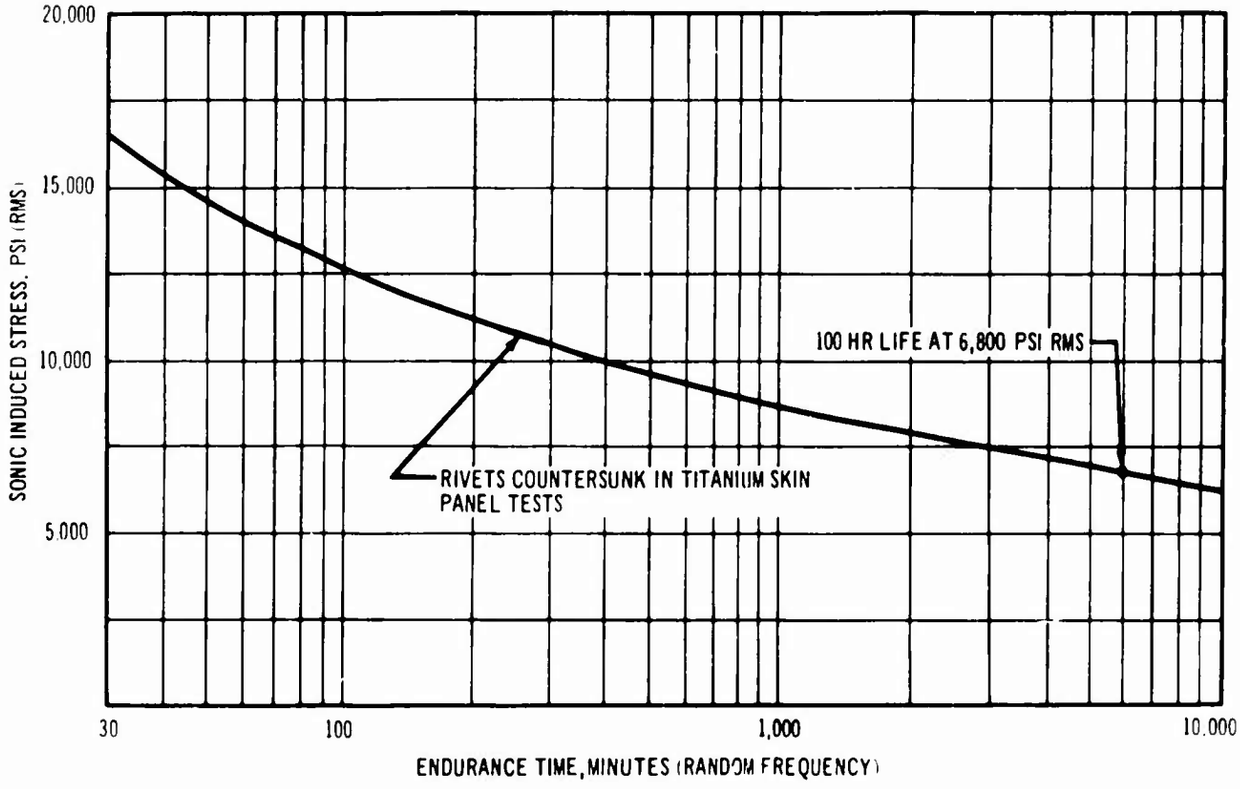


Figure 3-121. Sonic Fatigue S-N Curve

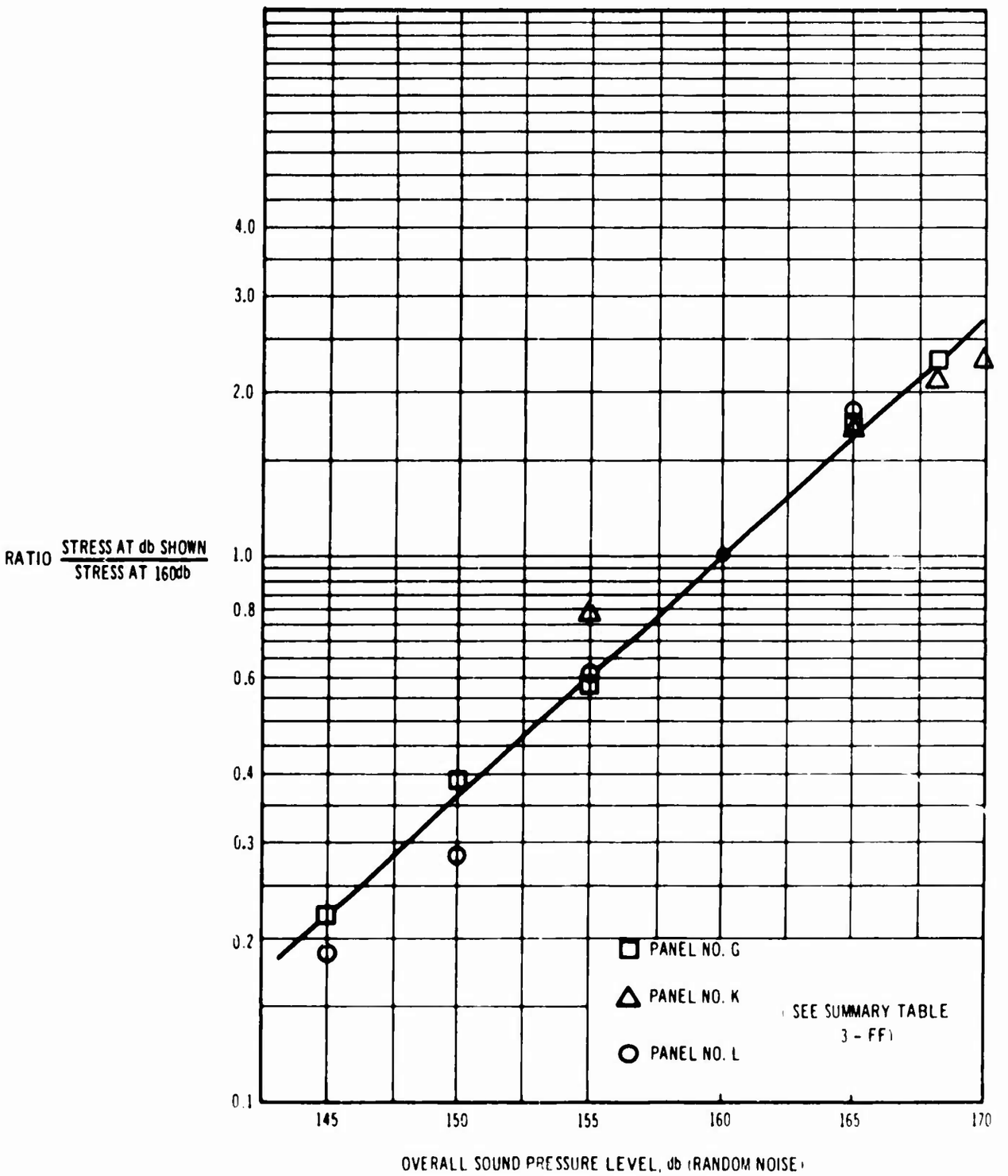


Figure 3-122. Variation of Stress With Sound Level

The riveted titanium panels have demonstrated excellent sonic-fatigue resistance. Where the spot-welded titanium skin stiffener panels were extremely sensitive to the higher db levels and detail design, the riveted panels have been so resistant to skin damage that failures are difficult to achieve. To date, no failures have been obtained for the proposed skin stiffener designs except along the free edges of the test panels where strain gage measurements indicate stress levels 50 to 100 percent greater than stresses in the representative structure.

Excellent sonic resistance has been demonstrated by honeycomb construction. The unique properties which are responsible for the high-sonic efficiency of honeycomb panels are low weight and high stiffness. A typical aircraft honeycomb panel has essentially one significant resonant frequency to which it responds in any sonic environment. The maximum discrete frequency sound level which produces failure is substantially lower (4 to 8db) than the random frequency overall sound level which produces failure. Honeycomb panels tested early in the development program were tested using a discrete frequency where all the noise energy was at the resonant frequency of the panel. The test results of these panels have been conservatively increased 4db to partially account for the severity of this type testing. Recent testing of honeycomb panels used jet engine type random noise at both room and elevated temperatures. Failure did not occur at up to 10 hrs exposure to 170db. The equivalent noise level for 100-hr life for these honeycomb panels was determined from the same S-N curve shape as for riveted panels. The 100-hr life level is conservative because the panels did not fail. Structure that sustains 10 hrs is being tested so near the endurance limit that testing might be continued indefinitely without producing significant additional information. Similar panels are currently being exposed to the SST thermal environment for extended time periods and will be sonic tested upon completion of exposure. A typical honeycomb panel is shown in Fig. 3-123.

The skin-stiffener and sandwich panel sonic test results are shown in Fig. 3-124. They show that the sandwich panels are lighter for a given sonic environment than skin-stiffener panels and that both types of construction have been improved over the proposed sonic-fatigued design criteria for Phase II-C.

Sonic testing has been done on some sandwich honeycomb panels that were deliberately damaged before testing. A 2-in. dia (1.36 lb) steel ball was dropped from heights of 4 and 6 ft on the 0.01 titanium exterior surface. Local core fracture was detected under the dents. Testing at 170db random environment for 3 hrs produced slight or no damage growth away from the point of impact. These tests showed that severe impact damage did not propagate rapidly, but no attempt was made to determine equivalent life on a damaged panel.

3.7.4 Conclusions and Future Work

Horn testing has clearly established the sonic resistance of panels of both riveted titanium skin-stiffener and honeycomb construction. Tests behind the engines have confirmed that horn testing is representative, so long as proper shaping of the horn noise is accomplished. Analytical methods are available to interpret short-term test life in terms of probable airplane life. Panel testing and analysis will continue to improve methods of evaluating strucural life. Outside work being done in Reference 6 "Modeling for Sonic Fatigue," Report AFFDL-TR-65-171 will be studied as soon as it is available. In addition to small panels, a full-scale test section representing the lower portion of the rudder is currently being fabricated and is scheduled for sonic testing in Phase II-C. The test section is 40 by 80 in. and is fabricated from both sheet titanium and typical honeycomb panels. Testing of this full-scale structure will be used to verify the results of panel testing and to evaluate the adequacy of the proposed empennage design including the internal structure and attachments.

3.8 HONEYCOMB SANDWICH STRUCTURE DEVELOPMENT TESTS

The development of stable high-temperature adhesives and resins made it possible to use the advantages of bonded sandwich structure on the B-2707. The structure development program has been marked by rapid improvements in both materials and processing. In many cases these improvements have made test results difficult to compare and sometimes show up as apparent inconsistencies in the data.

Extensive testing was conducted during the development of satisfactory honeycomb structure designs. This testing established the strength properties of the sandwich core and faces, and

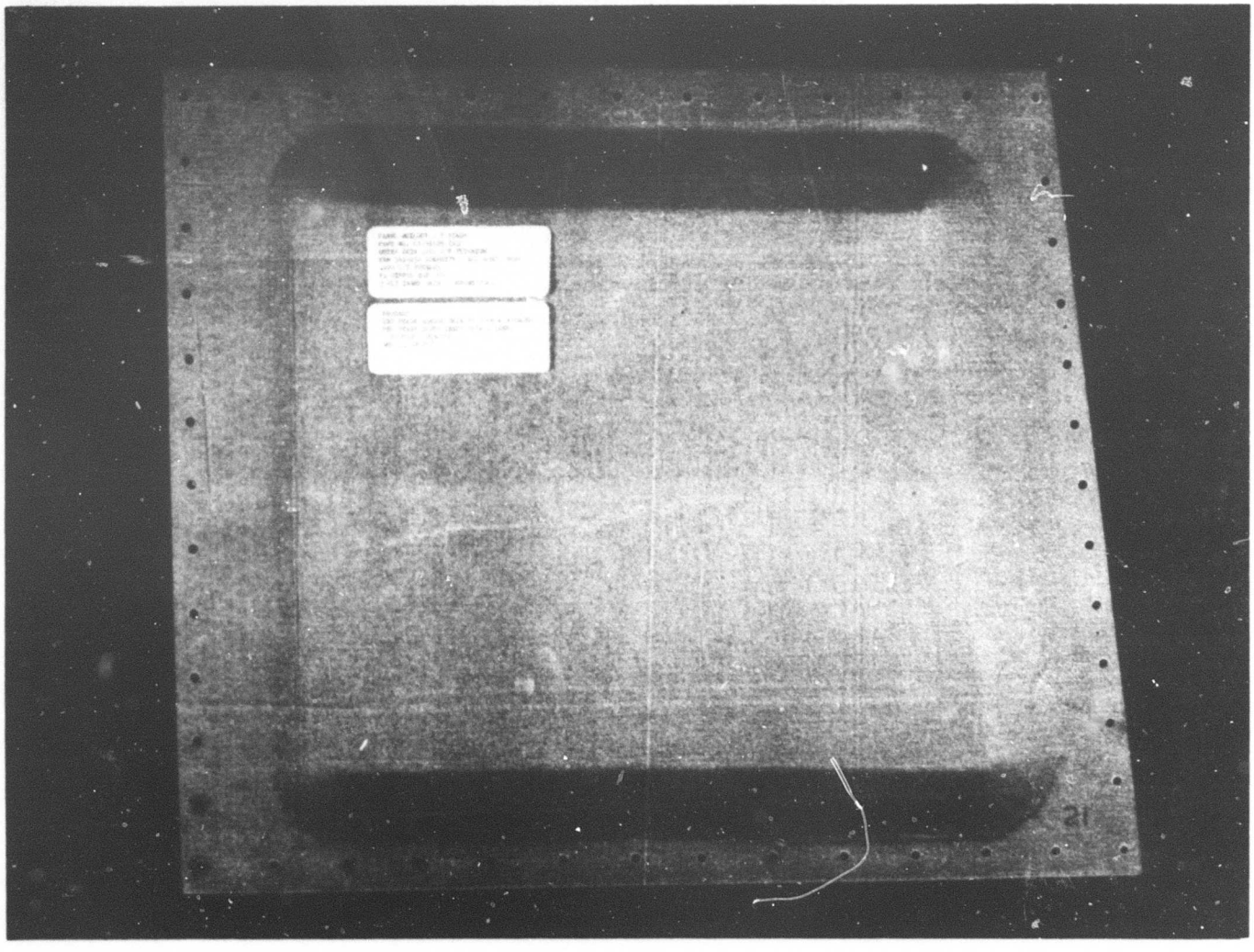


Figure 3-123. Honeycomb Sonic Test Panel

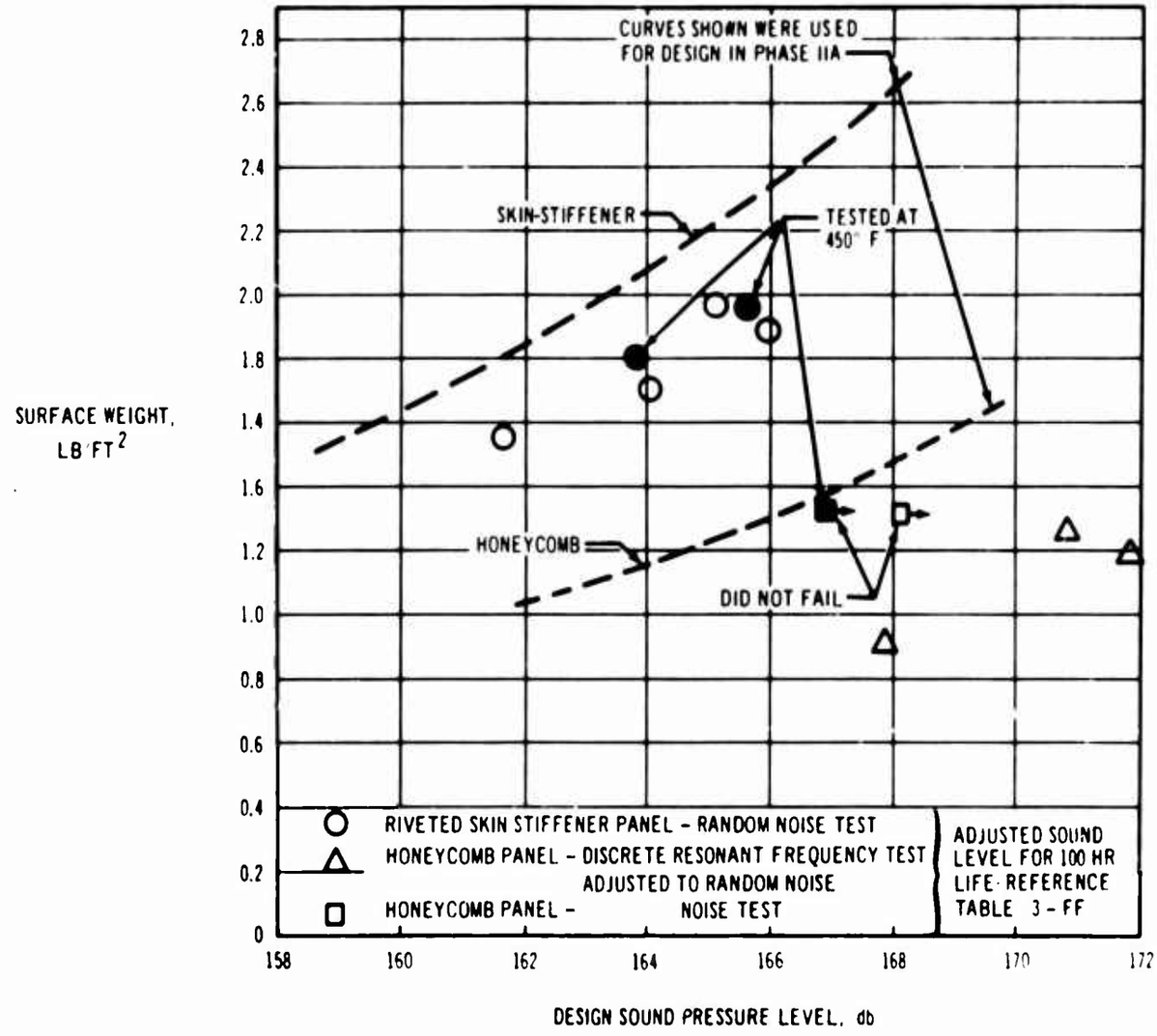


Figure 3-124. Development of Sonic Resistant Structure

the load carrying capability of the complete panel design. Data are presented and testing is continuing.

3.8.1 Basic Sandwich Testing

The bonded honeycomb structure is designed using a polyimide-glass core and titanium skins. Some areas are designed with an inner skin of polyimide-glass for increased formability. A few areas have special electrical properties requirements and are designed with both skins of polyimide-glass.

Each component material of the honeycomb sandwich was tested for strength properties after assembly in a bonded specimen.

Sandwich specimens with faces made from three different titanium alloys were tested for effects of elevated temperature exposure on the edgewise compression strength. This data is presented in Fig. 3-125 and demonstrates only minor strength reductions for all three alloys because of exposure.

Improvements in material and processes have been continuous and rapid. This was especially true of the polyimide-glass honeycomb core. Core of improved strength and quality has been received before testing of earlier lots were complete. Most of the data presented in Figs. 3-126 through 3-132 show core with normal weave glass fabric.

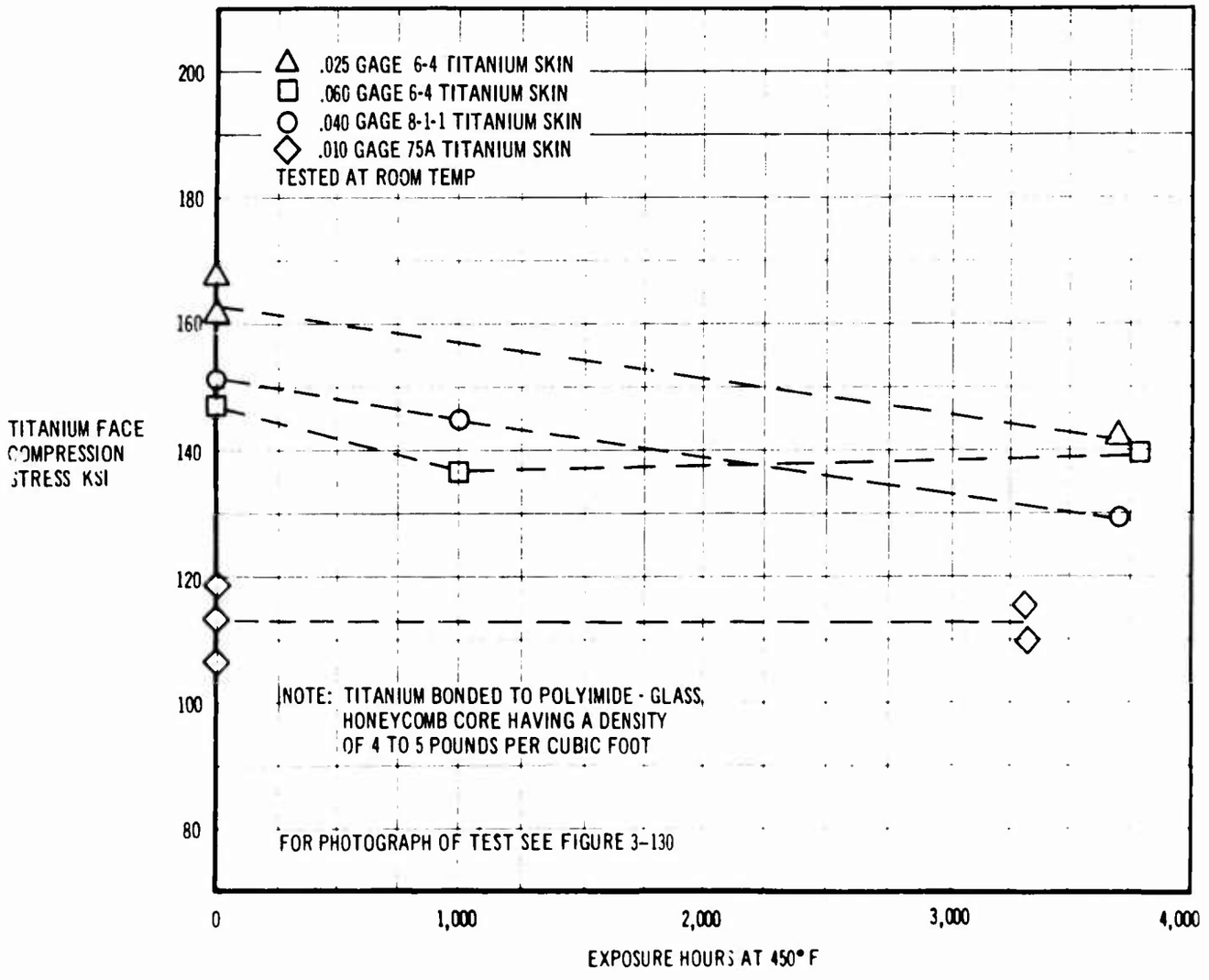


Figure 3-125. Exposure Effects on Titanium Face Compression

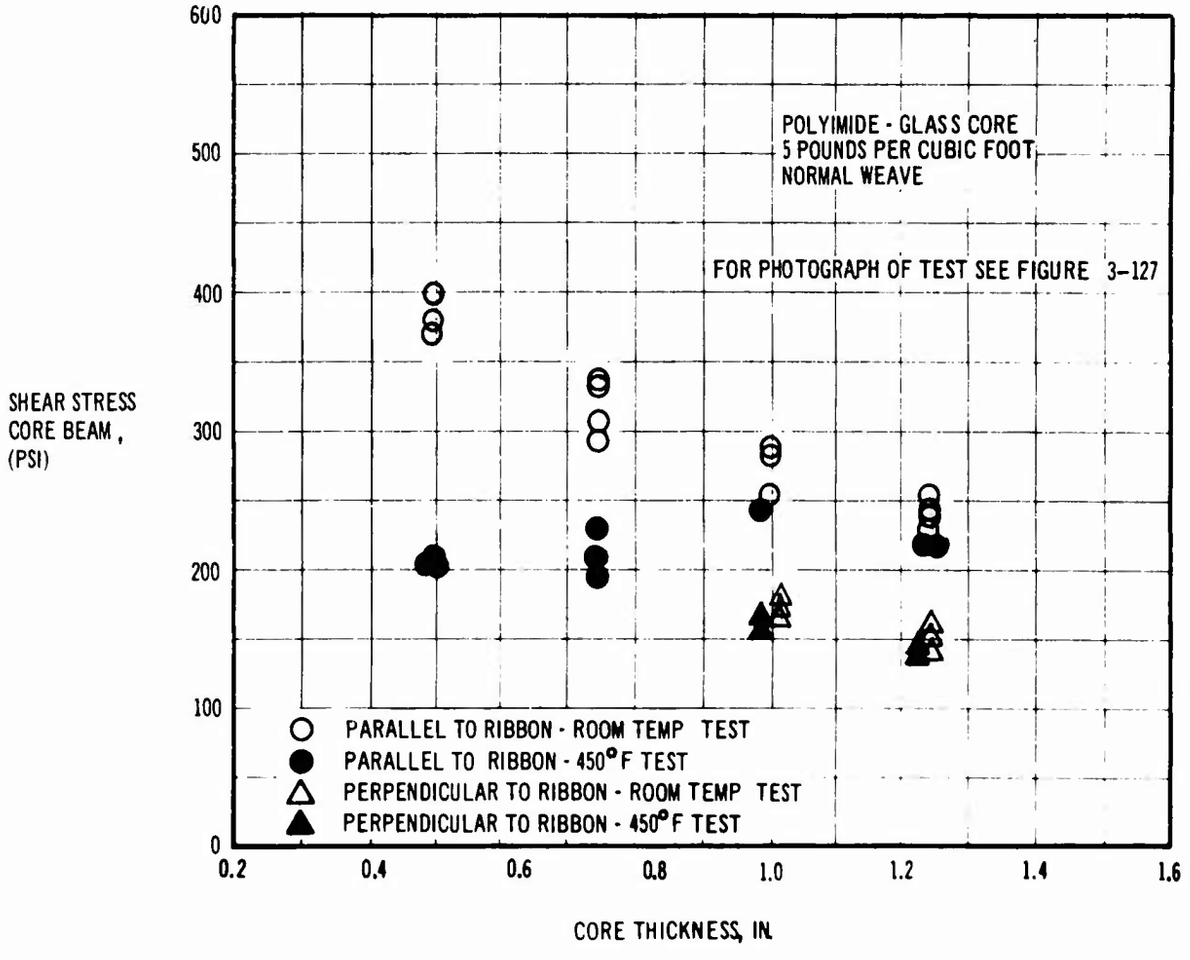


Figure 3-126. Core Shear Test Results

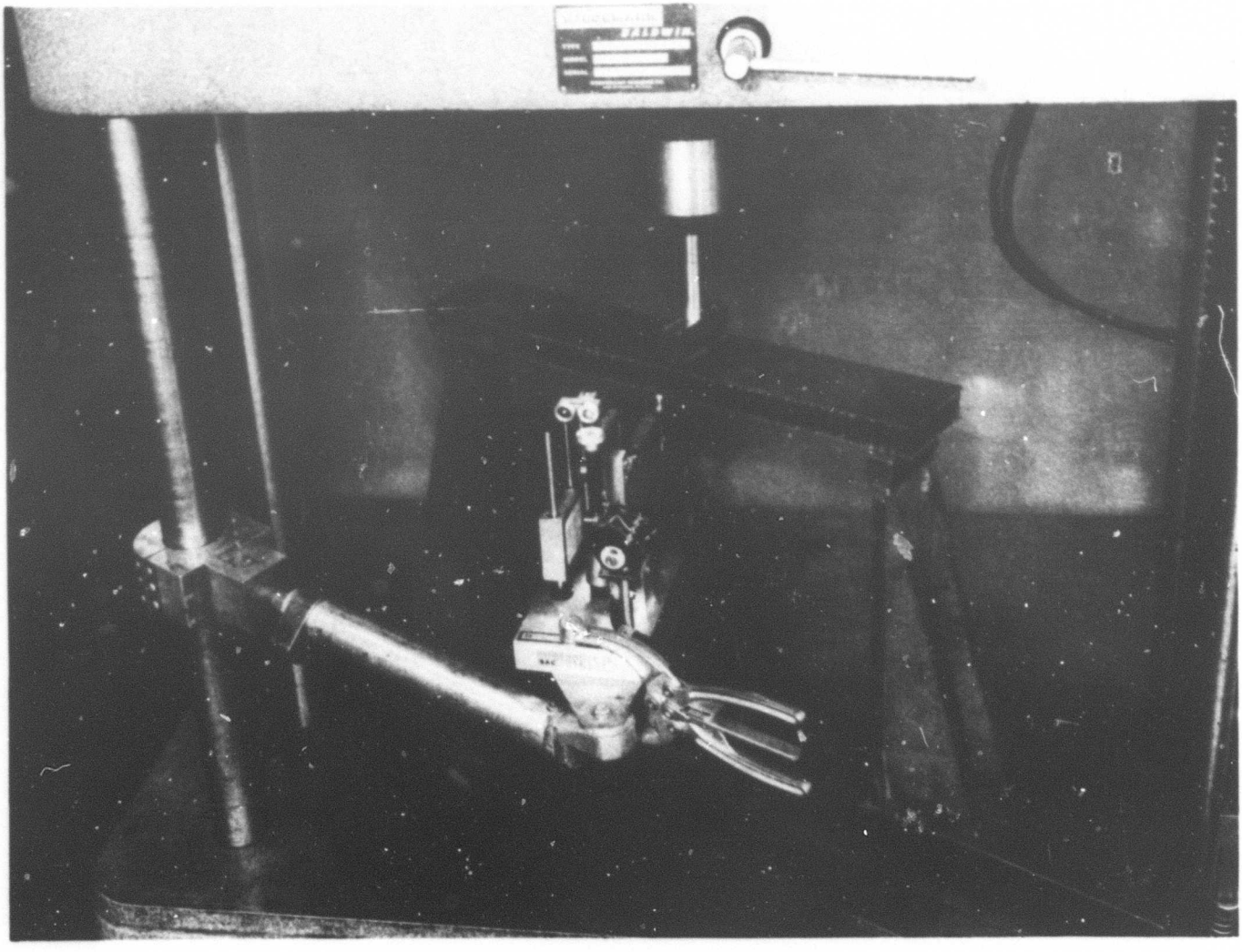


Figure 3-127. Beam Flexure and Core Shear Test Setup

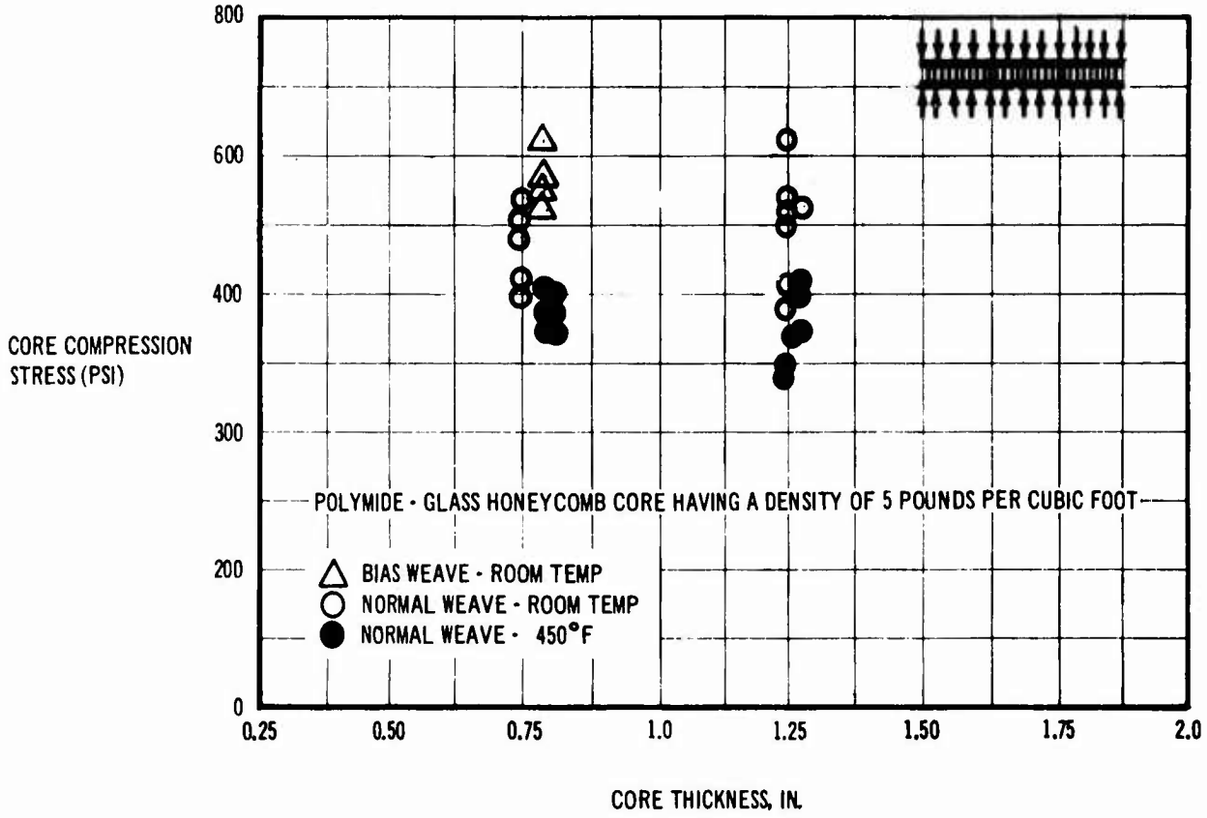


Figure 3-128. Core Compression Test Results

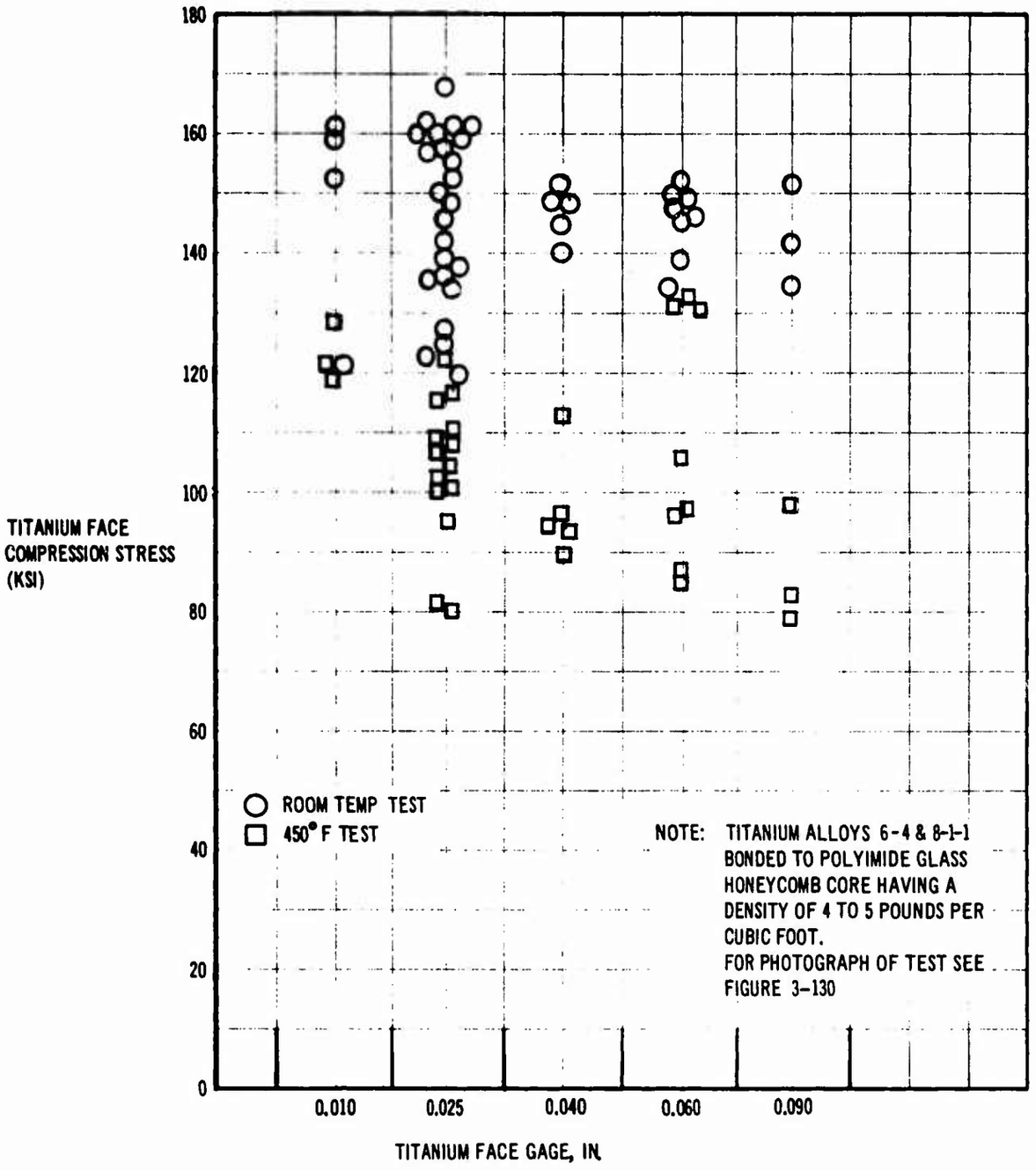


Figure 3-129. Titanium Face Compression Test Results

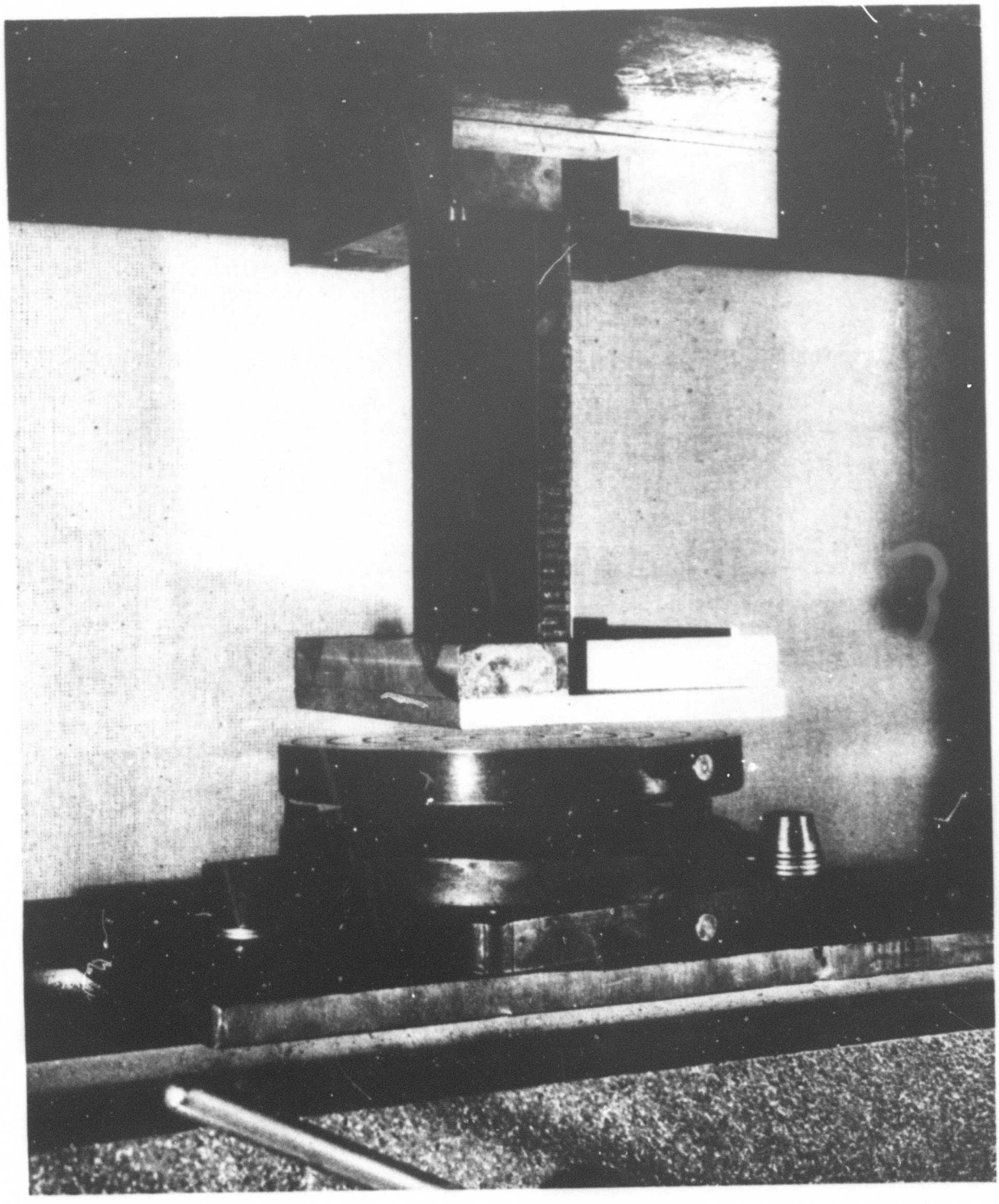


Figure 3-130. Edgewise Compression Test Setup

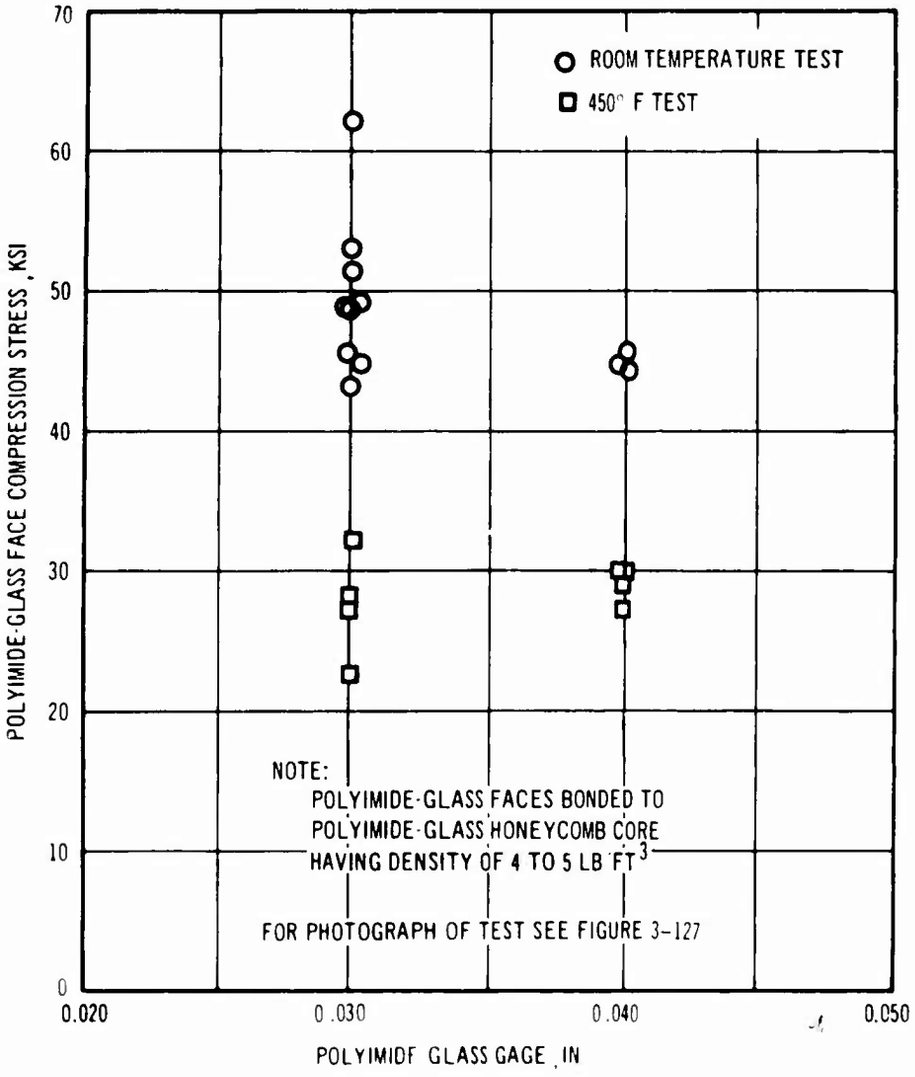


Figure 3-131. Polyimide-Glass Face Compression Test Results

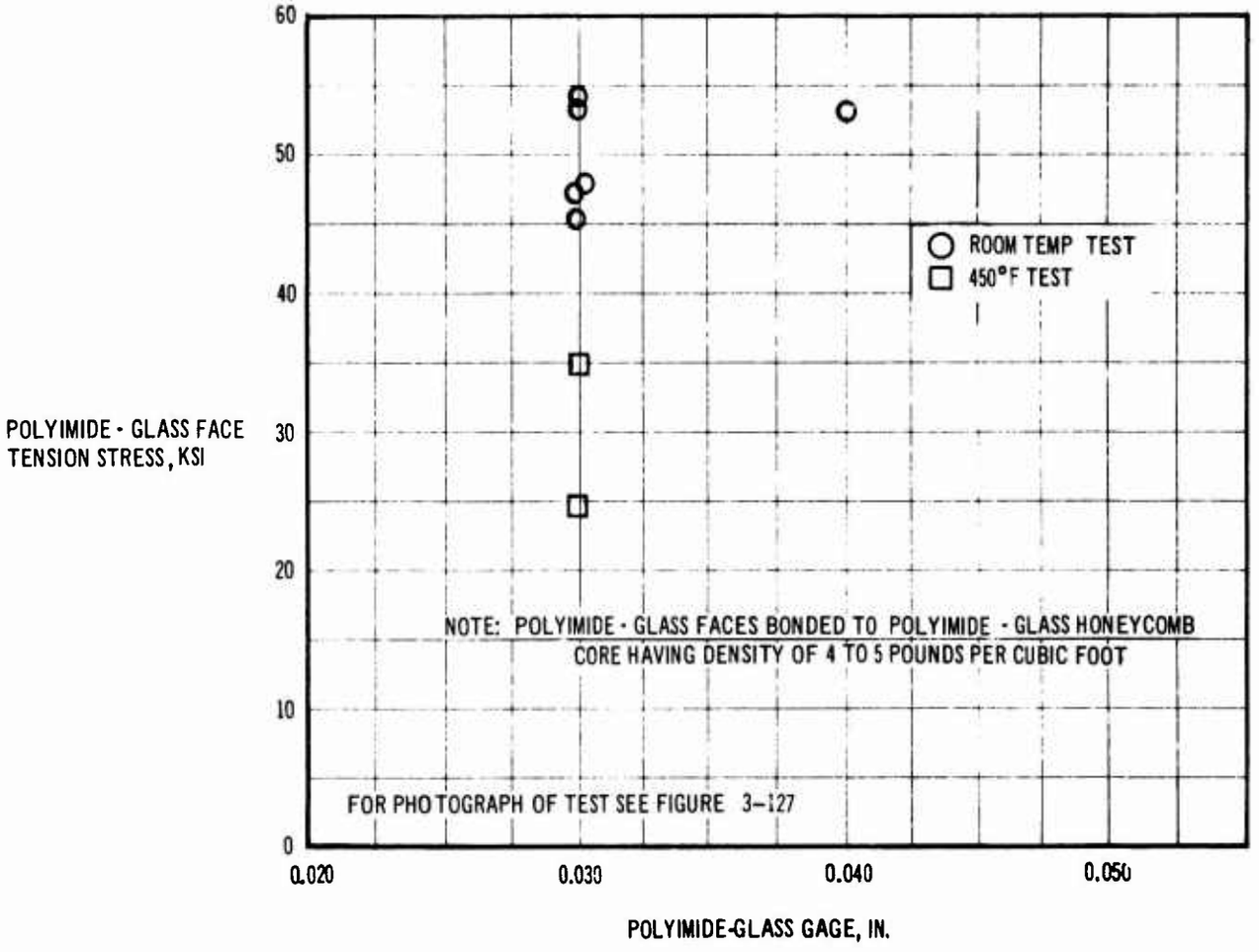


Figure 3-132. Polyimide-Glass Face Tension Test Results

Preliminary data on bias weave fabric indicate 25 percent increase in shear strength, over 200 percent increase in shear modulus and 50 percent decrease in compression modulus. Core material currently being supplied by Hexcell Inc. has satisfactory strength for design. Testing of improved core is continuing.

The effect of elevated temperature exposure on the polyimide-glass core and face strengths is shown in the Material and Processes part D of this Report (V2-B2707-8).

3.8.2 Honeycomb Sandwich Panel Testing Typical honeycomb panels were tested to substantiate their load capability and to develop improved panel designs. Structural panels were tested with compression, shear, and pressure loads.

The design of a panel to carry a compression load requires careful attention to design details in order to achieve a minimum weight structure. Eighteen honeycomb panels have been tested in compression and the results are presented in Fig. 3-133 with a photo of typical test setup shown in Fig. 3-134. Testing of improved designs and new ideas is continuing.

Figure 3-135 shows test results and test setup for a panel tested with internal pressure. The failure pressure of 10.1 psig was as predicted and demonstrates a satisfactory design for pressure loading.

Figure 3-136 shows test results and test setup for a panel tested in shear. The failure stress was 93 percent of basic material ultimate strength and demonstrates the excellent capability of honeycomb panels to carry shear loading.

3.9 LONG TIME EXPOSURE AND CREEP TESTS The purpose of this program is to evaluate the long-time exposure effects on the load carrying ability of titanium material. A further objective is to obtain data on the physical and chemical changes which take place when the material is subjected to environments simulating that of the actual airplane. Analytical efforts to extrapolate short-time testing or testing in which temperature and stress are scaled to give meaningful results for real time temperature exposure effects have been largely unsuccessful. The calendar time required to obtain long-time exposure data necessitated the selection of the then most promising titanium material for the SST. The Ti 8-1-1 duplex annealed alloy was selected for the investigation. Since initiation of this program, the material selected for the B-2707 was changed to the Ti 6-4 alloy. However, comparison of long-term exposure data for the two materials indicates that the general trends in residual material properties are similar.

Material specimens are subjected to either steady-state or cyclic exposure to evaluate effects of temperature only and, temperature in combination with stress. Steady-state exposure tests are being conducted at 500° F and 650° F at stress levels of 0 and 40 ksi. Cyclic exposure tests are being made at 500° and 650° F and to a maximum stress of 40 ksi. Exposures are for various intervals of time up to 30,000 hrs. In order to minimize calendar time required to accumulate 30,000 creep-producing hrs under intermittent exposure, a cycle, defined in Fig. 3-137, was selected in which the time spent at other than creep-producing conditions was minimized.

The several different exposure test specimens used in this investigation are shown in Figs. 3-138 and 3-139. The long-strip type specimens were designed to obtain several creep measurement gage lengths within the exposed region of each specimen and to provide for post-exposure sectioning into standard tensile and fatigue specimens. Basic material, spotwelded joints, and fusion welded specimens are included in the test program. The basic material and spotwelded joint specimens for steady-state cyclic and post-exposure testing are shown in Fig. 3-138.

The longitudinal and transverse weld specimens for both steady-state and cyclic exposure are shown in Fig. 3-139. The specimens were exposure tested in the company-designed creep testing facility shown in Fig. 3-140.

After various periods of exposure, residual creep strain, mechanical strength properties and metallurgical characteristics were determined and compared with that of unexposed baseline material. Creep measurements were obtained for all specimens before and after exposure. All measurements are made with fixed-gage length microscopes at room temperature in a controlled atmosphere so that conditions could be duplicated at each measurement.

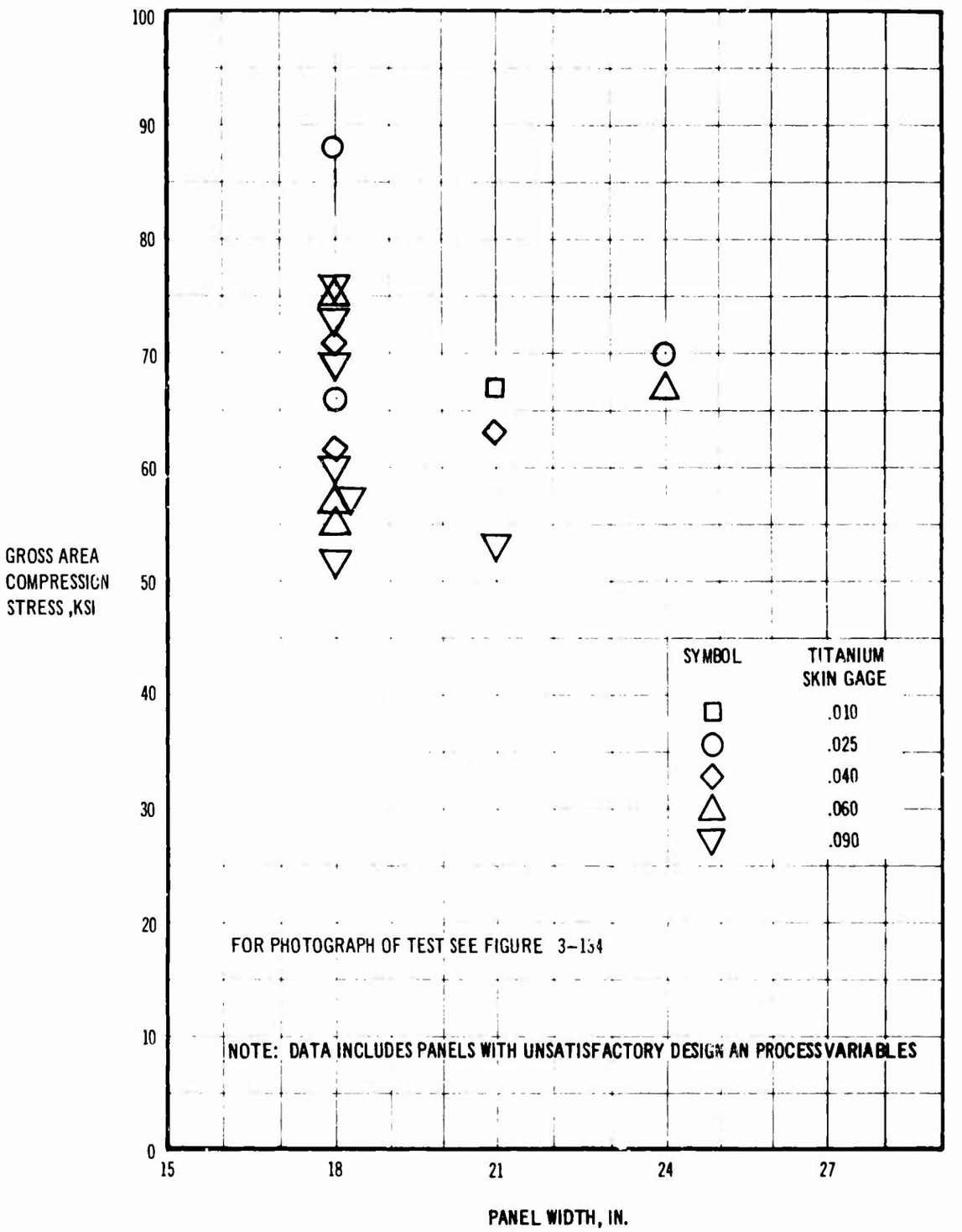


Figure 3-133. Compression Panel Test Results

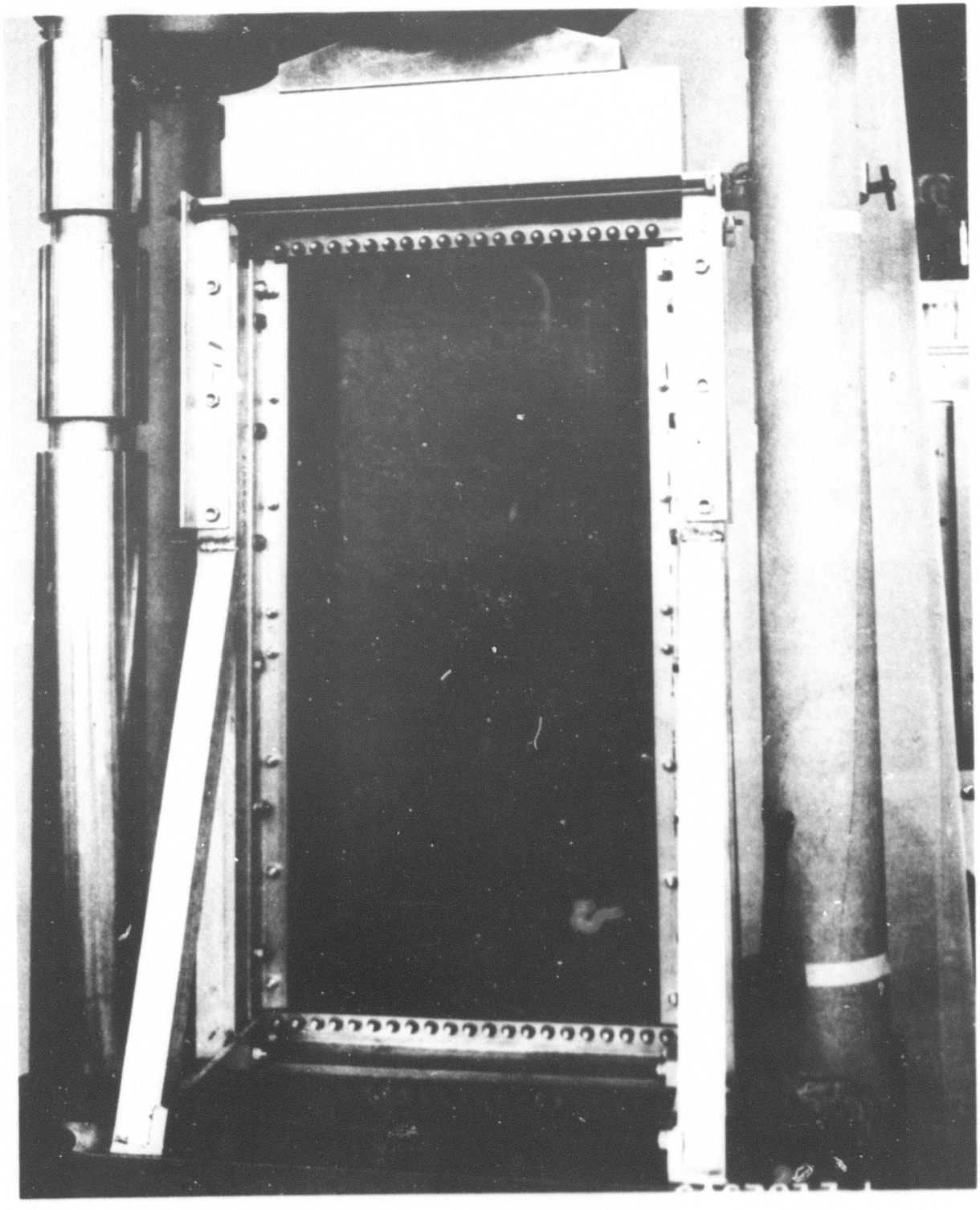
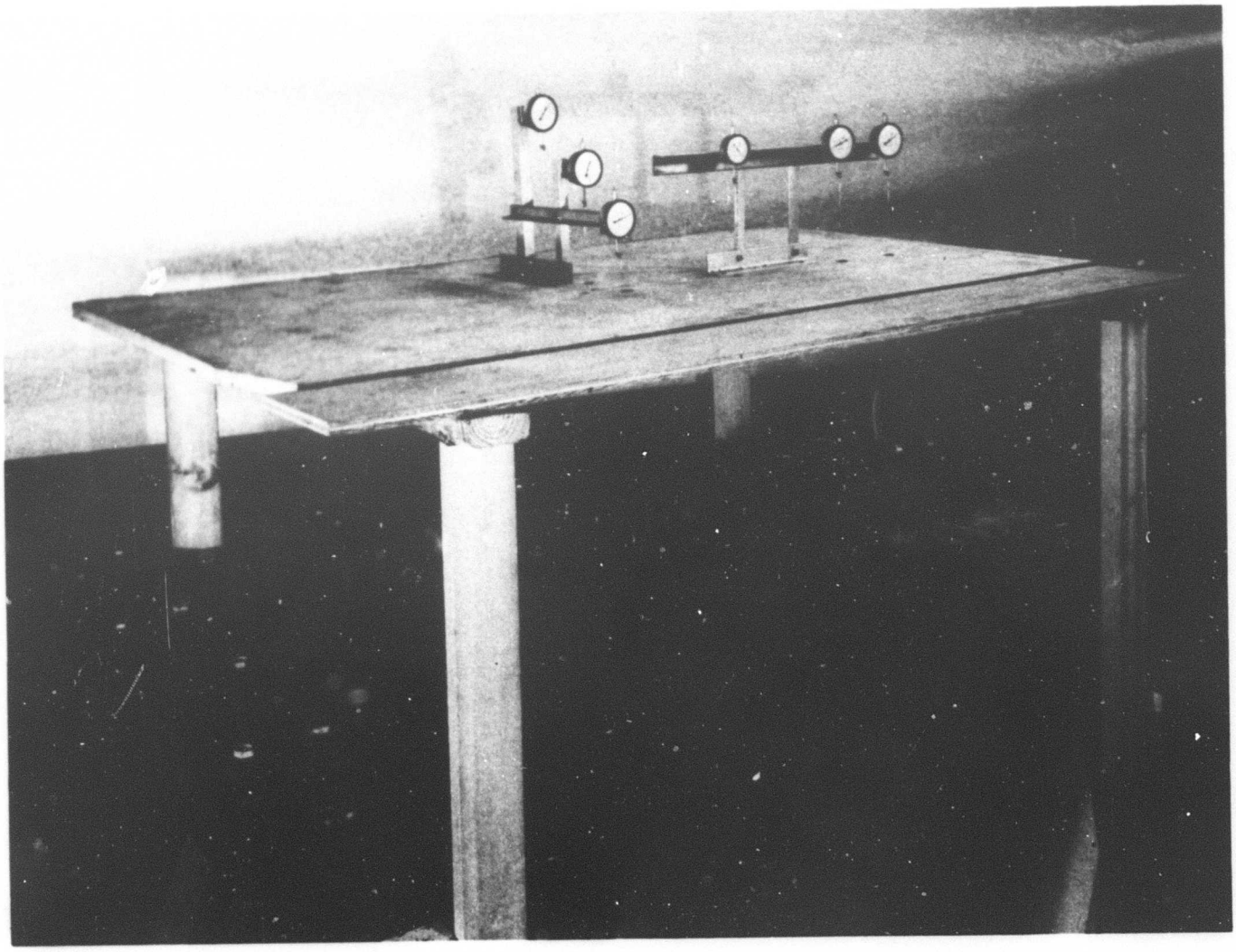
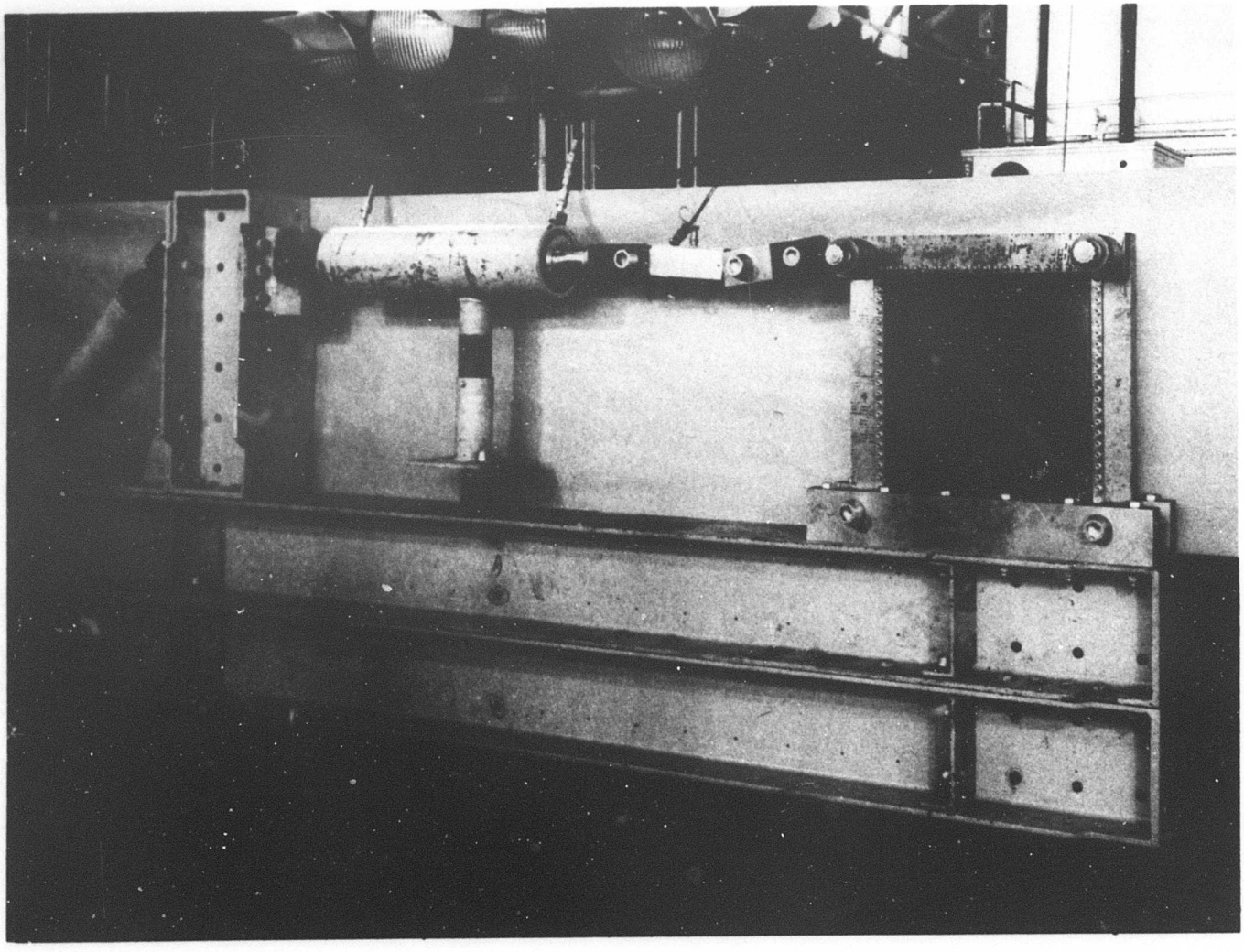


Figure 3-134. Compression Panel Test Setup



THIS 30 INCH X 60 INCH PANEL WAS CONSTRUCTED USING A .008 TITANIUM OUTER SKIN, POLYIMIDE-GLASS HONEYCOMB CORE 1½ INCHES DEEP, AND A .040 GAGE POLYIMIDE-GLASS INNER SKIN. FAILURE WAS OBTAINED AT 10.1 PSIG INTERNAL PRESSURE.

Figure 3-135. Pressure Panel Test Setup



THIS 23 INCH X 23 INCH PANEL WAS CONSTRUCTED USING A .040 GAGE TITANIUM OUTER SKIN, POLYIMIDE-GLASS HONEYCOMB CORE ONE-HALF INCH DEEP, AND A .030 GAGE POLYIMIDE-GLASS INNER SKIN. THE GROSS AREA FAILURE STRESS WAS 73 KSI AND REPRESENTS 93% OF THE ULTIMATE TITANIUM ALLOWABLE.

Figure 3-136. Shear Panel Test Setup

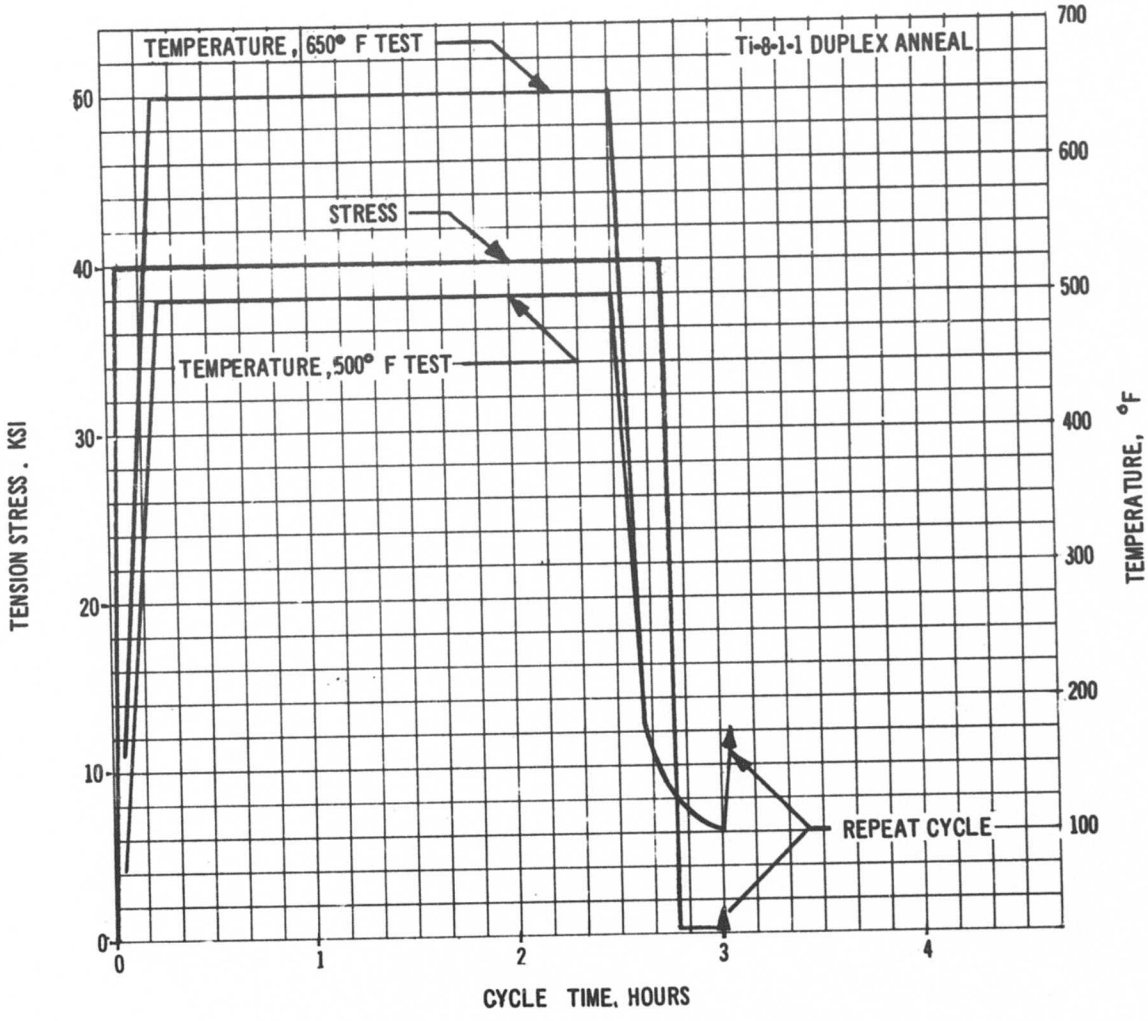


Figure 3-137. Temperature-Load Spectrum

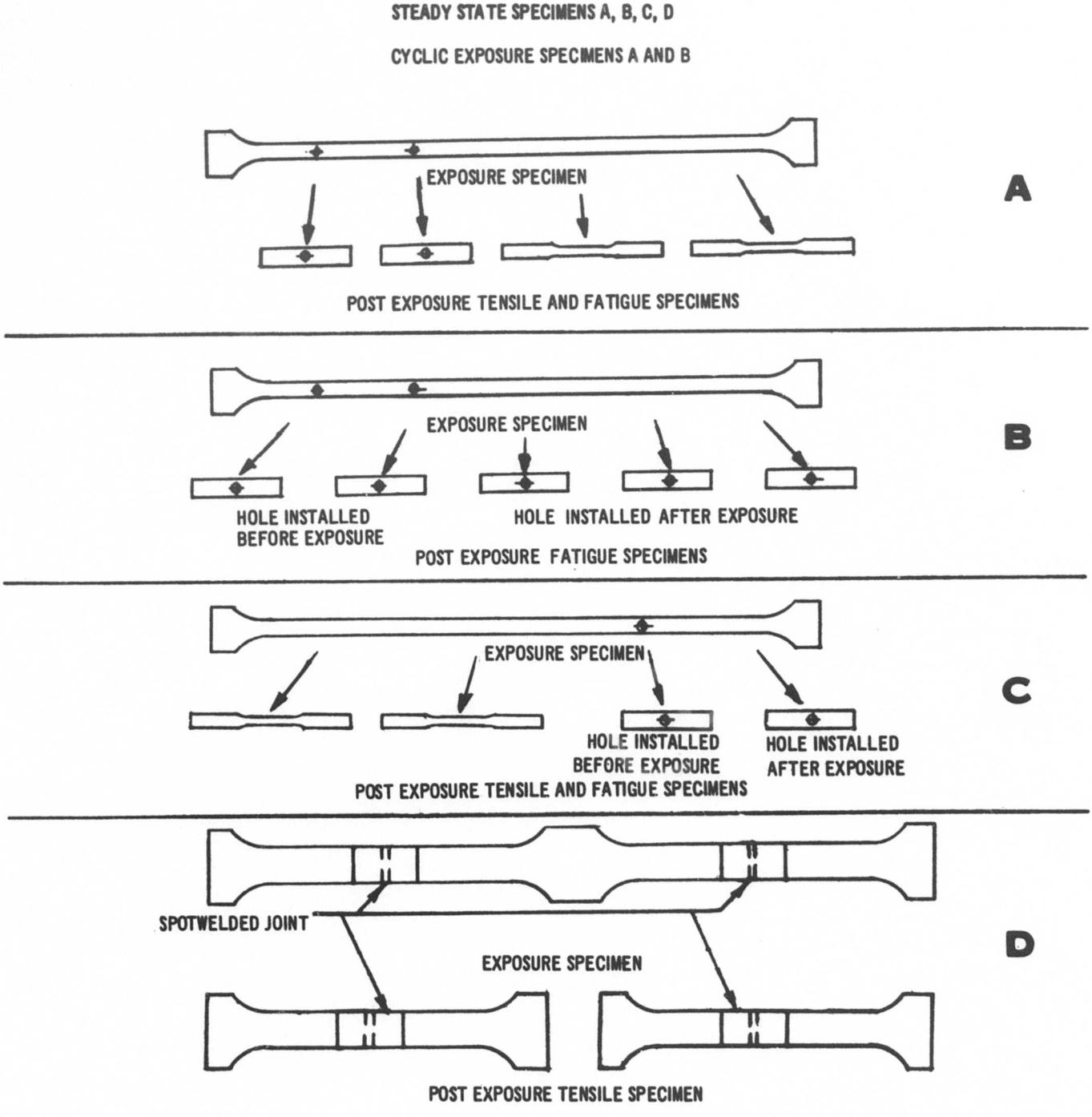
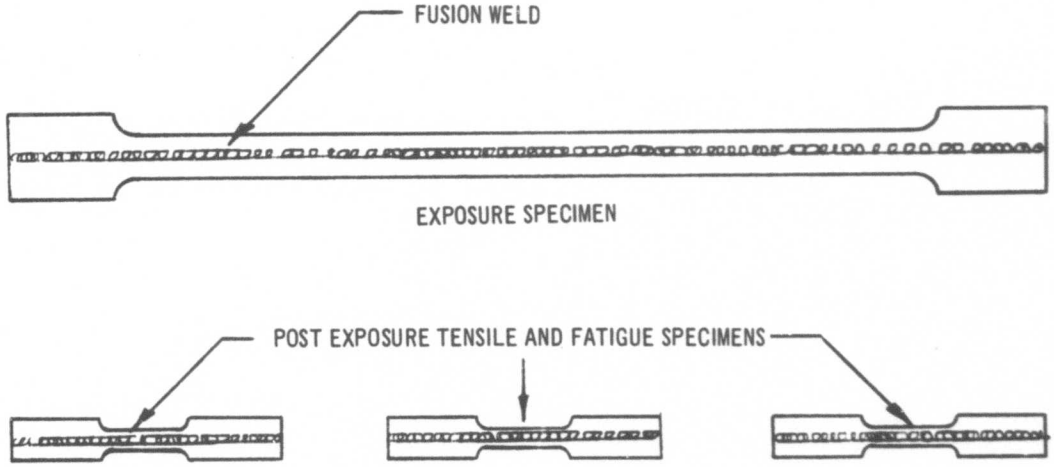


Figure 3-138. Basic Material Specimens



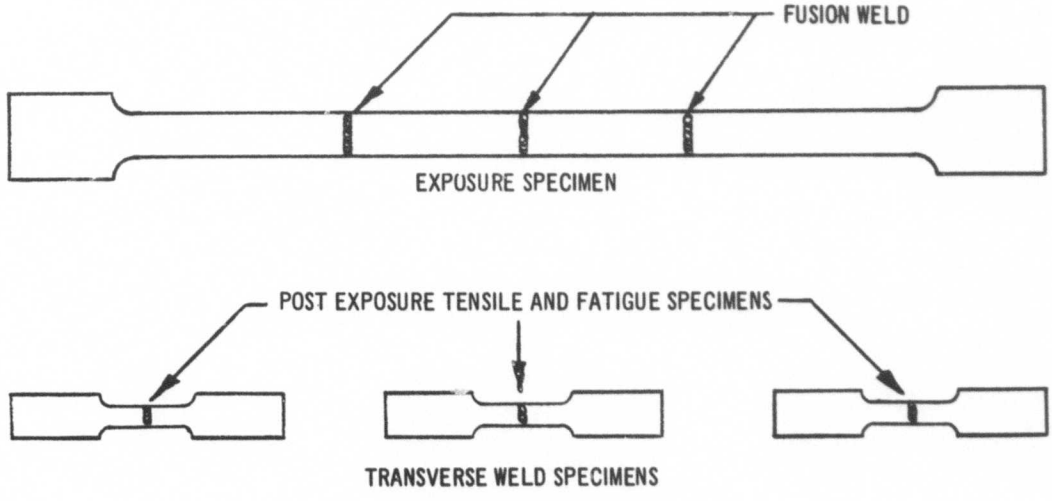


Figure 3-139. Fusion Welded Specimens

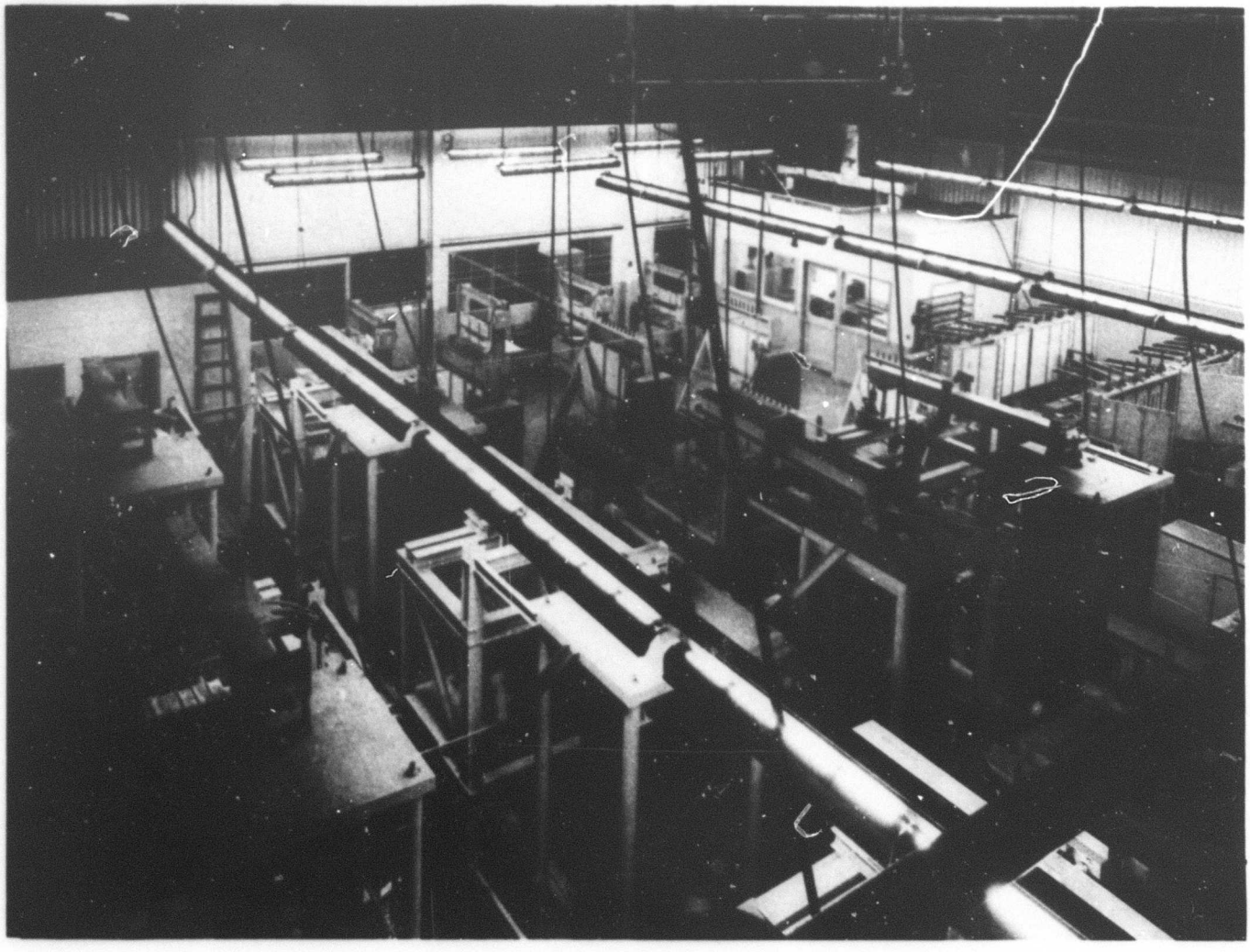


Figure 3-140. Creep Laboratory

Unexposed baseline material properties were obtained from specimens taken from the same sheets of material used to fabricate the exposure specimens.

Residual creep strains (unrecoverable creep) for steady-state and cyclic exposure specimens are shown in Fig. 3-141. The values shown are averages of 2 to 16 gage lengths for each condition. Data indicate that cyclic exposure conditions are more severe than those of steady-state; however, creep deformations will not be significant for temperature up to 650° F. Figure 3-142 compares creep data from this program with that of two other investigations. The Ti 8-1-1 mill-annealed data is from test conducted by Joliet Metallurgical Laboratories, Inc., Ref 6 and that for Ti-8-1-1 duplex annealed and Ti 6-4 mill annealed are data from General Dynamics Corp., Ref 7. The original test program of General Dynamics Corp. showed creep strains considerably larger than that obtained by other investigators. Revisions were made to their testing and measurement techniques and the data presented in Fig. 3-142 was obtained. A comparison of Ti-8-1-1 and Ti 6-4 creep data indicates that both materials have nearly identical residual creep strains. The steady-state exposure data of Ref. 6 are for a 67 ksi stress level and are considerably higher than the 40 ksi used in the program.

Following exposure, fatigue, and tensile tests were conducted on specimens obtained from the exposure specimens as shown in Figs. 3-138 and 3-139. Tensile test results of base material are shown in Fig. 3-143. The baseline material properties of the unexposed specimens are shown in Table 3-GG. Exposure results in an increase in F_{tu}, F_{ty} and modulus of elasticity and in decreased elongation. The effect of exposure is small and is evident in comparison to the scatter of unexposed data in Table 3-HH. These results are in agreement with the data trend as found by Joliet Metallurgical Laboratories, Inc., and General Dynamics Corp. The tensile tests of the exposed spotwelded joints and fusion-welded specimens indicated the same typical results as found for the base material specimens. The results of temperature exposure on spot-welded joints is given in Fig. 3-144 and for the fusion welded specimens in Figs. 3-145 and 3-146.

The fatigue life of center hole, spotwelded joints and fusion-welded specimens for exposed are unexposed conditions are given in Par. 3.6.1. To investigate the effect of creep exposure on fatigue life, a number of specimens were exposed with a centrally located hole (Fig. 3-151) to represent a moderate stress concentration on the airplane. In other specimens, the hole was installed after exposure.

Metallurgical examinations of exposed specimens have indicated no detectible material changes.

Testing has been completed on the fusion-welded specimens. The base material specimens have completed 10,000 hrs of steady-state and cyclic exposure and testing is continuing to 30,000 hrs. Post exposure testing results have been included for all except the 10,000 hrs base material cyclic exposure specimens. Post exposure testing of these specimens is presently being conducted. The 30,000 hrs steady-state specimens have accumulated 19,000 hrs and will require 1.25 yrs of additional exposure.

Comparison of exposure test results obtained from this program and from other investigators indicate that residual exposure effects will not impose limitations on the design of the B-2707.

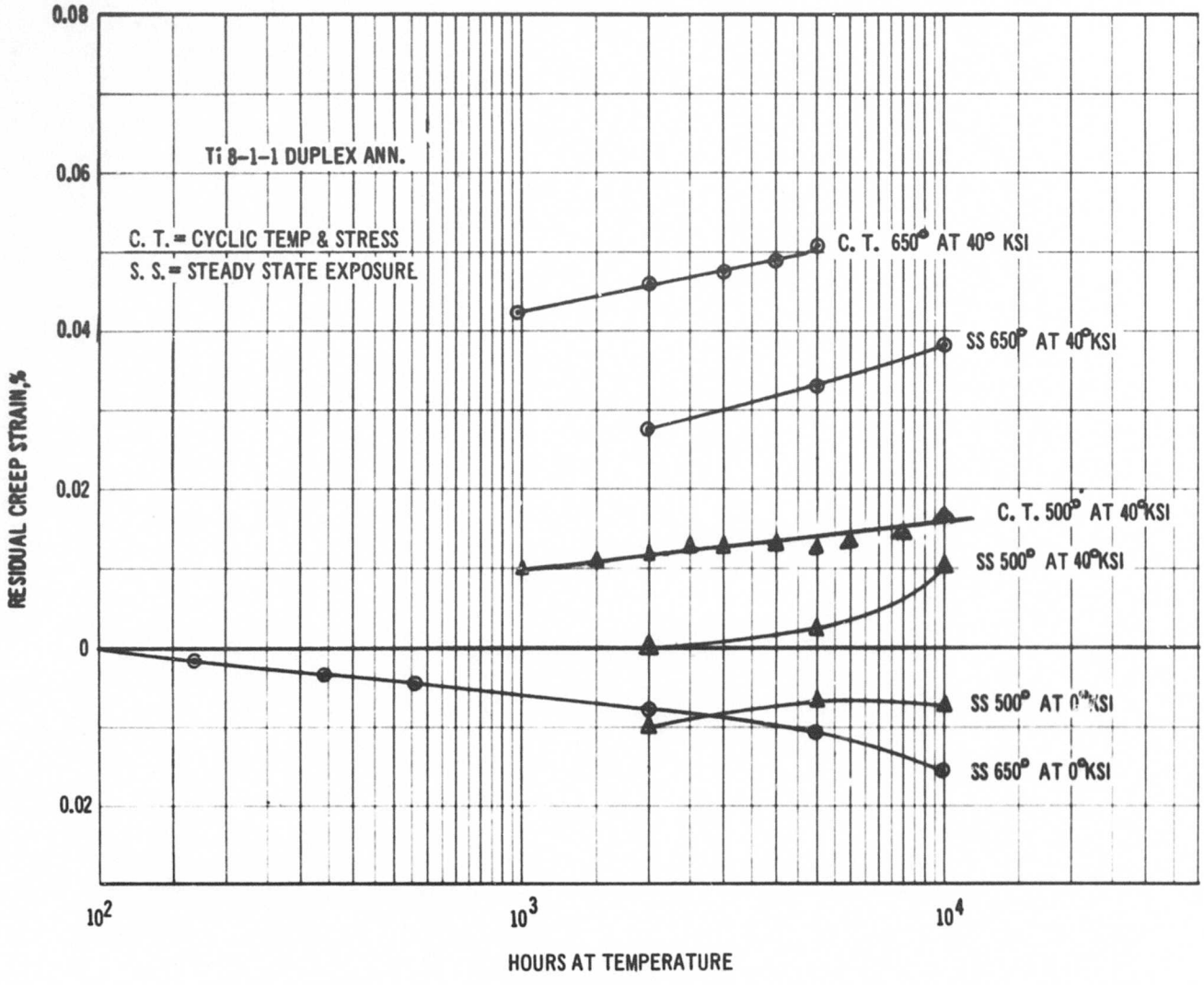


Figure 3-141. Residual Creep Strains

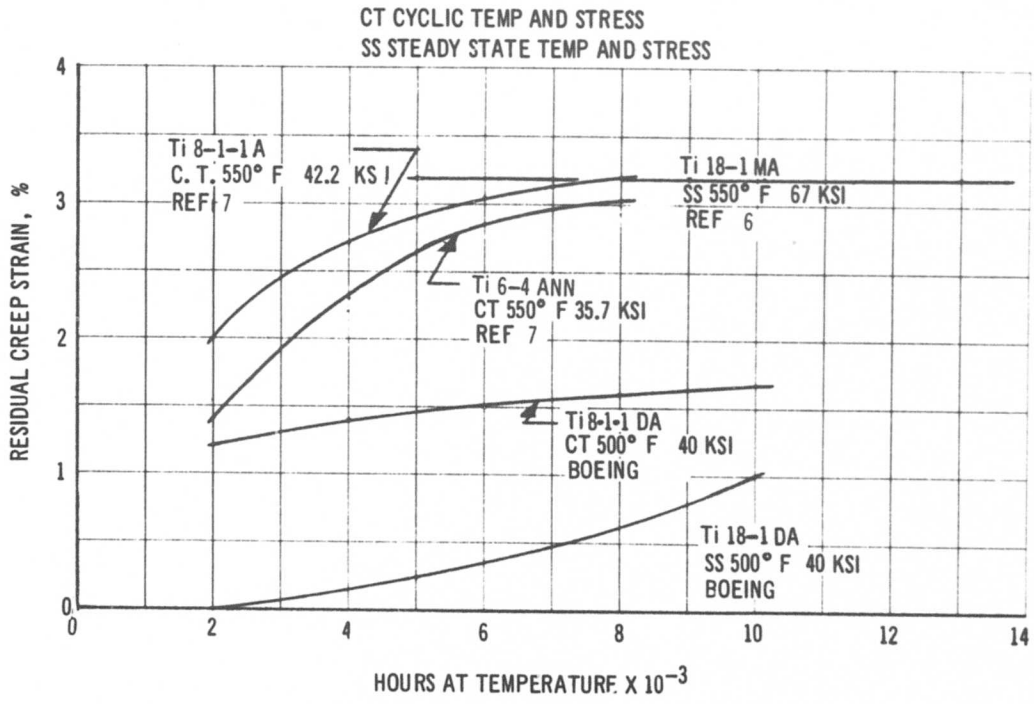


Figure 3-142. Residual Creep Strain Comparison

Table 3-GG. Baseline Material Properties

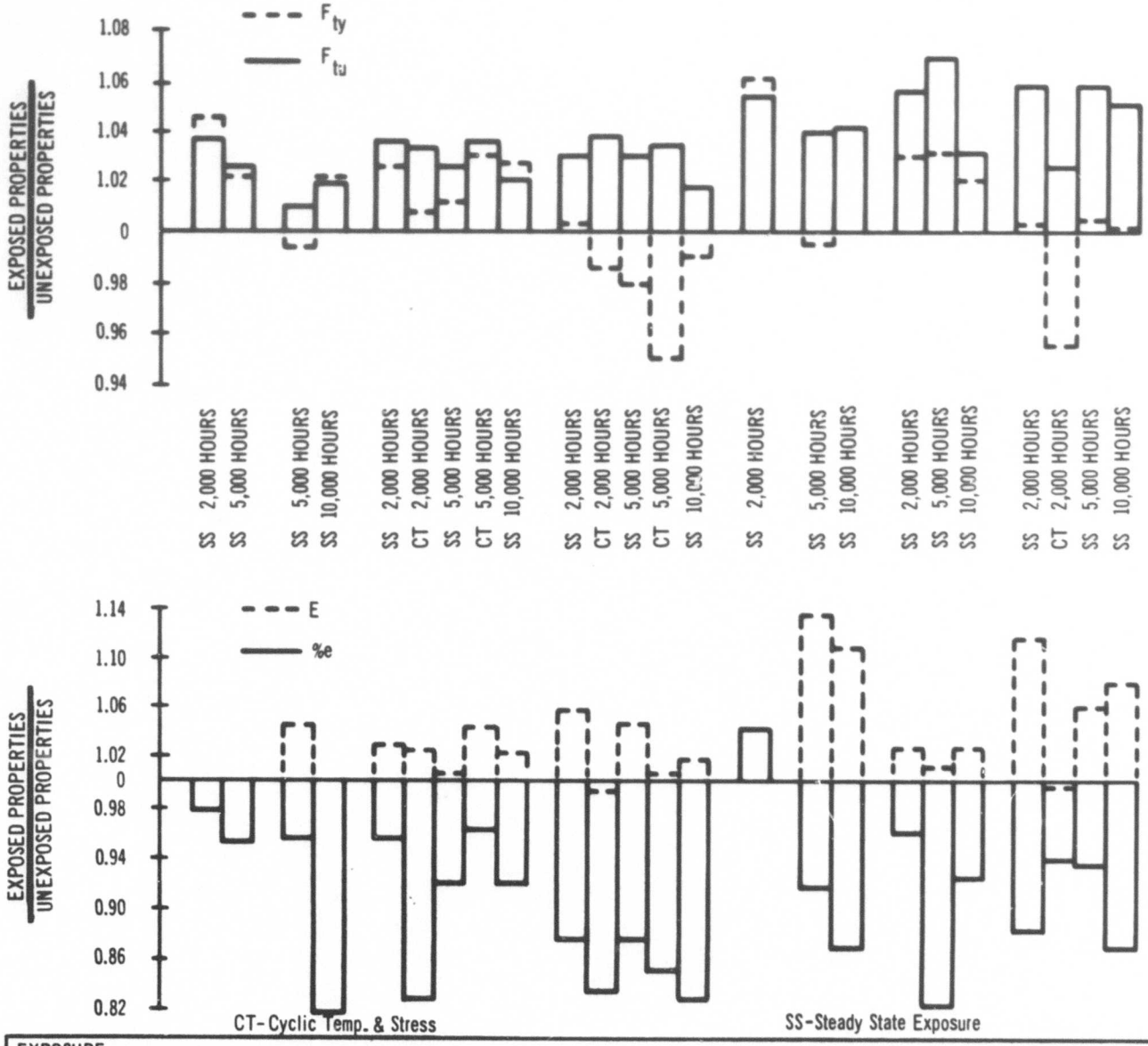
PROPERTIES OF UNEXPOSED Ti 8-1-1 MATERIAL USED IN CREEP TESTS

Prop. / Cond.	F_{tu} ksi	F_{ty} ksi	% Elong.	$X10^{-6}E$ psi
R.T.	140.0	127.7	16.3	17.0
500°F	110.7	88.9	15.2	15.6
650°F	105.6	82.0	15.0	14.3

Table 3-HH. Baseline Material Properties Scatter

SPREAD OF MAXIMUM AND MINIMUM TEST VALUES USED TO DETERMINE UNEXPOSED MATERIAL PROPERTIES

Prop. / Cond.	F_{tu} ksi	F_{ty} ksi	% Elong.	$X10^{-6}E$ psi
R.T.	±0.1%	±0.02%	$^{+1}_{-2}$ %	±1%
500°F	±0.9%	±0.3%	$^{+5}_{-8}$ %	±2%
650°F	±0.2%	±0.4%	$^{+4}_{-6}$ %	$^{+7}_{-6}$ %



EXPOSURE TEMP. °F	500	500	500	500	650	650	650	650
EXPOSURE STRESS ksi	0	0	40	40	0	0	40	40
SPECIMEN TEST TEMP. °F	70	500	70	500	70	650	70	650

Figure 3-143. Basic Material Properties

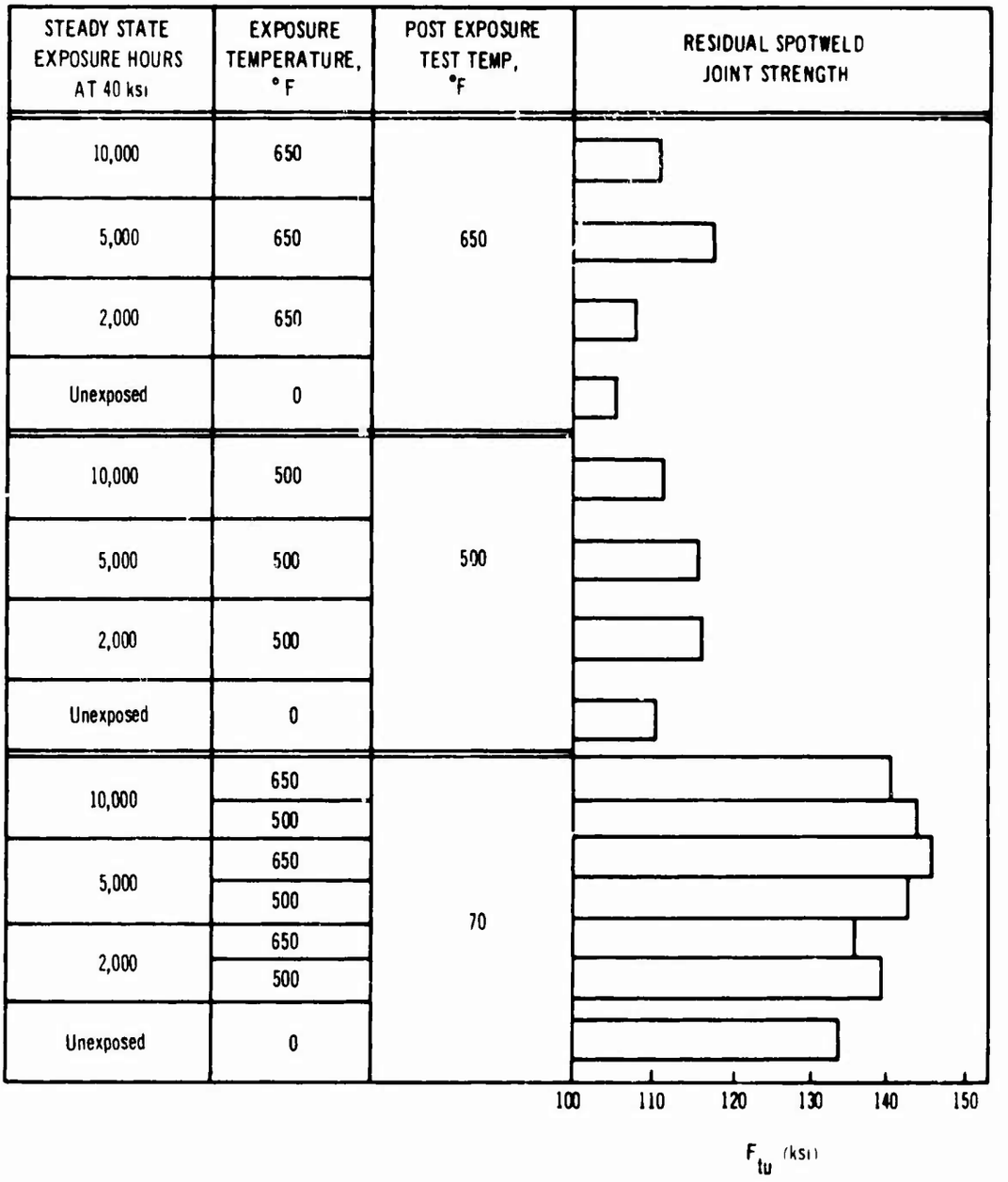


Figure 3-144. Spotweld Joint Strength

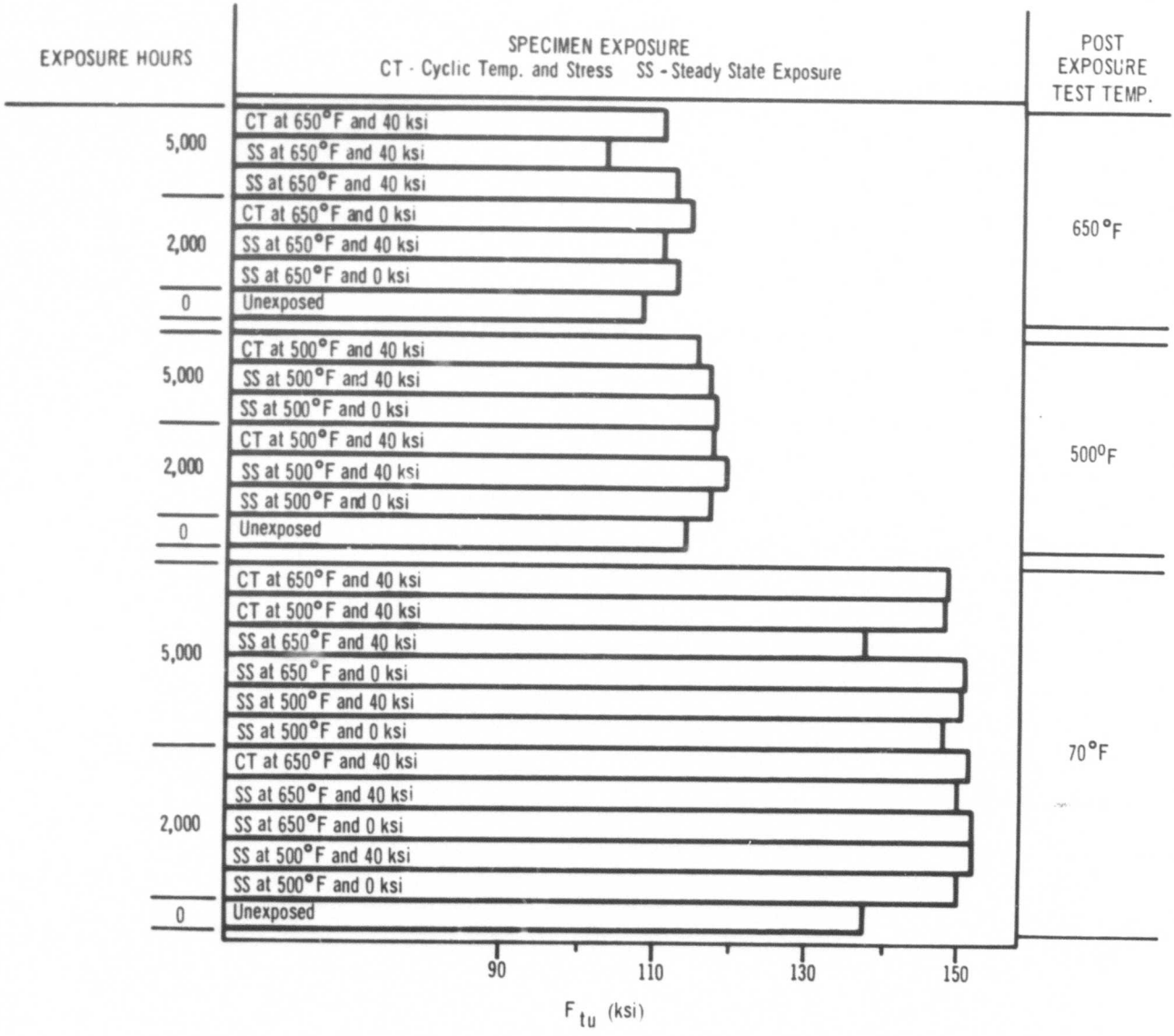


Figure 3-145. Longitudinal Weld Properties

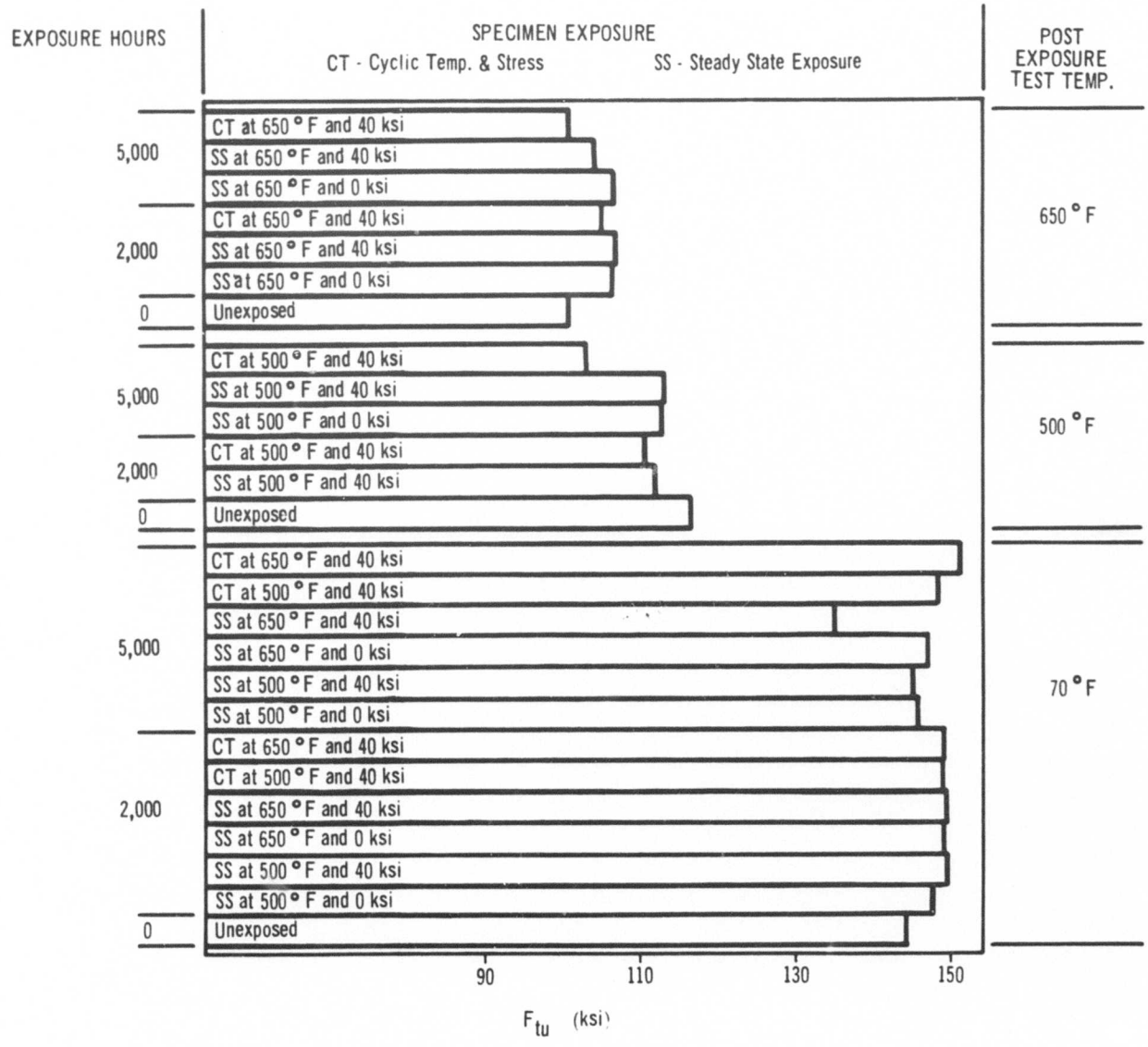


Figure 3-146. Transverse Weld Properties

218
4
226

REFERENCES

The following references are available at The Boeing Company, SST Division:

1. P. Kuhn, J. P. Peterson, and L. K. Levin, "A Summary of Diagonal Tension, Part I, Methods of Analysis," NACA TN 2661

2. A Method for the Calculation of the Approximate Stress Distribution and Surface Waviness of a Conventionally Stiffened Wing Box Subject to Thermal Buckling, D6-17340, The Boeing Company

3. Boeing Thermal Analyses AS-0315, The Boeing Company, August 1963

4. Stress Analysis of SST Empennage Test Structure, D6A10235-1, The Boeing Company, June 15, 1966

5. "Structural Design for Acoustic Fatigue," ASD-TDR-63-820, ASD Contract No. AF 33(657)-8217, Douglas Aircraft Company, Inc.

6. "Engineering Effort to Obtain Long Time Creep Data on Structural Sheet Materials," ASD Contract No. AF33(616)-8348, Task No. 73812, Joliet Metallurgical Laboratories, Inc.

7. "Intermittent Creep and Stability," ASD Contract No. AF33(657)-8907 and AF33(657)-11687, General Dynamics Corporation